Pro-drug strategies for pancreatic cancer therapy

By

Mohanad Alfahad

A thesis submitted in partial fulfilment of the requirements of Keele University for the degree of Doctor of Philosophy at the School of Pharmacy

March 2018

Abstract

Pancreatic cancer is the fourth main cancer in the western world. Currently the only chemotherapy available clinically is gemcitabine. However, gemcitabine treatment only proves effective in 23.8% of patients. Nano-structures (<120 nm) are capable of entering the highly permeable blood capillaries which supply the rapidly growing tumours. Once inside the capillaries they accumulate and are retained in the tumour as a result of the poor lymphatic drainage. This allows for a deeper tissue penetration which is otherwise difficult to achieve. Hybrid nanoparticles with an iron oxide core covered by gold shell (HNPs) have shown great potential for anti-cancer therapies. The magnetic iron oxide cores and the surface plasmon resonance (SPR) properties of the gold surface provide the HNPs with the capabilities of diagnostic imaging and drug delivery, making them true theranostic agents.

A novel prodrug of gemcitabine has been developed by a regioselective coupling of gemcitabine and lipoic acid, itself a potent antioxidant. Gemcitabine-*N*-lipoate (GL) was obtained in a one-pot synthesis and the optimum conditions for the reaction were established. GL prodrug loading on to the HNPs surface was confirmed and the release profile of gemcitabine from the GL-HNPs formulation was studied at pH 3.6, 5.6 and 7.4 utilising different temperature conditions (20, 37, 44 °C) using RPMI serum free media under sink conditions.

The data showed the stability of the formulation at pH 7.4, 20 °C while the optimum release conditions for gemcitabine from the GL-HNPs formulation were at pH 5.6, 44 °C with the highest release of 41.1% recorded after 24 hrs.

Preliminary *in vitro* MTT assay together with the drug uptake study show the superior inhibitory effect of the GL-HNPs formulation on the cell viability over gemcitabine after 24 hrs which indicates faster uptake of the formulation, however the overall effect of gemcitabine is greater after 48 hrs which is mainly due to the slow release of gemcitabine from the formulation.

The behaviour of the GL-HNPs formulation as a drug delivery system shows a great potential for the system to act as a theranostic tool and to overcome the significant drawbacks associated with gemcitabine.

"This thesis is the result of the author's original research. The copyright of this thesis belongs to the author under the terms of the United Kingdom Copyright Acts as qualified by Keele University. Due acknowledgement must always be made of the use of any material contained in, or derived from, this thesis."

Acknowledgements

Table of Contents

XI

Table of Figures

XIV

XV

XVII

Abbreviation

µM	micromolar
BNIHexamine	Bisnaphthalimido heptaethylhexamine
BNIPDi	Bisnaphthalimido diaminoicosan
BNIPDodecan	Bisnaphthalimidopropyl diaminododecan
BNIPds	Bisnaphthalimidopropyl diaminopropyldithiobutane
BNIPSpm	Bisnaphthalimidopropyl spermine
Boc	*tert*-butoxycarbonyl
br	broad
d	doublet
DCC	*N,N'*-Dicyclohexylcarbodiimide
DCM	dichloromethane
DEPT-135	Distortionless Enhancement of Polarisation Transfer
DIPEA	*N,N*-Diisopropylethylamine
DMAP	*N,N*-dimethylaminopyridine
DMF	dimethylformamide
DMSO	dimethyl sulfoxide
EDCI	1-Ethyl-3-(3-dimethylaminopropyl)carbodiimide
EDTA	Ethylenediaminetetraacetic acid
EtOH	ethanol
GL	gencitabine-lipoic acid prodrug
HATU	1-[Bis(dimethylamino)methylene]-1H-1,2,3-triazolo [4,5-b]pyridinium 3-oxid hexafluorophosphate
HEAEN	*N*-[2-(2-hydroxylethylamino)-ethyl]-1, 8-naphthalimide
HMBC	Heteronuclear multiple-bond correlation
HNPs	Hybrid ironoxide core gold shell nanoparticles
HPLC	High Performance Liquid Chromatography
hr	hours
HSQC	heteronuclear single quantum correlation
IC$_{50}$	Inhibitory Concentration
IR	infrared
J	coupling constant
m	multiplet
MeOH	methanol
Min	minute
mL	millilitres
Mmol	millimoles

Mp	melting point
MS	mass spectrum
Mts	Mesitylenesulfonyl chloride
Mts spermine	*N1,N5,N10,N14*-Tetramesitylatedspermine
Mts TET	*N1,N4,N7,N10*-Tetramesitylatedtriethyltetramine
MTT	3-(4, 5-dimethylthiazol-2-yl)-2, 5-diphenyl tetrazolium bromide
NADH	Nicotinamide adenine dinucleotide phosphate
NHS	*N*-Hydroxysuccinimide
NMR	nuclear magnetic resonance
PBS	Phosphate Buffered Saline
PEHA	pentaethylenehexamine
q	quartet
RPMI-1640	Roswell Park Memorial Institute 1640 medium
RT	room temperature
s	singlet
Spd	Spermidine
Spm	Spermine
t	triplet
TEA	Triethylamine
TEM	Transmission electron microscope
TET	triethyltetramine
THF	tetrahydrofuran
TLC	thin layer chromatography
TMSCl	trimethylsilyl chloride
Ts-Cl	Toluenesulfonylchloride
UV	Ultraviolet

CHAPTER 1: INTRODUCTION

1.1 Cancer

''Cancer is the name given to a collection of related diseases. In all types of cancer, some of the body's cells begin to divide without stopping and spread into surrounding tissues'' (National cancer institute 2016).

There are more than 200 types of human cancers causing a significant mortality rate for over a third of all population all over the world. Of these lung, breast, prostate and bowel cancer stand for about half of all cases. In 2012 more than 14 million new cases of cancer were diagnosed throughout the world, and over 300 thousand people were diagnosed with the disease in the United Kingdom alone in 2011 (Siegel *et al*. 2013; Cancer Research 2016).

Cancer is a leading cause of death in developed countries and accounting for about 25% of all deaths. Cancer was considered in the past as an incurable disease, nowadays patients could survive their disease if it is diagnosed in the early stage of development and before metastasis (Park *et al,* 2008).

Risk factors linked to cancer are either non-preventable like aging (patients over 75 account for more than 30% of all patients developing cancer (Yancik 2005)) and hereditary factors which are linked to certain types of cancers, and preventable risk factors which include environmental factors (like ultraviolet radiation, chemical toxins, and cigarette smoking) and dietary habits (like high fat diet and alcohol). All these factors together account for about 40% of cases in the United Kingdom (Surh 2003; Yancik 2005; Moiseeva & Manson 2009; Cancer Research 2016).

1.1.1 Pancreatic cancer

1.1.1.1 Pancreas

The pancreas is an endocrine-exocrine gland sited in between the liver, stomach and the small intestine (Figure 1). According to the shape of the pancreas, the organ was described to have head, body and tail. The endocrine part of the pancreas is responsible for secretion of glucose regulatory hormones (insulin and glucagon) and it is made up with islets of Langerhans, while the exocrine part which is made up with ducts and acini is responsible for secretion of digestive enzyme (Nabeel Bardeesy & DePinho 2002; Dintzis & Liggitt 2012).
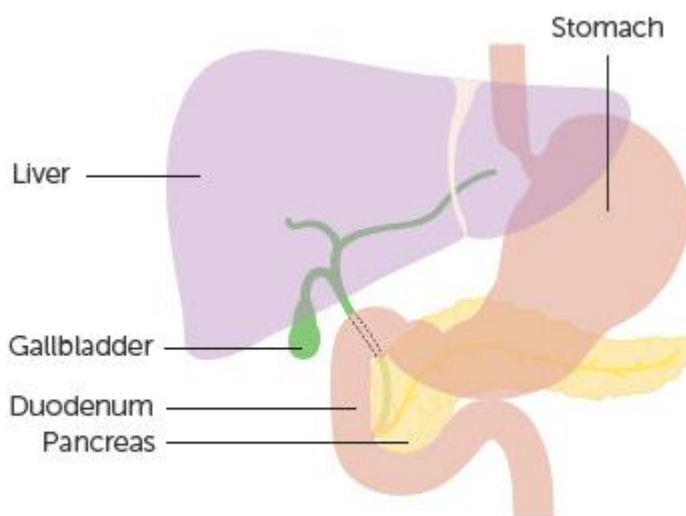
Figure 1: The pancreas location inside the body (Cancer Research UK 2016)

1.1.1.2 Types of pancreatic cancer

Pancreatic cancers are classified according to the origin of the tumour into exocrine pancreatic tumour which accounts for about 95% of all pancreatic cancers where the tumour affects the exocrine part of the pancreas and the endocrine pancreatic tumour which is involved in the endocrine part of the organ. In addition a range of rare pancreatic malignancies are observed, like; adenosquamous carcinoma and mucinous non-cystic carcinoma (Ryan *et al.* 2014).

1.1.1.3 Pancreatic ductal adenocarcinoma (PDAC)

PDAC is the major solid exocrine pancreatic tumour originating from the epithelial lining of the pancreatic ducts. It could be found anywhere in the pancreas but the majority of the PDAC's are found in the head part of the organ (about 75% of pancreatic cancers develop at the head of the pancreas) (Alexakis *et al.* 2004; Hidalgo 2010; Cancer Research 2016; *Kamisawa et al.* 2016). Furthermore spreading of cancerous cells into adjacent or remote tissues, via lymphatics like the spleen and peritoneal cavity are frequently witnessed. Metastatic growth is also commonly seen in both the liver and lungs (Hezel *et al.* 2006).

1.1.1.4 Epidemiology of pancreatic cancer

According to Cancer Research UK pancreatic cancer was in the eleventh position for the most common cancers in UK in 2014 (12th most common cancer for male and 9th for female). It also accounts for 3% of all new cases of cancer. People aged over 75 in the UK are more susceptible to the disease (47% of new cases of

pancreatic cancer are diagnosed in the elderly) and PDAC accounts for over 90% of all cases. The fifth cause of cancer related death within the UK is due to pancreatic cancer. In 2014, 9600 patients were diagnosed with pancreatic cancer, and 8,800 deaths were documented as a result of this aggressive disease (Cancer Research 2016). The deep location of the pancreas prevent early notice of size increment of the organ mounting the disease (pancreatic cancers), so early diagnosis is usually not applicable until the late stage where clinical symptoms start to appear, once diagnosed most patients will have a maximal survival of 12 months, with a less than 5% chance of surviving up to 5 years (Jemal *et al.* 2010). Long term survival can only be expected for an individual fortunate enough to have a primary localised tumour treatable via curative resection at the time of diagnosis (Hezel *et al.* 2006; Li *et al.* 2007; Singh *et al.* 2015).

1.1.1.5 Treatment of pancreatic cancer

Pancreaticoduodenectomy (surgical removal of the pancreas and duodenum) is the only possible curative treatment available for pancreatic tumour; even so unaided surgery will not succeed (N Bardeesy & DePinho 2002). Unfortunately surgery is only beneficial for patients in the early stages of the disease and it only prove to be effective in a rate ranging from 3-4% up to 27% as the 5 years survival rate report said (Ferrone *et al.* 2012; Shrikhande *et al.* 2007).

Most of the failures of the surgery treatment of pancreatic cancer are due to recurrent relapse of the disease after operation which is normally refers to failure of detection and elimination of metastatic cancer within the pancreas at time of

diagnosis so adjuvant chemotherapy in addition to surgery is usually required to increase the survival rate (Ferrone *et al.* 2012).

Adjuvants chemotherapies for pancreatic cancer are usually gemcitabine or Fluorouracil. Gemcitabine is the first line chemotherapeutic agent commonly used in the treatment of pancreatic cancer although it is only effective in 23.8% of patients (Sa Cunha *et al.* 2005). Many reports state that there is no extra benefit from using gemcitabine over Fluorouracil in pancreatic cancer therapy (Neoptolemos *et al.* 2010; O'Reilly 2011; Neoptolemos JP *et al.* 2012; Tuveson & Neoptolemos 2012).

The management choices for patients unable to have their tumour removed by surgical resection is either chemoradiation (chemotherapy+radiotherapy) or chemotherapy with gemcitabine as the ordinary choice, currently no alternative choice other than palliative treatment is available (Vincent *et al.* 2011).

New approaches (nanoparticle formulation) which adapt a pre-existing antitumor drug to be active against pancreatic cancer were recently developed and approved for clinical use in pancreatic cancer therapy. Abraxane[®] or nab-paclitaxil is a nanoparticle formulation of paclitaxel (anticancer), where the drug is bound to albumin nanoparticle to reduce the clinical side effect associated with the solvent used for the drug delivery. Studies conducted using co-administration of nab-paclitaxil with gemcitabine compared with gemcitabine alone for metastatic pancreatic cancer therapy, seems to increase total survival rate (Von Hoff *et al.* 2011; Von Hoff *et al.* 2013).

1.2 Cancer chemotherapy

Treatment of cancer typically involves a combination of surgery, chemotherapy and radiotherapy. Surgical treatment of cancer relies upon the use of invasive techniques and usually requires concurrent intravenous delivery of a chemotherapeutic agent. Chemotherapy can be used alone to reduce the size of any tumours or cancerous tissues, including tissue which may remain following other interventions. Radiotherapy is also used but it is usually employed in combination with administration of a chemotherapeutic agent.

The primary goal of any chemotherapy is to eradicate the cancerous cells preferentially and selectively in the presence of normal cells; this relies upon the fact that cancerous cells may grow and multiply faster than non-cancerous cells in normal tissue. New discoveries in the field of chemotherapy and optimisation of existing chemotherapeutic treatments over the past few decades have led to significant increases in patient survival and improvements in the quality of life, but efforts are still required to develop.

A chemotherapy or antineoplastic agent refers to a chemical compound which has the ability to prevent new growth of cells, and because they are designed to kill cells they do so regardless of being healthy or diseased. In general all cytotoxic mechanisms of killing cells involves a block to cell synthesis pathway or affect DNA, RNA and protein function (Avendano & Menendez 2008).

An ideal cytotoxic drug should be both tissue specific (i.e. affect only the diseased organ) and cell specific (*i.e.* affect only the diseased cells within the diseased organ), but unfortunately this is not yet applicable. Major adverse reactions

resulting from chemotherapy are cytotoxic effect on the short lived normal cells (*e.g.* gastrointestinal cells, hair follicle and bone marrow cells) leading to serious complications like nausea, vomiting, hair loss and susceptibility to infections. However there are other late irreversible major side effect associated with many cytotoxic agents affecting vital organs (heart, kidneys and lung) (Avendano & Menendez 2008).

1.2.1 Dosing of chemotherapy

Chemotherapeutic agents are frequently given in sequences to reduce the severity of side effects; the frequency of drug administration is usually several days to weeks. The dose for each cytotoxic agent that has to be given in each round is calculated according to the fact that each round of antineoplastic agent can kill a certain percent of tumour cells and this percent increases proportionally with the dose. If the agent(s) are capable to shrink the tumour to less than 10,000 cells, normal defence system will be able to eradicate them, therefore the dose should balance between the patient health conditions (their ability to tolerate the results side effect) and the active required dose (which depends on the size of tumour and the extent of tissue invasion) (Avendano & Menendez 2008).

1.2.2 DNA alkylators class of anticancer

DNA alkylators or DNA cross-linking agents are one of the prominent classes of cancer therapeutic agents; it includes the compounds that target the active DNA molecule by interfering with DNA replication and transcription process (Anderson *et al.* 2009). All DNA alkylators are characterised being very reactive electrophile (bearing a positive charge), and typically have planar or heteroaromatic chromophores, that stack between base pairs of the DNA double helix (Martínez & Chacón-García 2005).

The mechanism of alkylation of DNA molecule is the complexation reaction that happens between the nucleophilic groups of DNA (mainly but not solely the guanine base) with the electrophilic drug causing irreversible alkylation of the molecule, some alkylating agents has the ability to bind two distinct DNA bases or bind two DNA bases from two different DNA molecule (Kamal *et al.* 2007). Topoisomerase II enzyme (crucial enzyme in DNA shaping process) is also a target of some DNA cross-linkers, inhibition of Topoisomerase II lead to raise numbers of DNA strand breaks which may activate apoptosis (Fortune & Osheroff 2000; BrañaBraña *et al.* 2001).

Bisnaphthalimides (a new class of anticancer agents) also act by intercalating DNA molecule irreversibly by the aromatic rings implanting between the pairs of the DNA double helix, which alters DNA shape, leadings to cell death for a panel of human cancer cell lines (Braña *et al.* 1980; Braña & Ramos 2001; BrañaBraña *et al.* 2001; BrañaBrañaLin *et al.* 2003).

9

1.2.2.1 Naphthalimide and Bisnaphthalimide based anticancer agents

Napthalimides (Figure 2) were created in the 1970s to have the structural components of several cytotoxic agents into a single molecule.
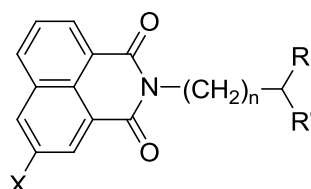
Figure 2: General structure of naphthalimides

The compounds were made by simple condensation of 3-nitro-1,8-naphthalic anhydride with the amine side chain. Afterwards, more derivative of naphthalimides were synthesised by changing ring substituents, and side chain (Braña & Ramos 2001; Braña *et al*. 2001).

Mitonafide and amonafide (Figure 3) were selected from a library of naphthalimides and thoroughly studied (go through Phase I and Phase II) because of their potent cytotoxic action against a group of cell lines. Both compounds exert their action by binding to DNA by intercalation and inhibit Topoisomerase enzyme II action while, other naphthalimides are unable to inhibit Topoisomerase enzyme II (Allen & Lundberg 2011; Braña & Ramos 2001).
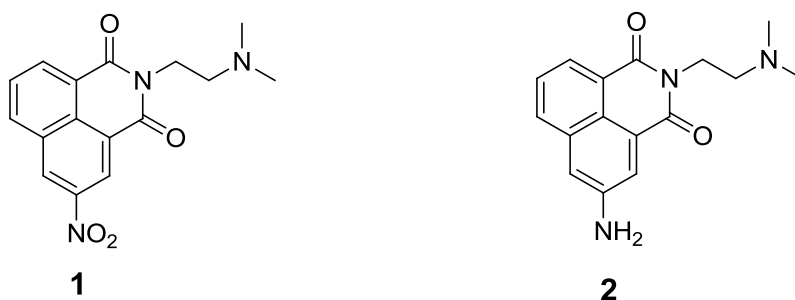
Figure 3: Chemical structure of Mitonafide **1** and Amonafide **2**

Derivatives of naphthalimides similar to amonafide have been made to increase the cytotoxic effects of the naphthalimides family. One approach was to design and synthesis new symmetrical derivatives of naphthalimide (Bisnaphthalimides). Bisnaphthalimides, in comparison with naphthalimides have greater cytotoxic effect due to their stronger binding ability to DNA (Braña & Ramos 2001).

Biological activity of bisnaphthalimide compounds are changed dramatically by changing both the chromophore substituents (in the order NO_2 > H > NH_2 > CH_3CONH) and the linker chain character (length and nature) (Braña & Ramos 2001).

Elinafide (Figure 4), a bisnaphthalimide derivative selected for phase I and phase II study, has no substituents in the chromophore and has seven methylene groups in the linker chain. Elinafide has the highest cytotoxic effect among the other bisnaphthalimide derivatives but unfortunately its anti-cancer effects were restricted by its side effects (Bousquet *et al.* 1995; Bailly *et al.* 1996; Braña & Ramos 2001).

3
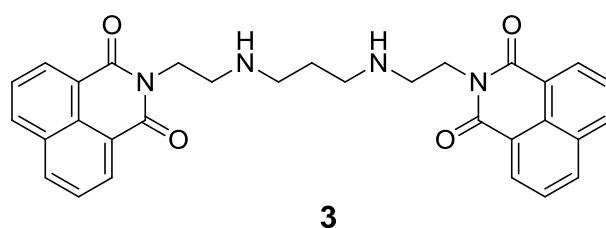
Figure 4: Chemical structure of Elinafide **3**

Asymmetric bisnaphthalimide derivatives were synthesised in an attempt to solve poor solubility problems of previously known bisnaphthalimide based compounds,

yet cytotoxicity of these compounds decreased without great improvement of aqueous solubility of the parent compound (Braña & Ramos 2001).

DNA intercalation (bifunctional intercalation via the major groove of double helix) and inhibition of Topoisomerase II enzyme are the way bisnaphthalimides exert their action. However, bisnaphthalimides structure requirements are (a) a nitro group in the naphthalimide rings, (b) two nitrogen atoms or (c) at minimum 3 methylene groups in the linker chain (Bailly *et al.* 1996).

Introduction of polyamines into the linker chain of bisnaphthalimides in order to increase their aqueous solubility and activity were found to be of great advantages as has been shown by Lin and colleagues (Lin & Pavlov 2000; Pavlov *et al.* 2001).

1.2.2.1.1 Polyamines

Polyamines in general are organic compounds having at least two primary amines in its structure. Naturally occurring polyamines (putrescine **4** ($C_4H_{12}N_2$), spermidine **5** ($C_7H_{19}N_3$) and spermine **6** ($C_{10}H_{26}N_4$) (Figure 5)) are known to be involved in living cell growth cycle. Polyamines levels inside the cell are linked to cell growth rate (low polyamine levels are associated with a decrease in cell growth) (Pegg 2009).
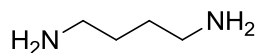
4
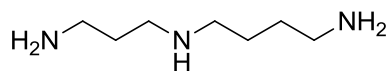
5
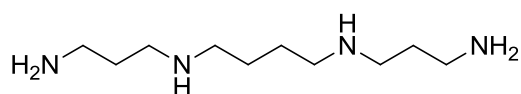
6

Figure 5: naturally occurring polyamines (putrescine **4,** spermidine **5** and spermine **6**)

Furthermore, cancer development is also thought to be controlled by polyamines, as high polyamines level were observed in cancer cells of breast and colon compared to normal cell, however high polyamines level were found in patients with psoriasis, cystic fibrosis, or even during pregnancy (Casero & Marton 2007). Protein synthesis have been shown to be stimulated by polyamines through stimulation of DNA and RNA synthesis (Childs *et al.* 2003), additionally scavenging of reactive-oxygen species by polyamines leads to protection of DNA, proteins and lipids (Nayvelt *et al.* 2010).

1.2.2.1.2 Polyamines derivatives as anticancer agents

Research over the last twenty years considers the inhibition of the anabolic pathways of polyamines. Inhibitors for anabolic enzymes in the biosynthetic pathway of polyamines were identified, but none of them go forward because of their low efficacy as anti-cancer agents (Casero & Woster 2001).

Taking the benefit of polyamine transporters as a tool for improving the uptake of potential anticancer agents by including the polyamines in their structures, was a big field of research aiming to produce analogues with better cytotoxic activity in addition to or apart from inhibition of polyamines biosynthesis (Casero & Woster 2001; Muth *et al.* 2014).

1.2.3 Antimetabolite as anticancer agents

Antimetabolites are compounds with great structural similarity to naturally occurring compounds, with an ability to inhibit the natural metabolic pathway by interfering with their formation and utilisation (Avendano & Menendez 2015).

Fluorouracil (5-Fu) and gemcitabine are cytotoxic drugs used to treat pancreatic cancer by inhibition of tumour growth by interacting with the processes involved in the synthesis of new proteins vital for cell proliferation. They also inhibit cell growth by also inhibiting DNA replication or causing enough stress to the cells leading to apoptosis (Batmani & Khaloozadeh 2013).

1.2.3.1 Gemcitabine

Gemcitabine **7** is a deoxycytidine **8** analogue (deoxycytidine is a naturally occurring nucleoside) (Figure 6).
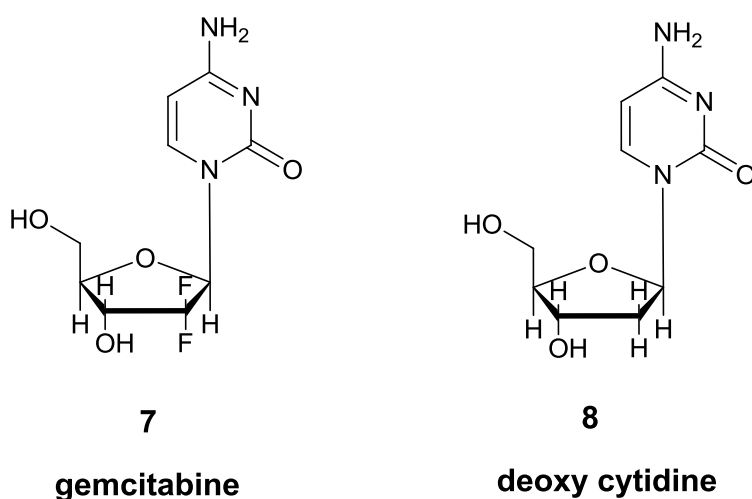
Figure 6: Chemical structures of deoxycytidine and gemcitabine

The chemical name of gemcitabine is 2′, 2′ diflourodeoxycytidine as the only difference between gemcitabine and deoxycytidine is the two fluorine atoms in the 2′ position on the carbohydrate ring. Gemcitabine was introduced in 1986 for the first time as an antiviral agent, ten years later (in 1996) the drug was approved by the (FDA) for pancreatic cancer therapy (metastatic adenocarcinoma of pancreas). The drug also has established effects against solid human tumours (lung, breast, and ovarian cancer) (Heinemann 2001). Gemcitabine is commonly used in combination with other anticancer agents (acting by DNA demolition) like paclitaxil, and cisplatin (Li *et al.* 2010; Weigt & Malfertheiner 2010).

1.2.3.1.1 Mechanism of action of gemcitabine

Gemcitabine is hydrophilic in nature so it can't enter the cell by passive diffusion; the nucleotide transporter proteins across the cell membrane are the means by which gemcitabine drug enters the cell (Mackey *et al.* 1998).

Once gemcitabine is inside the cell it undergoes enzymatic phosphorylation (deoxycytidine kinase) into gemcitabine monophosphate **9** which is then transformed into gemcitabine diphosphate **10** and finally gemcitabine triphosphate **11**, which is the active form of gemcitabine. The rate limiting step in this activation is the first step (conversion of gemcitabine into gemcitabine monophosphate). Gemcitabine triphosphate is then integrated with other nucleotides within the developing DNA strand followed by another nucleotide to mask gemcitabine and prevent the DNA repair action (Plunkett *et al.* 1995). Incorporation of false metabolite resulted in blockade of DNA synthesis and consequent cell deaths.

Incorporation of gemcitabine into RNA is also established but the RNA synthesis inhibition effect as a mechanism for gemcitabine action is still in debate (van Haperen *et al.* 1993).

Gemcitabine diphosphate and triphosphate have an ability to inhibit several enzymes including ribonucleotide reductase leading to the block of the de novo DNA synthesis as well as enhancement of their effects by feedback inhibition of metabolising enzyme (Wang *et al.* 2009) Figure 7 illustrates the mechanism of action of gemcitabine in brief.
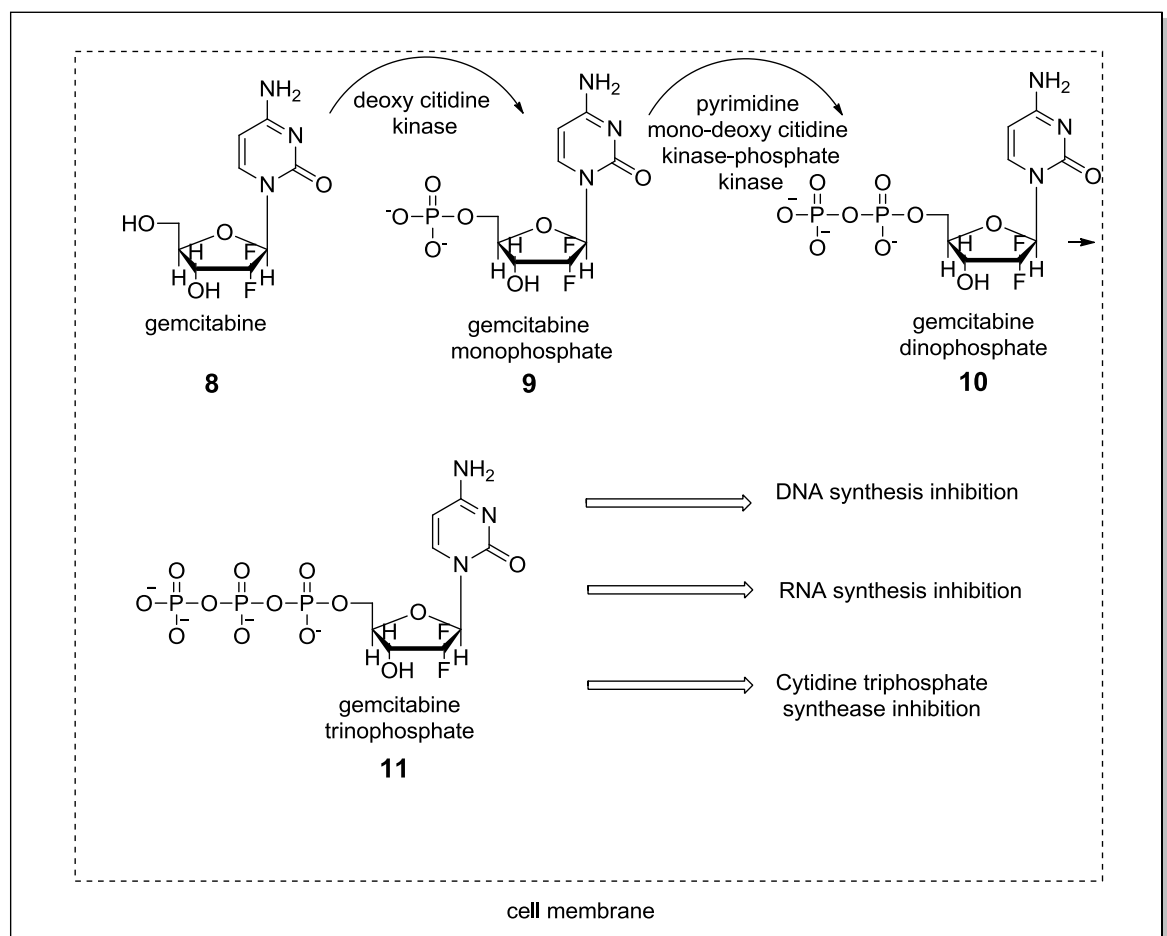
Figure 7: mechanism of action of gemcitabine

1.2.3.1.2 Metabolism of gemcitabine

As shown above in the mechanism of action of gemcitabine, gemcitabine is a prodrug that requires activation first by phosphorylation prior to exhibit its it is anticancer effect.

Deactivation of gemcitabine prior to being phosphorylated may occur by the action of cytidine deaminase enzyme while gemcitabine monophosphate **9** is deamination by deoxycytidylate deaminase enzyme (Bergman et al. 2002a).

The product of deactivation of gemcitabine by deamination is the 2′,2′ diflourodeoxyuridine **12**. This metabolite also displays cytotoxicity and it plays a role in ruling the passage and build-up of gemcitabine inside the cell (Veltkamp et al. 2008; Rudin et al. 2011a).

Deamination of gemcitabine monophosphate results in 2′, 2′ diflourouridine monophosphate **13** which has an inhibitory effect an thymidylate synthase enzyme affecting the deoxynucleotide triphosphate levels inside the cell (Bergman *et al.* 1999). De-phosphorylation of gemcitabine monophosphate is another form of deactivation of gemcitabine by the action of 5′-nucleotidases enzyme which transforms nucleotides to nucleosides (Enrico Mini et al. 2006)

(Figure 8) illustrates gemcitabine metabolism in brief.
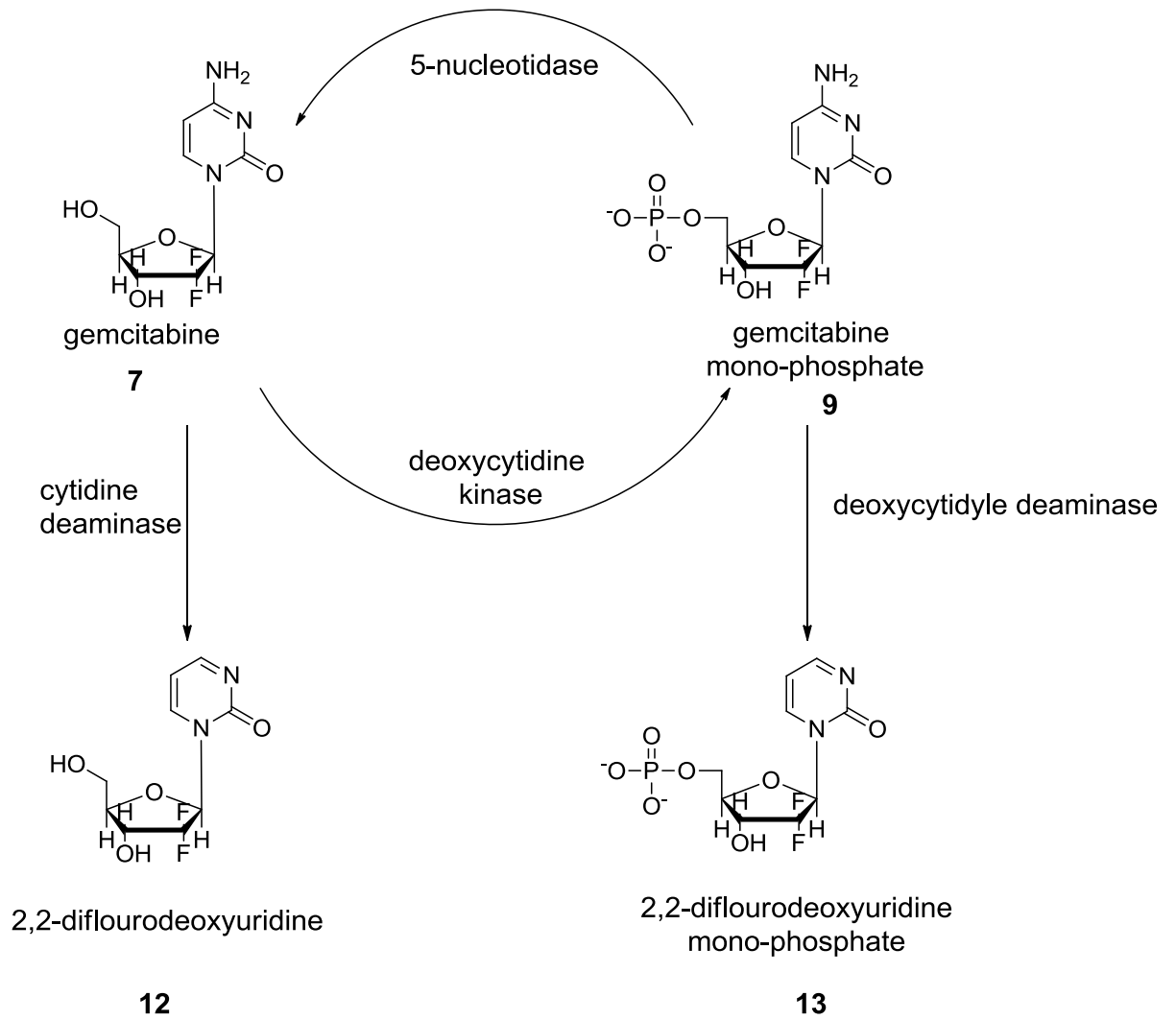
Figure 8: metabolism of gemcitabine

1.2.3.1.3 Resistance to gemcitabine

Cancer resistance to chemotherapy is a common practice in clinical cancer treatment, this chemo resistance may be intrinsic or acquired during treatment cycle (Kleger *et al.* 2014). Drug resistance can develop because of several reasons. like, changes in the drug target caused by mutations (Ling *et al.* 2005), over expression of proteins responsible for producing efflux pumps like p-glycoprotein or an immune response to the drug/drug transporter, or even. Because cancer drugs are cytotoxic, macrophages may become increasingly sensitive to their presence and increase the rate of drug metabolism (Markman *et al.* 2013). The liver is responsible for much of the detoxification within the body and may improve the rate of drug metabolism after repeated doses (Tsume *et al.* 2014).

One of the significant intrinsic factors associated with pancreatic cancer resistance to chemotherapy, including gemcitabine, is the tumour environment itself because pancreatic cancer is categorised as a solid tumour, which is very difficult to penetrate by drugs (as well as the immune system) due to its dense stroma and poor vascularisation (90% of pancreatic tumour volume might be due to desmoplastic reaction) (Neesse *et al.* 2011). In addition, just like other chemotherapeutic agents, gemcitabine could suffer from chemo resistance; a number of mechanisms are involved in developing resistance to gemcitabine of which the metabolic pathways are the most noticeable (Walker & Ko 2014). As gemcitabine needs to be inside the cell to be activated and cause the consequent cell death, gemcitabine transporter proteins in the cell membrane are one of the

targeted causes of chemo-resistance; genetic factors play an important role in defining intrinsic resistance to nucleotide analogues (Zhang *et al.* 2008).

1.3 Targeted cancer chemotherapy

Traditional chemotherapeutic lines alone or in combination with other therapeutic measures (surgery and radiotherapy) form the major therapeutic approach to cancer treatments (whether being localised or metastasised) (Rang *et al*. 2011), yet the high toxicity of the chemotherapeutic agents on the normal healthy tissues, together with low water solubility and the increasing probability of cancer cells developing multi drug resistance greatly limits their benefits as anticancer (Stavrovskaya 2000; Kwon 2003; Moorthi *et al*. 2011).

Chemotherapeutic agents are not suitable for long term treatment of cancers due to their poor selectivity, the consequence of which is that the drug will affect all types of highly proliferative normal cells within the body, such as bone marrow cells, gut epithelia, hair follicles and red blood cells not just the rapidly-growing neoplastic tissue. Furthermore, drugs used in cancer chemotherapy have little effect on solid tumours since these tumours develop slowly and most do not have a high rate of proliferation.

As a result, high-doses of chemotherapeutic drugs are required to inhibit the proliferation of tumour cells effectively, especially when treating resistant solid tumours. However, this high dose could also be the main reason behind discontinuation of chemotherapy due to the high degree of toxicity observed in adjacent tissues before the complete eradication of the cancerous cells is achieved (Mahato et al. 2011; Q. Sun et al. 2013a).

Failure of chemotherapeutics to exert their cytotoxic effects could be the reason of multi drug resistance; the systemic route of administration is the main route of drug delivery in cancer therapy and variation in metabolism, distribution and uptake by targeted tissues could play an essential role in determining the outcome of cancer treatments (Szakács *et al.* 2006). Research focussing on the mechanisms of multidrug resistance in cancer chemotherapy indicates three mechanisms of cellular drug resistance that have major contributions to the final therapeutic effect. These mechanisms are first, decreased uptake of membrane transporters dependent anticancer (such as nucleoside analogues), these compounds are usually highly water soluble in nature. Second, cell adaptation to counter act the effect of the cytotoxic drugs (including DNA damage repair and alteration of cell cycle and drug metabolism) and third, increased rates of energy dependent export of passively diffusing hydrophobic drugs through the plasma membrane (Szakács *et al.* 2006).

Several rapidly progressing approaches have been developed aimed for solving the problems associated with conventional drug delivery systems. Of these prodrug strategies and nanoparticulate drug delivery systems draw the vast attention (Luo *et al.* 2014).

Prodrugs (prodrugs are defined as bio-reversible, chemically modified derivatives of drug molecules that undergoes biotransformation *in vivo*, either chemically or enzymatically, to release the active compound (Rautio *et al.* 2008; Mahato *et al.* 2011)) have been widely used to increase the anticancer efficacy by altering physicochemical properties of the drug that hinder the active delivery to the site of action (such as the water solubility, lipid solubility and poor drug stability) (Bildstein *et al.* 2011; Luo *et al.* 2014)

Nanocarriers have shown potential advantages as anticancer drug delivery vehicles by improving the drug bioavailability, and provide a passive way of tumour targeting and increased tumour accumulation via the unique (enhanced permeability and retention effect (EPR)) characteristics of the nanoparticulate systems. In addition there is great potential for nanoparticle systems to be fabricated as targeted and controlled drug release systems (Minko *et al.* 2013; Luo *et al.* 2014).

Stages of drug distribution experienced by the drug loaded nanoparticles after IV administration (Figure **9**) should be considered at the time of developing a new nanoparticulate system. These stages are presenting the formulation into the systemic circulation, filtration of the nanoparticles throughout the blood vessel wall, deep tumour penetration, nanoparticulate system uptake by cancerous cell and disposition of drug within the cancer cell (Sun *et al.* 2013b; Luo *et al.* 2014).
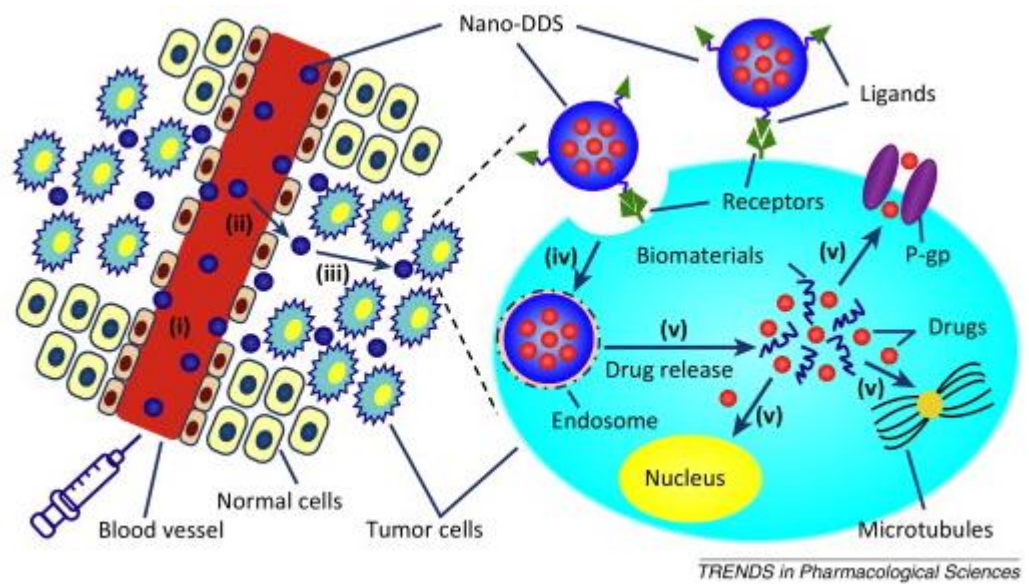
Figure 9: schematic presentation of nanoparticles distribution after intravenous administration: (i) circulation in blood; (ii) filtration via capillary wall; (iii) deep tumour penetration; (iv) uptake by tumour cells; and (v) release of nanosystems Nano-DDS: nanoparticulate drug delivery systems; P-gp: P-glycoprotein.(Luo *et al.* 2014)

1.3.1 Prodrug strategy of targeted drug delivery

Prodrug techniques have become an established tool for improving the physicochemical properties of a drug as well as the pharmacokinetic properties and they provide potential strategies for improving the selectivity of chemotherapeutic agents in comparison with other techniques for enhancing drug targeting (Rautio *et al.* 2008).

The strategy behind using prodrug techniques is usually to alter the physicochemical properties of the active drug through some structural modification, this usually results in (for example) enhanced solubility in aqueous media, improved chemical stability, masking of any bitter taste associated with the parent drug molecule, avoidance of inactivation of the drug by systemic circulation through the liver, and reduction in irritation and allergies, reduced toxicity and pain associated with the parent compound (Singh *et al.* 2008; Müller 2009).

More importantly, a prodrug approach could be used to improve the targeting and selectivity of chemotherapeutic agents in which ligands or polymers which recognise and bind to specific cell types are attached to the active drug by means of a cleavable linker. This approach is usually dependent on the over expression of a specific antigen and/or enzyme in tumour cells and cancerous tissue compared to the normal cells (Han & Amidon 2000; Mahato *et al.* 2011).

Prodrug formation requires the parent drug to have a functional group ready to be joined to a linker via chemical bond formation; the linker should be either self-cleavable or responsive to a certain trigger condition (like enzyme cleavage or pH) to allow the release of the parent drug. Additionally the linker should provide the

essential properties to overcome the problems faced by the drug on its way to the target cell. Ester and amide bonds (Figure 10) are among the most common bonds utilised in the design and synthesis of prodrugs, both bonds being characterised by being easy to synthesise and their functional groups are widely available in both linker molecules and parent drugs, in addition to the ability of the bonds to be cleaved by enzymes (Rautio *et al.* 2008; Mahato *et al.* 2011).

Amide bonds are more stable than ester bonds towards enzymatic breakdown and most amide bonds are stable in plasma (from several hours to several days) in the absence of specific metabolising enzyme (Mahato *et al.* 2011).
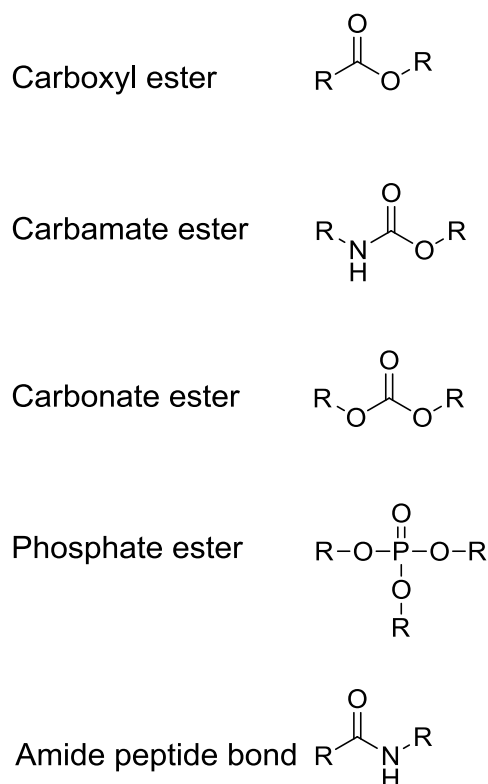
Figure 10: Esters and amide linkers used in prodrug design

Targeted prodrugs may be taken up by cells and then activated in the intracellular medium. For example, passive diffusion and endocytosis are common modes by which targeted therapies enter the cell prior to activation (Bildstein *et al*, 2011). Figure 11 shows the most common prodrug design for a chemotherapeutic agent containing as many as four distinct parts: (1) the active drug or its derivative; (2) a chemical linker to link the active compound to the rest of the prodrug; (3) a spacer or polymer susceptible to cleavage by a specific enzyme; (4) a targeting moiety with the ability to guide the molecule precisely to the site of action. (Mahato *et al,* 2011).

Targeting moiety	Spacer	Chemical linker	Drug
▪ Antibody ▪ Aptamer ▪ Peptide ▪ Folic acid	▪ Polymer ▪ Enzyme cleavable peptide	▪ Ester ▪ Amide ▪ Disulfide ▪ Thioether ▪ Oxime/imine	
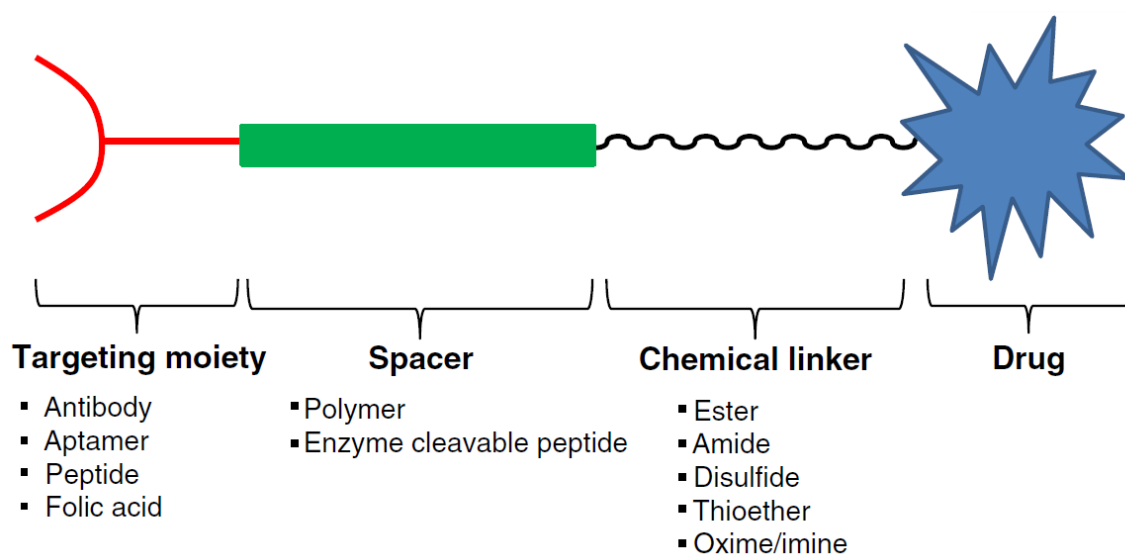
Figure 11: General design of a prodrug (reproduced from Mahato, *et al* 2011).

1.3.1.1 Prodrugs of Gemcitabine

Changes to gemcitabine structure by addition of a cleavable moiety to form a prodrug are a very well-known approach to overcome gemcitabine disadvantages. Prodrugs of gemcitabine are generated either to overcome the deactivation process by cytidine deaminase enzyme, change the mechanisms by which gemcitabine enter the cell and to prolong the release of gemcitabine by increasing time of storage inside the cytosol (this outcome is achieved by blocking the N 4 position of gemcitabine or changes to 5′ position in the carbohydrate fraction of gemcitabine). Or provide the gemcitabine monophosphate (the rate limiting step in gemcitabine activation) by phosphoramidate functioning of the 5′ position.

Many prodrugs of gemcitabine have been synthesised (by addition of PEG **14**, **15** valproate, squalene, linear acyl derivatives **16** and phosphoamidate **17**) (Figure 12) and studies show their ability to protect against the action of cytidine deaminase enzyme, and also show the enhancement of the bioavailability of gemcitabine as well as modification to the route of drug entry suggesting motivating approach to treat difficult cancers (Moysan *et al.* 2013).
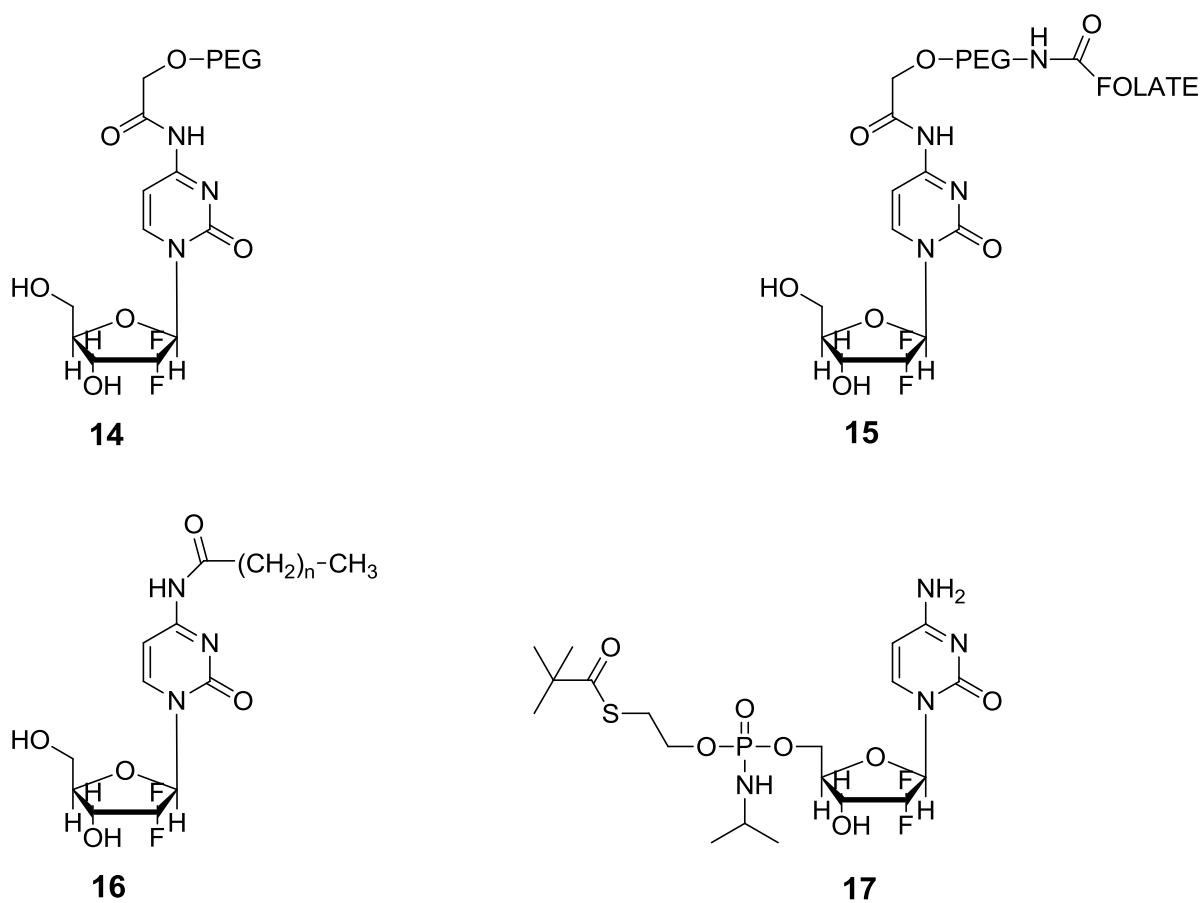
Figure 12 : *e.g* of gemcitabine prodrug derivatives (**14**: PEG-gemcitabine.; **15**: Folate-PEG-gemcitabine.; **16**: 4-(N)-acyl-gemcitabine.; **17**: -gemcitabine phosphoramidatediester (Moysan *et al.* 2013).

1.3.2 Targeted nanoparticles for drug delivery to cancer cells

Nano sized particles or more easily nanoparticles (NPs) are 1-100 nm size particles defined as a very small object acting as one system in term of properties and transport. NPs have been used in humans since 1983 when the US FDA approved the first micellar drug (Sandimmune®), and later on in 1990, the first polymer-drug conjugate (Adagen®) (Knop *et al.* 2010; Dreaden *et al.* 2012). After that much research has been done on a range of biomedical nanotechnologies (including inorganic nanoparticles and polymer drug conjugation) providing a potential tool for disease monitoring, diagnosis and treatment (Harris & Chess 2003; Thakor *et al.* 2011; Dreaden *et al.* 2012).

Targeted NPs can be classified in general into two main categories, passive and active targeting. Active targeting of cancerous cells by nanoparticles is achieved by targeting specific cellular components of tumour tissues such as over-expressed cellular receptors and other membrane bound proteins that enable active transport of the nanoparticulate system into the cell, and hence reducing the unwanted exposure of healthy tissues to the cytotoxic drugs. Interactions between the ligands and the cellular receptors may also facilitate the process of NPs endocytosis, including antibodies, peptides, and folic acid (Patra *et al.* 2008; Yu *et al.* 2010; Bazak, *et al.* 2014a).

Passive targeting of tumour tissues by nanoparticles is the result of the well described phenomena of enhanced permeability and retention effect (EPR) which is built on the specific structure of tumour vasculature and the size range of the nanoparticles (Bazak, *et al.* 2014b).

Among all the physicochemical properties of nanoparticles (including shape, size and surface charge) the size of the nanoparticles makes a significant contribution to the ability of the particles to penetrate tumour tissues and being taken up and cleared by cells. Size is also the main regulator of nanoparticle biodistribution inside the body and hence on the overall therapeutic effects (Tang *et al*. 2014).

Nanoparticle sizes range between 100-200 nm for most approved anticancer nanomedicines (Uster *et al*. 1998; Gradishar *et al*. 2005). Smaller sized anticancer nanomedicines have shown higher therapeutic effects in vivo, especially nanoparticles with 50 nm size (Cabral *et al*. 2011; Tang *et al*. 2014)

Very small nanoparticle (< 2 nm) and relatively small nanoparticles (<10 nm) have been shown to travel freely into tumour tissues and to be cleared rapidly into the blood stream without effective accumulation inside the tumour (Matsumura & Maeda 1986; Dreher *et al*. 2006).

The optimal size range of nanoparticles intended to be used for cancer treatments should also consider both the renal clearance (renal clearance threshold (<10–15 nm) (Choi *et al*. 2011; Shilo *et al*. 2012)) and interstitial/lymphatic clearance (<20 nm) (Moghimi *et al*. 2005).

A study by Tang *et al.* 2014 demonstrated that 50 nm size nanoparticles show the highest tumour retention time by comparing the use of 50 nm silica nanoparticles as a drug carrier for breast cancer treatments to a 20 nm and 200 nm size silica nanoparticles. The tumour retention time used was taken in the study as a parameter to reflect the deep tumour penetration, nanoparticle uptake by cancer

cells, the rate of nanoparticle clearance from tumour tissues, and consequently the anticancer efficacy (Tang *et al*. 2014).

Passive tumour targeting by Nano-particulate systems are basically thought to be due to the enhanced permeability and retention effect (EPR). Nanoparticle drug carrier systems, including liposomes and polymeric micelles, tend to accumulate in the tumour tissues more preferentially than normal tissues because of the undeveloped "leaky'' tumour blood vessels and also due to the absence of lymphatic drainage inside the tumour.

EPR phenomena (Figure 13) which have been first described and termed by Matsumura and Maeda, in 1986 will eventually lead to accumilation of nano-sized particles in the cancerous tissue (Matsumura & Maeda 1986).
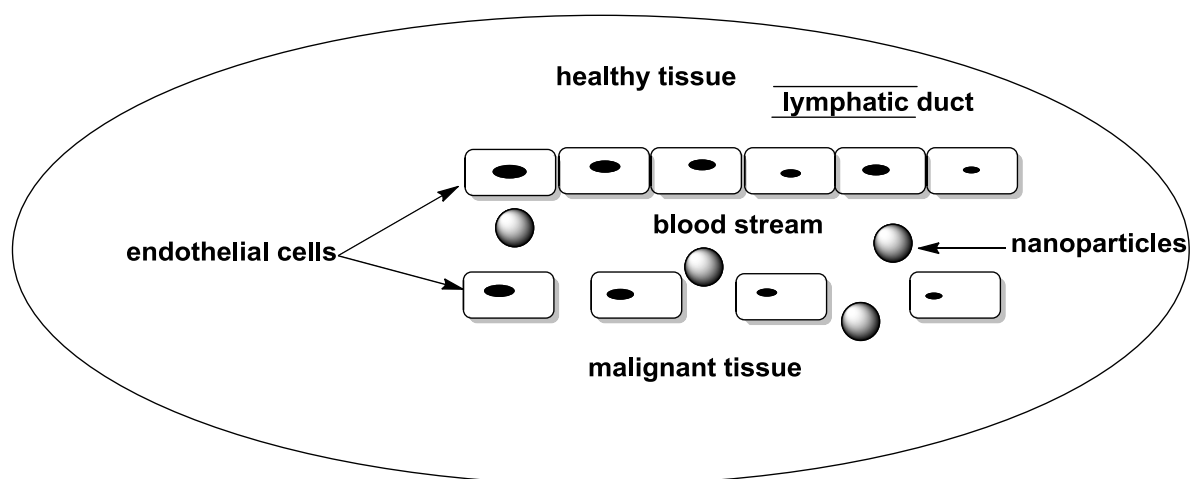
Figure 13: Diagram explaining EPR criteria of tumour vasculature.

The differences between the blood vessels of solid tumours and normal tissues in both physiological and morphological character were examined and described (Ruoslahti 2002; Bae *et al.* 2011; Jain 2012). Due to the rapid angiogenesis in cancerous tissues an irregular blood vessel arrangement resulted in comparison to the structured vasculature of normal tissues (Morikawa *et al.* 2002; Campbell 2006). Additionally the permeability of the tumour vasculature (the gap size in the tumour vessel wall is remarkably higher than the healthy tissues blood vessels) and the rate of endothelial cell growth is higher than in the healthy tissues (Yuan *et al.* 1995).

Furthermore, retention of accumulated nanoparticles within the tumour tissues was observed because of the absence of a lymphatic system which is normally present for drainage of macromolecules in normal tissues (Peer *et al.* 2007).

As a result, the EPR effect provides a passive way for nanosystem accumulation and retention permitting potential effective anticancer therapy with minimum drug toxicity (Bae *et al.* 2011).

1.3.3 Hybrid nanoparticles

Combining different materials into a single system makes it a hybrid system and when this system is nano sized, then these are termed hybrid nanoparticles. Hybrid nanoparticles display a dual or a core/shell nanostructure which combines different physicochemical properties and have great potential in the area of biomedicines. They can be functionalised by different reactive groups or charges

on the surface with great stability and compatibility (Leung *et al*. 2012). Several hybrid nanoparticles have emerged that are directed towards tackling the problems associated with tumour diagnosis and treatments, including cancer imaging and targeting (Sailor & Park 2012). Hybrid nanoparticles generated by joining both diagnostic and therapeutic functions of nanoparticles in one system are known as "theranostic" systems. Theranostics offers the potential monitoring of the biodistribution *in vivo* and also tracking the fate of therapeutic nanoparticles. Theranostics may also provide guided delivery of nanotheraputics payload and hence reduce the accompanying side effects of conventional nanodevices (such as affecting healthy tissues by cytotoxic agents or hyperthermia induced by external stimuli). Furthermore, theranostics may provide potential monitoring of the treatment efficacy by tracking the progress of the disease status (Kim *et al*. 2006; Kim *et al.* 2008; Sailor & Park 2012).

1.3.3.1.1 Hybrid iron oxide core gold shell nanoparticles (HNPs)

Both iron oxide and gold nanoparticles are prominent in the field of advanced nanoparticles. Their unique physicochemical character is the main reason behind the thorough investigation of them and hence their use in a wide range of applications (such as magnetic fluids, catalysis and bio-separation (magnetic nanoparticles) and cellular optical imaging, hyperthermia, and sensitive bio-detection for DNA (gold nanoparticles)) (Leung *et al. 2012)*.

The biomedical applications of magnetic iron oxide nanoparticles include targeted therapy, drug delivery, enhanced resolution contrast agents for MRI, hyperthermia,

early detection of inflammatory, cancer, diabetes, and atherosclerosis (Patra et al. 2008; V. V Mody et al. 2010) All these biomedical applications rely on the high magnetisation values of the nanoparticles so as to provide high-resolution MR images (V. V Mody et al. 2010).

Other advantages of iron oxide nanoparticles in biomedicine are their ability to be fabricated easily into different sizes and shapes, and also their ability to be influenced by an external magnetic field to produce local hyperthermia (Pankhurst *et al*. 2003).

Iron oxide nanoparticles intrinsic magnetic character may cause the particles to gather in clusters resulting in a large size nanoparticles and hence long term instability of the biomedical system. Furthermore cell toxicity may result from free radical production from degradation of iron oxide into iron in physiological environments. Many efforts aiming to tackle such problems by surface coating of the nanoparticles by organic macromolecules such as polyacrylic acid, dextran and poly(ethyleneimine) (PEI) or coatings such as silica, carbon or precious metals like gold (Thorek *et al.* 2006; Mahmoudi *et al.* 2009; Mody *et al.* 2010. ; Hoskins *et al.* 2012; Leung *et al.* 2012).

Gold nanoparticles or colloidal gold is a suspension of nano-sized gold particles. Colloidal gold nanospheres are especially promising because of their simple and fast preparation and ease of bioconjugation. Gold spherical nanoparticles have a direct relation between their size and their light absorption/scattering character. Michael Faraday, in the 1850s, was the first to describe the difference in properties

between colloidal and bulk gold as shown in Figure 14 where the colloidal gold solution (<100 nm) is an intense red colour solution while the larger particles solution have a dirty yellowish colour. The unique interactions of gold nanoparticles with light are termed the localized surface plasmon resonance (LSPR). LSPR is the oscillation of the free electrons of the metal in response to the oscillating electromagnetic field of the light, This process is resonant at a specific frequency of the light. After absorption, the surface plasmon decays radiatively resulting in light scattering or non-radiatively by converting the absorbed light into heat. Furthermore the LSPR effect is also dependent on the shape of the gold nanoparticles (Jin *et al*. 2010; V. V Mody *et al*. 2010).
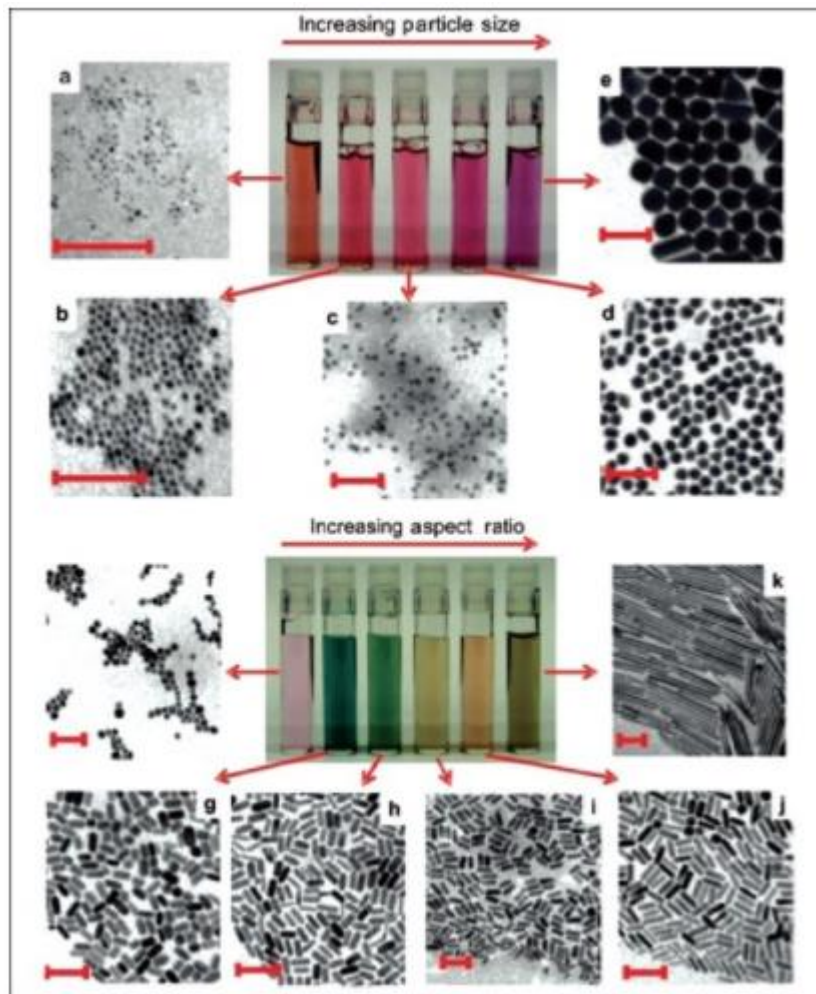
Figure 14: TEM images of gold nanospheres (upper panels) and gold nanorods (lower panels) as a function of increasing dimensions. (all scale bars 100 nm) (V. Mody *et al.* 2010)

By using both iron oxide and gold within a single drug delivery vehicle, a multifaceted system can be developed which exploits the surface chemistry of the gold whilst retaining the magnetic character of the iron oxide, allowing for biologically compatible drug delivery and imaging (Jin *et al.* 2010). This leads to a rigid nanoparticle structure which eliminates the potential of degradation of the iron oxide core and, hence, generation of toxic free radicals, thus giving an overall system, that is much more biocompatible.

Various structures and sizes of HNPs can be obtained by utilising different synthetic methods. The HNPs structure can be defined in general into two main categories including monodispersed layers and aggregates particles, monodispersed layer of particles could involve the fabrication of core/shell, dumbbell shape and shell/core/shell particle while aggregates type of HNPs involve the mosaic assembly of particle component within a defined matrix (Wu *et al.* 2008; Yu *et al.* 2008; Leung *et al.* 2012).

Core/shell nanostructure is a single core nanoparticles totally covered with a shell. In comparison to the core/satellite structure (a single core with many smaller nanoparticles attached to the surface of the core to form a star like shape hybrid nanoparticles) the surface is entirely covered by the shell, omitting the properties of the core material. Additionally, a low surface area to volume ratio would be obtained, in contrast to the core/satellite structure (Leung *et al.* 2012).

1.3.4 Theranostic Application of HNPs

The term "theranostic" is applied to any system which possesses the ability of both diagnostic and therapeutic functions. Several potential applications of HNP nanosystems as theranostics have been hypothesised and tested by many researchers (Leung *et al.* 2012). The following list of applications have been chosen to emphasise the importance of HNPs in relation to work contained in this thesis.

1.3.5 Magnetic resonance imaging (MRI)

MR imaging is a non-invasive imaging techniques widely used in human clinical diagnostic practice. MRI techniques are based on hydrogen nuclei properties of alignment under a powerful applied magnetic field (Sun *et al.* 2008).

Differentiation of tissues by MRI can be enhanced by contrast agents. Iron oxide magnetic nanoparticles have the ability to act as a powerful contrast agent by shortening the relaxation parameters of water by resulting the magnetic field (Sun *et al.* 2008).

Gold iron oxide hybrid nanoparticles theranostic properties involving MRI are affected by the nanosystem structure. In the case of the core/shell structure (HNPs) the nanosystem displays a relatively lower magnetic response in contrast to other structures of the hybrid system, which is mainly due to the effect of the gold shell that covers the iron oxide and hence, lowers the magnetic effect of the particles. Furthermore, MR response of HNPs is directly proportional to the nature of the iron oxide core and size (large solid iron oxide cores have more MR response than the small porous particles) (Janib *et al.* 2010; Leung *et al.* 2012).

1.3.6 Remotely induced hyperthermia

Heat induced cell death can be utilised as a therapeutic means to manage the tumour. Cell death occurs at a temperature above 42℃ (more specifically between 41 - 47℃ apoptosis starts while necrosis happens at 50℃) (Cherukuri *et al.* 2010).

Hyperthermia can be generated by using radio-frequency, microwave and laser which involve the introduction of a probe into the body region.(Cherukuri *et al.* 2010).

Hyperthermia generated by hybrid iron oxide-gold nanoparticles is classified according to the way by which heat is generated into magnetic induced hyperthermia (for iron oxide part of the nanosystem) and photo induced hyperthermia (for the gold part of the nanosystem).

HNPs are supposed to induce individual photo induced hyperthermia because of the utilisation of the magnetic properties of the nanosystem for MRI imaging.

Application of a near infra-red (NIR) laser can cause the selective hyperthermia of the gold surface. The time and power of the NIR laser's irradiation of the HNPs hybrid system are usually similar to the irradiation of the gold nanoparticles alone. However, the gold nanoparticle criteria have a great effect on the photo induced hyperthermia (hyperthermia requires the gold nanoparticles to be either aggregated in clusters or being in specific shape (nanorod and nanoshell)) (Minelli *et al.* 2010; Leung *et al.* 2012). While in the case of the HNPs hybrid system, gold already absorbs in the NIR region, so hyperthermia can be achieved in its original form (Leung *et al.* 2012).

1.3.7 Chemotherapeutic drug delivery

A study by Xu *et al.* 2009, where cisplatin (an anti-cancer drug) had been attached to the gold surface of a dumbbell shape gold-iron oxide nanosystem and the whole nanocomposite guided to the site of action by means of Herceptin® (HER2 antibody) attached to the surface of an iron oxide part of the nanosystem (Figure 15), showed the advantages of using tow functional ligands within one system without interference between their actions. The study showed the selective targeting of SKBR3 cells and also the *in vitro* release profile of the drug at the physiological environments. Finally the improvement of therapeutic effect of the system was compared to the naked drug (Xu *et al.* 2009).
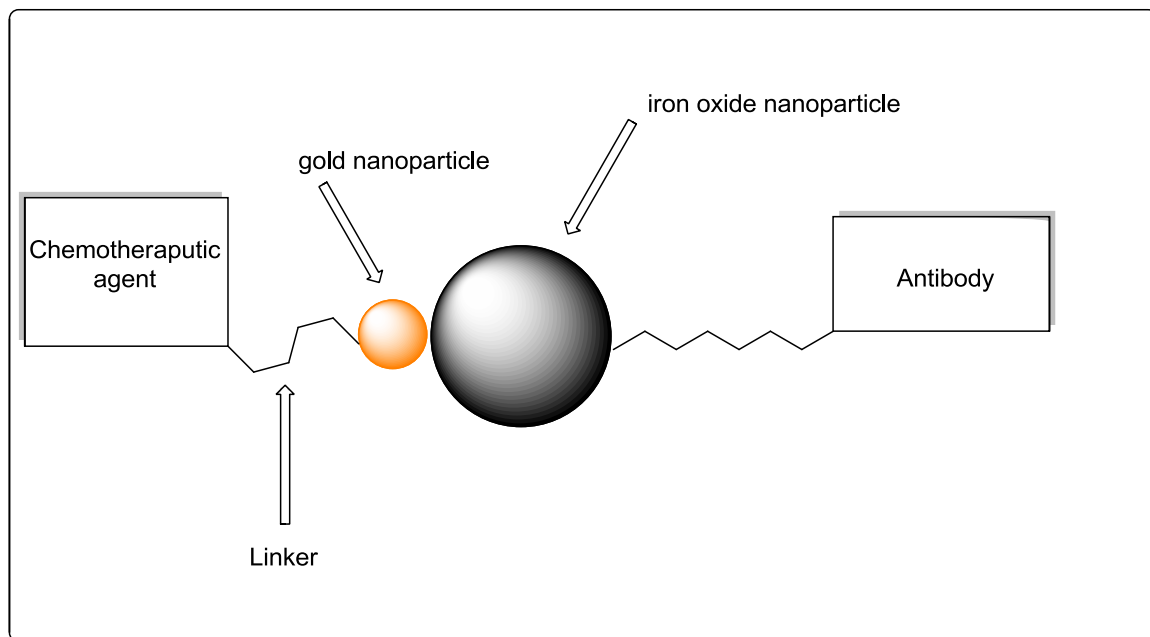
Figure 15: graphical representation of drug delivery and the cell targeting of gold-iron oxide dumbbell shape nanosystem

In addition a study whereby doxorubicin was successfully loaded onto gold-coated iron oxide nanoparticles (Au-Fe$_3$O$_4$ nanoparticles) saw the same retention of magnetism and a sustained release of the drug (Kayal & Ramanujan 2010). Recent literature has shown the maghemite form of iron oxide preferentially binds gold compared with the magnetite form and is a more stable and biocompatible form of iron oxide. The presence of the gold shell on the magnetic core makes it possible to functionalise the nanoparticles with thiolated molecules by exploiting gold-sulfur chemistry. In particular, it facilitates the attachment of biological molecules with inherent self-assembly properties onto the surface of nanoparticles. This opens up new ways for assembling magnetic nanoparticles

rationally into well-organised and functional complexes through the lock and key functionality provided by the biological molecules on the surface (Robinson *et al.* 2010).

1.4 Aim

The theranostic potential of iron oxide core gold shell hybrid nanoparticles (HNPs) together with the potential advantages of bioavailability, chemical stability and surface plasmon resonance properties of gold nanoparticles in addition to the loading ability of gold surfaces provides possibilities for novel drug formulation for treating pancreatic cancer.

The first aim of this project involves the design and synthesis of a small library of bisnaphthalimide base compounds characterised by having twenty atoms in their linker chain and bearing different number of positively charged atoms (nitrogen atoms), as well as synthesising a bisnaphthalimide derivative with a sulfide functionality in the linker chain. These compounds are then used within the nanopharmaceutical group to test the electrostatic interaction and hence loading and release profiles of these compounds onto and from the gold surface of the HNPs.

The second aim is to synthesise mutual prodrugs of gemcitabine with an ability to bind actively to the surface of the HNPs and test this ability by preparing and characterising the HNPs, and testing the loading and release profile of the prodrug.

The third aim is the biological investigations of the prodrugs of gemcitabine, the prodrug-HNPs formulation and comparing the resulting effects against a pancreatic cancer cell line with the effects of gemcitabine alone.

CHAPTER 2: SYNTHESIS AND CHARACTERISATION OF BISNAPHTHALIMIDE DRUGS

2.1 Background

In order to test the hypothesis that hybrid iron oxide core gold shell nanoparticles (HNPs) can carry compounds possessing multiple positively charged residues as effectively as compounds which bear thiol or sulphide functionalities, a series of compounds was proposed, synthesised and screened against pancreatic cancer cell lines. Some of these compounds are known to be effective as anticancer agents (Lin & Pavlov 2000; Barron et al. 2010) and others were novel compounds. All of the compounds were derived from the basic symmetrical bisnaphthalimide structure characterised by having identical naphthalimide terminal residues and the same linker chain length of 20 atoms. However, the compounds differed in the number of positively charged atoms within the linker chain and one of them having disulfide residues included within the linker chain.

2.1.1 Bisnaphthalimidopropyl polyamines

In the 2000s Lin and Pavlov (2000) designed and synthesised a series of novel bisnaphthalimidopropyl polyamine (BNIPP) compounds, by using naturally occurring polyamines as linker chains between two identical bisnaphthalimide residues (Figure 16).
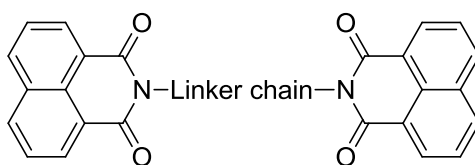
Figure 16: General structure of bisnaphthalimidopropyl polyamine (BNIPP) compounds

Lin and Pavlov (2000) suggested that increasing the number of positively charged heteroatoms within the linker chain, would increase their water solubility and hence their overall cytotoxic activity (Lin & Pavlov, 2000). The BNIPP derivatives introduced by Lin and Pavlov consisted of two naphthalimidopropyl residues with connected linkers derived from naturally occurring polyamines: Putrescine **4**, spermidine **5**, spermine **6** and oxaputrescine **18** (Figure 17).
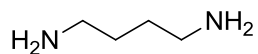
putrescine
4
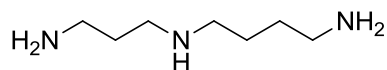
spermidine
5
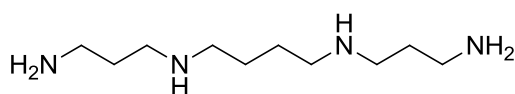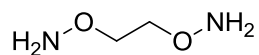
spermine
6

oxaputrescine
18

Figure 17: structures of naturally occurring polyamines: Putrescine **4**, spermidine **5**, spermine **6** and oxaputrescine **18**

The BNIPP derivatives prepared by Lin and Pavlov (2000) from the naturally occurring polyamines were summarised in (Figure 18) (Lin & Pavlov 2000).
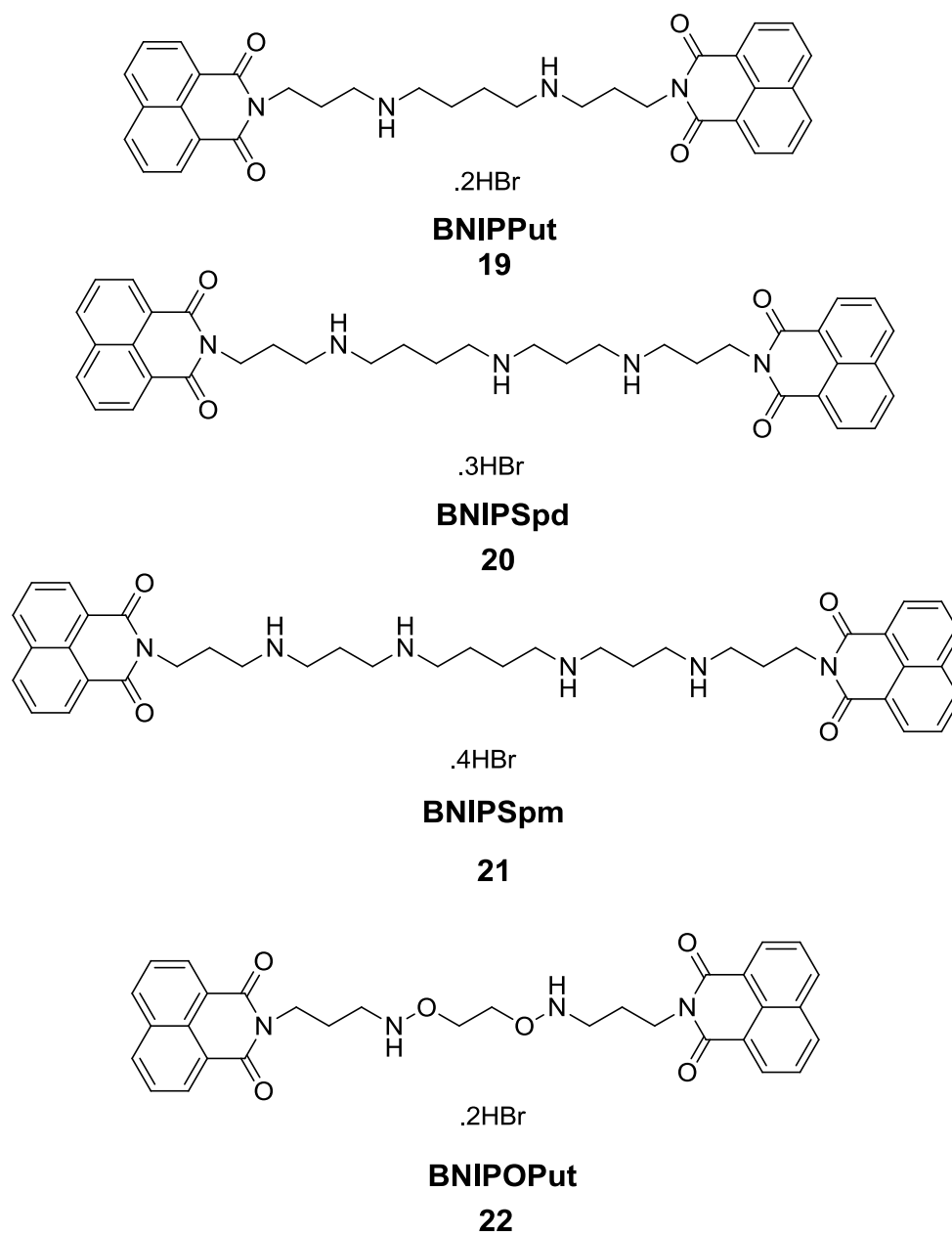
Figure 18: Structures of BNIPP derivatives prepared from the naturally occurring polyamines were bis(naphthalimidopropyl)putrescine (BNIPPut) **19**, bis(naphthalimidopropyl)spermidine (BNIPSpd) **20**, bis(naphthalimidopropyl)spermine (BNIPSpm) **21** and bisnaphthalimidopropyl)oxaputrescine (BNIPOPut) **22**

The cytotoxicity of the BNIPP derivatives was first studied using the National Cancer Institute (NCI) screen who examined the BNIPP compounds against a number of human cancer cell lines (breast, colon, CNS, lung, leukaemia, renal, ovarian, and prostate cancer). The study revealed that the cytotoxic activity of the BNIPP derivatives was in the order BNIPPut **19** > BNIPSpd **20** > BNIPSpm **21** > BNIPOPut **22** (Lin & Pavlov 2000).

In contrast, the aqueous solubility of the compounds was greatly affected by the number of heteroatoms in the linker chain: compounds with more positively charged heteroatoms (Nitrogen atoms) in the linker chain were more soluble in water (Lin & Pavlov 2000).

A similar finding was obtained by Pavlov *et al* (2001) who examined the cytotoxic effect of BNIPSpd **20**, BNIPSpm **21** and BNIPOSpm **23** (Figure 18 and Figure 19) against the human breast cancer MCF-7 cell line: the study showed growth inhibition of the cell line by the compounds was affected in the same order: the cytotoxicity went down with increasing either the length of linking chain or the number of positively charged heteroatoms in the linker (Pavlov *et al.* 2001; Lin *et al.* 2003; Barron 2010).

.4HBr
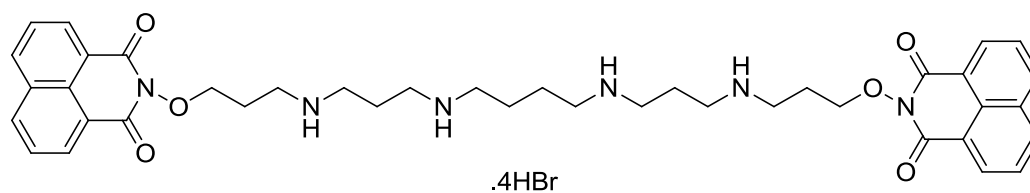
BNIPOSpm

23

Figure 19: Chemical structure of bis(naphthalimidopropyl)oxaspermine (BNIPOSpm) **23**

Another study predicted that introducing an oxygen atom into the linker directly attached to the nitrogen of the naphthalimide ring would result in enhancing the solubility without affecting the cytotoxicity of the original compounds (Dance *et al* 2005). In this study, they synthesised three compounds BNIPOPut **24**, BNIPOSpd **25** and BNIPOSpm **23** (Figure 19 and Figure 20) and compared their aqueous solubility and cytotoxicity to that of the parent compounds BNIPSpd **20** and BNIPSpm **21**. The results showed an increase in the aqueous solubility but a decrease in the anticancer effect against the MCF-7 cancer cell line (Dance *et al.* 2005).

All the studies repeatedly confirmed that the cytotoxic effect of the BNIPP compounds is greatly dependent on the structure of the polyamine linker (Lin & Pavlov 2000; Pavlov *et al.* 2001; Lin *et al.* 2003; Dance *et al.* 2005; Barron *et al.* 2010).

BNIPOPut

24

BNIPOSpd

25
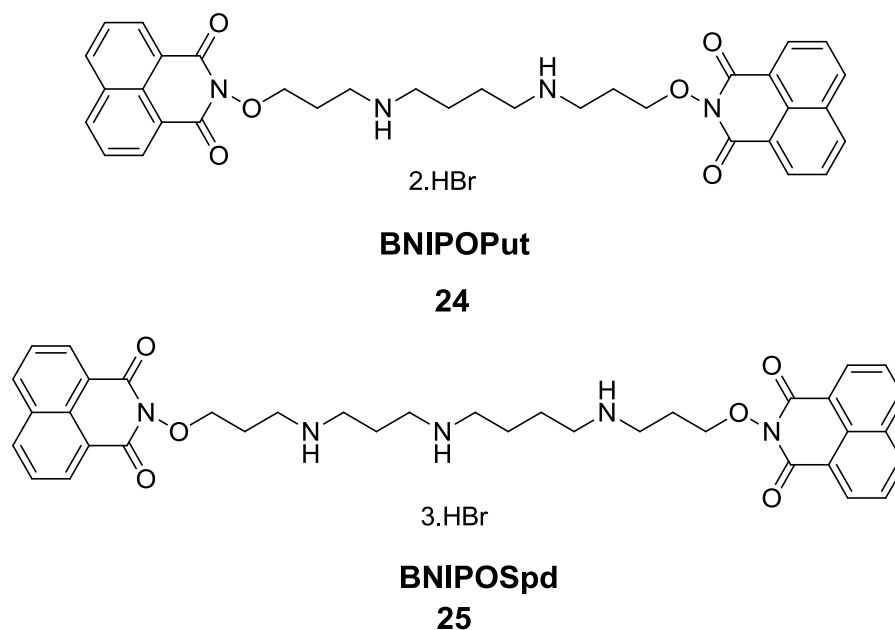
Figure 20: Chemical structure of bis(naphthalimideoxapropyl)putrescine (BNIPOPut) **24** and bis(naphthalimidooxapropyl)spermidine (BNIPOSpm) **25**

Further analogues of BNIPP compounds were synthesised (Figure 21) by modifying the length and number of heteroatoms in the linker chain, and their cytotoxicity against the human colon cancer cell line (Caco-2) and the parasite *Leishmania infantum* were examined using the MTT assay. The results showed that compounds with the same linker-chain length but one nitrogen atom less can have similar cytotoxic effects (Oliveira *et al.* 2007; Barron *et al.* 2010).

Other investigations into analogues of BNIPP compounds focused on introducing cyclic or heterocyclic moieties into the linker chain. These studies also screened the compounds against a number of human cancer cell lines (Filosa *et al.* 2009; Barron *et al.* 2010).
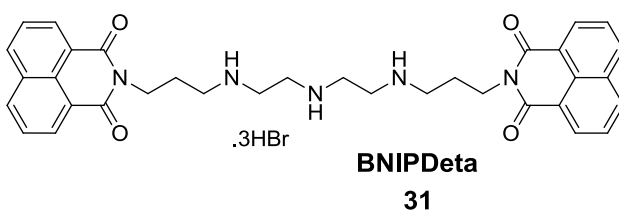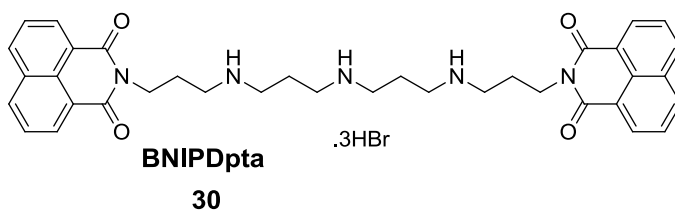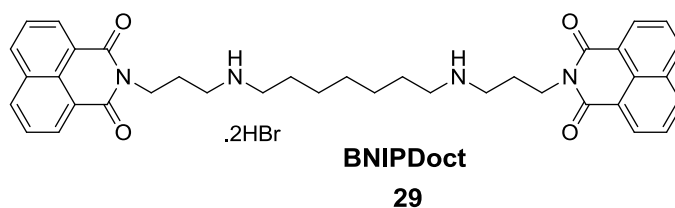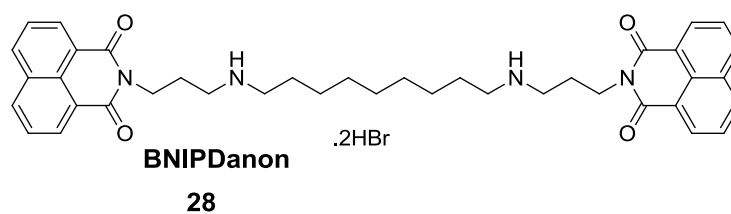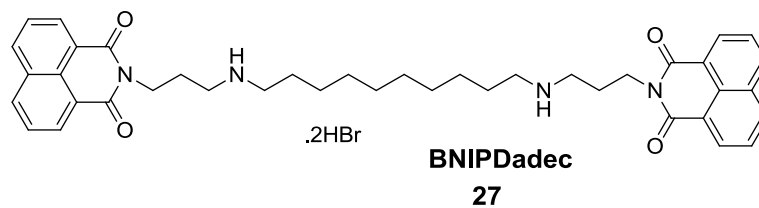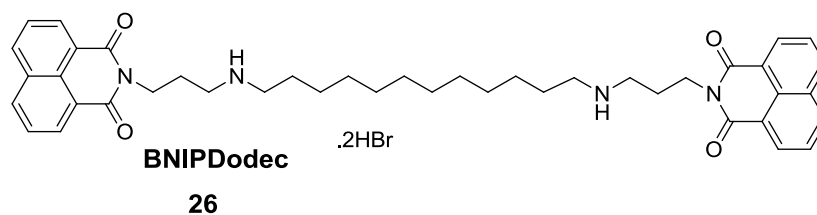
Figure 21: Chemical structure of BNIPdiaminododecan (BNIPDodec) **26**, BNIPdiaminodecan (BNIPDadec) **27**, BNIPdiaminononan (BNIPDanon) **28**, BNIPdiaminooctan (BNIPDaoct) **29**, BNIPdipropyltriamine (BNIPDpta) **30**, and BNIPdiethyltriamine (BNIPDeta) **31**

The aim of this chapter is to present results obtained from the synthesis of the group of BNIPP analogues shown in (Figure 22) which includes previously known compounds BNIPSpm **21** and BNIPDodecan **26**, and the novel compounds (BNIPDi) **32**, (BNIHexamine) **33**, and (BNIPds) **34** in order to compare their ability to associate with HNPs as drug delivery system.

BNIPSpm
21

.4HBr

BNIPDodec
26

.2HBr

BNIPDi
32

BNIHexamine
33

.6HBr
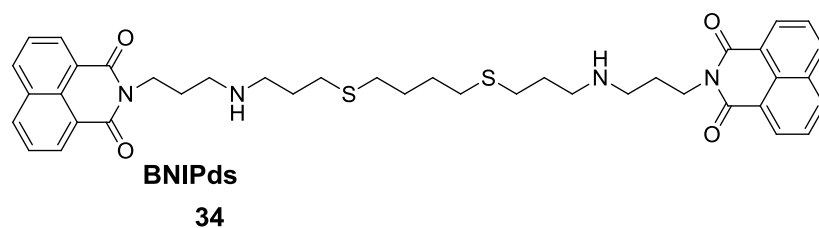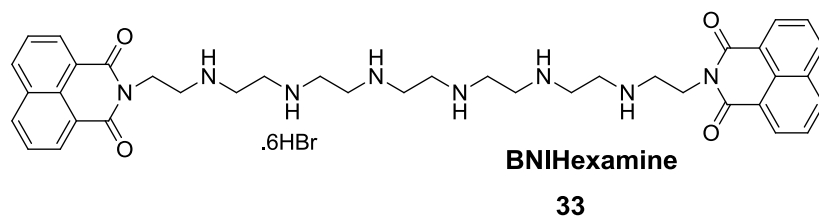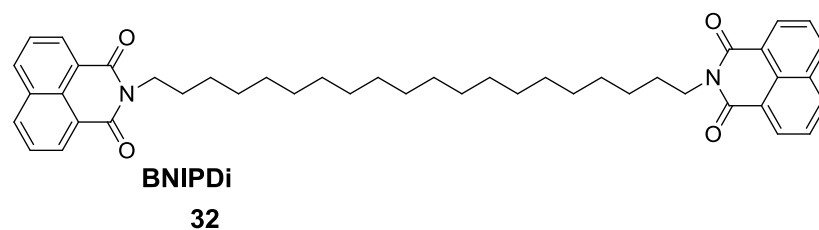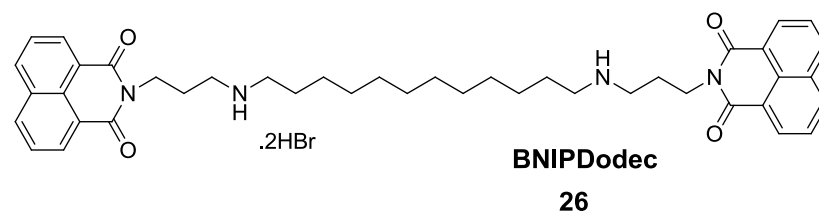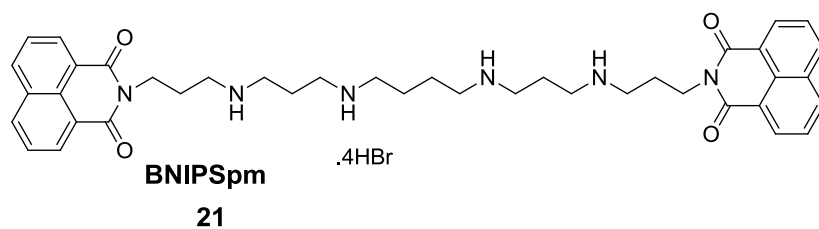
BNIPds
34

Figure 22: Chemical structure of BNIPSpm **21**, BNIPDodec **26** and proposed compounds (BNIPDi) **32**, (BNIHexamine) **33**, and (BNIPds) **34**

2.2   Attempt to synthesise bisnaphthalimido diaminoicosan (BNIPDi) 32

The synthesis of bisnaphthalimide derivatives was adopted from the successful synthesis of mitonafide **37** which is a compound with high cytotoxic activity among mononaphthalimide derivatives. The synthetic strategy described by Braña *et al.* for delivering mitonafide involve the use of equimolar amounts of both reactants (3-nitro 1,8-nphthalic anhydride **35** and *N1,N1*-dimethylethane-1,2-diamine **36**) (Scheme 1) in a one-step reaction (Braña *et al.* 1993; Braña *et al.* 1996).

The synthesis of bisnaphthalimide compounds was carried out generally by the same mechanism, which involves nucleophilic reaction of the 1,8-naphthalic anhydride with the corresponding polyamine in a 2:1 molar ratio respectively (Scheme 1) (Braña & Ramos 2001).
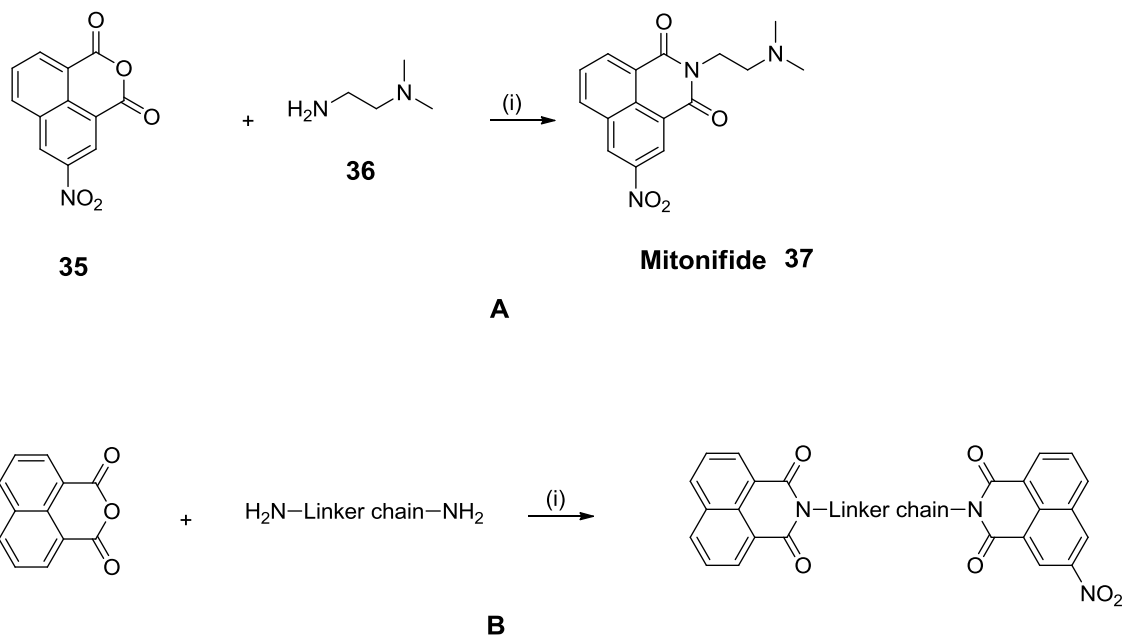
Scheme 1: Synthesis of (A) mitonifide **37** and (B) bisnaphthalimide. Reagents and conditions: (i) absolute ethanol, reflux, 12 hrs

The strategy for the synthesis of BNIPDi **32** (Scheme 2) was adapted from the method previously described for synthesis of bisnaphthalimide derivatives by Braña *et al.* (Scheme 1). The rationale behind preparing BNIPDi **32** was to make an analogue of BNIPSpm **21** without any heteroatoms in the linker chain in order to confirm that the ability of the BNIPSpm **21** to be loaded on the HNPs surface is due to the charge-charge interaction between the compound and the gold surface.

1,20-Eicosanedicarboxylic acid **38** acid was utilised as a starting material in order to synthesise the required linker chain (1,20-Eicosanediamine **41**) for the synthesis of compound **32** (Norrehed *et al.* 2013). The process of synthesis of the linker chain **41** was carried out accordingly without prior purification of the intermediate product. Furthermore, the obtained yield from the reactions was quantitative. Regarding compound **41**, the product was obtained in the final step as an off-white solid with a yield of 70%.
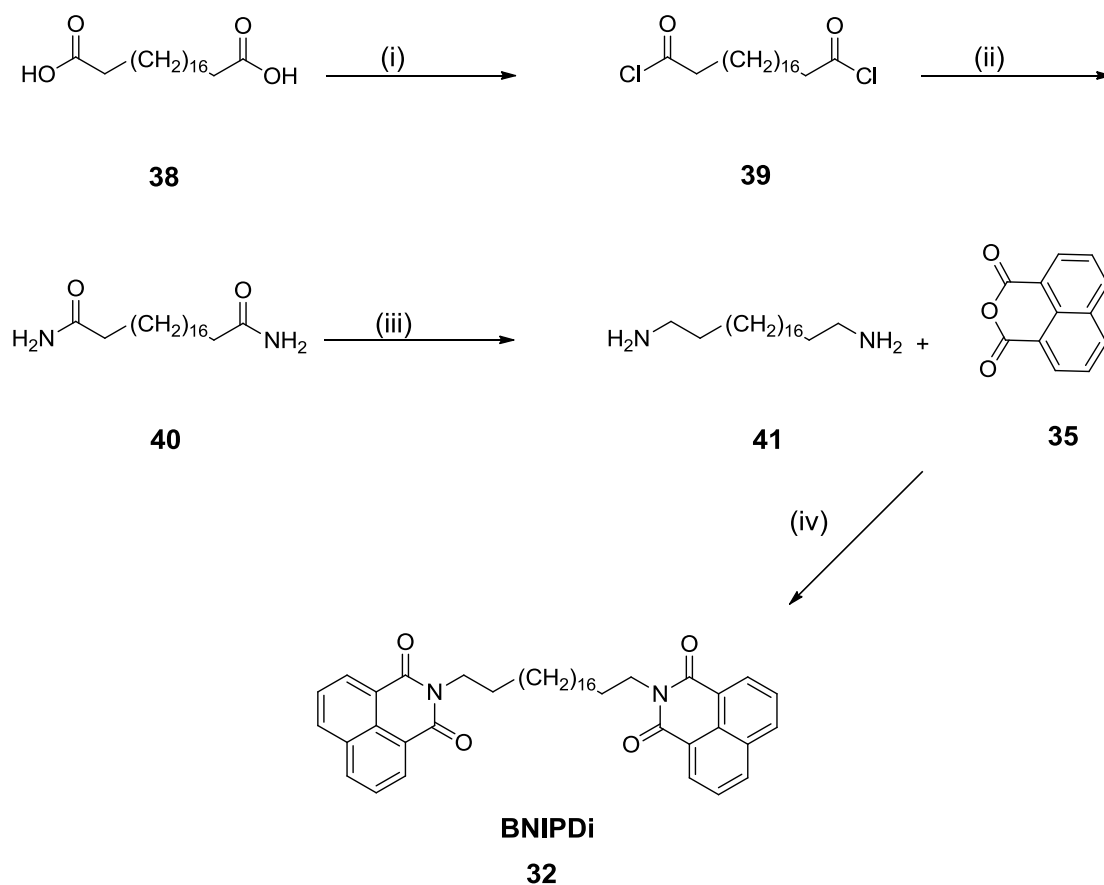
Scheme 2: Strategy for the synthesis of bis(naphthalimido)diaminoicosan (BNIPDi) **32**. Reagents and conditions: (i) thionyl chloride, reflux 18 hrs, (ii) dioxan, ammonium hydroxide solution, 4 hrs (iii) Lithium aluminum hydride, THF 12 hrs, reflux (iv), absolute ethanol, reflux, overnight

2.2.1 Synthesis of compound 39 (the acid chloride derivative of 38)

Activation of carboxylic acids by forming the corresponding acid chlorides is one of the simplest methods for activating otherwise unreactive carboxylic acids towards nucleophilic attack (Montalbetti & Falque 2005). Numerous reagents are commonly used to make the acid chloride from their parent acids, including thionyl

chloride (SOCl$_2$) **42**, phosphorus pentachloride (PCl$_5$) **43**, oxalyl chloride **45** ((COCl)$_2$), phosphorus oxychloride (POCl$_3$) **46** and phosphorus trichloride (PCl$_3$) **44** (Figure 23).

Thionyl chloride

42

Phosphorus pentachloride

43

Phosphorus trichloride

44

Oxlyl chloride

45

Phosphorus oxychloride

46
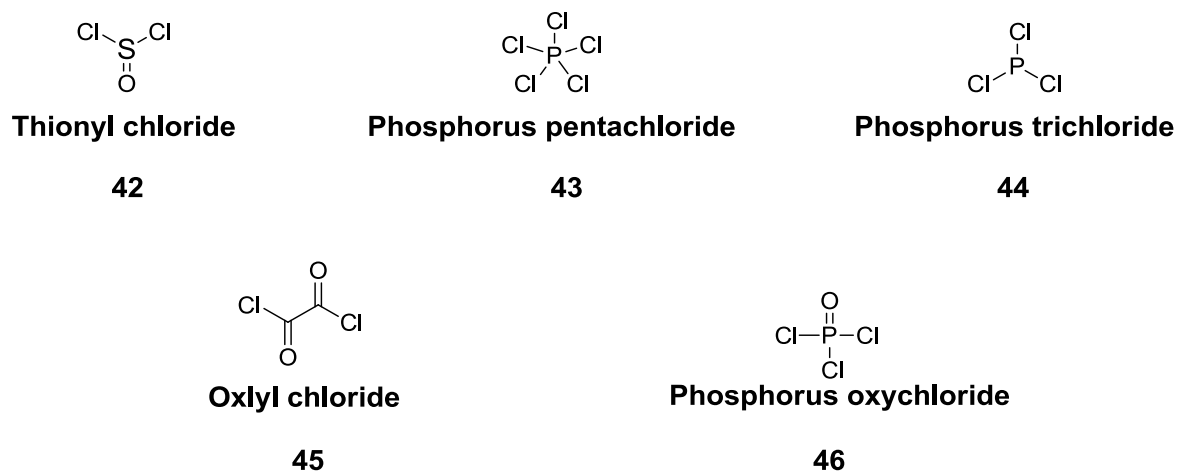
Figure 23: commonly used reagents for acid chloride formation

The general mechanism for making an acid chloride using thionyl chloride is shown in Scheme 3. The major drawback of this method of acid activation is the formation of hydrochloric acid and sulfur dioxide as by-products of the reaction, which can affect acid-sensitive compounds and the environment (Montalbetti & Falque 2005).
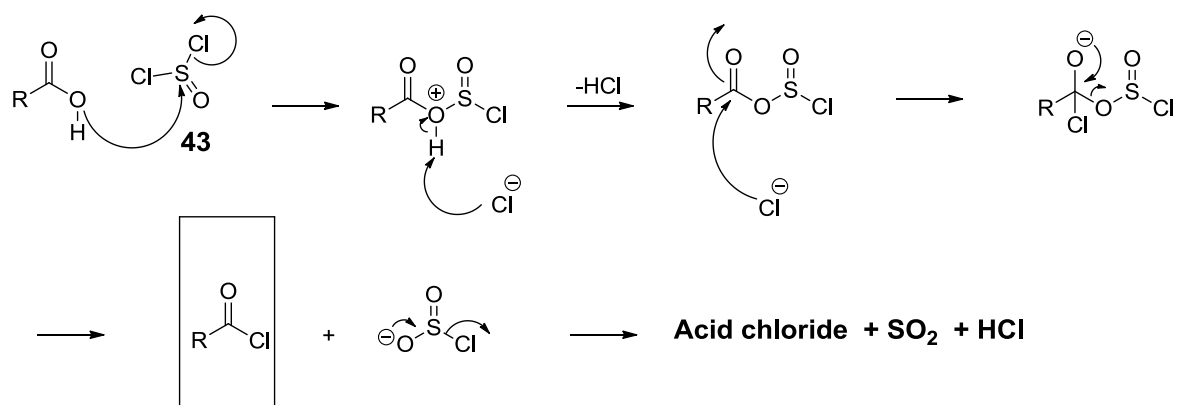
Scheme 3: Mechanism of acid chloride formation by using thionyl chloride (Montalbetti & Falque 2005)

Two molar equivalents of thionyl chloride are required to react with eicosanedicarboxylic acid **38** to give the corresponding di-acid chloride derivative **39**. In practice, an excess of thionyl chloride was used to ensure that all the acid residues had been converted to the analogous acid chloride.

2.2.2 Synthesis of 1,20-Eicosanediamide (40) towards making 1,20-Eicosanediamine (41)

Reaction of an acid chloride with an amine results in amide bond formation
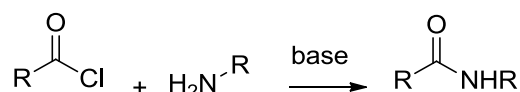
Scheme 4: General reaction of acid chloride with amines (Montalbetti & Falque 2005)

HCl is formed as a by-product of this reaction so addition of base is necessary to trap the formed acid. In the synthesis of 1,20-eicosanediamide, ammonium hydroxide acts as both base and the source of amine nitrogen. It is used in excess to overcome the formation of the acid by-product (Scheme 4).

The obtained white product (1,20-eicosanediamide **40**), was reacted with LiAlH$_4$ in dry THF at elevated temperature overnight in order to ensure complete reduction of compound **40**.

2.2.3 Synthesis of BNIPDi 32

Once the diamine linker chain had been synthesised the subsequent step was to react it with 1,8-naphthalic anhydride **35**. The mechanism of such a reaction involves intramolecular diamide bond formation facilitated by the short distance between the secondary amine and the carbonyl carbon atom. This favours the

intramolecular reaction rather than the potential for intermolecular polymerisation (Figure 24).
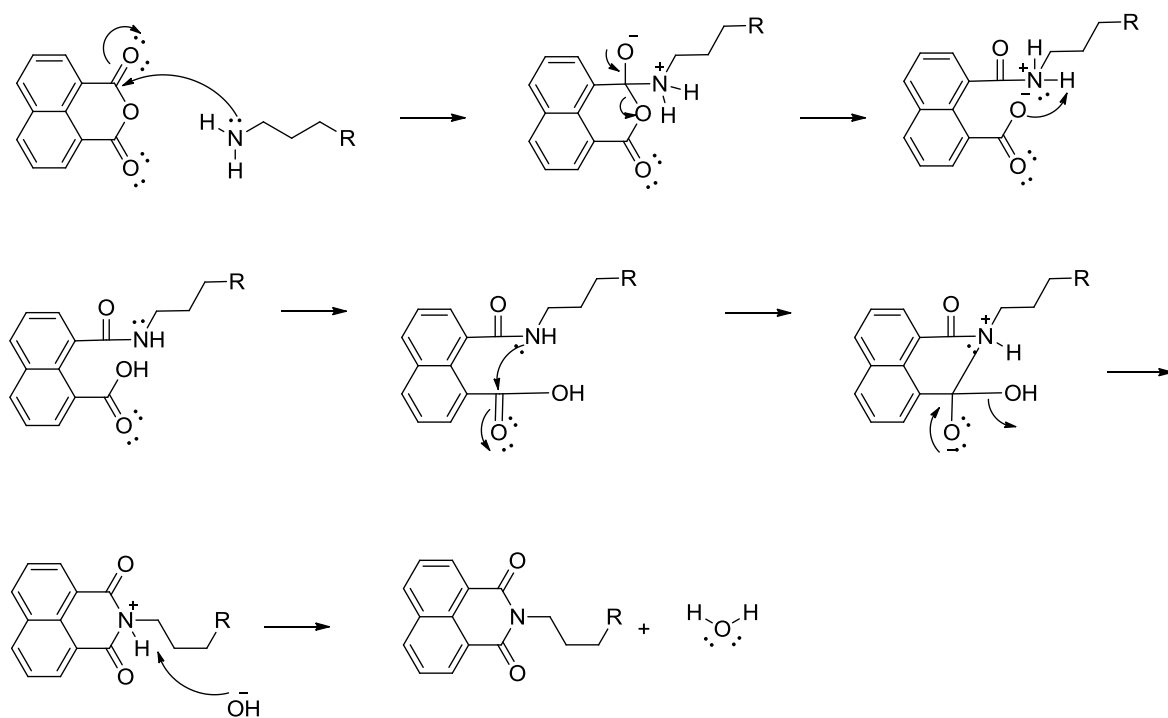
Figure 24: Mechanism of naphthalimide formation

2.3 Synthesis of BNIPSpm 21 and BNIPDodec 26

2.3.1 General method of BNIPP synthesis

The general synthesis of BNIPP derivatives (Figure 25) first appeared when Lin and Pavlov merged the strategies of synthesising bis(alkyl) polyamine derivatives (Figure 26) (Bergeron *et al*. 1988) and bisnaphthalimide derivatives (Scheme 1B) (Braña *et al*. 1993; Lin & Pavlov 2000).
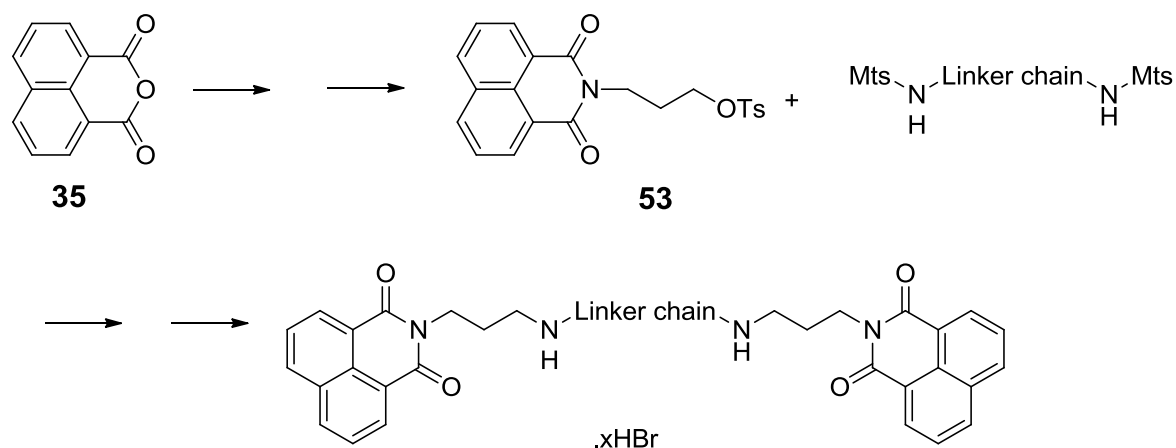
Figure 25: General synthesis of BNIPP compounds

The strategy involves *N*-alkylation of a fully mesitylated polyamine linker with *O*-tosyloxypropyl)naphthalimide **53** to yield the fully protected analogue of the final product. Deprotection using hydrobromic acid delivers the hydrobromide salt (Lin & Pavlov 2000; Pavlov *et al*. 2001; Dance *et al*. 2005; Barron *et al*. 2010).
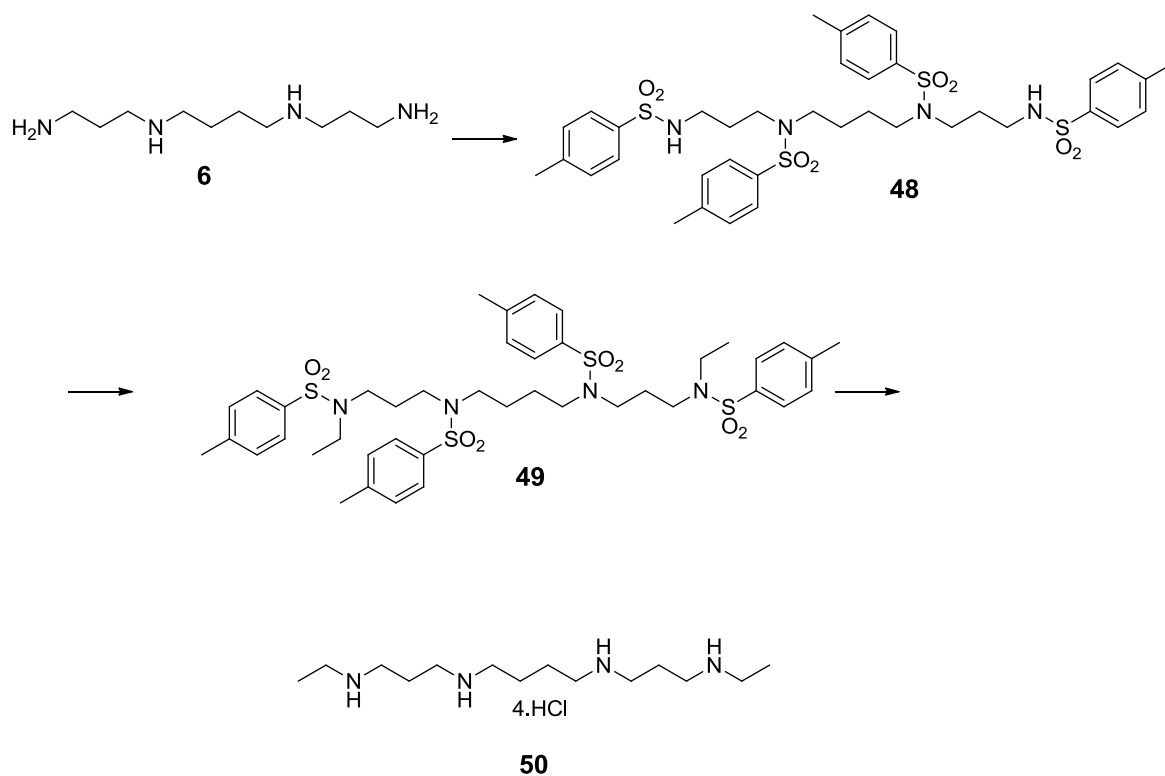
Figure 26: Synthetic scheme of a dialkyl spermine **50**

2.3.2 Synthetic strategy of BNIPSpm 21 and BNIPDodec 26

The strategy used to deliver the two compounds BNIPSpm **21** and BNIPDodec **26** was analogous to the previously published work by Lin and Pavlov (2000) and Barron *et al.* (2010).

The plan was to prepare the fully mesitylated polyamine linker (Mts Spermine **58** and Mts Diaminododecane **60**) (Scheme 7 and Scheme 8), the mutual intermediate *O*-(tosyloxypropyl)naphthalimide **53**) and couple them together in 1:2 molar ratio respectively followed by elimination of the mesitylene protecting group (Scheme 5 and Scheme 6).
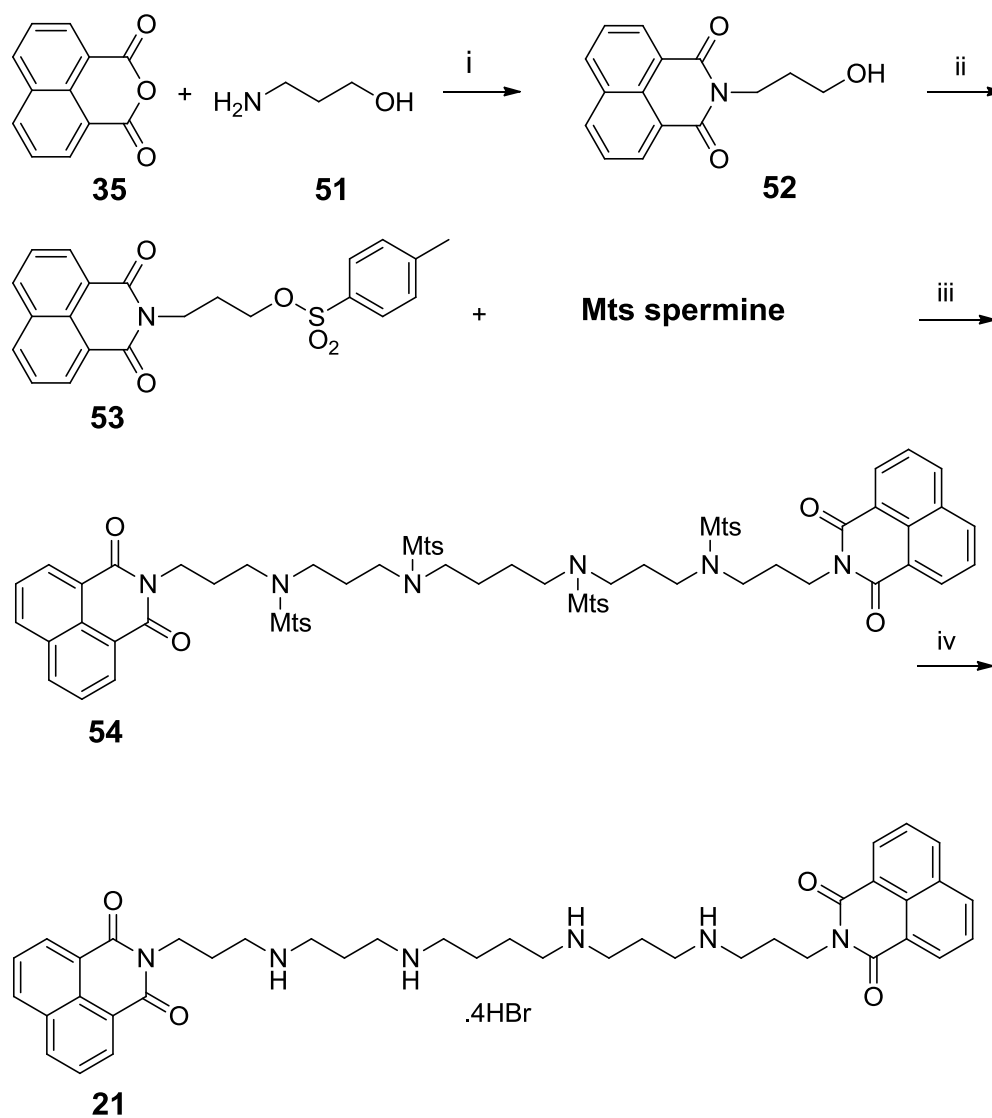
Scheme 5: Synthesis of BNIPSpm **21** reagents and conditions:(i) absolute ethanol, reflux, overnight (ii) tosyl chloride, pyridine, 12hrs (iii) CsCO$_3$, DMF. (iv) HBr/glacial aceticacid, CH$_2$Cl$_2$
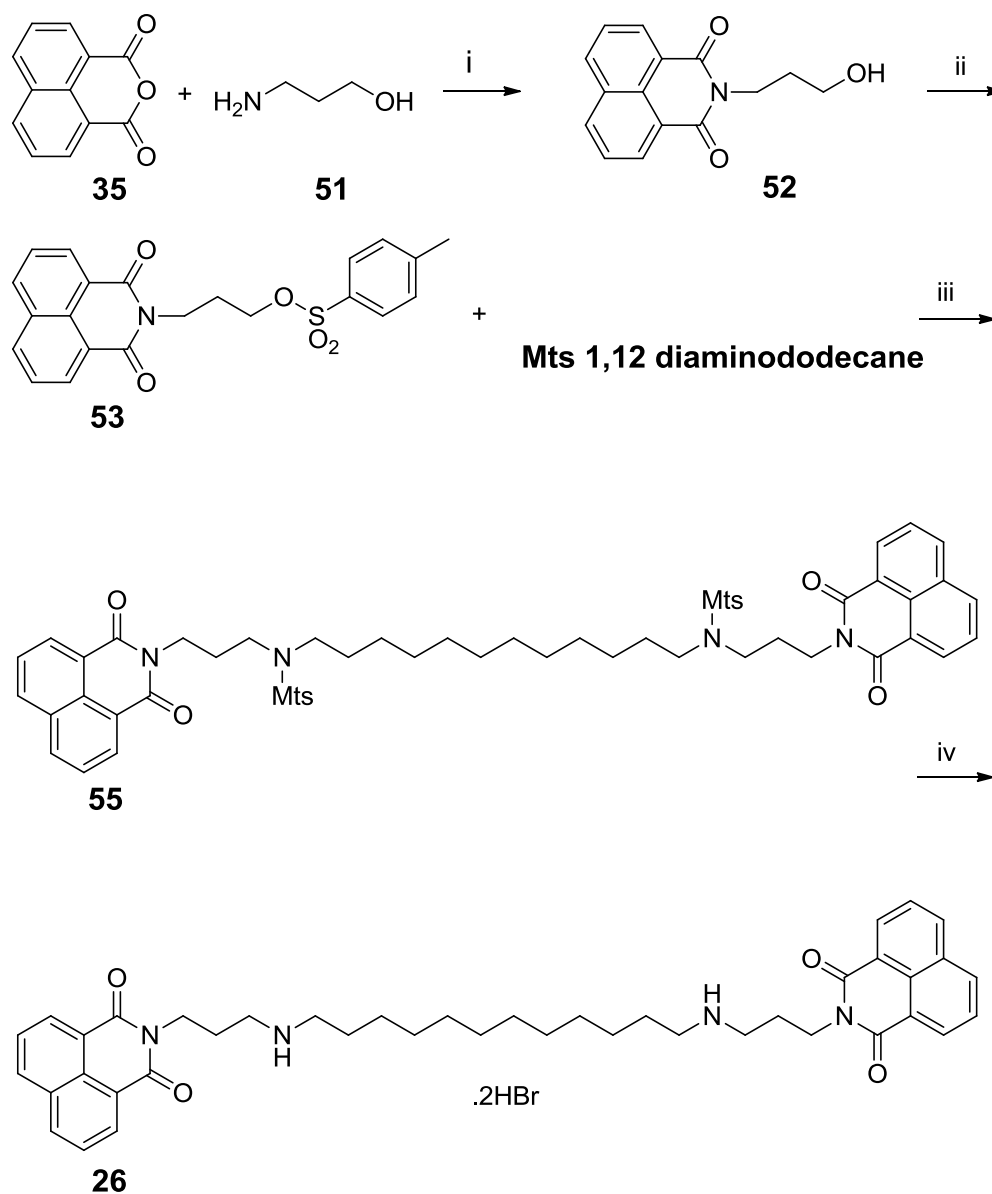
Scheme 6: Synthesis of BNIPDodec **26** reagents and conditions :(i) absolute ethanol, reflux, overnight (ii) tosyl chloride, pyridine, 12hrs (iii) CsCO$_3$, DMF. (iv) HBr/glacial aceticacid, CH$_2$Cl$_2$
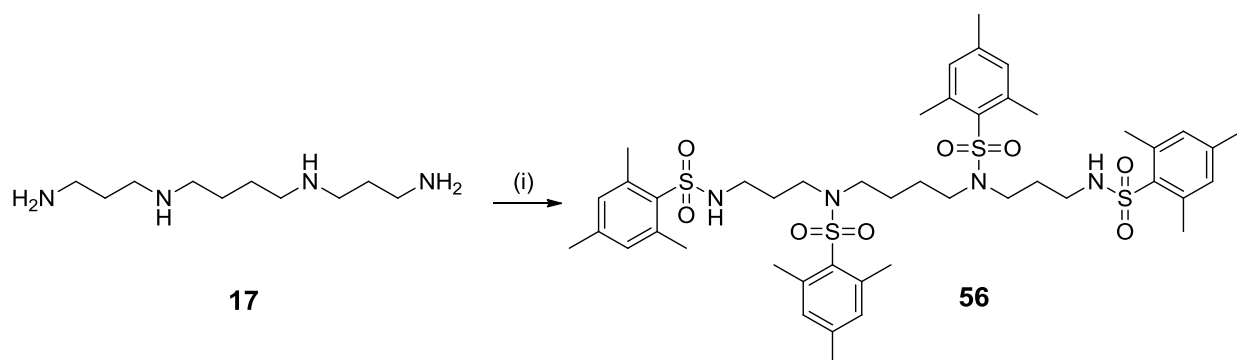
Scheme 7: Synthesis of mesitylated derivatives of spermine Reagents and conditions: (i) mesitylene chloride, pyridine, RT 12 hrs
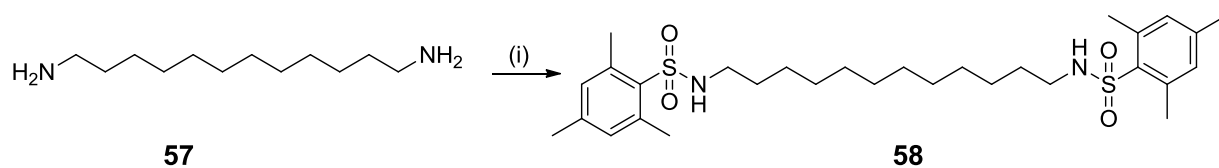
Scheme 8: Synthesis of mesitylated derivatives of diaminododecane Reagents and conditions: (i) mesitylene chloride, pyridine, RT 12 hrs

2.3.3 Synthesis of fully protected polyamines (tetra-mesitylated spermine 56 and di-mesitylated diaminododecane 58)

Spermine **7** and diaminododecane **57** were obtained from commercial sources and reacted with mesitylene sulfonyl chloride using pyridine as both a solvent and a base to trap the liberated hydrochloric acid by-product from the reaction. The reactions proceed smoothly to yield the products N^1, N^5, N^{10}, N^{14}-tetra-mesitylspermine **56**, and N^1,N^{14}-di-mesityl dodecane **58** in a yield 30% and 50% respectively after purification and recrystallisation from ethanol. Both compounds give one spot in TLC and their spectroscopic data which showed the right number of carbon atoms (in both aliphatic and aromatic region) match with the reference data provided by the original authors (Figure 27 and Figure 28), though the yields obtained were less than those reported in the literature (60% and 66%, respectively) (Lin & Pavlov 2000; Barron *et al.* 2010).
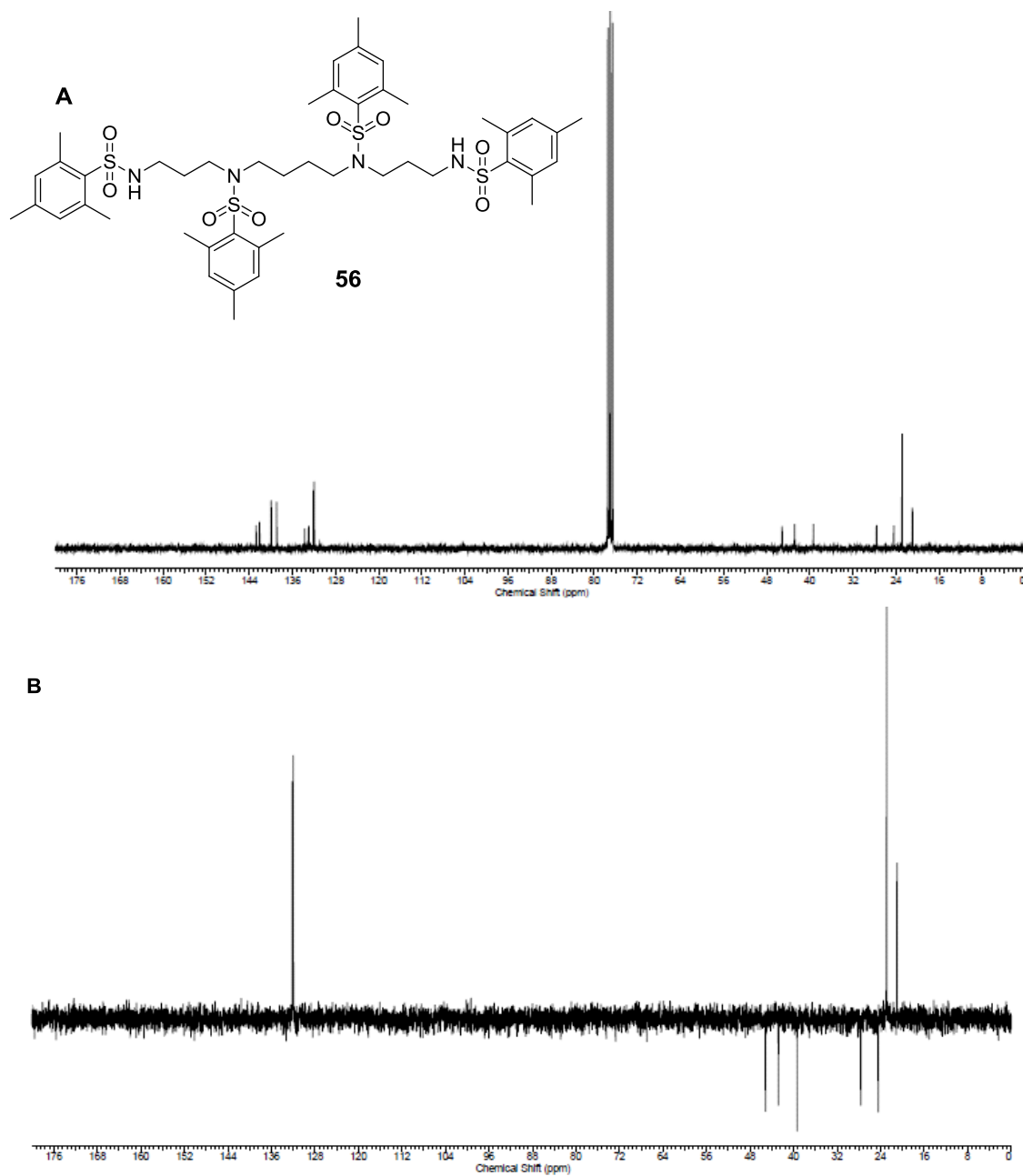
Figure 27: **A**: 13C NMR data of mesitylated spermine **56**, **B**: DEPT 135 NMR data of mesitylated spermine **56**
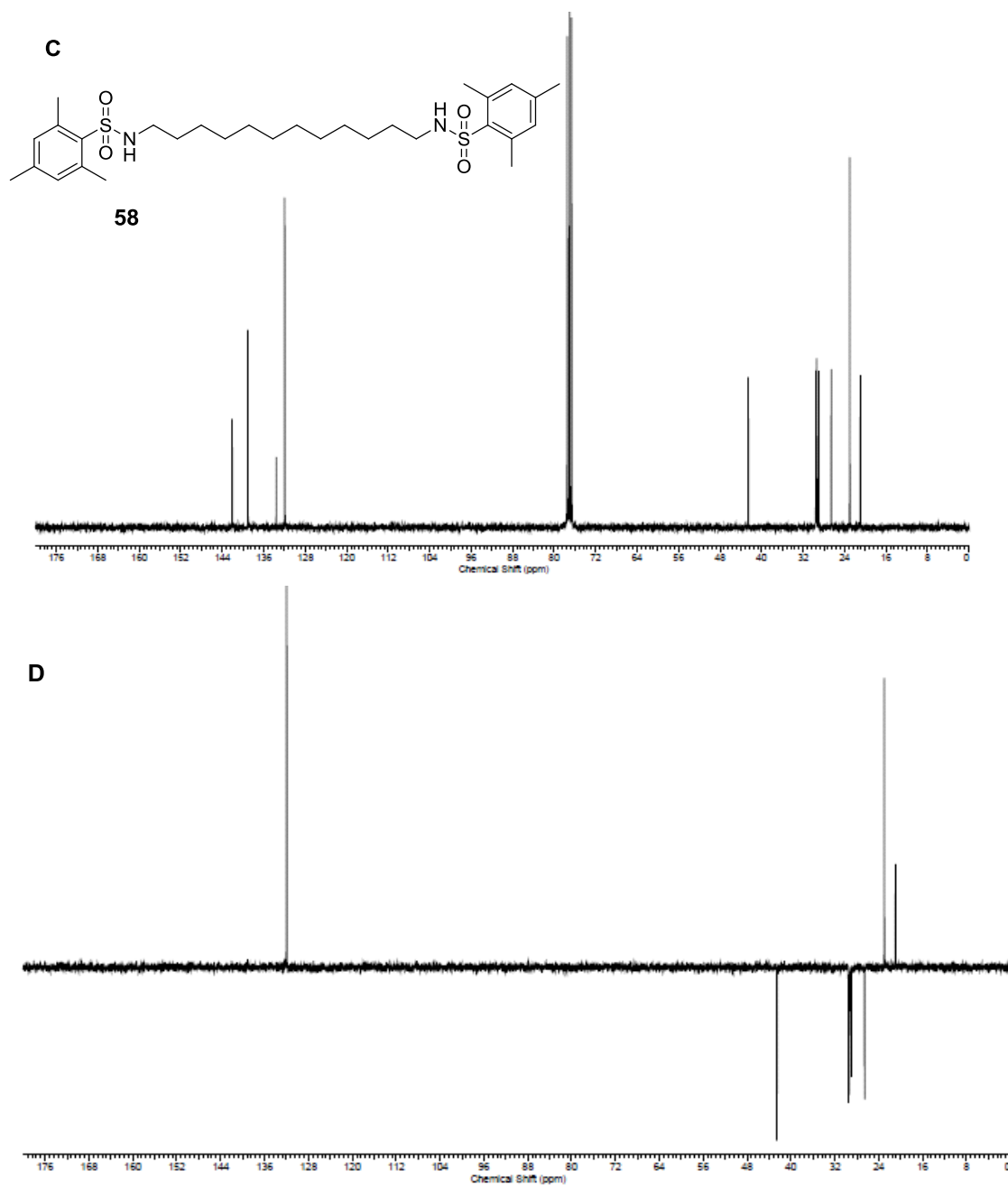
Figure 28: **C**: ^{13}C NMR data of mesitylated dodecane **58**, **D**: DEPT 135 NMR data of mesitylated dodecane

2.3.4 Synthesis of *N-(3*-hydroxypropyl) naphthalimide 52

Synthesis of the *N*-(3-hydroxypropyl) naphthalimide **52** was reported in literatures mainly by two ways both of them stated a high yield product, the difference between the two methods is the type of solvent used (absolute ethanol or DMF) and the presence of catalytic amount of DBU base in case of using DMF as a solvent. The method chosen was refluxing 1, 8 naphthalic anhydride **35** with propanol amine **51** in absolute ethanol for 12 hrs to get the product in a very good yield. The ^{1}H NMR data (Figure 29) show all the peaks at the right position (aromatic protons at 7.7-8.6, methylene protons at 2.0-4.5) which match the reference data.
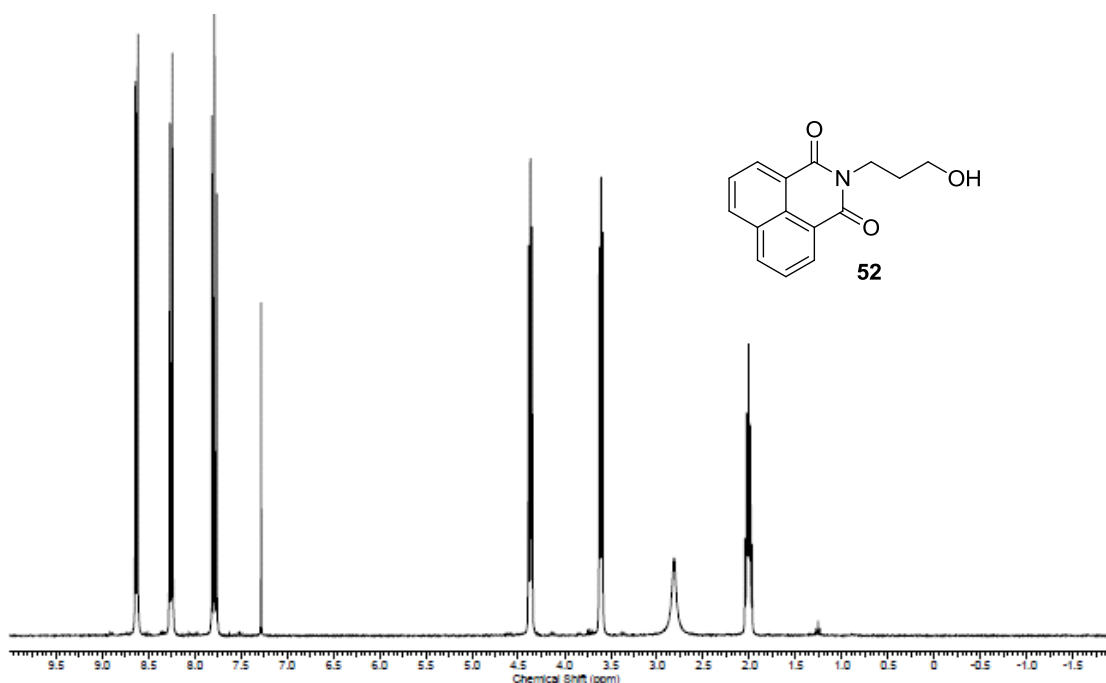
Figure 29: ^{1}H NMR spectrum of *N*-(3-hydroxypropyl) naphthalimide **52**

72

2.3.5 Synthesis of (*O*-tosyloxypropyl)naphthalimide 53

Tosylation of the hydroxyl of *N-(3*-hydroxypropyl) naphthalimide **52** activates the hydroxyl group into a leaving group which is more easily replaced by a nucleophile. However, tosylation using an equimolar amount of the reactants under the conditions employed can result in one of either two products **53** and **59**, or a mixture of the two (Figure 30), which affects the yield and makes purification difficult. To avoid this happening, a fourfold excess of *para*-toluenesulfonyl chloride can be used. (Lin & Pavlov 2000).

Figure 30: Compounds which are potentially delivered from tosylation of **52**

Tosylation was performed in pyridine using an equimolar amount of reactants at room temperature for 16 hrs and the product purified by recrystallisation from ethanol to give **53** in a yield of 40% (Lin *et al.* 2003), sufficient to proceed to the next step.

The ^{1}H NMR data showed the methyl of the tosyl group and the methylene groups at (2.2-4.5 ppm) together with the aromatic proton of both the tosyl- and naphthalene group at (6.6-8.6 ppm) (Figure 31).

Figure 31: ^{1}H NMR spectrum of tosylated **53**

2.3.6 Synthesis of compound 54 and 55

The fully protected versions of BNIPSpm **54** and BNIPDodecan **55** were obtained by *N*-alkylation of the correspondence mesitylated polyamines with *O*-tosyloxypropyl)naphthalimide **53** in 1:2 molar ratio respectively using DMF as a solvent and caesium carbonate as a base. The products were characterised by ^{13}C and DEPT-135 NMR analysis (Figure 32 and Figure 33) which show the aliphatic hydrocarbon (between 22 and 77 ppm) and aromatic hydrocarbon from mesitylene and naphthalene group (between 122 and 138). It also shows the inversion of CH$_2$- peaks and disappearance of the quaternary carbon from the mesitylene group and the amide group. All the data acquired were matched with the reference data from the literature.
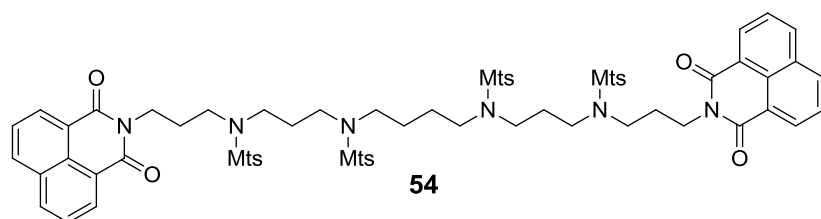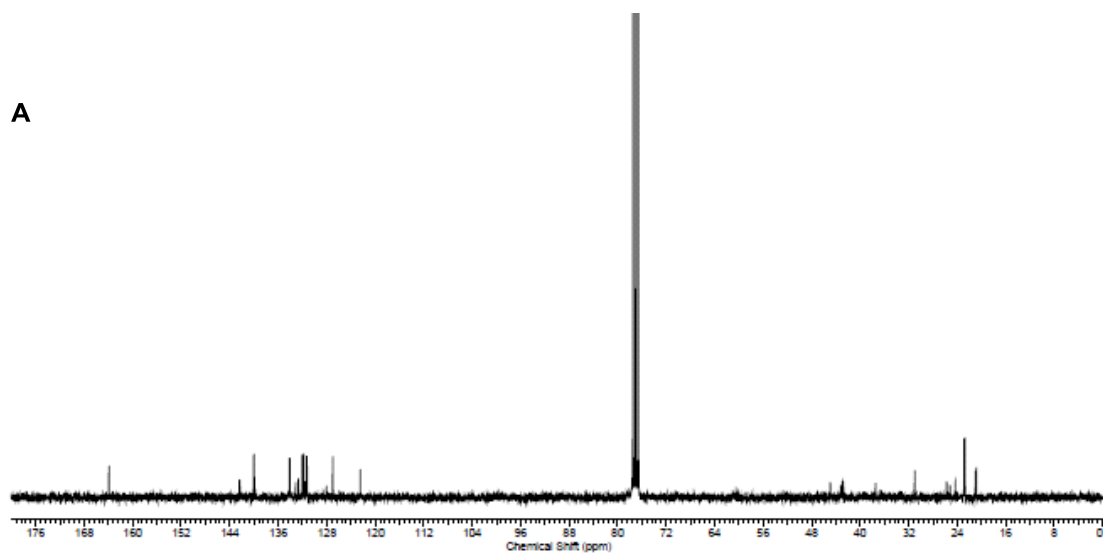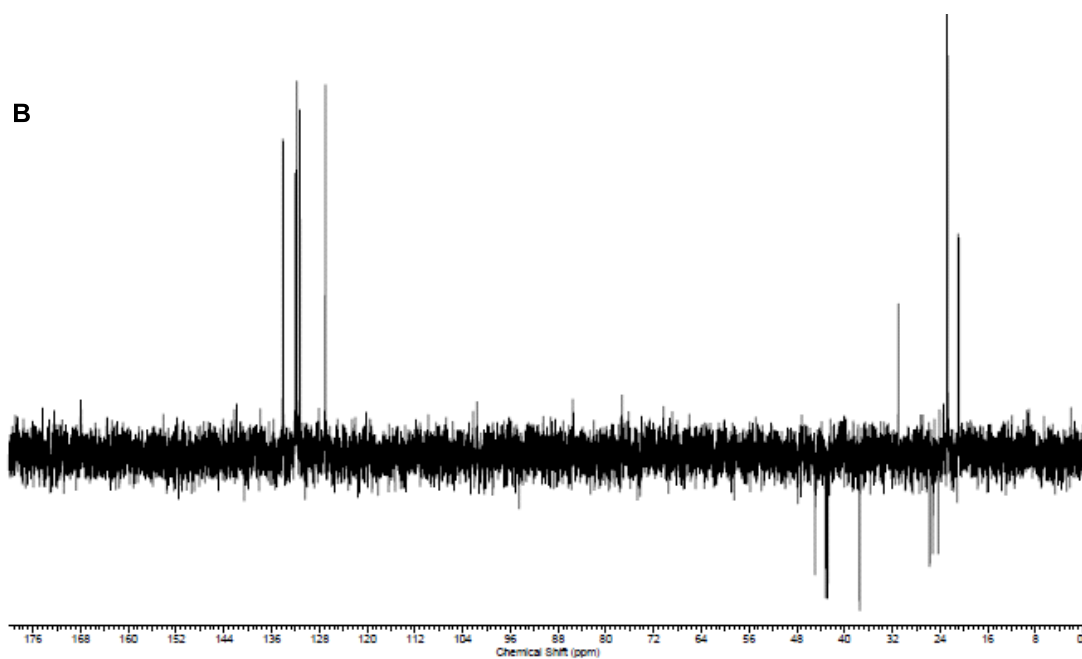
Figure 32: ^{13}C (**A**) and DEPT135 (**B**) NMR spectrum of mesitylated analogue of BNIPSpm **54**
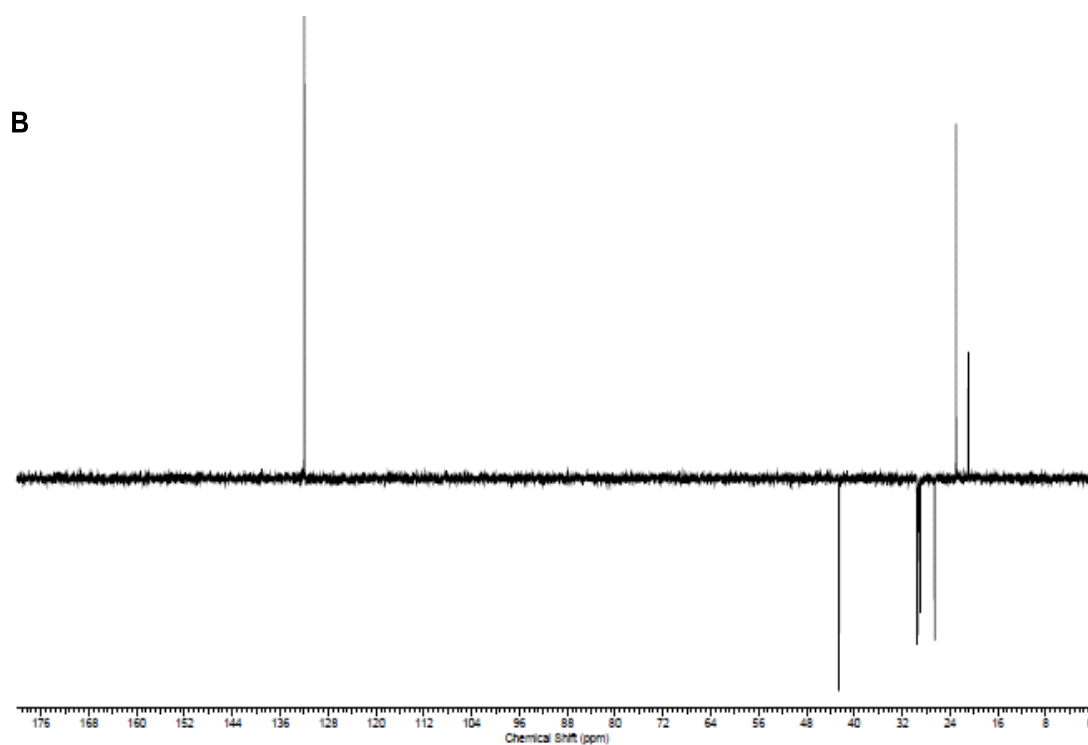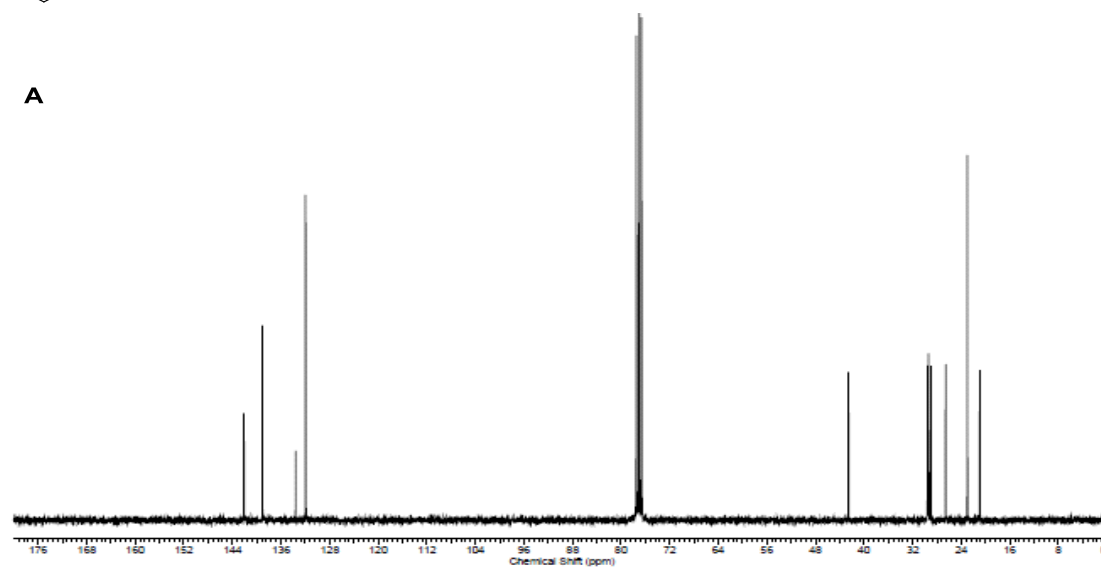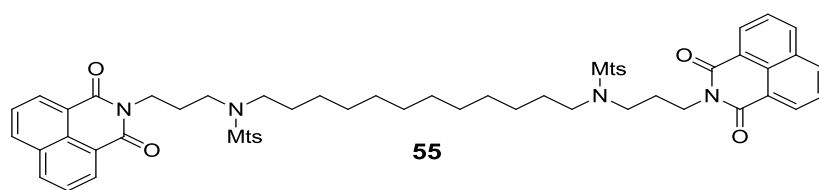
Figure 33: ^{13}C (**A**) and DEPT135 (**B**) NMR spectrum of mesitylated analogue of BNIPDodec **55**

2.3.7 Deprotection of mesitylated analogue of BNIPSpm 21 and BNIPDodecane 26

The target compounds BNIPSpm **21** and BNIPDodecan **26** were prepared by the demesitylation of the protected analogues **54** and **55** by HBr/glacial acetic acid at room temperature using anhydrous dichloromethane as a solvent. As before, the compounds were characterised by ^{13}C and DEPT-135 NMR analysis (Figure 34 and Figure 35) which show the aliphatic carbons (between 27 and 77 ppm) and aromatic carbons from the naphthalene group (between 122 and 138), it also show the inversion of CH_2- peaks and disappearance of the quaternary carbon, all the data acquired matched the reference data from the literature.
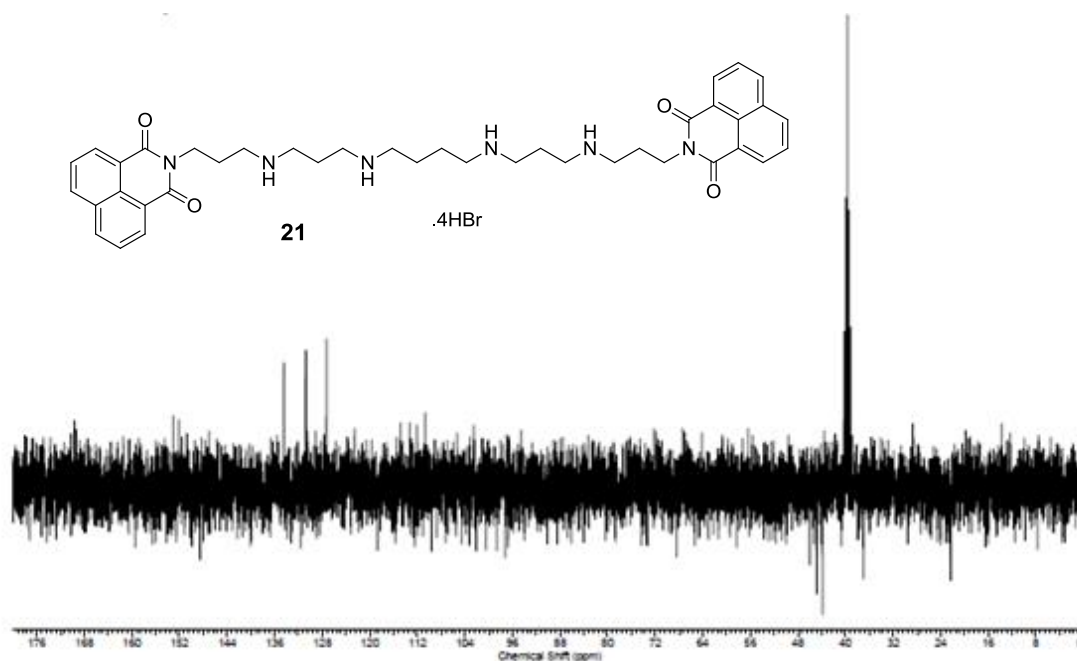
Figure 34: DEPT135 NMR spectrum of BNIPSpm **21**
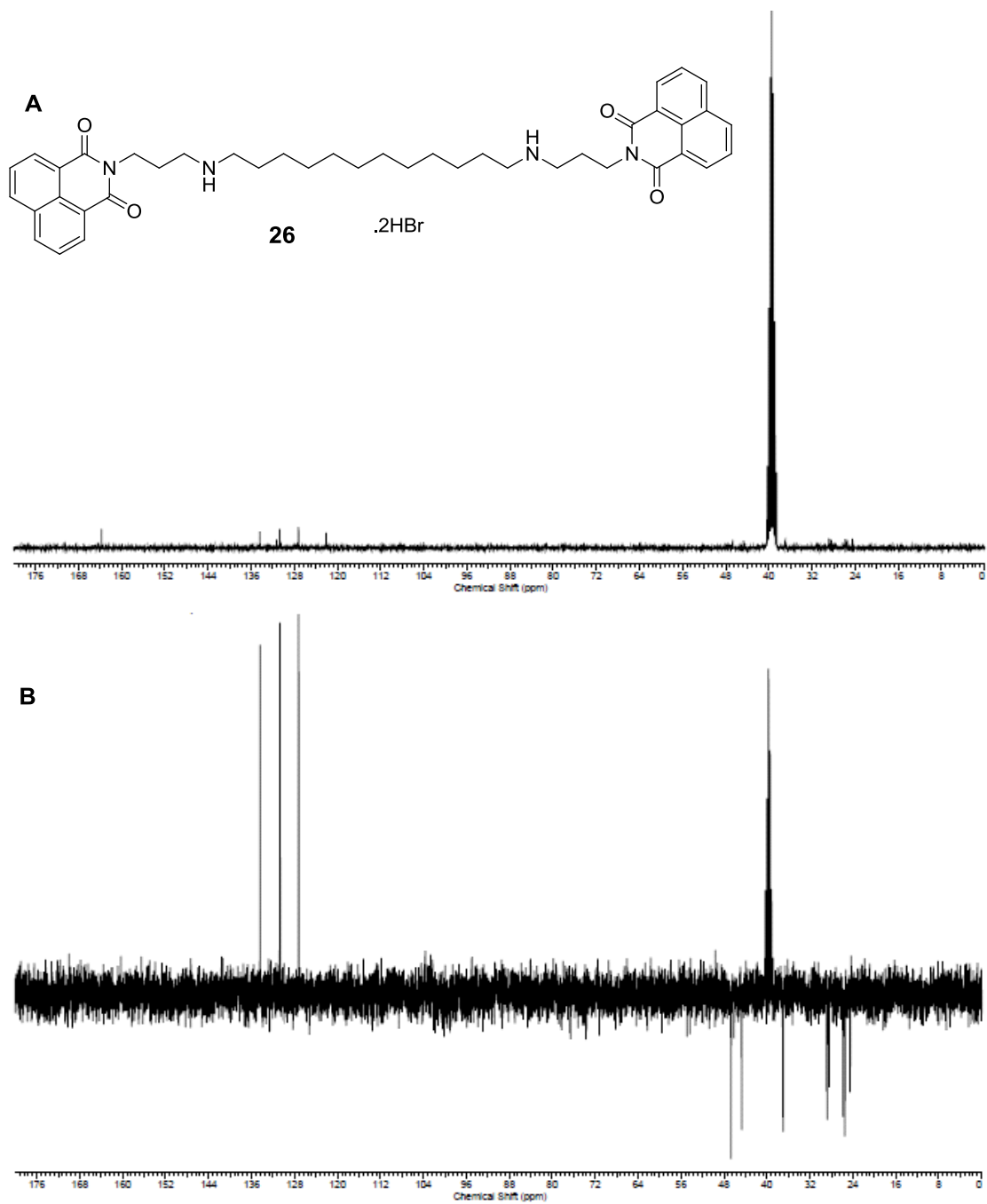
Figure 35: ^{13}C (A) and DEPT135 (B) NMR spectrum of BNIPDodec **26**

2.4 Synthetic strategies for bisnaphthalimido heptaethyl hexamine (BNIHexamine) 33

Unfortunately, all strategies which were employed to deliver the target compound (BNIHexamine **33**) failed to deliver the desired product. Two main strategies were extensively studied and two others were examined to see if they were applicable or not.

2.4.1 First strategy

The simplest way to obtain the six amino linker analogue of BNIPSpm **33** is explained in (Figure 36) were pentaethylenehexamine **60** can be used as a linker chain to reacted after mesitylation with tosylated *N-(2*-hydroxyethyle) naphthalimide **63** to make the desired analogue of BNIHehexamine**33.**
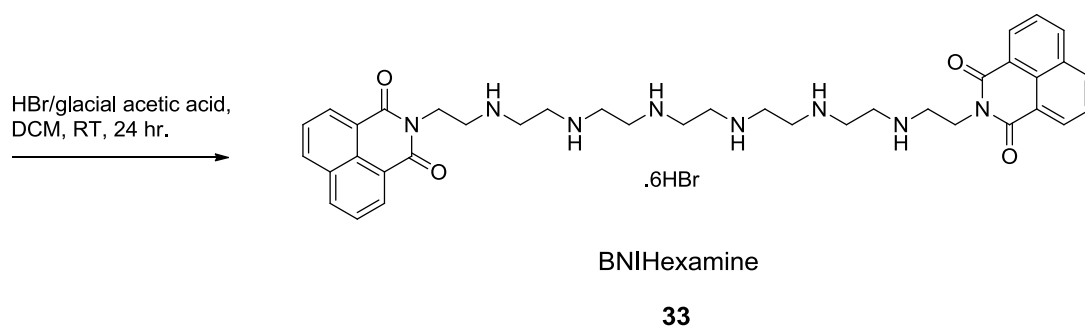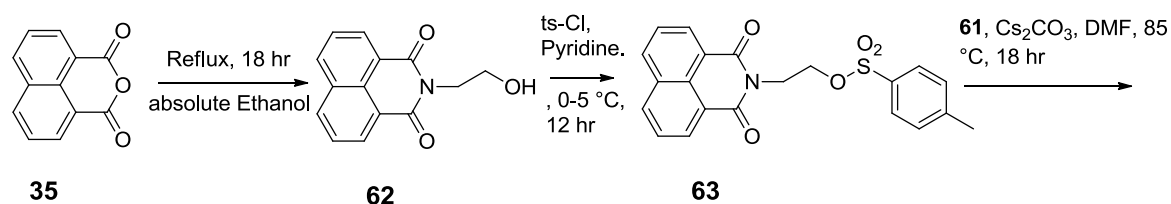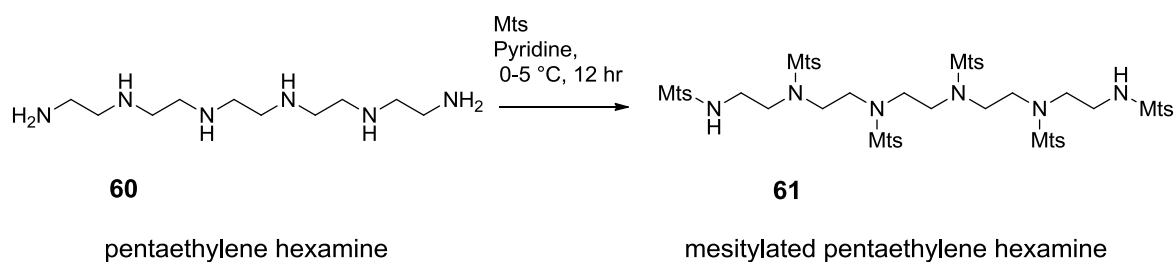
Figure 36: First strategy for synthesising BNIHexamine **33**

In this strategy, the first problem faced was the absence of a commercial source

for pure pentaethylenehexamine (PEHA) **60**. The only available product was

technical grade which contains 70% PEHA **60** as a mixture with other unspecified

amines. Purification was attempted by simple distillation at atmospheric pressure

and at reduced pressure using Kugelrohr apparatus. Purification of the PEHA **60**

from this mixture was not feasible as most of the contaminant polyamines had a

very similar boiling point. An attempt to mesitylate the technical grade PEHA **60** without prior purification was undertaken in order to find a way to facilitate separation of the desired product but the resulting mixture contained compounds with a very similar Rf value which made their separation very difficult to achieve. However, it was decided to proceed with this strategy by coupling *O*-(tosyloxyethyl) naphthalimide **63** to mesitylated PEHA **61** with the aim to obtain a product which would be easier to separate from the mixture which included the mesitylated polyamines.

Surprisingly, the result of this process was that no reaction between *O*-(tosyloxyethyl) naphthalimide **63** and mesitylated PEHA **61** was observed, though spectroscopic analysis showed the original starting compound (*N*-(2-hydroxyethyl)naphthalimide) **62**. This finding was confirmed by reacting (*O*-(tosyloxyethyl) naphthalimide **63**) with mesitylated spermine **56** the result was the same, *i.e.* no reaction between **63** and **56** but compound **62** could be isolated readily.

The proposed mechanism for this unexpected finding is presented in (Figure 37). The short distance (2 carbon atoms) between the nitrogen atom of the naphthalimide and the tosylated oxygen could be the reason that the detosylation is occurring.
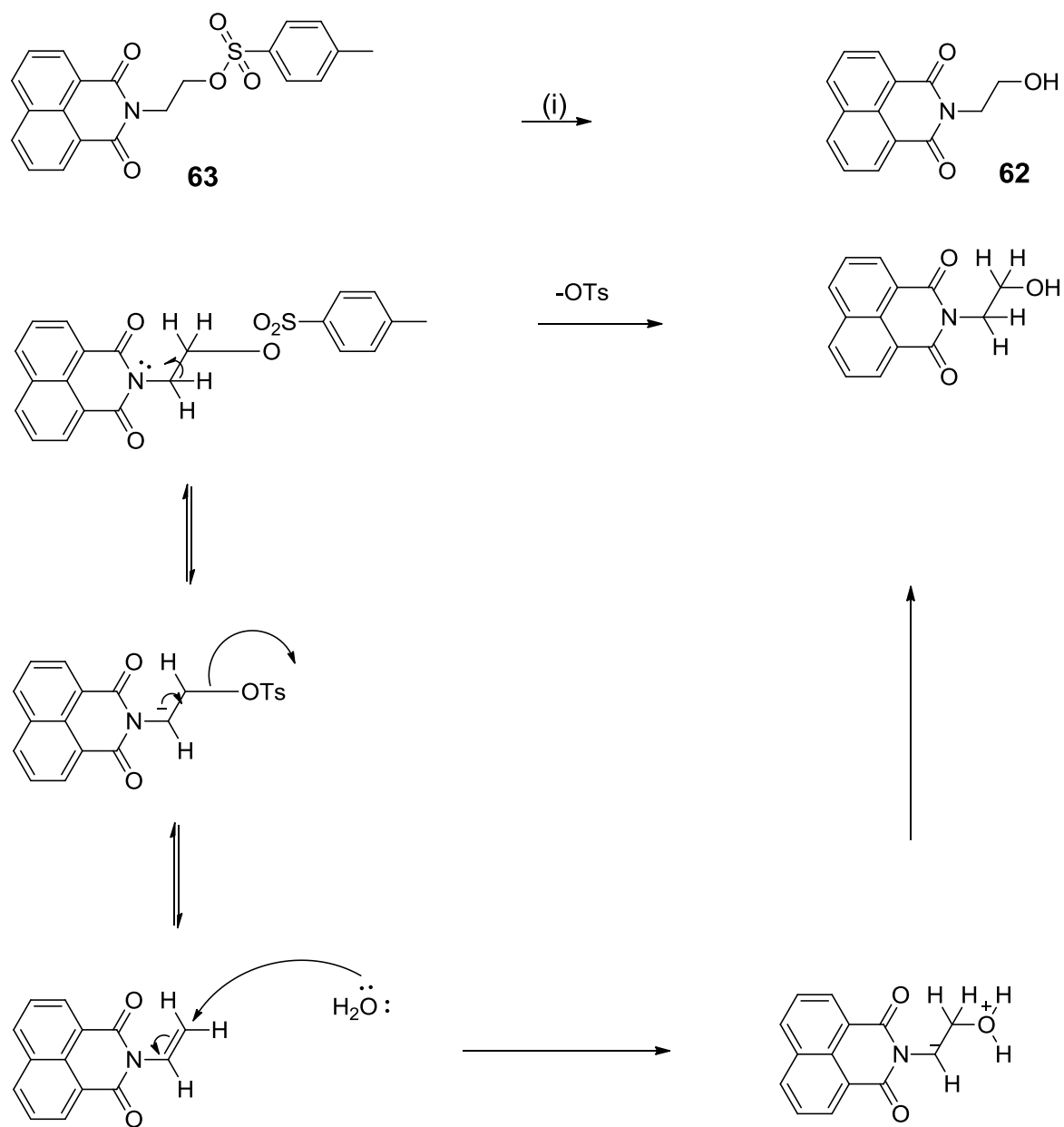
Figure 37: Proposed mechanism of de-tosylation of **63**

2.4.2 Second strategy

In the following strategy, a commercial source of relatively pure triethylenetetramine (TET) **64** was utilised as a corner stone of the synthetic plan in (Figure 38).
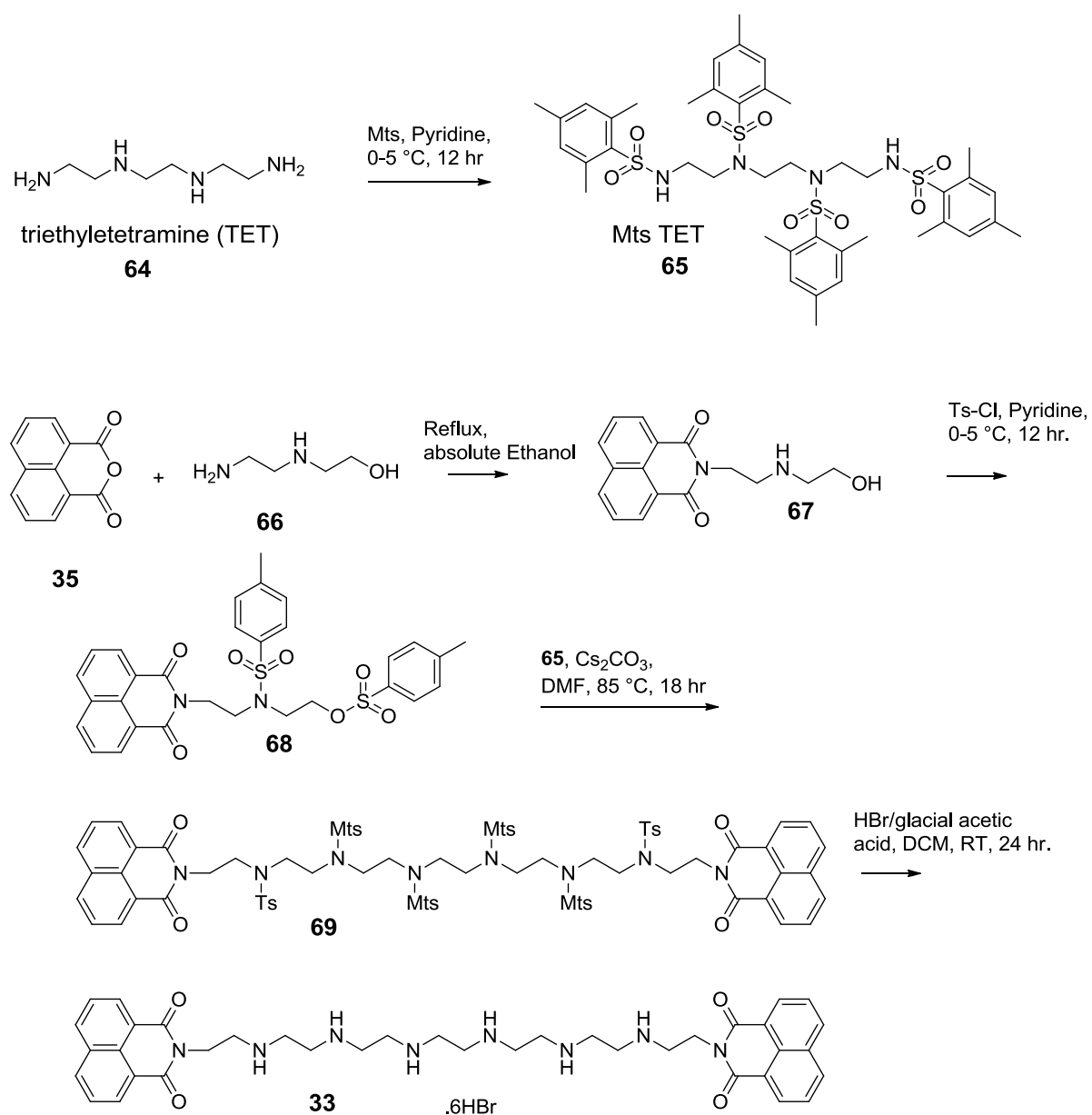
Figure 38: Schematic explanation of the second strategy of **33** syntheses

Mesitylation of TET **64** was performed following the same procedure reported for the synthesis of mesitylated polyamines described previously. The result was promising and a good yield of the pure compound was obtained (Figure 39).
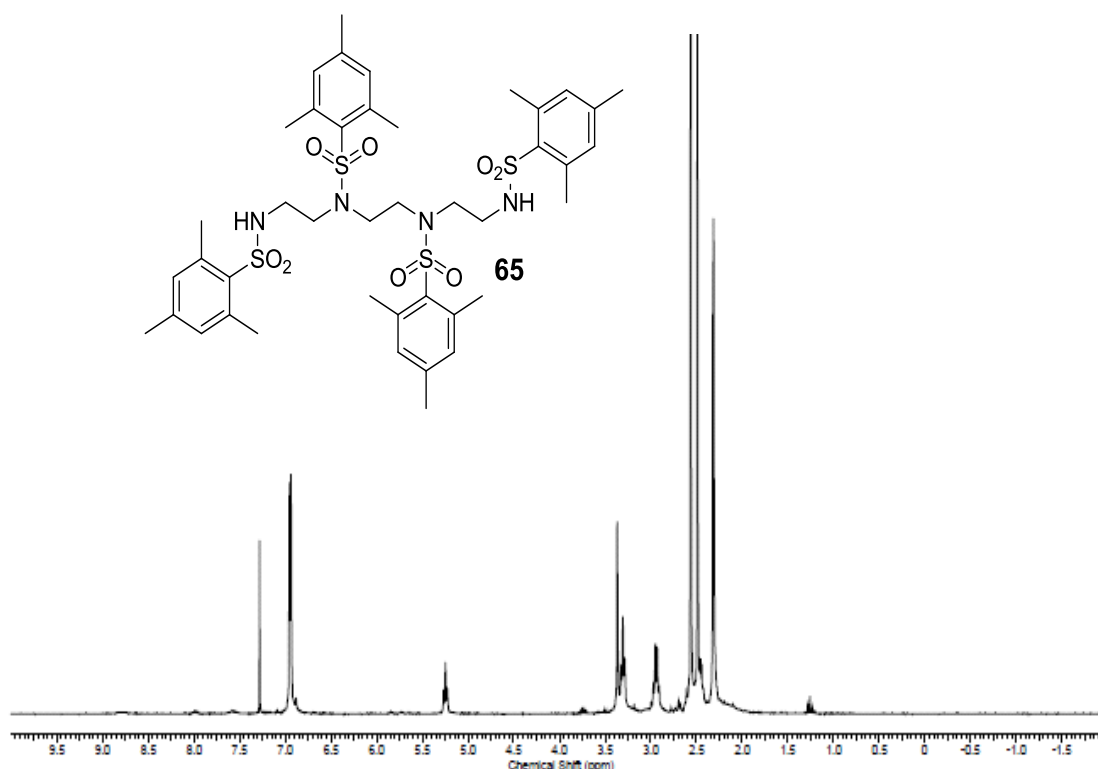
Figure 39: ¹H NMR spectrum of mesitylated TET **65**

2.4.2.1 Synthesis of the *N*-[2-(2-hydroxylethylamino)-ethyl]-1, 8-naphthalimide (HEAEN) 67

Synthesis of **67**was achieved according to the procedure reported by Chen *et al.* which required refluxing the two starting materials (**35** and **66**) in solution in ethanol to obtain the product in almost quantitative yield. The ¹H NMR data acquired for the compound (Figure 40) shows the peaks at position 7.7-8.6 for

aromatic protons, and 2.0-4.5 for the aliphatic protons which perfectly match the reported spectroscopic data (Chen *et al.* 2009).
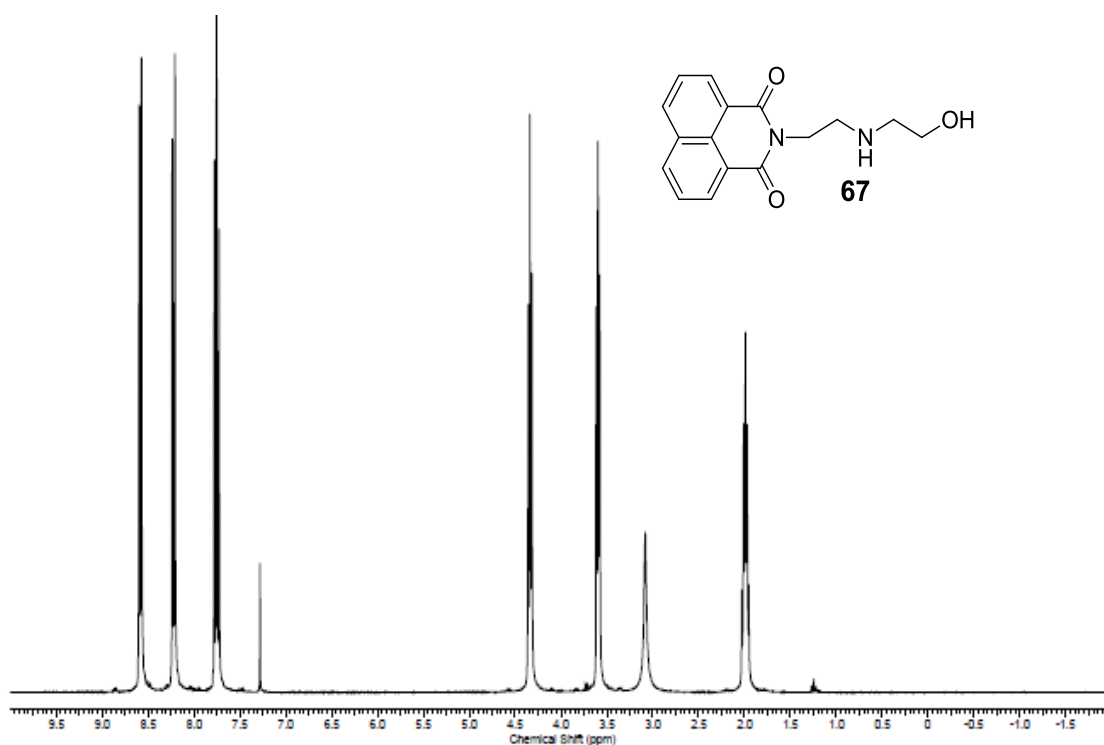
Figure 40: ^{1}H NMR of HEAEN **67**

2.4.2.2 Synthesis of di tosylated *N*-[2-(2-hydroxylethylamino)-ethyl]-1, 8-naphthalimide (HEAEN) 68

Tosylation of HEAEN **67** was also undertaken following a slightly modified method than that used for tosylation of N-(2-hydroxypropyl)naphthalimide **53** and *N*-(2-hydroxyethyl)naphthalimide **63**. Using pyridine as a solvent, the reaction resulted in an apparent mixture of two compounds, the monotosylate **70** (tosyl group substituted on the amine and the *di*-tosyl derivative **68**) (Figure 41).
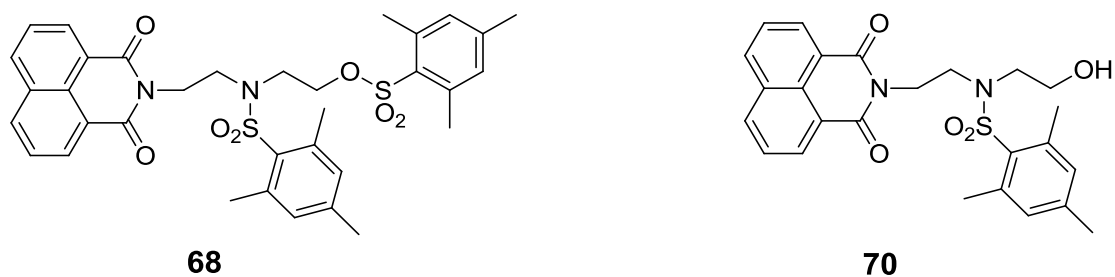
Figure 41: Chemical structure of **68** and **70**

Fortunately the reaction could be easily directed towards favouring the ditosyl derivative **68** by changing some reaction conditions (increasing the duration of stirring at 0 ℃ and using three molar equivalents of tosyl sulfonyl chloride) The ^{13}CNMR data acquired from both compounds is presented in (Figure 42) and highlights the difference in the number of aromatic peaks between 120-144 and the absence of a second methyl peak from the monotosylate derivative at 21.25 ppm as compared to the ditosylate.
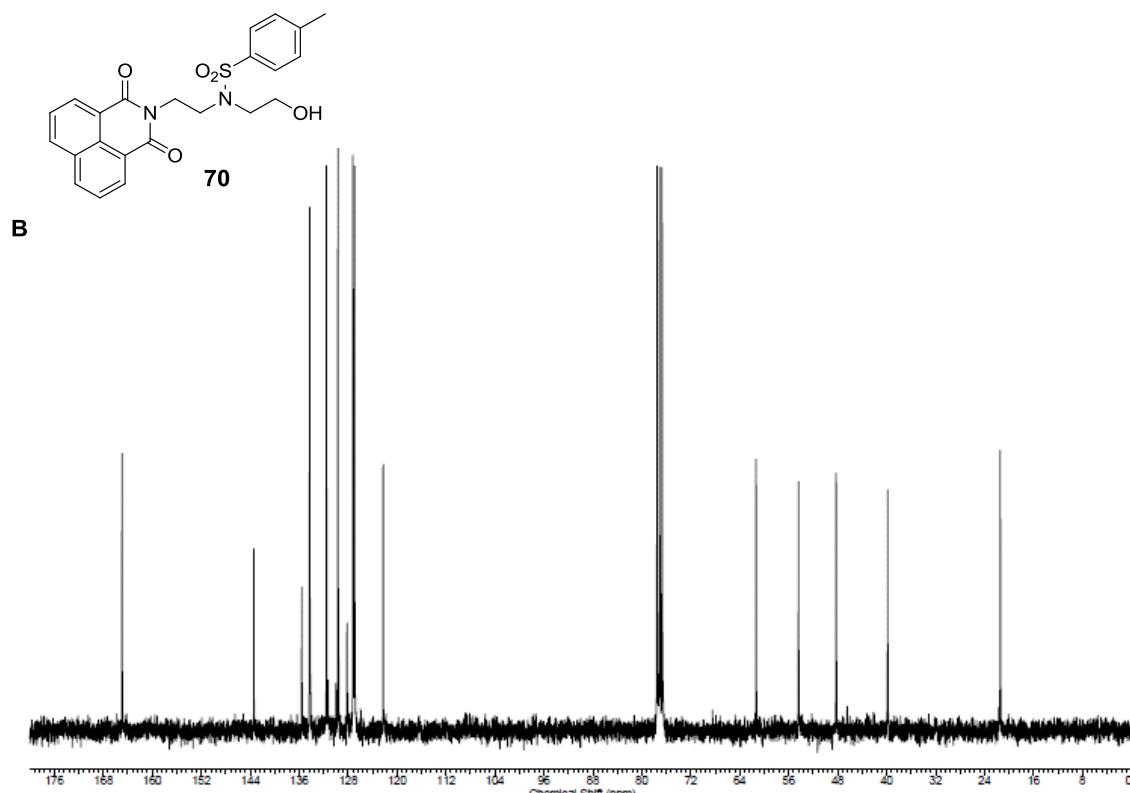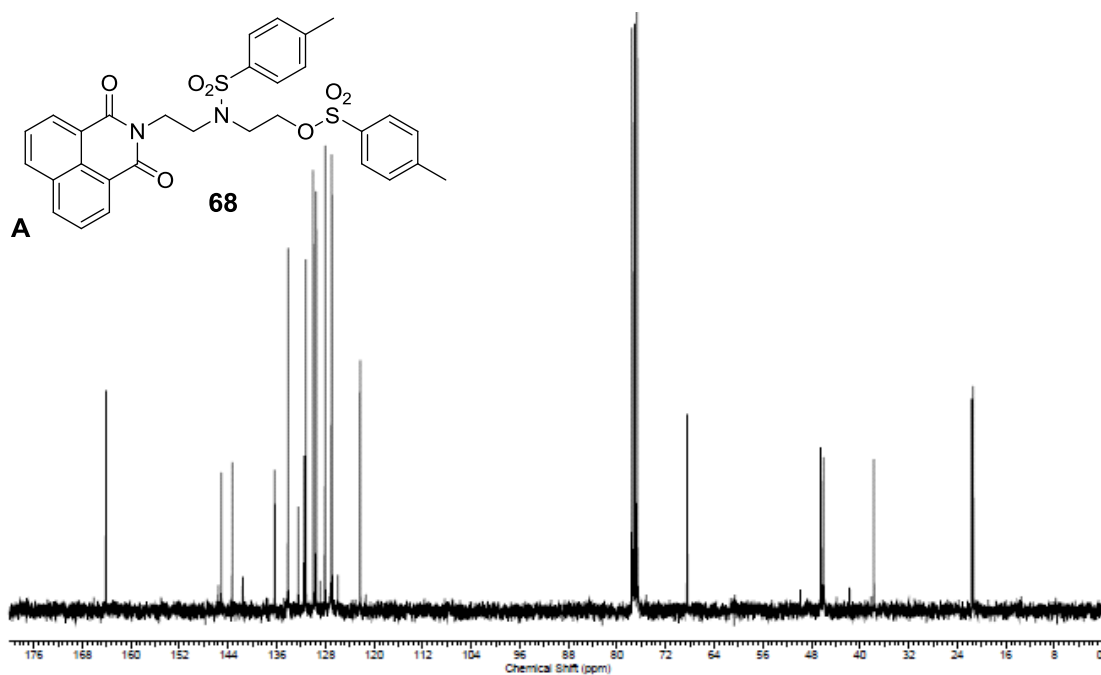
Figure 42: ^{13}C NMR spectrum of (A) di-tosylated HEAEN **68** and (B) mono tosylated HEAEN **70**

2.4.2.3 Synthesis of the mesitylated analogue of Bisnaphthalimido heptaethyle hexamine (Mts BNIHexamine) 69

Following the success in synthesis of the required building blocks of desired compound BNIHehexan **33** it was envisaged that the subsequent coupling step will be equally facile, but it was not.

Attempts of coupling the two reactants (ditosylated HEAN **70** with mesitylated TET **69**) were failed and no reactions were observed between the two reactants even though different reagents and conditions applicable for *N*-alkylation of polyamine had been applied (Table 1).

Table 1: Reagents and conditions used in the attempted coupling of di-tosylated HEAEN **68** to mesitylated TET **65**

Reagents	Conditions	Results
Caesium carbonate 7equ.	Dry DMF, RT, 12 hrs	No reaction
Caesium carbonate 7equ.	Dry DMF, 60C 12 hrs	No reaction
Caesium carbonate 10equ	Dry DMF, RT, 24 hrs	No reaction
Caesium carbonate 10equ	Dry DMF, 60C, 24 hrs	No reaction
Triethylamine 5, 10 equ.	Dry DMF, RT, 12 hrs	No reaction
Triethylamine 5, 10 equ	Dry DMF, 60C, 12 hrs	No reaction
Diisopropylamie 5, 10 equ	Dry DMF, RT, 12 hrs	No reaction

2.4.3 Other strategies

A few other plans were examined before moving on to the second strategy, most of which are highlighted in (Figure 43). They were time consuming and difficulties were faced during purification of the products or the product obtained was not consistent with that described in the reference literature source.

The strategies were basically divided into two parts, the first being the attempt to make the linker ($C_{14}H_{28}N_8$) **71** and react it directly with 1,8 naphthalic anhydride **35**, or the synthesis of pure PEHA **62** and couple it to *N*-(3-hydroxypropyl)naphthaliimide **53.**

The second strategy was to attempt to make compound **72** first and then couple the two residues together using a smaller linking fragment, ditosylated ethylenediamine **73**) (Figure 43).

Figure 43: Schematic explanation of different attempts to synthesise compound **33**

2.5 Synthesis of Bisnaphthalimidopropyl diaminopropyldithiobutane (BNIPds 34)

The final compound in the proposed series of BNIPSpm analogues was BNIPDodithiobutane **34** which has two sulfur atoms in the middle of the linker chain in place of the two nitrogen atoms present in the BNIPSpm **21** linker chain (Figure 44).

The plan for synthesis is explained in (Figure 44). The spermine-like linker has to be synthesised first from the starting material (butane-1,4-dithiol) **75** which was extended by reaction with acrylonitrile **76** followed by reduction of the resulted bis-nitrile **77** to bis-amine **78**, synthesis of the required bisnaphthalimide analogue was achieved following the same procedure of *N*- alkylation, but this could be achieved without prior mesitylation of the linker chain.
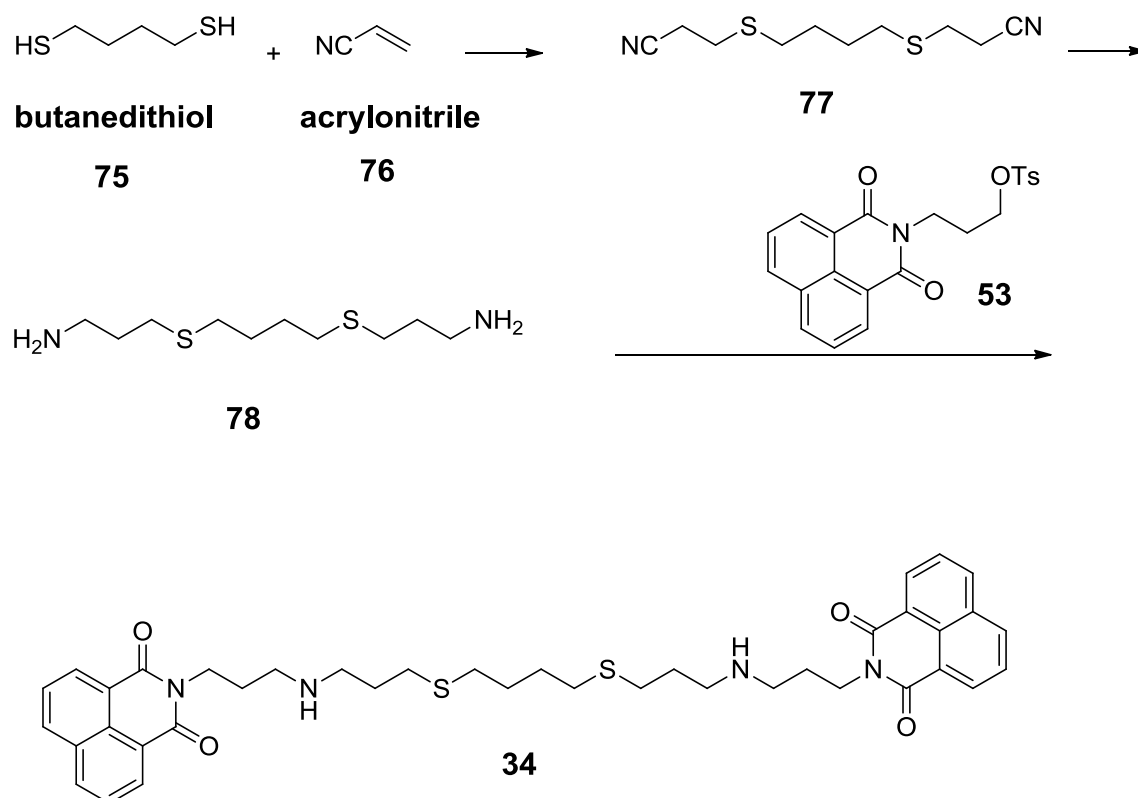
Figure 44: BNIPds **34** synthetic strategy

2.5.1 Reaction of butandithiol 75 with acrylonitrile 76

Acrylonitrile **76** was chosen as a starting material after it proved extremely difficult to purify the product obtained from the analogous reaction of butandithiol with bromopropionitrile **74** (Figure 45).
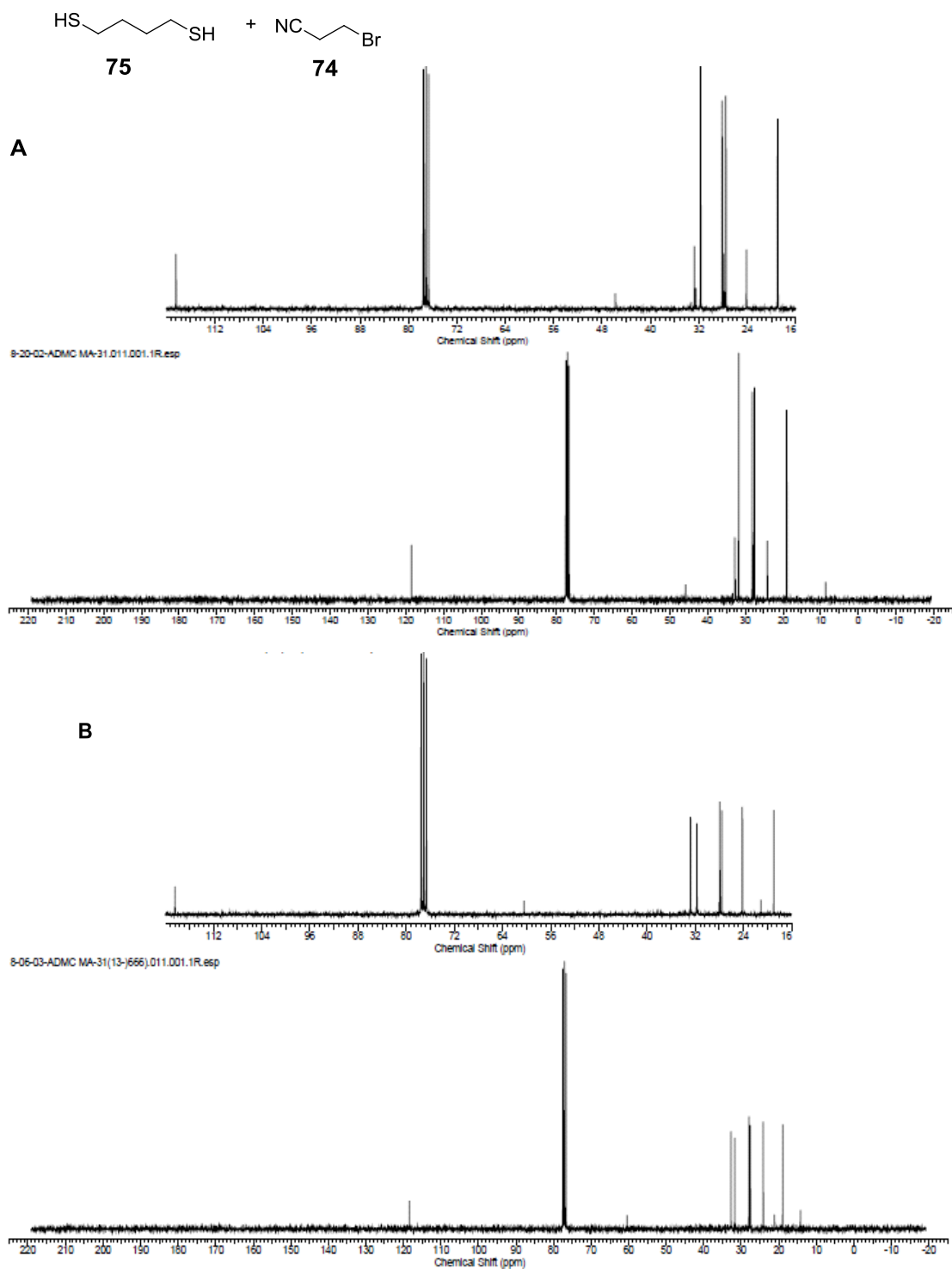
Figure 45: ^{13}CNMR spectrum show effect of column purification on the product of butandithiol (**75**) reaction with bromopropionitrile (**74**), **A**: crude product, **B**: compound recovered after column purification

Fortunately, the reaction of acrylonitrile **76** and 1,4-butandithiol **75** delivered a pure product which could be used without further purification. The reaction was complete after 4 hrs and the yield was quantitative. ^{13}C NMR data show the five characteristic peaks of the product at 18.95 -31.56 and 118.53 (Figure 46).
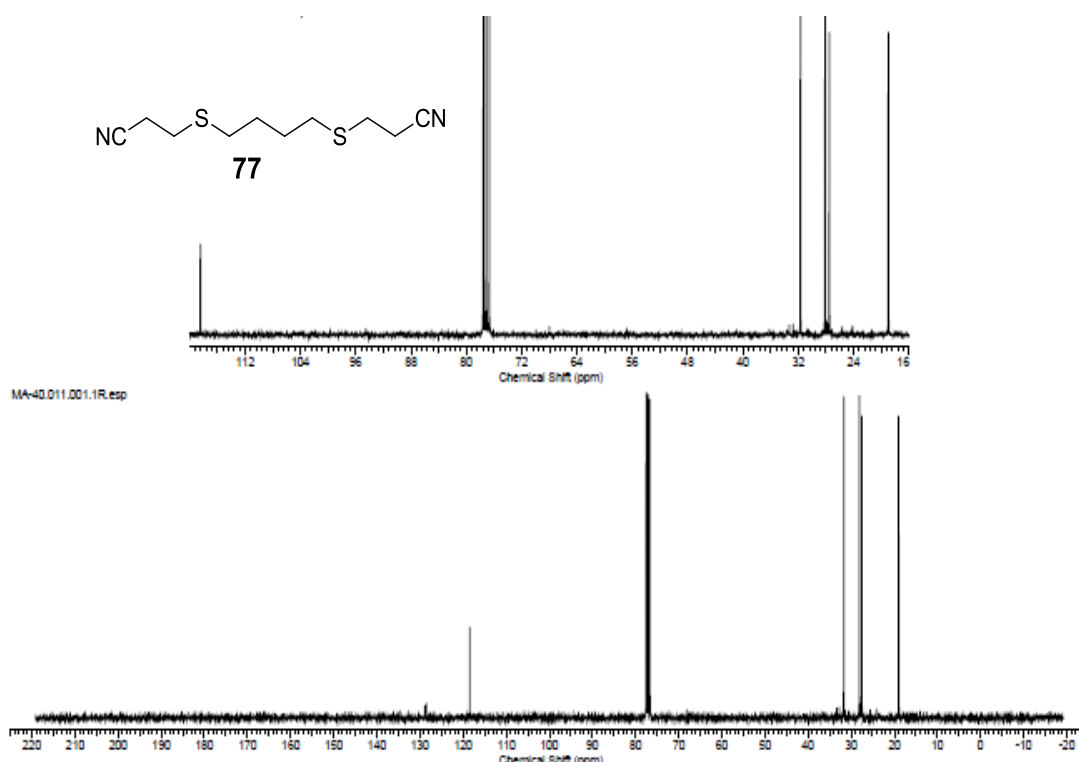
Figure 46: ^{13}CNMR spectrum of bisnitrile **77**

2.5.2 Reduction of bisnitrile 77 to bisamine 78

The next step was reduction of bisnitrile **77** to bisamine **78**. The reaction was tried using borane dimethylsulfide complex. ^{13}C NMR of the product shows the disappearance of peaks at 118.53 ppm and appearance of a fifth peak in the aliphatic region (Figure 47).
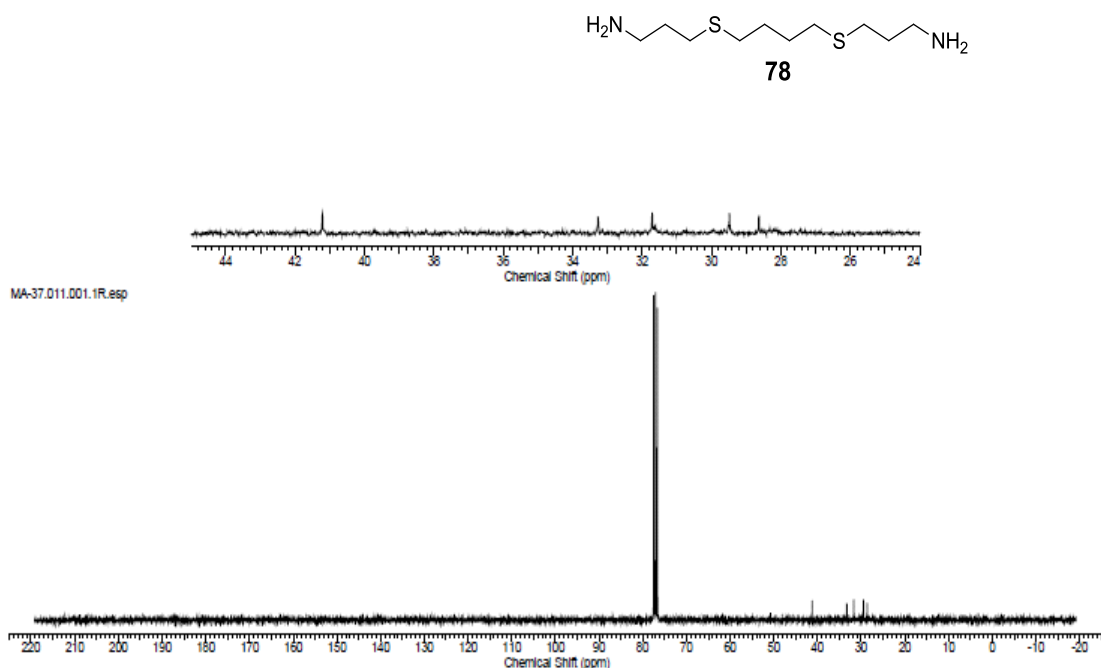
Figure 47: ^{13}CNMR spectrum of bisamine **78**

2.5.3 Synthesis of compound 34

Coupling the sulfide containing linker chain to **53** following the same procedure acquired from the synthesis of compound **22** and **26** was carried out without previous mesitylation of the two amino ends of the linker chain, and the rationale behind doing the reaction in this way is because mesitylation of the linker chain was ended with a mixture of compounds difficult to be purified. A direct reaction

96

between **53** and **78** in 2:1 molar ratio proceeds smoothly to yield compound **34** in a quantitative yield.

Synthesis of the dihydrobromide salt of **34** was conducted following the same method applied for the deprotection step of **56** and **57** which involves deprotection using hydrobromic acid/glacial acetic acid in anhydrous CH_2Cl_2 under an inert atmosphere.

2.6 Conclusions

Two previously known compounds **21** and **26**, together with two novel compounds **32** and **34** have been synthesised successfully following an established procedure. The compounds were utilised by the Keele nanopharmaceutics research group to examine their ability to bind the gold surface of the iron oxide core gold shell hybrid nanoparticles, and investigate their cytotoxic effect against a pancreatic cancer cell line.

Different strategies had to be applied to tackle the problems which arose during the synthesis of compound **33**, but these were not successful, though the second strategy applied was very promising.

The synthetic route chosen to produce compound **34** was an *N*-alkylation reaction without prior mesitylation of the diamine in the linker chain. This reaction has been used successfully and was found to be simple, reproducible, and did not produce by-products. Production of the dihydrobromide salt of **34** was successful but the compound was found to be unstable.

CHAPTER 3: SYNTHESIS AND

CHARACTERISATION OF

GEMCITABINE PRODRUGS

3.1 Background

Following the successful experiments conducted previously within the Keele Nanopharmaceutics Research group which demonstrated the potential advantages of hybrid iron oxide core gold shell nanoparticles (HNPs) as a carrier for positively charged cytotoxic compounds and their potential effects as a powerful tool to tackle the problems presented by the deep stroma caused by pancreatic cancer, derivatives of gemcitabine were proposed which could actively bind to the surface of the HNPs and be delivered into the pancreatic cancer cell. The hypothesis being that this would increase the efficacy of gemcitabine which is the preferred chemotherapy for pancreatic cancer.

3.1.1 Nucleoside, Nucleotide and Nucleic acid

Genetic information is codified within living cells inside the nucleic acids DNA (deoxyribonucleic acid) and RNA (ribonucleic acid). Nucleic acids are polymeric sequences of nucleotides, which themselves are phosphorylated nucleosides which consist of a basic heterocyclic residue attached to ribose (RNA) or 3-deoxyribose (DNA).

The basic heterocyclic residue within nucleosides are nitrogen-containing heterocycles which are either purine- or pyrimidine derivatives. The purine nucleosides are adenine **80** and guanine **81**, both of which are found in both DNA and RNA. The pyrimidine nucleosides are cytosine **82**, thymine **83** and uracil **84**: cytosine **82** is found in both DNA and RNA, whereas thymine **83** is present in DNA only and uracil **84** is only found in RNA. The heterocyclic residues are attached to

the pentose carbohydrate via a glycosidic linkage to the anomeric position of the pentose.

Nucleic acids are polymeric macromolecules which contain the genetic information to code for the synthesis of proteins and other biomolecules. DNA consists of two strands and is essentially a complementary dimer which has the shape of a double helix. RNA exists as discrete single strand molecules. Genetic information stored within the nucleic acids is coded according to the sequence of the nucleotides within the molecule (Lodish *et al.* 2000; Neidle 2008).

Figure 48 shows the basic structure of nucleic acid, nucleotides and nucleosides.
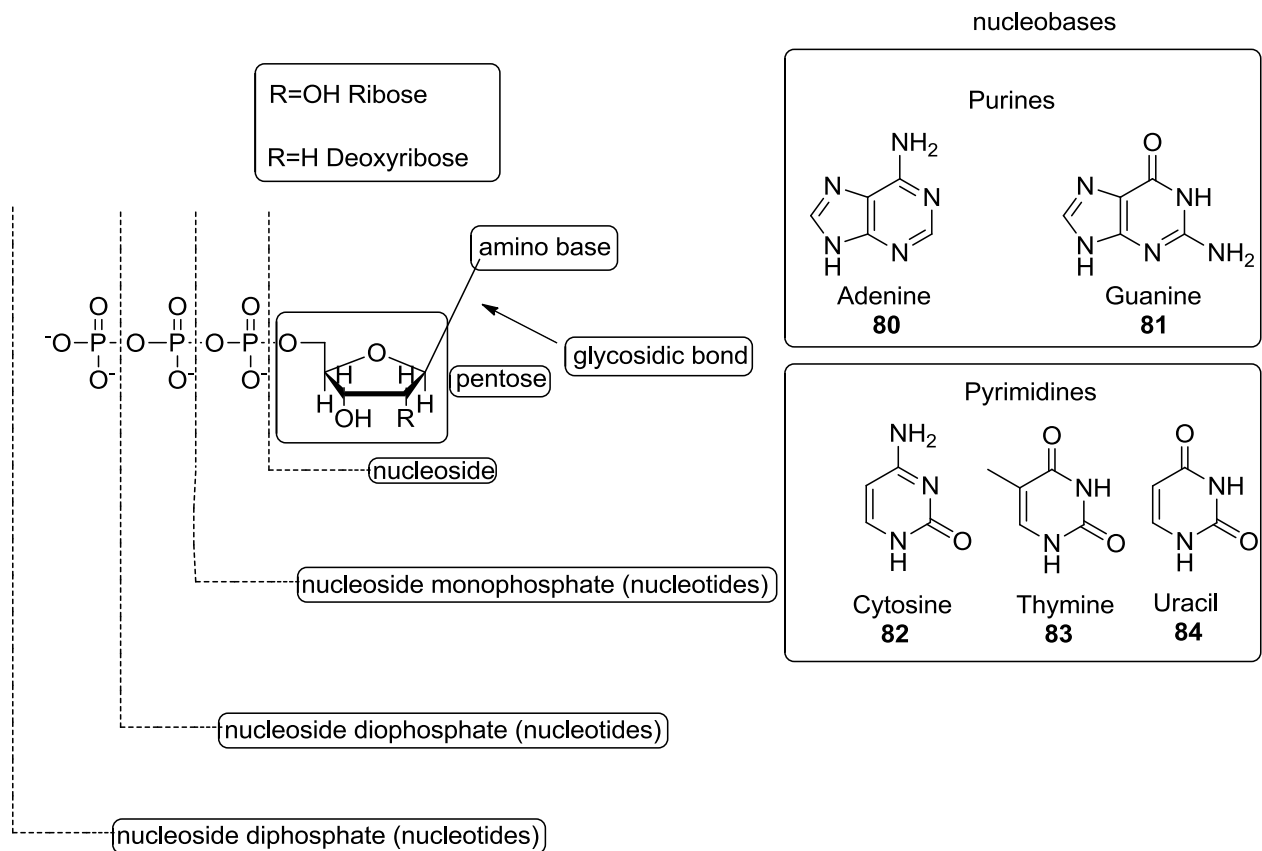
Figure 48: Structures of nucleobase, nucleosides and nucleotides

3.1.2 Nucleoside analogues

Nucleoside analogues, as the name indicates, are analogues very close in structure to the naturally occurring nucleosides which form the building blocks of the nucleic acids. This similarity allows these analogues to be integrated within the structures of DNA and/or RNA by the action of the DNA- or RNA polymerase enzymes which lack the ability to distinguish between nucleosides and their analogues.

The integration of the false nucleoside within the replicating DNA molecule cause a deformity in the shape of the outspreading polymer. This deformity will consequently inhibit chain elongation, and eventually prompt apoptosis (a programmed cell death).

The nucleoside analogues class of cytotoxic agents has shown significant clinical effects against several malignancies and solid tumours (Lodish *et al.* 2000; Simons *et al.* 2005; De Clercq & Field 2006; Neidle 2008; Madela & McGuigan 2012).

3.1.3 Resistance to nucleoside analogues

Resistance to chemotherapy developed within cancer cells remains one of the major drawbacks of chemotherapy using cytotoxic drugs. Consequently, more effective treatment is in great demand, either by finding new ways of removing chemoresistance or making known therapeutic agents more efficient (Gottesman 2002).

The cytotoxic action of nucleoside analogues within the cell is determined by their ability to enter the cell through transporters in the cell membrane and subsequent activation by nucleoside kinases to give the active phosphorylated form of the analogue (Fukuda & Schuetz 2012). Resistance to nucleoside analogues is developed when the processes of transportation and/or activation are disturbed by modulation of the enzymes involved or by the action of the natural catabolic enzymes that deaminate or deposphorylate the analogues (Galmarini *et al*. 2001; Damaraju *et al*. 2003; Fukuda & Schuetz 2012). However, nucleoside analogues continue to be of great value in attempts to overcome tumour chemoresistance, especially when used in combination therapy with other chemotherapeutic agents, mainly because the majority of nucleoside analogues have little tendency to cause cross-resistance with other cytotoxic agents (Galmarini *et al*. 2010).

3.2 Gemcitabine a nucleoside analogue

Gemcitabine **7** is an analogue of deoxycytidine **8**: it has two fluorine substituents in the 2' position of the ribose residue. The clinical outcomes using gemcitabine are very good but its efficacy is restricted by inactivation by deaminase enzymes. Several prodrug derivatives of gemcitabine have been developed to protect the drug from deamination and to increase drug lipophilicity but the high toxicity of these derivatives have rendered the compounds to have low value in term of clinical efficacy (Plunkett et al. 1995; Bergman et al. 2002b; Alexander et al. 2005; Enrico Mini et al. 2006; Frese et al. 2012; De Sousa Cavalcante & Monteiro 2014).
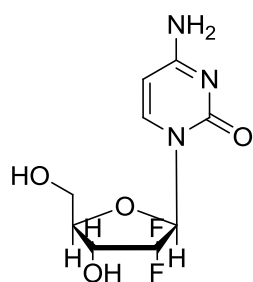
7

gemcitabine
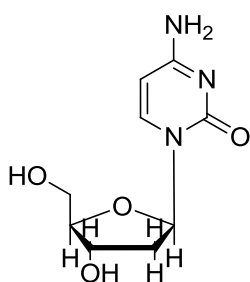
8

deoxy cytidine

The aim of this chapter is to describe the design and synthesis of a derivative, possibly a prodrug, of a clinically relevant drug, gemcitabine, to enable it to covalently or electrostatically bind to the gold surface of the hybrid nanoparticles (HNPs) described elsewhere in this thesis. The hypothesis is that the analogue will be taken up by the cell in quantity and have a greater efficacy as a consequence because it is bound to the HNPs.

3.3 Attempt to synthesise positively charged prodrug of gemcitabine

Unmodified gemcitabine is unable to attach to the gold shell of the HNPs because it lacks the required functionality for creating a dative covalent or electrostatic bond with the outer shell; it lacks positively charged atoms or any sulfur-containing residues. Therefore, an analogue of gemcitabine is required which does contain the requisite functionality for bonding to the gold surface and is also able to exert a cytotoxic effect once in the cell, either by itself or through the liberation of gemcitabine. In this case, a prodrug approach was considered in order to release gemcitabine after the nanoformulation has been taken up by the cell.

Work conducted previously within the Keele Nanopharmaceutics Research Group, which used bisnaphthalimide anticancer agents as model agents to investigate the electrostatic binding of positively charged drugs to the gold surface of HNPs, demonstrated that compound **21,** derived from spermine **6** and bearing four positively charged amino groups in its structure, bound most efficiently to the negatively charged gold surface of the HNPs through electrostatic bonding association.
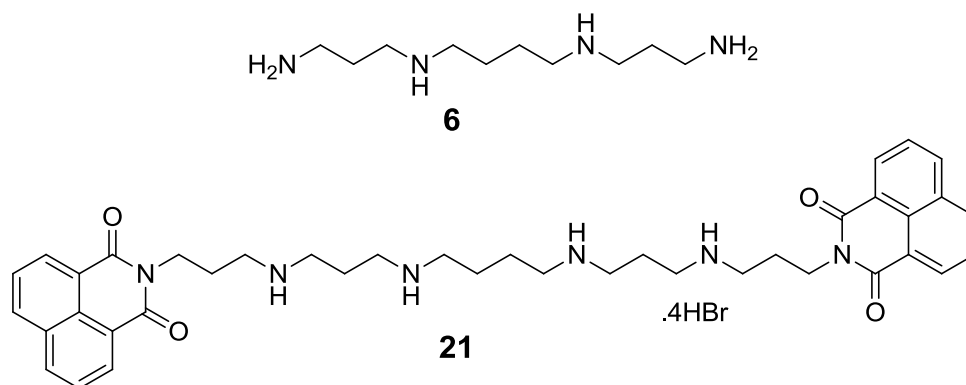
3.3.1 Spermine

Spermine **6** is a natural polyamine; Polyamines are components of nearly all living cells: spermine is found in all eukaryotic cells but different species form additional, different ranges of polyamines. Putrescine **4**, spermidine **5** and spermine **6** are the only polyamines produced by mammals (Kusano *et al.* 2007).
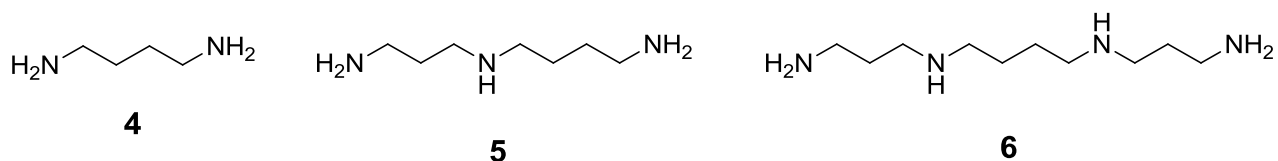
The structure of spermine was first established in 1926 by a group of scientists, however Antonie van Leeuwenhoek had described crystals of spermine phosphate in human semen as early as 1678, while the name spermine was used first in 1888 by Ladenburg and Abel. Spermine is found as a polycation at physiological pH and it is the compound that gives the semen fluid its characteristic smell (Kusano *et al.* 2007; Bachrach 2010).

The role of spermine in cell metabolic pathways is well established. Together with other polyamines it plays an important role in many cell activities, including acting as a protective barrier against oxidative damage, the regulation of ion channels, conservation of membrane structure and function, affecting cell proliferation by regulating the process of transcription and translation, modulation of some kinase enzyme activity and stabilising the helical structure of nucleic acid (Khan *et al.* 1992; Pedreño *et al.* 2005; Casero & Pegg 2009; Pegg 2009; Mandal *et al.* 2013; Pegg 2014).

3.3.2 Strategy applied for coupling gemcitabine to spermine

The proposed strategy (Figure 49) was designed to provide a way of coupling a spermine molecule with gemcitabine without losing the ability to protonate all the remaining primary and secondary amine groups in the polyamine. The strategy was based upon published work on the selective protection of polyamines and coupling of a carboxylic acid to a primary amine group to form an amide using dicyclohexylcarbodiimide (DCC) as a coupling agent. Functionalisation of the spermine molecule by addition of a free carboxylic acid arm was required to achieve the goal, the carbonyl group of the carboxylic acid arm should be at least one carbon atom away from the amine coupling site of spermine to prevent possible protonation of the amine group reducing the reactivity of the carbonyl group towards amide bond formation.

The potential advantages of amide bond formation between the proposed derivative of spermine and gemcitabine to produce a prodrug was the main reason behind choosing this kind of coupling.
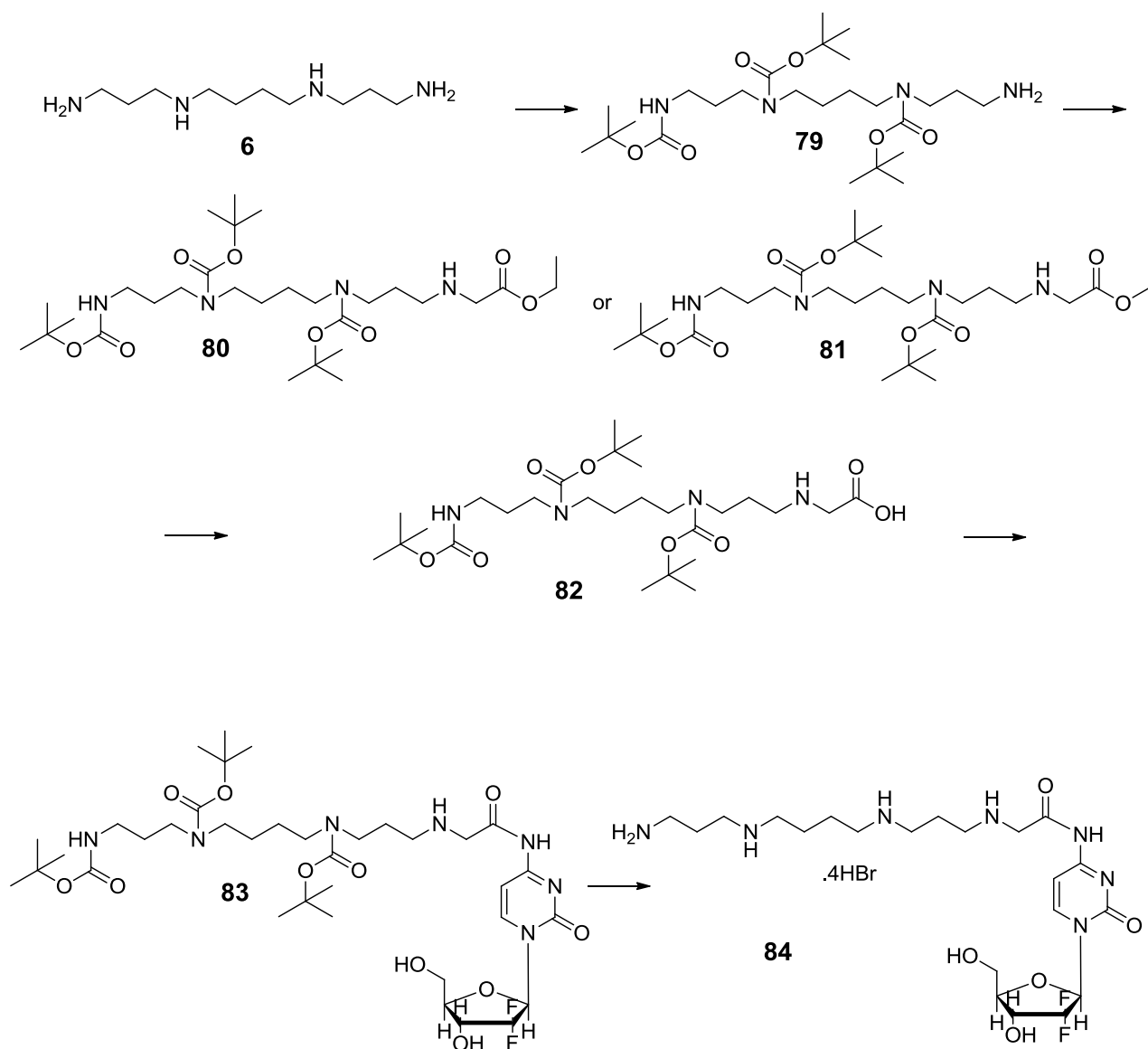
Figure 49: Proposed synthetic strategy for the formation of a gemcitabine-spermine prodrug (Jørgensen *et al.* 2005; Zhang *et al.* 2009; Kölmel *et al.* 2014; Jagu *et al.* 2015)

3.3.2.1 Regioselective Boc protection of spermine

Boc refers to the *tert*-butoxycarbonyl protecting group **91** which is commonly used to protect amine functional groups during synthesis. Reaction of a primary or secondary amine with di-*tert*-butyl dicarbonate **92** yields the corresponding Boc protected *N*- *tert*-butoxycarbonyl derivatives **93**. The term Boc protection is applied because of the ability of the Boc group to alter the reactivity of the amine group towards most bases and nucleophiles. The Boc protecting group can be readily removed using moderately strong acids.
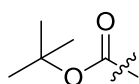
tert-butyloxycarbonate
91
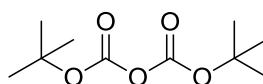
Di-*tert* butyl dicarbonate
92
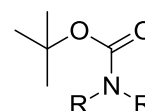
N- *tert*-butoxycarbonyl
93

The chosen strategy to make the polyaminated gemcitabine analogue began with a regioselective protection of spermine. Reaction of spermine with di-*tert*-butyl dicarbonate **92** under standard conditions resulted in complete reaction of the primary and secondary amine groups in spermine to give the tetra-Boc derivative where all of the nitrogens have been protected. The selective protection of both secondary amino groups and one of the primary amino groups in spermine was reported by Geall and Blagbrough (2000): reaction of spermine with an equimolar quantity of ethyl trifloroacetate at -78 ℃ gave a crude mixture of mono-, di- and tri-

trifluoroacetamide derivatives of spermine, with the mono-substituted derivative in which only one of the primary amino groups was protected being the dominant species. An excess of di-*tert*-butyl dicarbonate **92** was added to the flask containing the crude mixture of spermine trifluoroacetimidates and reacted under standard conditions in order to protect any unreacted amino functional groups. Finally, the trifloroacetate groups were cleaved by raising the pH of the mixture to pH 11. The tri-Boc-protected spermine **85** was obtained in 50% yield after purification by flash column chromatography (Geall & Blagbrough 2000).

85
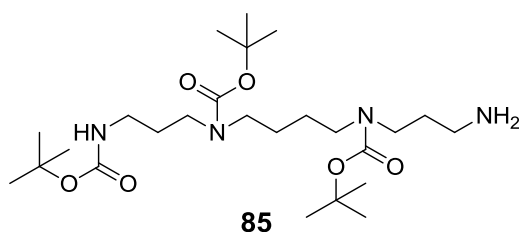
Purification of the reaction mixture described above was actually rather challenging and it proved almost impossible to separate the desired product from those derivatives protected by only two Boc groups which may be on the primary or secondary amino groups. A minor change to the procedure was introduced, inspired by Wellendorph *et al* (2003) who held the reaction temperature between -48℃ and -52℃ while adding the trifluoroacetylation reagent to the solution of spermine. The temperature control favours the production of the tri-Boc-protected spermine **85** over other by-product of the reaction (*i.e.* di-Boc-protected spermine **94**) while addition of di-*tert*-butyl dicarbonate **92** was undertaken at 0℃ and the reaction temperature was left to reach the ambient temperature spontaneously (Wellendorph *et al.* 2003; Emanuela *et al.* 2012).

94
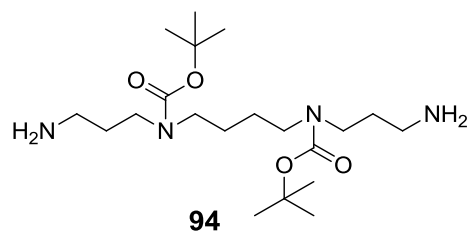
3.3.2.2 Synthesis of compound 88

Synthesis of a spermine derivative bearing a carboxylic acid functional group **88** required reaction of the tri-Boc protected spermine **85** with either methyl or ethyl bromoacetate to yield **86** and **87,** respectively, followed by ester hydrolysis to yield compound **88**. These were effectively one-pot reaction monitored by TLC.

86　　　　　**87**

88
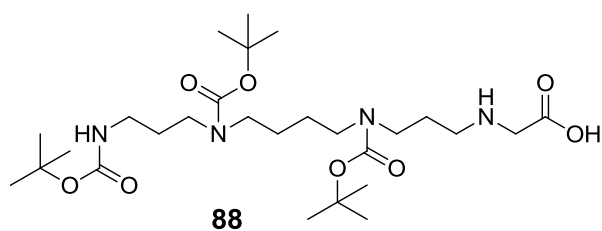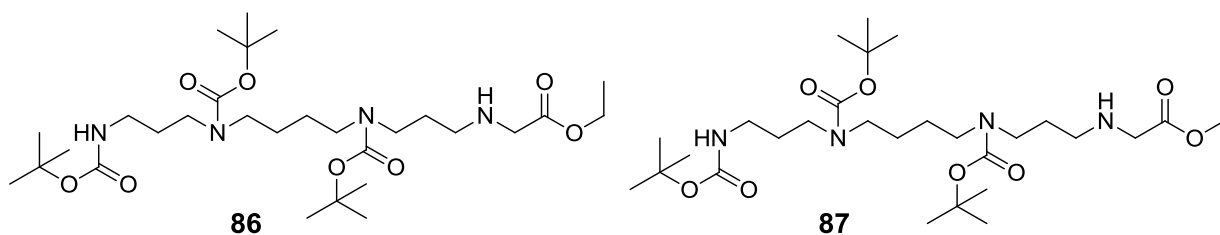
3.3.2.3 Reaction of gemcitabine with compound 88

The coupling of gemcitabine to compound **88** using DCC as the coupling agent was unfortunately unsuccessful: the reaction was repeated many times using slightly modified conditions, reaction times, etc but no product could be identified in each case, with only starting materials being observed. Due to time constraints and the prolonged complex multi-step synthesis and purification of the starting materials, the coupling of a polyamine derivative of spermine with gemcitabine to create a potential prodrug was abandoned.

3.4 Synthesis and characterisation of sulfur bearing derivative of gemcitabine

In order to use the hybrid nanoparticles as a diagnostic and/or therapeutic tool in biomedicine the appropriate strategy to load the payload compound or species to the particle has to be chosen carefully (Cao-Milán & Liz-Marzán 2014).

Both chemical and physical bonding interactions can be involved in molecular attachments to the gold surface of the HNPs used in this study (Figure 50): such interactions between the gold HNP surface and payload molecules may be achieved via chemisorption of thiol derivatives, electrostatic attraction between two differently charges species, hydrophobic attraction between the particle surface and the payload molecule and dative covalent bonding between electrons on the gold surface and sulfur atoms within the molecule (Day *et al.* 2010; Jazayeri *et al.* 2016).
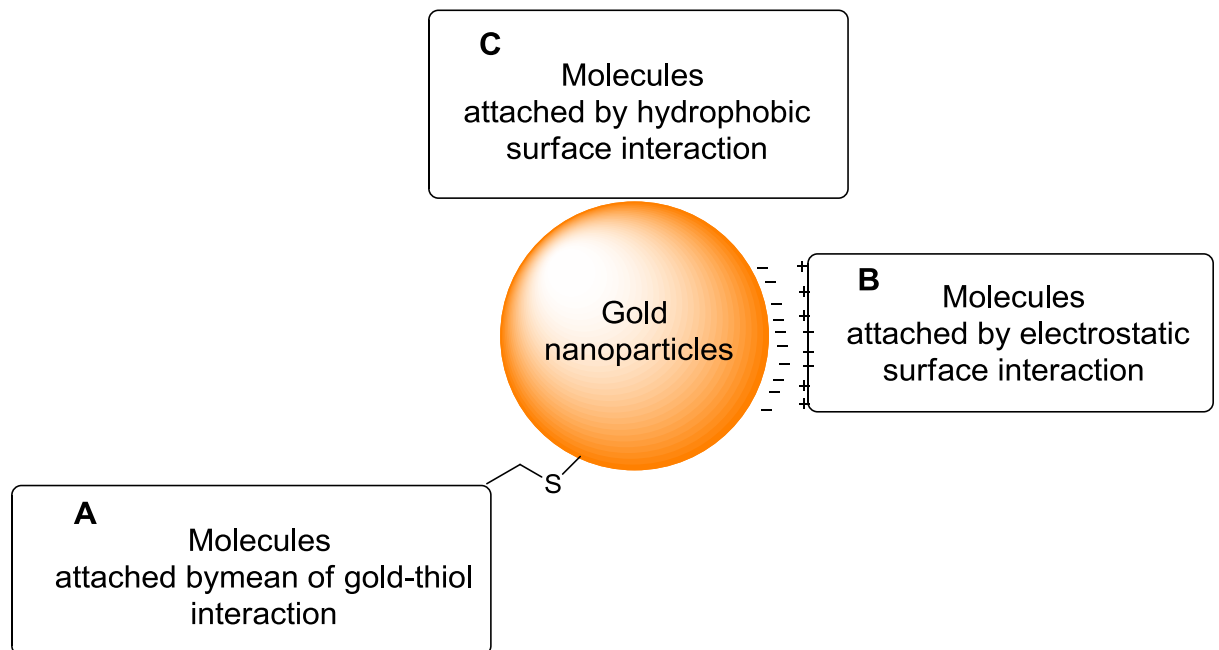
Figure 50: Interactions between gold nanoparticle surfaces and molecules A) a dative covalent binding, B) ionic interaction, C) hydrophobic interaction

3.4.1 Lipoic acid

α-Lipoic acid **95**, also known as thioctic acid, is a naturally occurring compound. Lipoic acid is synthesised enzymatically from octanoic acid in the mitochondria but it can also be acquired from nutritional sources. It has been found to accumulate in many tissues for a short period of time. The compound plays an important role in energy metabolism as it acts as a critical cofactor for the α-ketoacid dehydrogenase enzyme located inside the mitochondria. However, evidence has been shown that lipoic acid from dietary sources may not act as a metabolic cofactor.
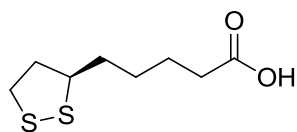
95

Lipoic acid from dietary supplement is thought to trigger key biochemical processes which can lead to a potential therapeutic effect. For example, in addition to the antioxidant effect of lipoic acid the compound has been described as part of a regime for controlling diabetes and as an aid to improve age-associated cardiovascular, cognitive, and neuromuscular deficits. It has also been shown to act as a modulator of various inflammatory signalling pathways (Packer *et al.* 1995; Biewenga *et al.* 1997; Shay *et al.* 2009; Vallianou *et al.* 2009; Gorąca *et al.* 2011).

3.4.2 Lipoic acid coupling to gemcitabine

Synthesis of cytidine analogues **96** and **97** was used as a model prior to the actual reaction of gemcitabine **7** with lipoic acid **95**. The result of the reaction of cytidine **8** with lipoic acid **95** in the presence of a coupling agent was not fully characterised but the TLC showed three spots which had different Rf values than those corresponding to the starting materials. Upon separation products were identified using NMR spectroscopy which gave a preliminary indication of the position where the lipoic acid substituent had attached to cytidine **8**: one product had a substituent on the primary amine **96** and another had the substituent attached to the primary alcohol of the ribose residue **97** (Scheme 9).

114
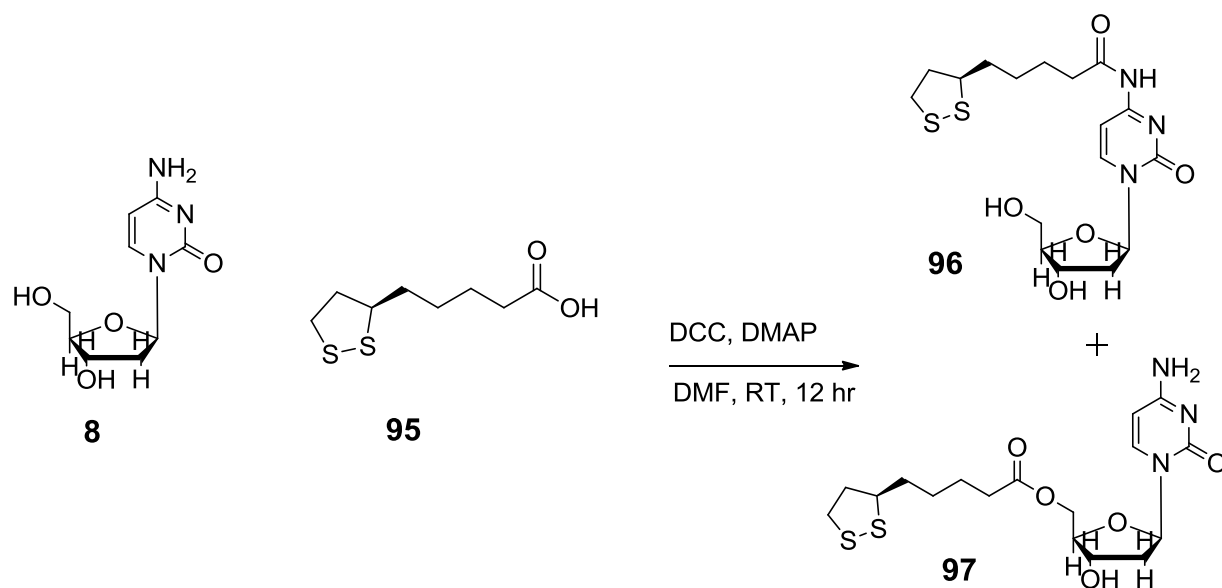
Scheme 9: Reaction between cytidine and lipoic acid

Following the reaction of cytidine **8** with lipoic acid **95** the same conditions were employed for the reaction of gemcitabine **7** with lipoic acid **95**. By using the same reagents and conditions only one product **98** was formed, as indicated by TLC and the NMR spectrum of the product obtained after chromatography.
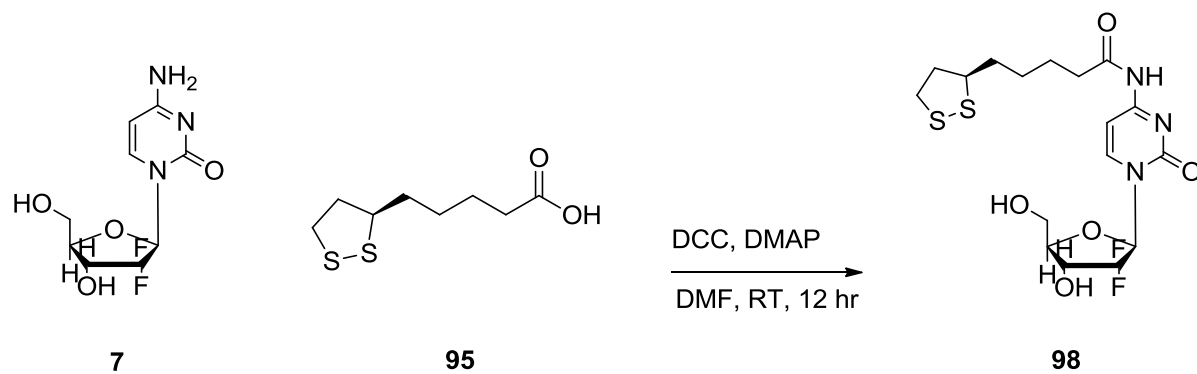
Scheme 10: Reaction between gemcitabine and lipoic acid.

3.4.3 Characterisation of gemcitabine–lipoic acid derivative

The goal of this reaction was to synthesise a prodrug of gemcitabine by coupling it with a lipoic acid residue to give the corresponding lipoamide. It was assumed that the reaction would yield a mixture of products as was observed in the cytosine model, i.e. substitution on either the primary amine and/or the primary hydroxyl of gemcitabine. This seemed a reasonable expectation since the gemcitabine was reacted without any prior protection of functional groups to avoid any unwanted products, a decision driven by a desire to remove any unnecessary steps from the synthetic strategy. Surprisingly, a single product was indicated by the spectroscopic data and following thorough characterisation of the product it was determined that the site of coupling of the lipoic acid residue to gemcitabine was the primary amino group attached to the pyrimidine moiety of gemcitabine (compound **98**)
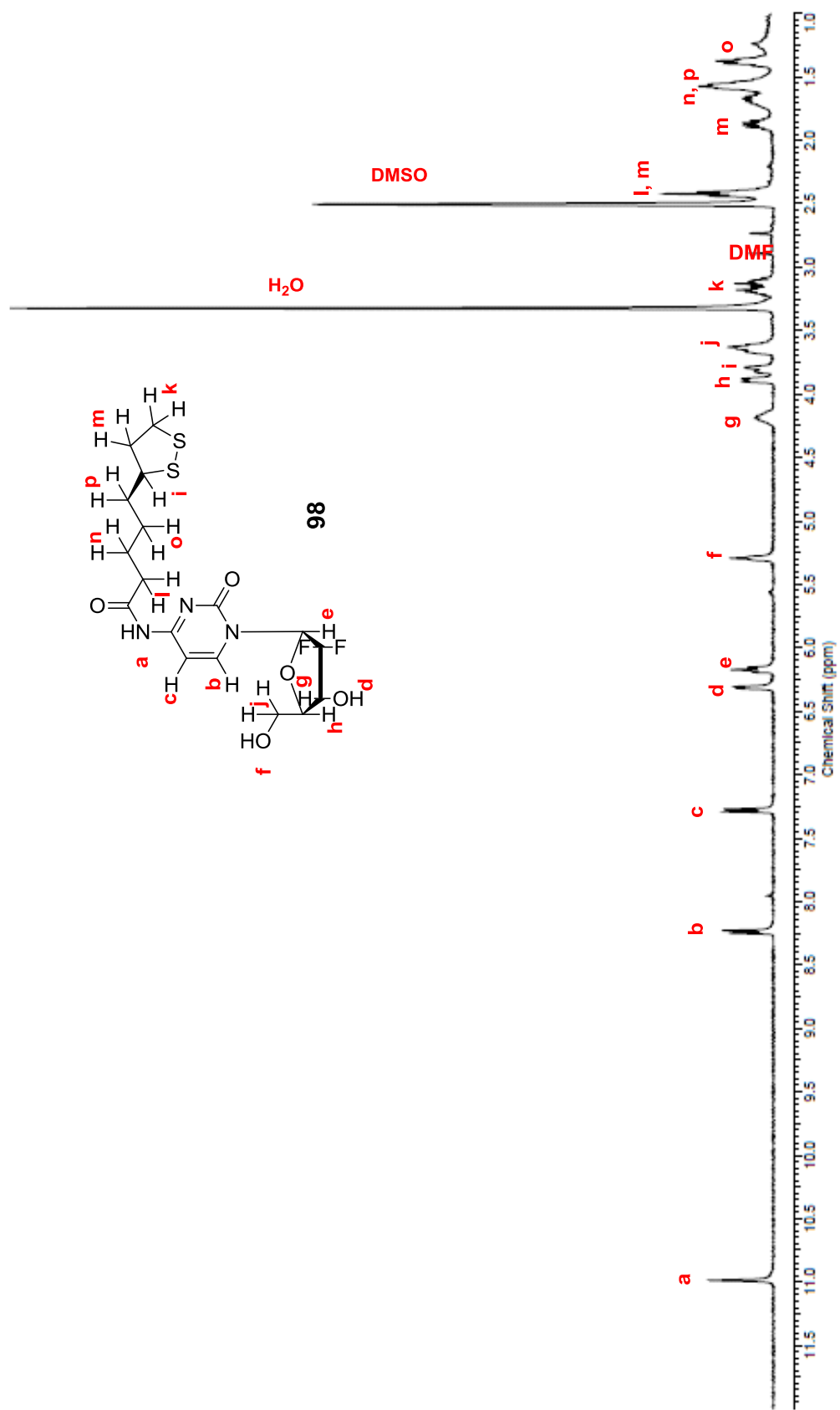
Figure 51: ¹H NMR spectrum of gemcitabine-lipoic cid prodrug in DMSO carried out using 400 MHz NMR machine at 25℃

3.4.3.1 ^{1}H NMR spectrum of 98

The ^{1}H NMR spectrum (Figure 51) of **98** (400 MHz DMSO-d6, 25°C) showed the following peaks: δ= 11.03 (s, 1H, a), 8.27 (d, 1H, b), 7.30 (d, 1H, c), 6.36 (d, 1H, d), 6.20 (t, 1H, e), 5.35 (t, 1H, f), 4.20 (m, 1H, g), 3.91 (m, 1H, h), 3.82 (m, 1H, i), 3.65 (m, 2H, j), 3.18 (m, 2H, k), 2.44 (m, 3H, l, m), 1.93 (m, 1H, m), 1.68 (m, 1H, n), 1.25 (m, 1H, n), 1.58 (m, 2H, p), 1.39 (m, 2H, o) ppm.

Comparing the data acquired for **98** with ^{1}H NMR data for the gemcitabine **7** starting material, the pyrimidine protons (b and c) had shifted from 8.19 (d 1H), 6.29 (d 1H), for gemcitabine hydrochloride to 8.27 (d [b], 1H), 7.30 (d [c], 1H) for **98** (Figure 52). These findings were the first indicator of lipoic acid coupling to the pyrimidine part of gemcitabine.
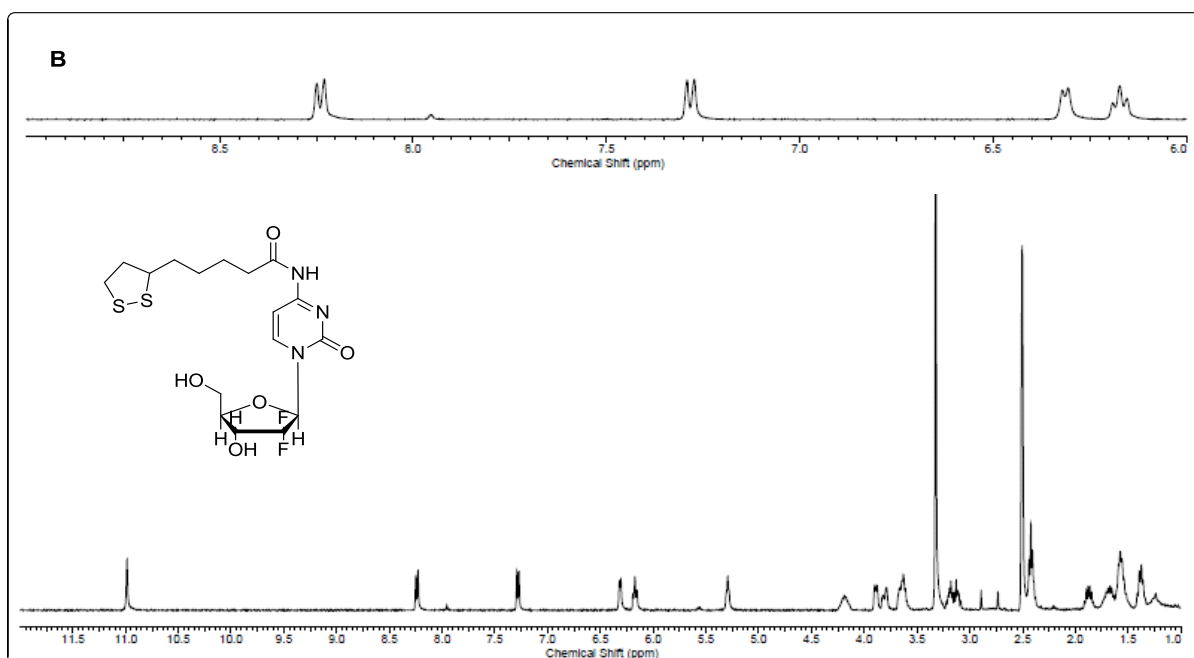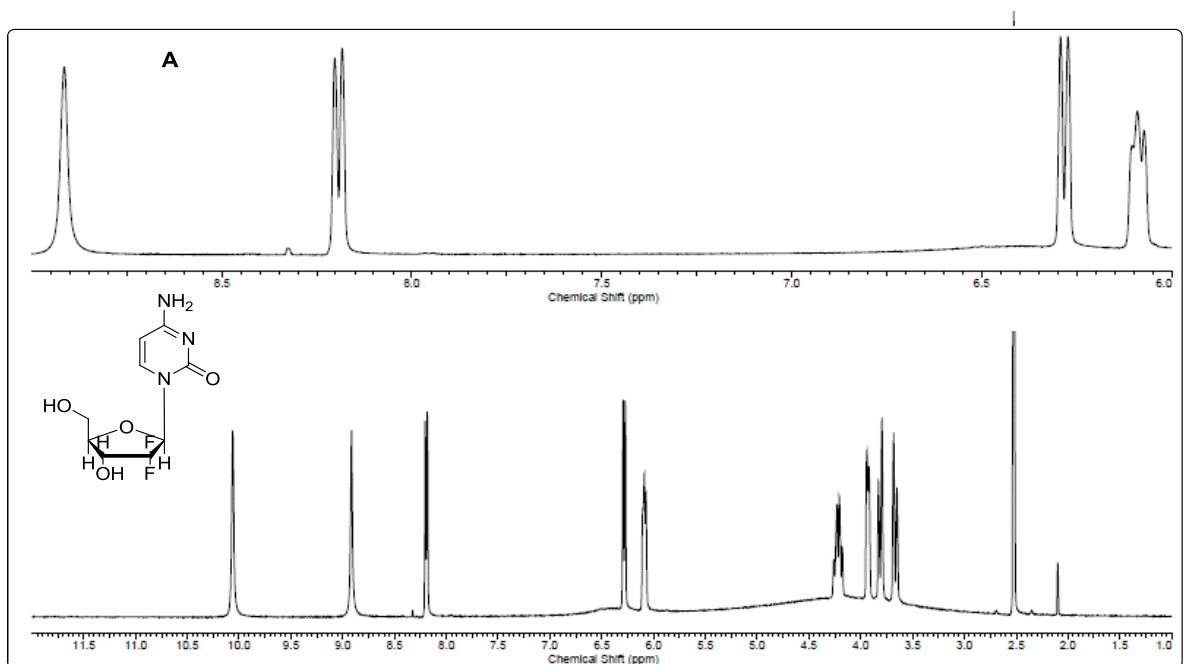
Figure 52: ^{1}H NMR spectrum of gemcitabine HCl (A) and GL pro-drug **98** (B) in DMSO-d6 carried out using 400MHz NMR at 25 °C

3.4.3.2 ^{13}C and DEPT-135 NMR Spectrum of 98

^{13}C NMR detects carbon nuclei. Distortionless Enhancement of Polarisation Transfer (DEPT) is another ^{13}C NMR experiment in which carbon nuclei may be differentiated based upon their substitution. In a DEPT-135 experiment the spectra shows the CH_3 and CH signals above the base line but the $-CH_2-$ signals appear inverted below the base line and quaternary carbons are not visible using this ^{13}C NMR experiment. Therefore, DEPT-135 can be used to confirm the number of hydrogens attached to carbons within a compound (Loudon 2002b).

Figure 53 and Figure 54 show the ^{13}C and DEPT-135 NMR data acquired for compound **98:** aliphatic hydrocarbons ($-CH_2-$) appear between 25 – 72 ppm with aromatic carbons from the pyrimidine group between 122 – 138 ppm. The amide (N-C=O) groups were observed at 174 ppm. The DEPT-135 spectrum (Figure 54) showed that the $-CH_2-$ groups present in the lipoic acid residue were inverted, between 25 – 40 ppm, and the quaternary carbons, for example the carbonyl peak from the amide (174 ppm) had disappeared.
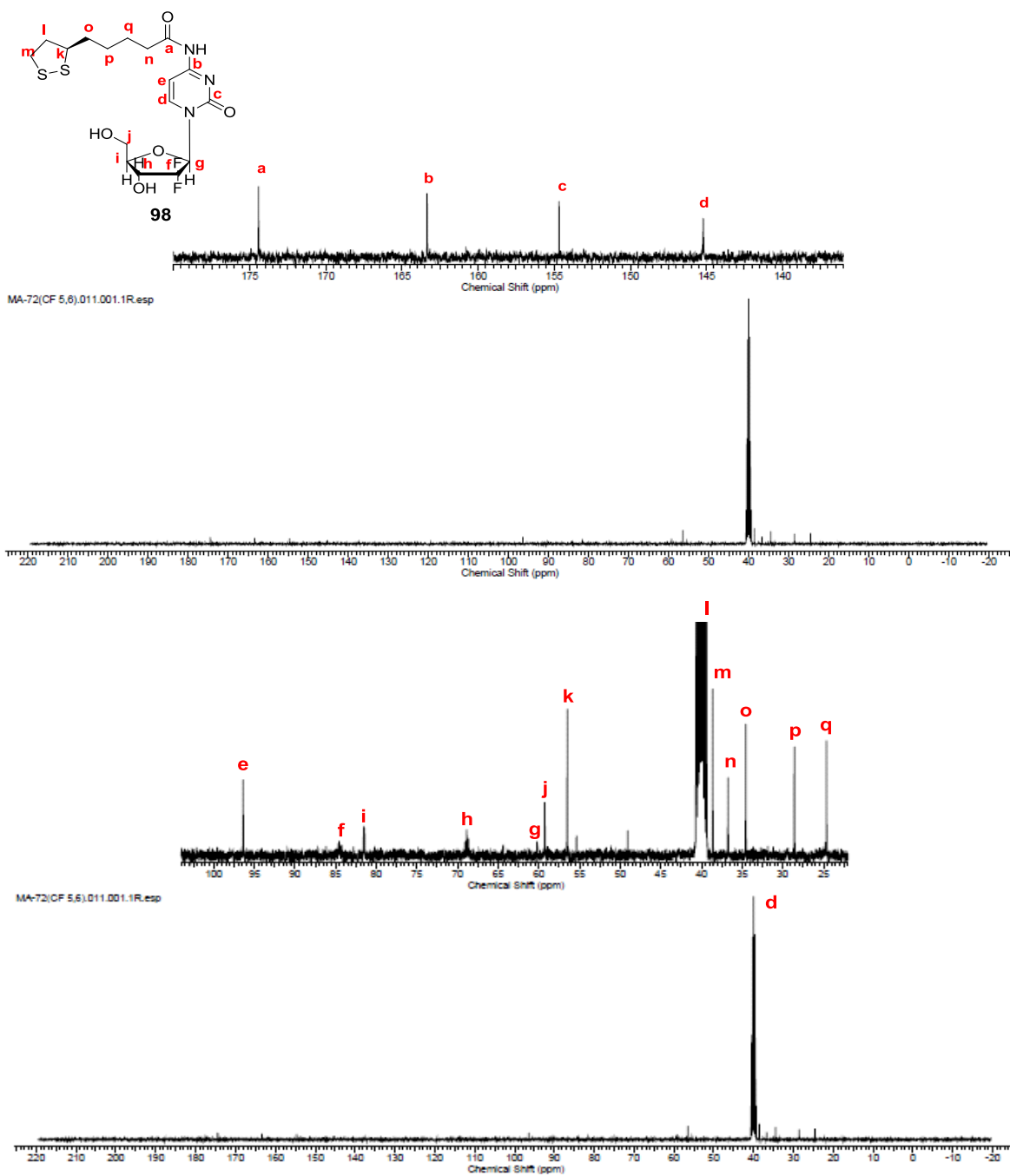
Figure 53: ^{13}C NMR spectrum of **98** in DMSO-d6 carried out using 400MHz NMR at 25 °C
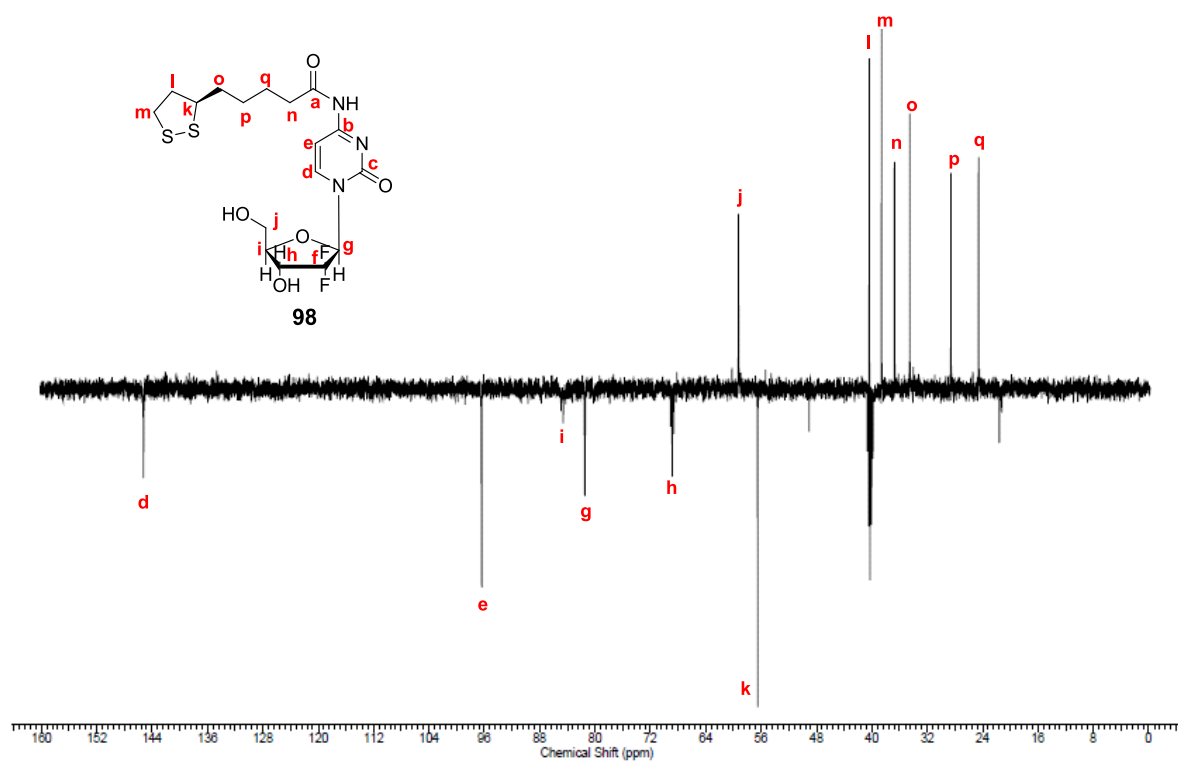
Figure 54: DEPT 135 NMR spectrum of **98** in DMSO-d6 carried out using 400MHz
NMR at 25 °C

3.4.3.3 Two-dimensional NMR spectrum of 98

Two-dimensional nuclear magnetic resonance spectroscopy (2D NMR) is an accustomed method of (NMR) spectroscopy measurements which provide data plotted in two frequency axes rather than one. 2D NMR afford additional information about a molecule in addition to the one-dimensional NMR spectra and are particularly beneficial in molecule structure determination, typically for molecules that are too complicated to work with using one-dimensional NMR (Aue 1976; Ernst *et al.* 1987).

Heteronuclear single-quantum correlation spectroscopy (HSQC) experiment (Figure 55 and Figure 56) which correlate ^{1}H NMR with the DEPT-135 of compound **98**, is just confirming the data acquired by both the ^{1}H NMR and ^{13}C, DEPT 135.

Heteronuclear multiple-bond correlation spectroscopy (HMBC) (Figure 57) detects heteronuclear correlations over longer ranges of bonds (about 2-4 bonds).

HMBC experiment was selected to be the one which could show the site of coupling of lipoic acid to gemcitabine (the primary amine site of gemcitabine). The data in (Figure 57) show the assignment of the singlet at δ= 11.03 (**a**) relation to the peak at 96 which belongs to the pyrimidine carbon atom next to tertiary amine (**e**) which could serve as strong evidence of the site of coupling.
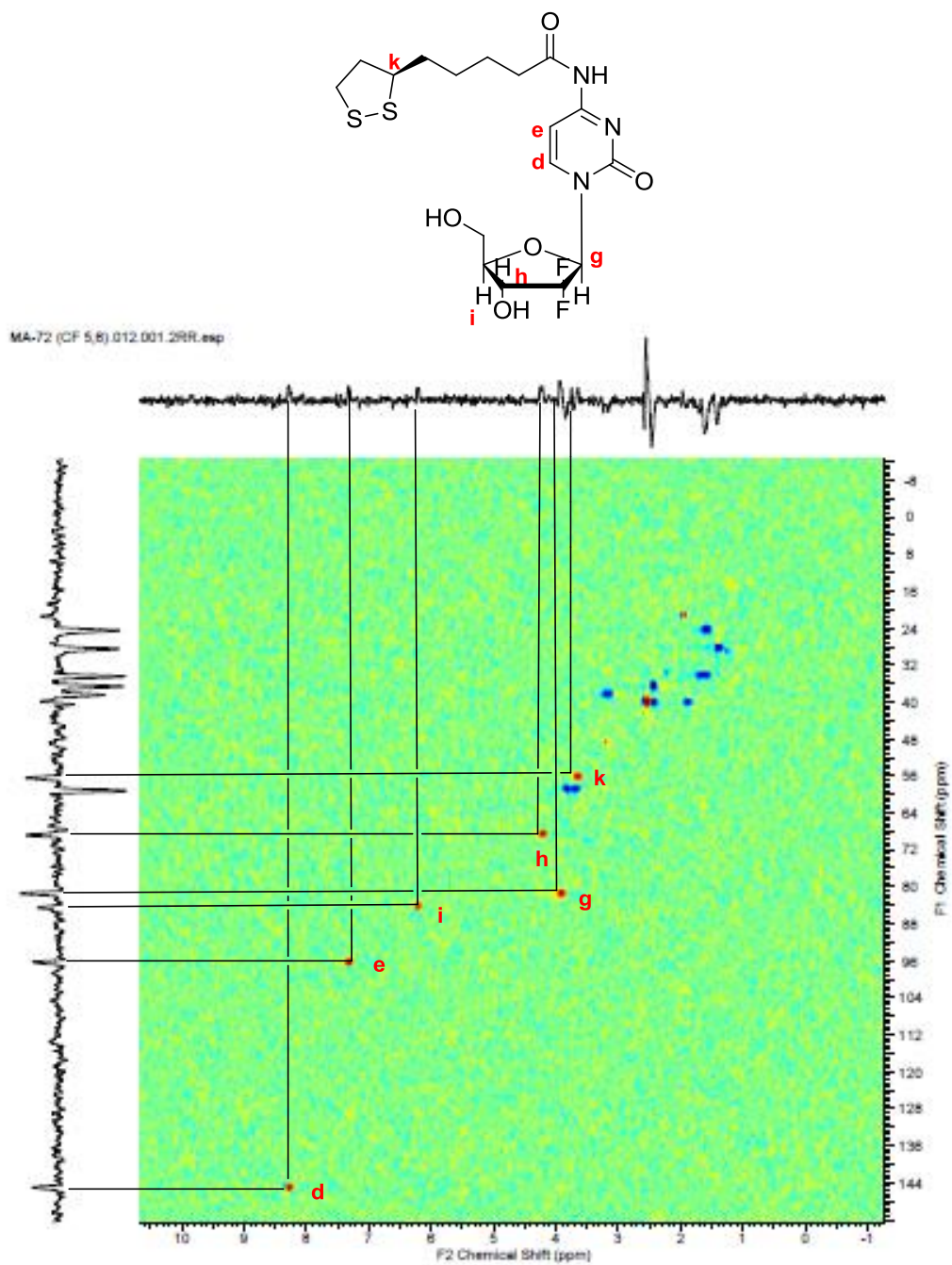
Figure 55: HSQC NMR spectrum of **98** in DMSO-d6 carried out using 400MHz NMR at 25 °C, showing CH and CH$_3$
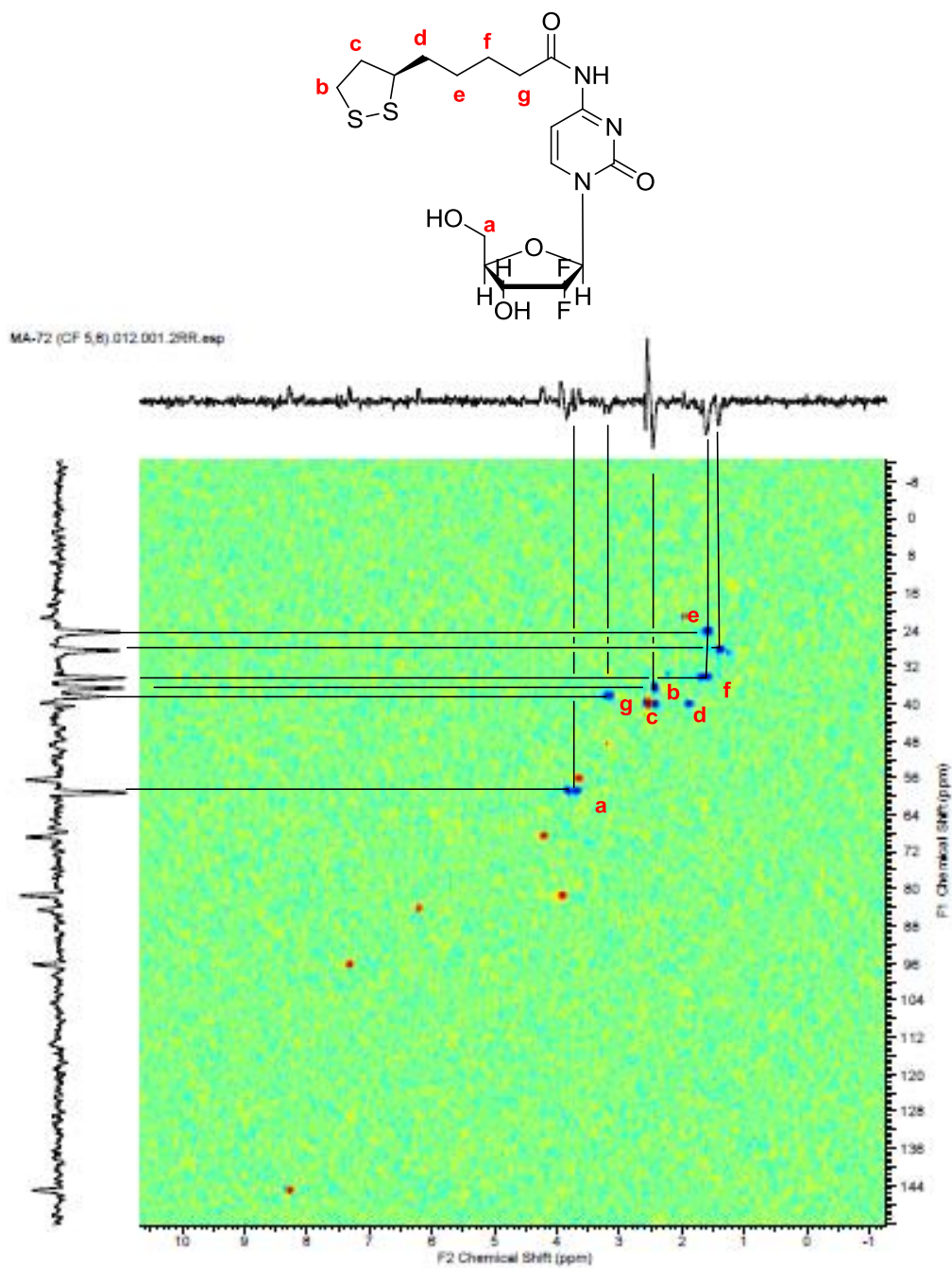
Figure 56: HSQC NMR spectrum of **98** in DMSO-d6 carried out using 400MHz NMR at 25 °C, showing CH$_2$
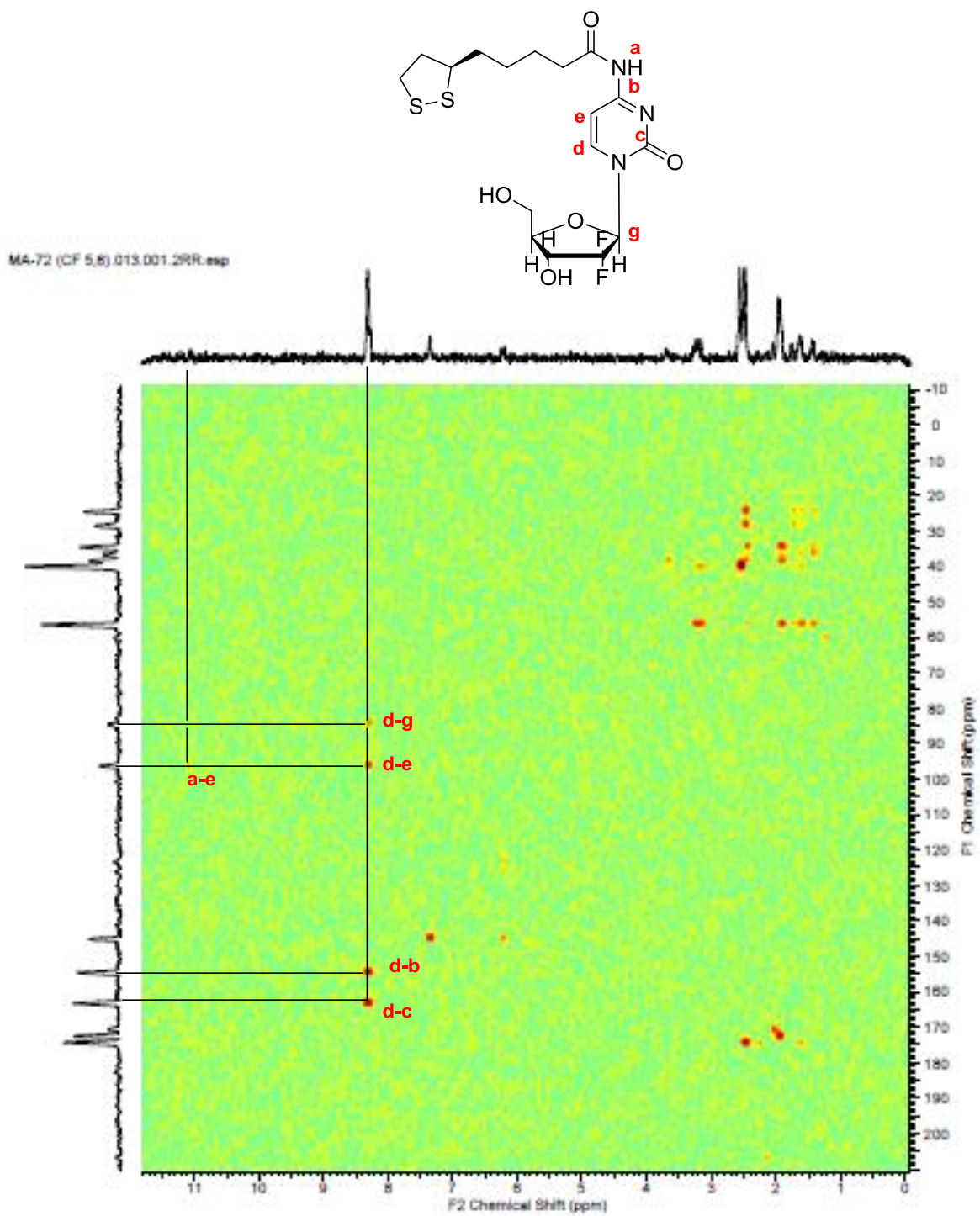
Figure 57: HMBC NMR spectrum of **98** in DMSO-d6 carried out using 400MHz NMR at 25 °C

3.4.3.4 Mass spectrometry analysis of gemcitabine-lipoic acid prodrug 98

Mass spectrometry applied in the field of analytical chemistry as a tool to characterise chemical (after ionizing them) according to their mass/charge ratio. Compounds masses measurement by mass spectrum is represented as a plot of ion signal to define the mass and hence to interpret the chemical structure.

The typical procedure of mass spectroscopy involves ionisation of the sample by bombarding it with electrons and then sorting the resulting charged fragments according to their mass/charge ratio by subjecting them to an electrical or magnetic field (Hoffmann & Stroobant 2007).

Mass spectrometry of the synthesised GL prodrug was acquired from NMSF (EPSRC National Mass Spectrometry Facility). The relevant area of the resultant spectrum is shown in (Figure 58). The formula mass of GL prodrug is 451.51 g/mol, and the most abundant peak occurs at an m/z value of 452.112 which is the mass/charge of a protonated (M+H+) form of GL prodrug **98.**
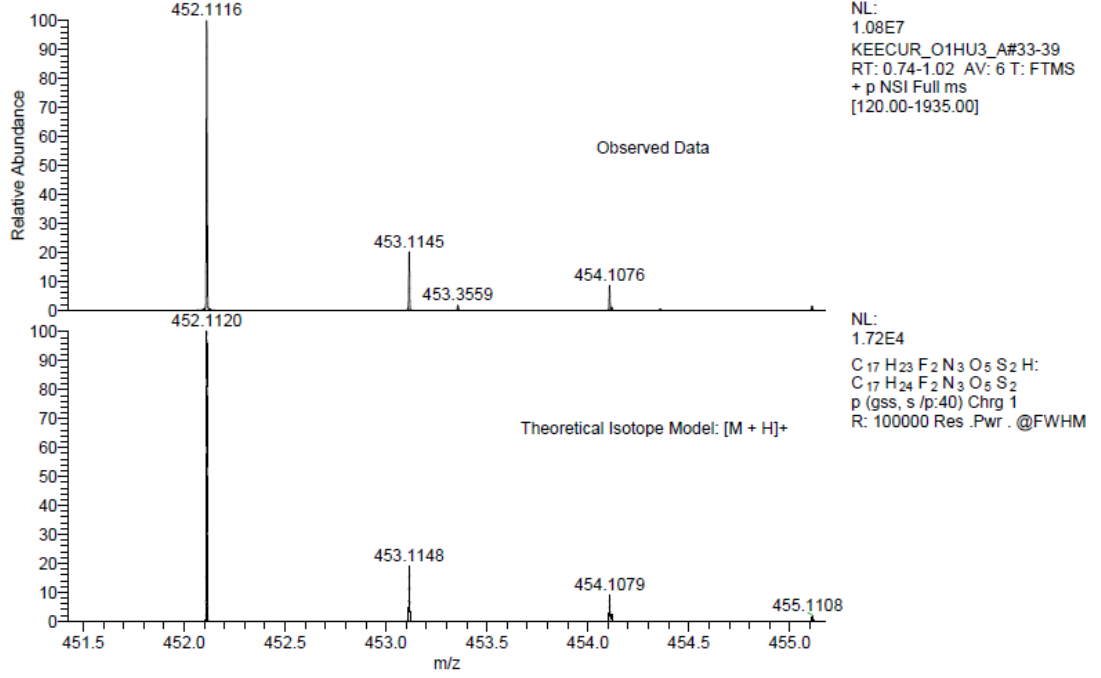
Figure 58: Mass spectrum of gemcitabine-lipoic acid (GL) prodrug **98**

3.4.4 Scaling up the synthesis of prodrug 98

The reaction conditions employed for the coupling of gemcitabine **7** to lipoic acid **95** were effective when the reaction was undertaken at a very low scale. However, the capricious yields obtained, often as low as 5% meant there was a great need to scale the reaction up in order to have a sufficient amount of the product in hand in order to be able to undertake the full battery of experiments with the hybrid nanoparticles later on in the project.

A scaled-up reaction was designed and conducted following the same procedures as applied for the small-scale synthesis of the prodrug **98** but unexpectedly no reaction was observed even though the reaction was monitored carefully by TLC and NMR spectroscopy. This reaction was repeated a number of times with the same outcome, no reaction observed and isolation of the starting materials.

3.4.4.1 Attempts to scale up the synthesis of prodrug 98

A number of other coupling reactions were designed utilising different strategies and performed in an attempt to isolate the product in a good yield but unfortunately not one of the reactions succeeded. These experiments focussed solely on obtaining compound **98** rather than trying to discover and isolate any other of products from the coupling of lipoic acid **95** to a hydroxyl group of gemcitabine.

Methods for formation of amide bonds using coupling agents have been reviewed (Albericio 2004; Montalbetti & Falque 2005; Valeur & Bradley 2009) and a significant number of these methods were used in small scale experiments in order to find a method which gave the highest yield. These attempts were in

addition to the initial attempts that had been tried to optimise the simple protocol applied originally in the synthesis of **98**.

Unfortunately, all the alternative protocols used either gave no reaction or yielded a very small quantity of a mixture of compounds which were difficult to purify. Efforts were divided into three broad strategies, the first being a one-pot method where the reactants are combined with the coupling reagents in one step. The second method focused on the prior protection of the reactive hydroxyl groups in the gemcitabine structure by selectively adding Boc groups to get the advantages of dealing with 3′, 5′-O-Bis Boc gemcitabine which is highly soluble in a variety of organic solvents (Guo & Gallo 1999). The third method was to pre-react lipoic acid with thionyl chloride or *N*-hydroxysuccinamide before further reaction with gemcitabine.

Figure 59 summarises the methods applied to obtain the prodrug **98**. It should be noted that each of these reactions were attempted a number times and using slightly different conditions in order to eliminate as many variables as possible.
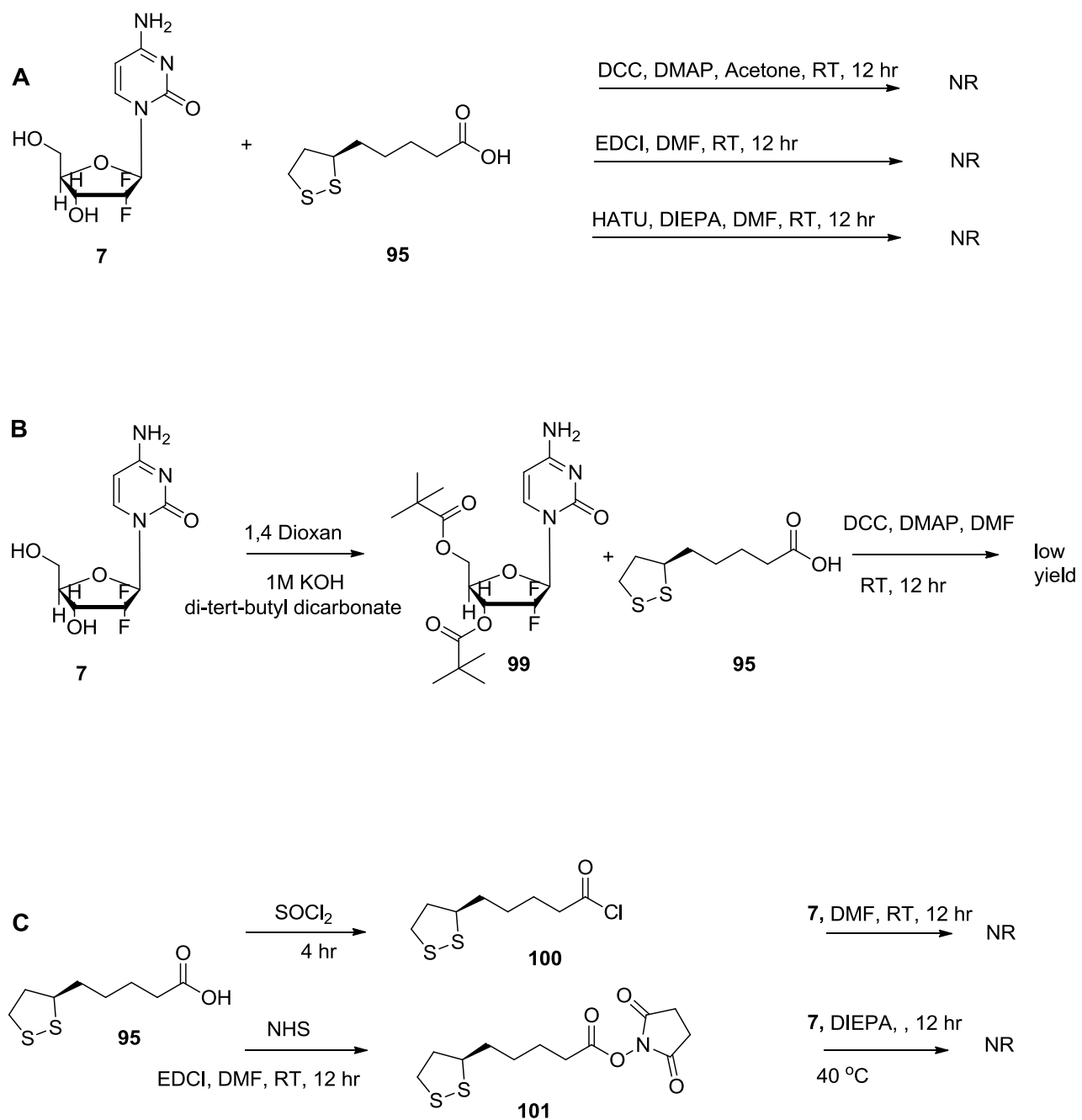
Figure 59: Schematic presentation of failed coupling attempts of lipoic acid and gemcitabine

It became clear from these numerous attempts to tackle the problem of low yield that obtaining a sufficient amount of prodrug **98** for further conjugation and release studies with HNPs as well as *in vitro* biological studies would be challenging.

The focus then returned to the protocol used for the small-scale synthesis of compound **98**. It was deduced that a step-wise addition of DCC to a solution of lipoic acid and waiting for a specific time to allow preformation of the acid-carbodiimide adduct intermediate was essential before addition of gemcitabine to the reaction mixture (Figure 60). The timing is critical in this process, as are anhydrous reaction conditions, but this proved to be the solution for the scaling up issue. This deduction was based upon the observation of a white precipitate from reaction of lipoic acid with DCC prior to addition of gemcitabine. Formation of this adduct is essential to form the prodrug **98** and further optimisation finally delivered a protocol that gives a good yield of the desired product **98,** which is consistently >40 %. Also, the yield of the expected products from reaction with the unprotected primary hydroxyl groups of gemcitabine did not increase and the desired product could be isolated readily. In summary, for the large-scale synthesis of prodrug **98** the key consideration is the time required to form the intermediate shown in (Figure 61)prior to the coupling with gemcitabine.
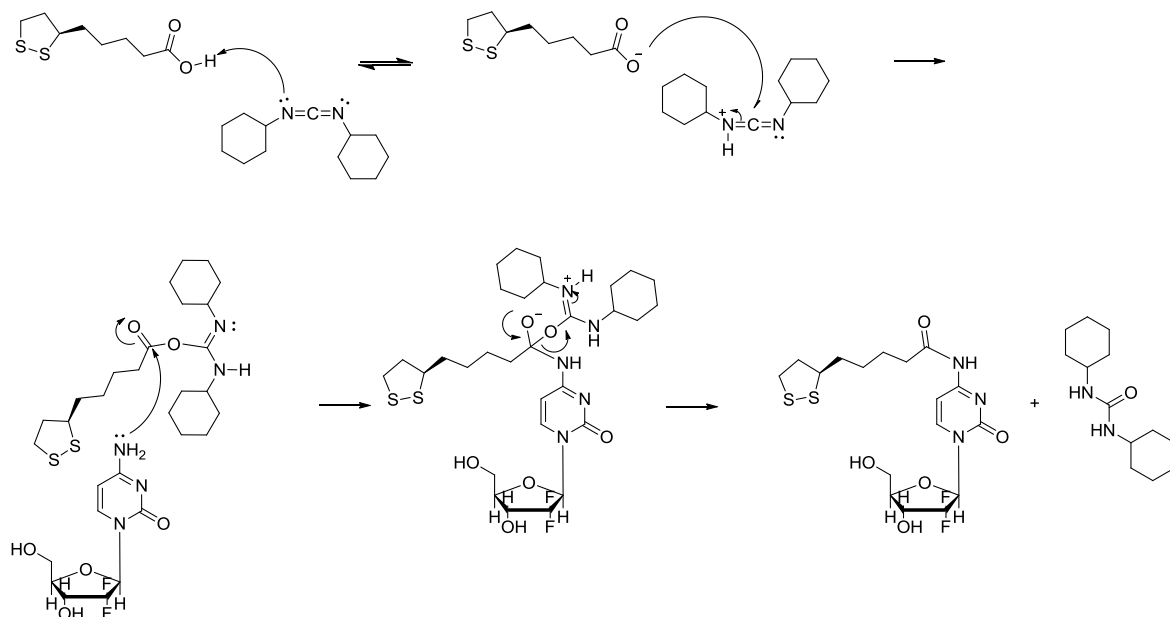
Figure 60: proposed mechanism of lipoic acid coupling to gemcitabine using DCC as coupling agent
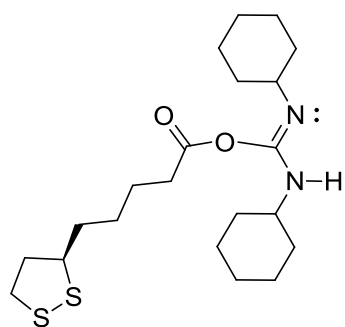
Figure 61: proposed structure of lipoic acid derivative prior to being coupled to gemcitabine

3.5 Conclusion

The synthesis of a prodrug derived from the reaction of gemcitabine with a spermine derivative was not successfully completed due to a series of difficult synthetic and purification steps. This remains a worthwhile challenge to face because the hypothesis is sound but the execution requires further investigation.

Synthesis and characterisation of a prodrug of gemcitabine **98** was successfully completed. Compounds bearing thiol or disulfide bonds can bind to gold nanoparticles by means of dative covalent bonds, a covalent bond in which one atom donates the electrons to be shared between the two atoms involved. The presence of disulfides on prodrug **98** may allow the formation of a dative bond with the gold surface of hybrid nanoparticles (Figure 62). The next task involved assessing the attachment of prodrug **98** to the hybrid nanoparticles and to test the drug release rates from the formulation, leading ultimately to an investigation of the impact of the formulation on cell proliferation.
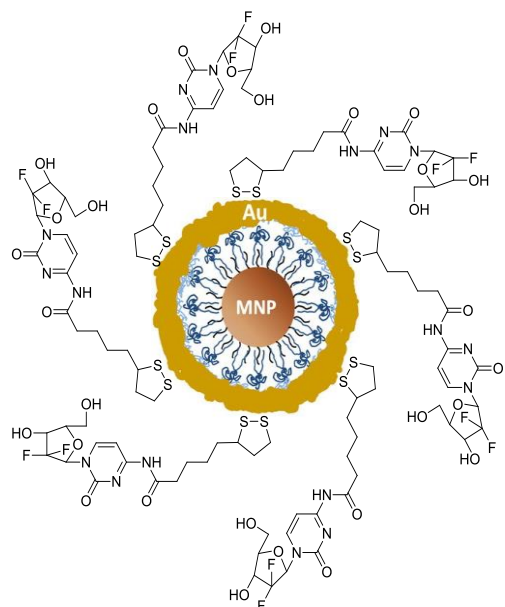
Figure 62: theorotical imagination of gemcitabine-lipoic acid prodrug coupling to the surface of the hybrid iron oxide core gold shell nanoparticles

CHAPTER 4: SYNTHESIS AND CHARACTERISATION OF HYBRID NANOPARTICLES AND GL PRODRUG RELEASE PROFILES

4.1 Background

The heterogeneous nature of cancer together with the common limitations of nearly all current cancer treatments, particularly the narrow patient population range in which such drugs are effective, mean that cancer remains a challenging disease to treat. For example, gemcitabine **7** is only effective in less than 25% of pancreatic cancer patient (Burris *et al.* 1997). Additionally, the effects of treatments might be confined to a certain stage of the disease which necessities the idea of combining diagnosis and treatment in one effective system. The term "theranostic" is used to describe agents with dual diagnostic and therapeutic abilities; theranostic might bring more promise to improve patient prognosis (Xie *et al.* 2010; Xie & Jon 2012).

Many materials have been investigated to explore their potential as imaging or therapeutic agents with many nanoparticulate systems being aimed towards the diagnosis or treatment of cancer (Nune *et al.* 2009). The combination of imaging and therapy in nanoparticle systems requires sufficient accumulation of such agents in diseased areas in order to overcome common specificity problems associated with chemotherapeutic agents and to achieve effective cancer treatment (Xie *et al.* 2010).

Theranostic nanoparticles, as the name indicates, are nano-sized particle systems designed to have diagnostic and therapeutic abilities, hopefully to provide more patient specific and tailored disease management. Ideal criteria for theranostic nanoparticles includes: being biologically safe, the ability to accumulate in the chosen area of interest, have the ability to carry and deliver the requisite amount

of drug(s) to the site of action without affecting the nearby organs, detect and report disease characteristics and be able to be cleared or metabolised by the body into a safe form (Xie *et al*. 2010; Jokerst & Gambhir 2011; Chen *et al*. 2014). Despite the fact that several potential theranostic nanoparticles had been synthesised and tested for cancer therapy none of them meet all the required ideal criteria (Xie *et al.* 2010; Lammers *et al*. 2011; Chen *et al*. 2014).

Nanoparticles with sizes ranging from 10-200 nm are favourable for active cellular uptake, high drug loading and specific targeting to the tumour, either through passive or active targeting (Duncan 2003; Davis *et al*. 2008).

Among all the physicochemical properties of nanoparticles, including shape, size and surface charge, the size of nanoparticles has a significant contribution to the ability of the particles to penetrate tumour tissues and being taken up and cleared by cells. The size is also the main regulator of nanoparticle bio-distribution inside the body and hence on the overall therapeutic effects (Tang *et al*. 2014).

Most approved anticancer nanomedicines comprise nanoparticles in the size range between 100-200 nm (Uster *et al*. 1998; Gradishar *et al*. 2005). Smaller sized anticancer nanomedicines have shown higher therapeutic effects *in vivo*, especially nanoparticles with 50 nm diameter (Cabral *et al*. 2011; Tang *et al*. 2014). Very small nanoparticles (< 2 nm) and relatively small nanoparticles (<10 nm) were shown to travel freely into tumour tissues and being cleared rapidly into the blood stream without effective accumulation inside the tumour (Matsumura & Maeda 1986; Dreher *et al*. 2006).

The optimal size range of nanoparticles intended to be used for cancer treatments should also consider both renal clearance (renal clearance threshold is<10–15 nm (Choi *et al.* 2011; Shilo *et al.* 2012)) and the interstitial/lymphatic clearance (<20 nm) (Moghimi *et al.* 2005).

A study by Tang *et al* (2014) demonstrates that 50 nm diameter nanoparticles show the highest tumour retention time: they compared the use of 20 nm, 50 nm and 200 nm diameter silica particles as drug carriers for breast cancer treatments. The tumour retention time observed in the study was used as a parameter to reflect the deep tumour penetration, nanoparticle uptake by cancer cell, the rate of nanoparticle clearance from tumour tissues and, consequently, the anticancer efficacy (Tang *et al.* 2014).

As described before in chapter one, passive tumour targeting by nanoparticulate systems is thought to be due to the enhanced permeability and retention effect (EPR), in which nanoparticle drug carrier systems, including liposomes and polymeric micelles, tend to be accumulated in the tumour tissues more preferentially than normal tissues because of the undeveloped "leaky" tumour blood vessels and also due to the absence of lymphatic drainage inside the tumour. The EPR phenomenon (Figure 13) leads to nano-sized particles being absorbed and preserved within the target cells (Matsumura & Maeda 1986).
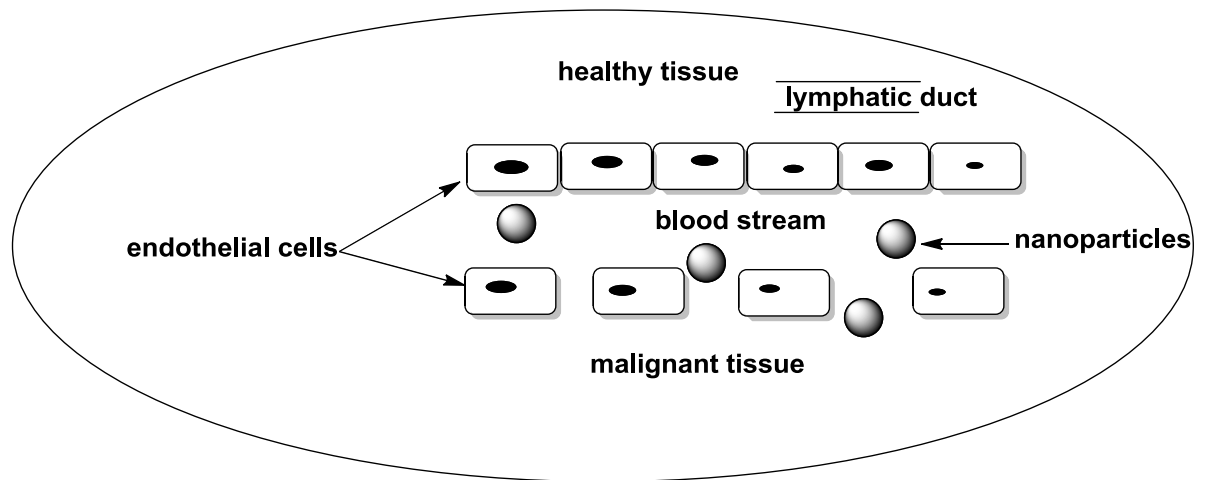
Figure 63: Diagram explaining EPR criteria of tumour vasculature

The differences between the blood vessels within a solid tumour and normal tissues in terms of both their physiological and morphological character has been examined and described (Ruoslahti 2002; Bae *et al.* 2011; Jain 2012). Due to the rapid angiogenesis in cancerous tissues an irregular blood vessel arrangement results when compared to the structured vasculature of normal tissues (Morikawa *et al.* 2002; Campbell 2006). Additionally, the permeability of the tumour vasculature, the gap size in the tumour vessel wall is remarkably higher than in healthy tissues. The rate of endothelial cell growth is also higher than in healthy tissues (Yuan *et al.* 1995).

Furthermore, retention of accumulated nanoparticles within the tumour tissues is observed because of the absence of a lymphatic system which is normally present for drainage of macromolecules in normal tissues (Peer *et al.* 2007).

As a result, the EPR effect provides a passive way of nanosystem accumulation and retention permitting potential effective anticancer therapy with minimum drug toxicity (Bae *et al.* 2011).

4.1.1.1 Hybrid iron oxide core gold shell nanoparticles (HNPs)

The hybrid nanosystem used in this present study is composed of both gold as the outer shell and iron oxide as a core and which may hold significant potential as a drug delivery vehicle (Barnett *et al.* 2013; Hoskins *et al.* 2012): The magnetic character of the iron oxide core permits imaging and potential guiding of the hybrid system together with the advantages of the gold shell which can be exploited for heating and the potential to be loaded with a drug, either by electrostatic interaction or by utilising the well described gold-thiol interaction.

Iron oxide metal nanoparticles have high magnetic character and a surface able to be functionalised by several biologically useful agents; the targeting of diseased tissues by magnetic iron oxide nanoparticles has been reported using functionalisation of nanoparticle surfaces with antibodies, nucleosides, proteins and enzymes (Peng *et al.* 2008; Hwu *et al.* 2009; Nune *et al.* 2009).

Surface coating of nanoparticles has been shown to alter the *in vivo* behaviour of the nanoparticles: many nanoparticle technologies use poly ethylene glycol (PEG) to prolong circulation times in the blood, reduce uptake by the reticuloendothelial system (RES), increase the circulation half-life and improve accumulation in target tissues.(Nune *et al.* 2009). Polymer coating of iron oxide nanoparticles using dextran and poly(ethylenimine), for example, has been shown to improve biocompatibility and stability (Sun *et al.* 2008; Nune *et al.* 2009; Karimazadeh *et al.*

2017). Poly (ethylenimine) is a polymer containing multiple amino groups each separated by two carbon atoms (Figure 64). Poly(ethylenimine) has a poly-cationic character which makes it suitable for coating iron oxide nanoparticles to provide both the advantage of preventing the iron oxide core from being aggregated into large particle and providing a functional surface for a gold seed to be settled on to the surface of the iron oxide core.
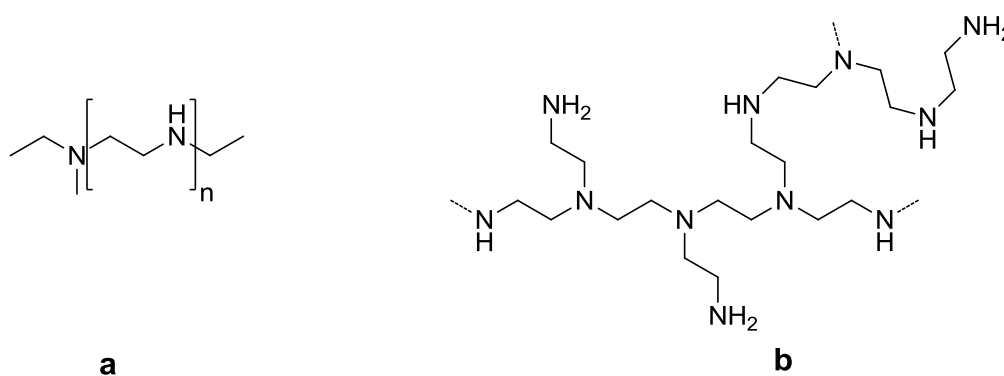
Figure 64: chemical structure of poly(ethyleneimine) polymer; **a**: repeating unit of poly(ethylenimine) polymer; **b**: typical branched poly(ethylemimine) fragment

Magnetic resonance imaging (MRI) of iron oxide nanoparticles is a non-invasive technique used routinely in clinical medicine for imaging the function and structure of tissues. MRI relies on the difference in behaviour of protons in the presence and absence of an applied magnetic field and within this field the iron oxide nanoparticles have a high saturation magnetisation and increased loss of magnetisation when the magnetic field is removed (Nune *et al.* 2009). Iron oxide

nanoparticles are associated with significant advantages as a contrast agents because of their biocompatibility and high sensitivity in low to moderate concentration (Bellin 2006; Jun *et a*l. 2008).

Thermal ablation of cancerous tissues using gold nanoparticles as a source of heat after irradiation by near infrared laser light is an almost non-invasive technique which is easy to apply with high potential ability to kill malignant tissues in vital regions, especially when surgical removal is not a choice (Vigderman & Zubarev 2013; Mocan *et al.* 2016). Cell death following irreversible cellular damage may eventually occur when tissue is heated to 42 °C (Cobley *et al.* 2010). Gold nanoparticles have the ability to convert the absorbed laser light into heat and, consequently, an increased temperature will result in the surrounding tissues where the nanoparticles are located. Laser irradiation is essential for tissue penetration during photothermal ablation procedures *in vivo* (Liu *et al.* 2008; Guo *et al.* 2013). A temperature of up to 80 °C has been recorded for gold nanoparticles after light absorption (Huang *et al.* 2006; Cai *et al.* 2008). The ability of gold nanoparticles to produce heat following light irradiation and the cell death observed subsequently is due to the basic physical properties of gold in response to light exposure. This behaviour is known as surface plasmon resonance (SPR). SPR happens when a gold particle is exposed to light at a specific wave length and free electrons on the surface of the particles start to oscillate in response to the oscillation of the electromagnetic field of the light. Electron oscillation on the particle surface causes a charge separation and hence dipole oscillation along the electrical field of light. The SPR intensity and wavelength is affected by particle

shape, size and other factors that might affect the electron density distribution on the surface of the particles (Huang & El-Sayed 2010).

Gold nanoparticles have been investigated in diverse areas including drug delivery (Cai *et al.* 2008). A heat triggered release study of a drug payload using HNPs as a Nano-carrier benefiting from the advantages of deep tumour penetration by nanoparticles aiming to increase the drug efficacy highlights the potential use of HNPs as thermal switches in heat triggered drug delivery (Curtis *et al.* 2015). The challenges highlighted by the Curtis *et al.* (2015) study of the HNPs as a thermally triggered system for targeted drug delivery, hypothesised the use of a heat responsive linker that holds the drug to the gold surface of the HNPs. The distance of the thermal labile linker from the gold surface and the heat control of gold surface to provide drug release before cell damage (Curtis *et al.* 2015).

4.1.1.2 Drug-nanoparticle formulation

A dumbbell shape nano-sized system in which cisplatin was coupled to a gold surface and guided by an antibody (HER2) attached on the surface of the accompanying iron oxide part of the system has been used as a drug delivery vehicle (Xu *et al.* 2009). The system has the advantages of multiple functionality and a diversity of ligands available which can act independently. The cisplatin release profile from the nanocomposite to the external environment showed that a low percentage of the drug was released from the nanosystem in the first two hours. Release increased when the pH was similar to the endosome/lysosome environment (low pH), demonstrating that the drug release would be enhanced after internalisation of the nanocomposites into the cells. The cell viability tests for

the drug-nanocomposite system, cisplatin, and control were compared which indicated that the cytotoxicity of the drug-nanocomposite system was greatly increased compared to the free drug (Xu *et al*. 2009; Leung *et al*. 2012).

Clinical trials using nanoparticles, including colloidal gold as therapeutic agents for pancreatic cancer treatment, have shown that nanoparticles in conjunction with chemotherapeutic agents can improve the efficacy of the anticancer agents by increasing the delivery, cellular targeting and also reducing associated adverse effects because nanoparticles have the ability to overcome some of the difficulties faced by conventional chemotherapeutic agents (Au *et al*. 2016).

In drug delivery approaches utilising nano-sized systems as a carrier, the drugs are either encapsulated inside or loaded on the surface of the nanoparticles. Regarding the iron oxide core gold shell hybrid nanoparticles it has been shown by Bhadra *et al* (2002) and Jokerst *et al* (2011) that this kind of nanoparticle coated with PEG has a chance to be an effective drug delivery system as it has a longer blood circulating period compared with conventional therapies (Bhadra *et al*. 2002; Jokerst *et al*. 2011).

4.2 Aim

The aim of the following study was to synthesise Hybrid iron oxide core gold shell nanoparticles (HNPs). Characterisation of the particulate species was performed at each step of the synthesis by determining the size and charge using Zeta potential measurements, the metal content of the HNPs by using ICP-OES, the UV/visible light absorbance of the metal particles by using UV/Vis. spectroscopy

and the shape and final size of the HNPs by using transmission electron microscopy (TEM).

The subsequent aim was to study the interaction of gemcitabine analogue-lipoic acid (GL) prodrug **98** with the surface gold of the HNPs with and without a thiol capped polyethylene glycol (Thiol-PEG) present. Subsequent investigations into the potential for the nanoparticulate formulation to act as a pH and/or heat responsive drug delivery system *in vitro* required prodrug loading and drug release studies to be undertaken, monitored by HPLC.

4.3 Materia and methods

4.3.1 Materials used

The following tables includes all the material used in the synthetic and characterisation procedures for HNPs as well as materials used in the following loading and release study of the GL prodrug onto the gold surface of the HNPs.

Table 2: Materials used in synthesis and characterisation of gold iron oxide hybrid nanoparticle

Material	Suppliers
Absolute ethanol	Sigma-Aldrich Co., UK
Chloroform	Sigma-Aldrich Co., UK
Copper grid	Agar Scientific Co., UK
Formvar	Agar Scientific Co., UK
$HAuCl_4$	Sigma-Aldrich Co., UK

Hydrochloric acid	Sigma-Aldrich Co., UK
Hydroxyl amine	Sigma-Aldrich Co., UK
Iron (II) sulfate	ACROS Organics Co., UK
Nitric acid	Sigma-Aldrich Co., UK
PEI (Mw = 2000 g/mol)	Sigma-Aldrich Co., UK
PEI (Mw = 750000 g/mol)	Sigma-Aldrich Co., UK
Potassium nitrate	Sigma-Aldrich Co., UK
Sodium borohydrate	ACROS Organics Co., UK
Sodium hydroxide	Fisher Scientific Co., UK
Sulfuric acid	Sigma-Aldrich Co., UK

Table 3: Materials used in the study of GL prodrug loading on to HNPs and gemcitabine release profile

Material	Suppliers
RPMI media	Fisher Scientific Co., UK
Hydrochloric acid	Sigma-Aldrich Co., UK
Sodium hydroxide	Fisher Scientific Co., UK
Acetonitrile	Fisher Scientific Co., UK
Dialysis Bag	Medicell Co., UK
Thiolated polyethylene glycol	Sigma-Aldrich Co., UK

4.3.2 Methods

4.3.2.1 Synthesis of iron oxide core

To a stirring solution of iron sulfate (3.89 g) in sulfuric acid (20 mL, 0.01 M) a solution of sodium hydroxide (1.03 g) and potassium nitrate (1.82 g) previously dissolved in deionised water (180 mL) at 90℃ and bubbled with nitrogen gas for 1 hr were added and the resulting mixture was stirred at 90℃ for 24 hrs under nitrogen (Sugimoto & Matijević 1980; Goon *et al.* 2009; Hoskins *et al.* 2012). The product of this reaction was separated magnetically using a strong magnetic field applied from outside the reaction flask to separate the iron oxide from the other reaction components. The iron oxide particles were then washed with deionised water six times successively and re-suspended in 15 mL of deionised water for the next step synthesis.

4.3.2.2 Iron oxide core coating

Poly(ethyleneimine) (PEI) with a molecular weight equal to 750 K g/mol was used in this step to coat the iron oxide core: a 50 mL solution of 5 mg/mL of PEI in deionised water was prepared and mixed with 5 mL of iron oxide nanoparticle (resulting from the previous step (4.3.2.1) suspension and sonicated for 1 hr using the Soniprep 150 Plus ultra-sonic disintegrator. The particles were then magnetically separated and washed successively (6 times 50 mL) with fresh deionised water to remove the excess of PEI. The particles were re-suspended in 5 mL deionised water (Goon *et al.* 2009; Hoskins *et al.* 2012).

4.3.2.3 Gold seeding step

Gold seed nanoparticles were prepared by reducing chloroauric acid (HAuCl$_4$) to small sized colloidal gold: a 4 % solution of HAuCl$_4$ was prepared and 375 µL of this solution was taken and mixed with sodium carbonate (500 µL, 0.2 M) in a 200 mL beaker filled with 100 mL ice cold deionised water. The solution was stirred for 10 min at this temperature before sodium borohydride (5 mL, 0.5 mg/mL) was added and the solution kept stirring for another 10 min.

2 mL of a suspension of PEI coated iron oxide nanoparticles (product of step 4.3.2.2) was stirred with 90 mL of the gold seed solution for 2 hrs at room temperature. The magnetic particles were magnetically separated and washed successively (6 times 50 mL deionised water) and re-suspended in 5 mL deionised water (Goon *et al.* 2009; Hoskins *et al.* 2012).

The magnetic particles with the gold seeds attached were then treated with a solution of poly(ethylenimine) 2000 g/mol (20 mL, 1 mg/mL) for 10 min to aid stabilising the gold seeds on the surface of the iron oxide nanoparticles (Hoskins *et al.* 2012). The particles were then magnetically separated and washed successively (6 times 50 mL deionised water) and re-suspended in 5 mL deionised water.

4.3.2.4 Gold coating (synthesis of HNPs)

Gold shells were applied on top of the earlier coated iron oxide core obtained from the previous step (4.3.2.3). A mixture of a suspension of coated iron oxide core (2 mL) and sodium hydroxide solution (110 mL of 0.01 M) was stirred at 60℃. HAuCL$_4$ solution (0.5 mL of a 1% solution) was added followed by hydroxyl amine

solution (0.75 mL, 0.2 M) and the mixture was kept stirring for 10 minutes. Four successive iterative reductions of gold were conducted by addition of HAUCl$_4$ (0.5 mL of a 1% solution) and hydroxyl amine (0.25 mL, 0.2 M) each time with 10 minutes time intervals (Goon *et al.* 2009; Hoskins *et al.* 2012).

An extra 0.5 hr of stirring is allowed before magnetic separation and washing (6 times 50 mL deionised water) of the final product is performed. The resulting nanoparticles were re-suspended in 10 mL deionised water.

4.3.2.5 Characterisation of hybrid nanoparticles

Characterisation of the gold shell-iron oxide core nanoparticles was undertaken using several techniques including: inductively coupled plasma-optical emission spectroscopy (ICP/OES), UV/Visible spectroscopy, photon correlation spectroscopy and TEM imaging.

4.3.2.6 Characterisation using ICP/OES spectroscopy

Inductively coupled plasma-optical emission spectroscopy (ICP/OES) was used to determine the amount of both gold and iron in nanoparticle samples. The instrument used was an Optima 7000 DV ICP-OES (PerkinElmer, Wokingham, UK).

An acid digestion was carried out on the samples using a mixture of concentrated nitric acid and hydrochloric acid (1:1) with heating to 100 °C (1:5 sample:acid mixture). The solution was then diluted with deionised water (1:1000) prior to analysis. A calibration was carried out using standard iron and gold solutions (1000 µg/mL) diluted with deionised water prior to analysis to (10, 5, 1, 0.5, 0.1,

0.05 µg/mL). A control sample of deionised water was also run. Gold was analysed at a wavelength of 242.794 nm while iron was analysed at a wavelength of 261.187 nm. A calibration curve (Figure 65) with a R^2 value = 0.999 for gold and 0.997 for iron was generated and both the gold and iron content of the nanoparticles was determined. The concentration of HNPs used in the subsequent experments was referred to the concentration of iron content of the HNPs.
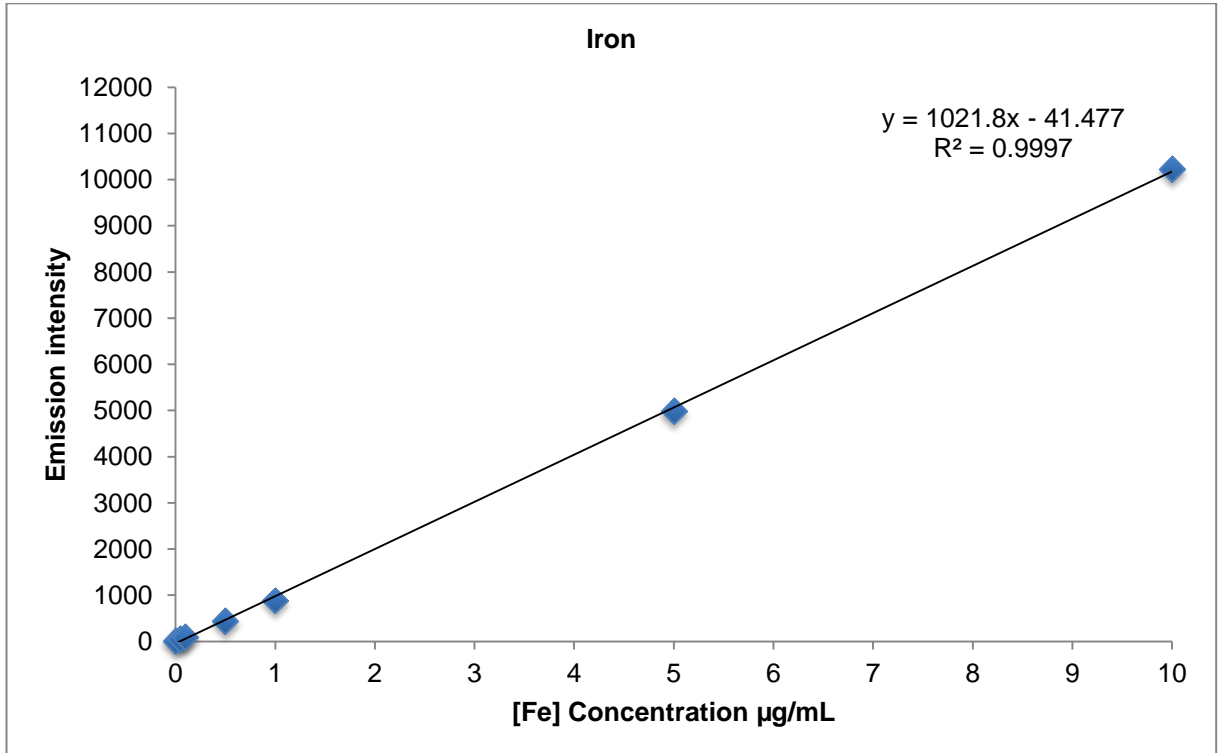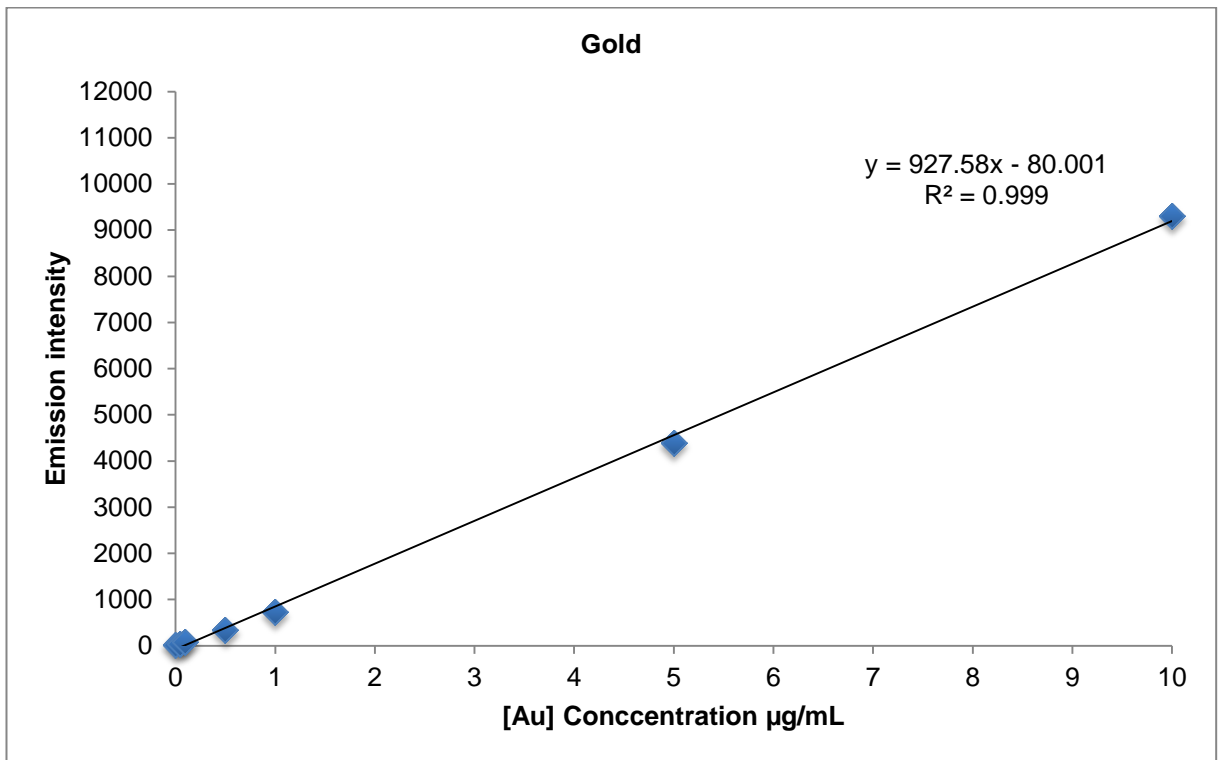
Figure 65: ICP/OES standard calibration curve for Gold and Iron

4.3.2.7 Characterisation using UV/Visible spectroscopy

Iron oxide nanoparticles, nanoparticles following the gold seed step and the final iron oxide core-gold shell hybrid nanoparticles (HNPs) were analysed using a Varian Cary 50 Bio Uv-Vis spectrophotometer over a wavelength range of 300-800 nm in order to determine the λ_{max} of the HNPs within this range. UV Peak absorbance was recorded for the aqueous samples in deionised water using quartz cuvettes. Uv-Vis absorption spectra were recorded between 300-800 nm, all readings were done in triplicate at room temperature and recorded as an average value (Hoskins *et al.* 2012).

4.3.2.8 Characterisation using photon correlation spectroscopy and zeta potential measurement

A diluted solution of nanoparticles in deionised water was prepared and sonicated in an ultrasonic bath prior to analysis. Hydrodynamic diameter, polydispersity index (PDI) and zeta potential measurements was performed using PCS on a Zetasizer Nano-ZS, Malvern Instruments, UK. The measurements were conducted at each step of the nanoparticle synthesis, all measurements were conducted in triplicate at 25℃ and an average value was determined.

4.3.2.9 Characterisation using Transmission electron microscopy (TEM)

Images of the nanoparticle products of each step in the synthesis of HNPs were obtained via using a JEOL 1200 EX-FDL5000 microscope (Jeol, Japan) transmission electron microscope. Sample preparation included diluting each suspension in deionised water and a small amount (10 µL) was dropped onto a formvar coated copper grid (previously prepared and dried for this purpose) and

allowed to dry at room temperature. The grids were placed into the TEM and directly imaged.

4.3.2.10   Loading of GL prodrug onto HNPs

Prodrug conjugation to the surface of the HNPs was performed by mixing a known amount of HNPs (based on the mass of iron oxide) in 5 mL of deionised water with a certain amount of the GL prodrug (prodrug mass was added in different ratios starting from 1:1 up to 6:1 prodrug: iron oxide respectively). The mixing was continued for 3 hrs at room temperature before the loaded HNPs were magnetically separated and washed with deionised water (5 mL).

The mixing was performed either in the presence of or the absence of different concentrations of a thiolated polyethylene glycol.

A calibration curve for measuring gemcitabine in various concentrations in aqueous solution was generated using HPLC (Perkin Elmer Flexar LC Autosampler connected to a UV detector set at a λ_{max} of 268 nm for the detection of GL prodrug XX and gemcitabine (Cavallaro *et al.* 2006). The mobile phase used was acetonitrile:water (1:1 v:v), the flow rate was 1 mL/min and the column used was a Pinnacle DB C18 reverse phase column. The mass of the prodrug in the "wash solutions" was obtained using the equation of this calibration curve (Figure 66).

The amount of the GL prodrug remaining in the wash waste was used to determine the amount of GL prodrug loaded on the HNPs by subtracting the

amount of GL prodrug **98** in the waste solution from the total amount of the GL prodrug used.

The resulting formulation produced in the presence of thiolated PEG was termed PEG GL-HNPs (polyethylene glycol-gemcitabine-lipoic acid prodrug-HNPs). When no PEG residues were present the formulation was referred to simply as GL-HNPs.
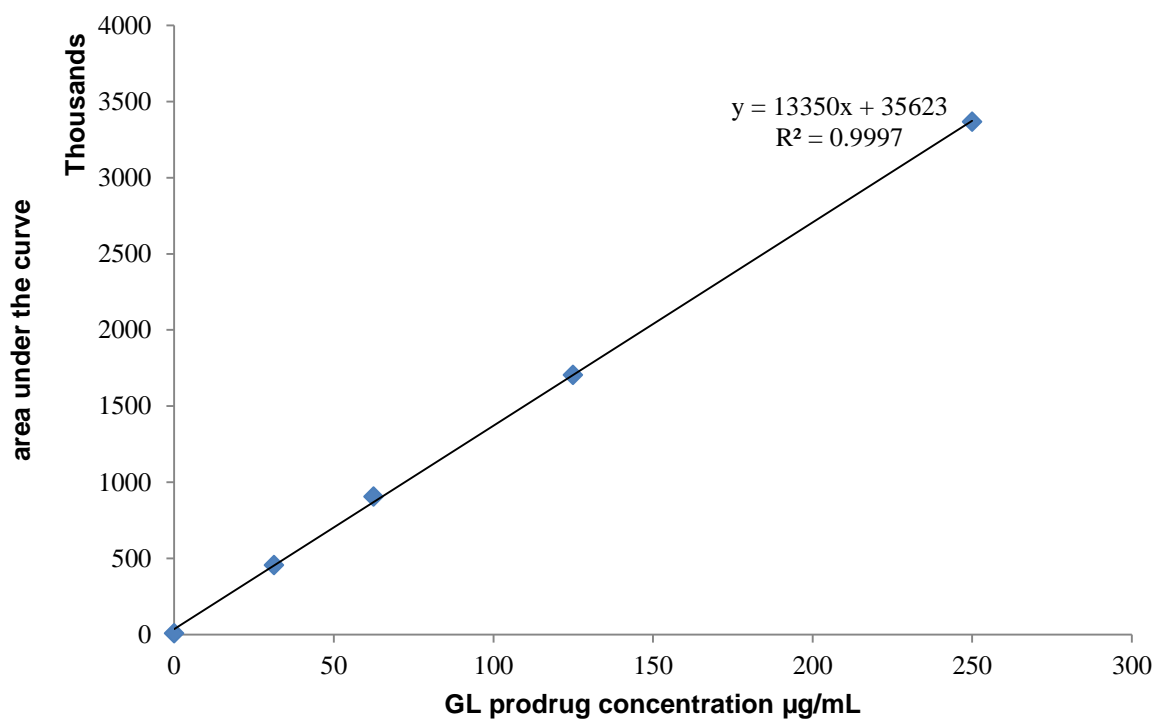
Figure 66: Graph of the calibration curve for GL prodrug concentration against HPLC retention peak area

4.3.2.11   *In vitro* drug release in aqueous media

A release profile study was conducted in aqueous solution at 20℃ by placing GL-HNPs formulation (2 mL of 500 µg/mL based on the iron oxide concentration of the HNPs) into a visking tubing (12-14 KDa) and dialysed against 200 mL of deionised water at 20℃.

At fixed time points (0, 10, 20, 30, 40, 50, 60, 90, 120, 180 minutes and finally after 1440 minute (24 hrs)) a sample of 1 mL from the exterior solution was taken and replaced by 1 mL of deionised water at the specified time point.

The amount of drug released was analysed by HPLC. The experiment was performed in triplicate and the data was expressed by the mean value.

4.3.2.12   *In vitro* drug release in biological media

In vitro study was performed by placing GL-HNPs formulation (2 mL, 500 µg/mL based on the iron oxide concentration of the HNPs) into a visking tubing (12-14 KDa) and dialysed against 200 mL of RPMI media (the pH of the RPMI media was adjusted to be 3.6, 5.6 and 7.4 by using concentrated HCl) at 20, 37 and 44℃, at fixed time points of (0, 10, 20, 30, 40, 50, 60, 90, 120, 180 minutes and finally after 1440 minute (24 hrs)). A sample of 1 mL from the exterior solution was taken and replaced by 1mL of the same environmental media solution at the specified time point.

The same procedures were repeated using PEG GL-HNPs formulation utilising the same pH and heat environments.

The amount of drug released was analysed by HPLC. The experiment was performed in triplicate and the data was expressed by the mean value. The overall number of experiments conducted is explained in Figure 67.
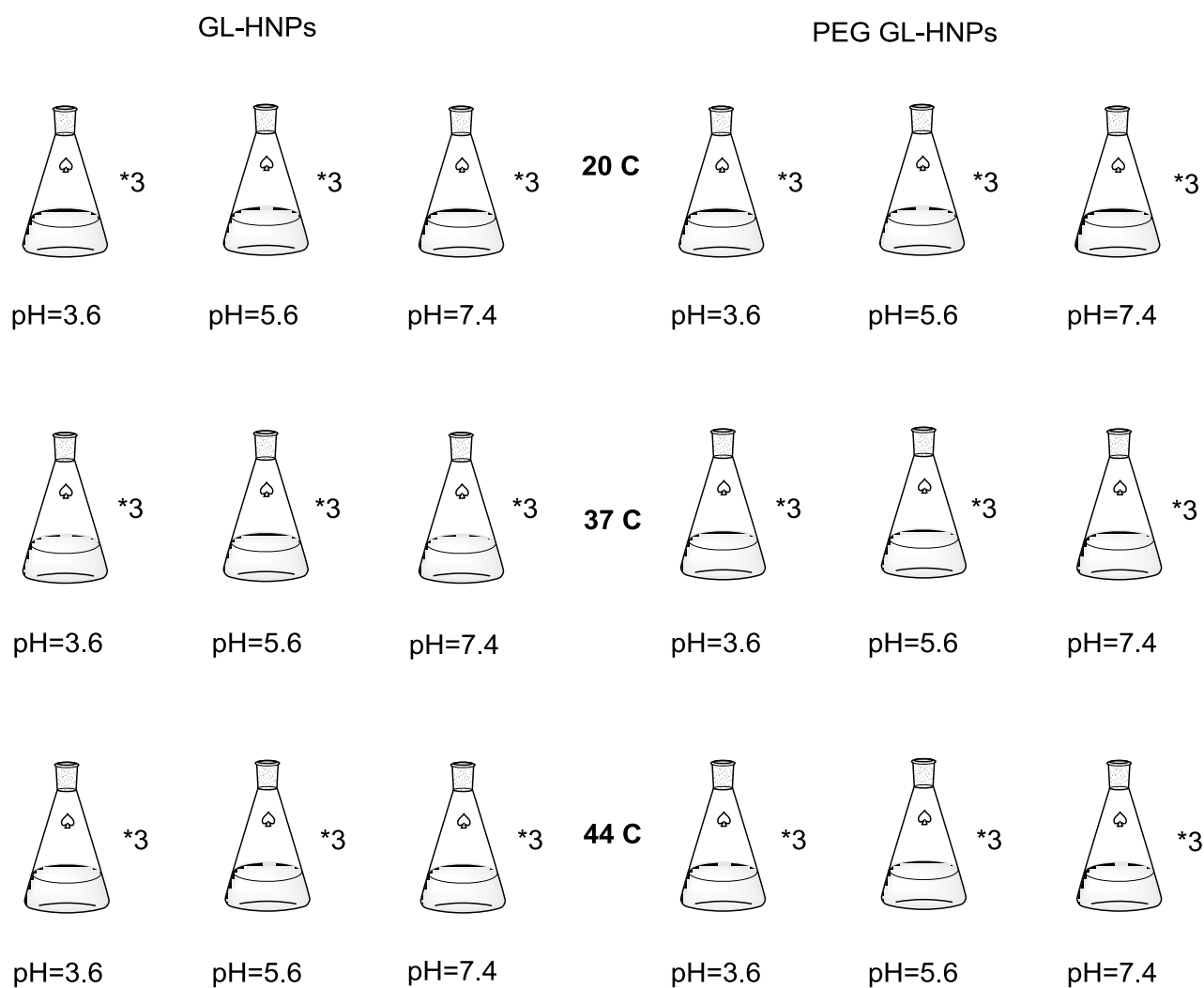
Figure 67: Total number of release experiments conducted in *in vitro* release study

4.4 Results

Characterisation of products from each of the intermediate steps and of the final HNPs prepared was undertaken and is described below.

4.4.1 Characterisation using UV/Visible spectroscopy

The UV/visible absorbance is regarded as an indicator of successful coating of the iron oxide core nanoparticle because of the difference in absorbance pattern between gold and iron oxide. Figure 68 shows a comparison between the UV/visible absorption spectra of the iron oxide core and the final HNPs, showing that the UV absorbance of gold starts to go up from 400 nm to reach the maximum absorption at 590 nm while at the same time the iron oxide spectra shows no absorbance change at the same wavelength.

The gold seeded iron oxide nanoparticles are also expected to have a maximum absorbance around the highest absorbance of gold seed solution which is at 480 nm (Hoskins *et al.* 2012). However, the data shows similar absorbance to the iron oxide core. The absence of a similar pattern of absorbance between the gold seed solution and the gold seeded on the surface of PEI coated iron oxide core was mainly due to the difference in concentration of gold seed within the two solutions.
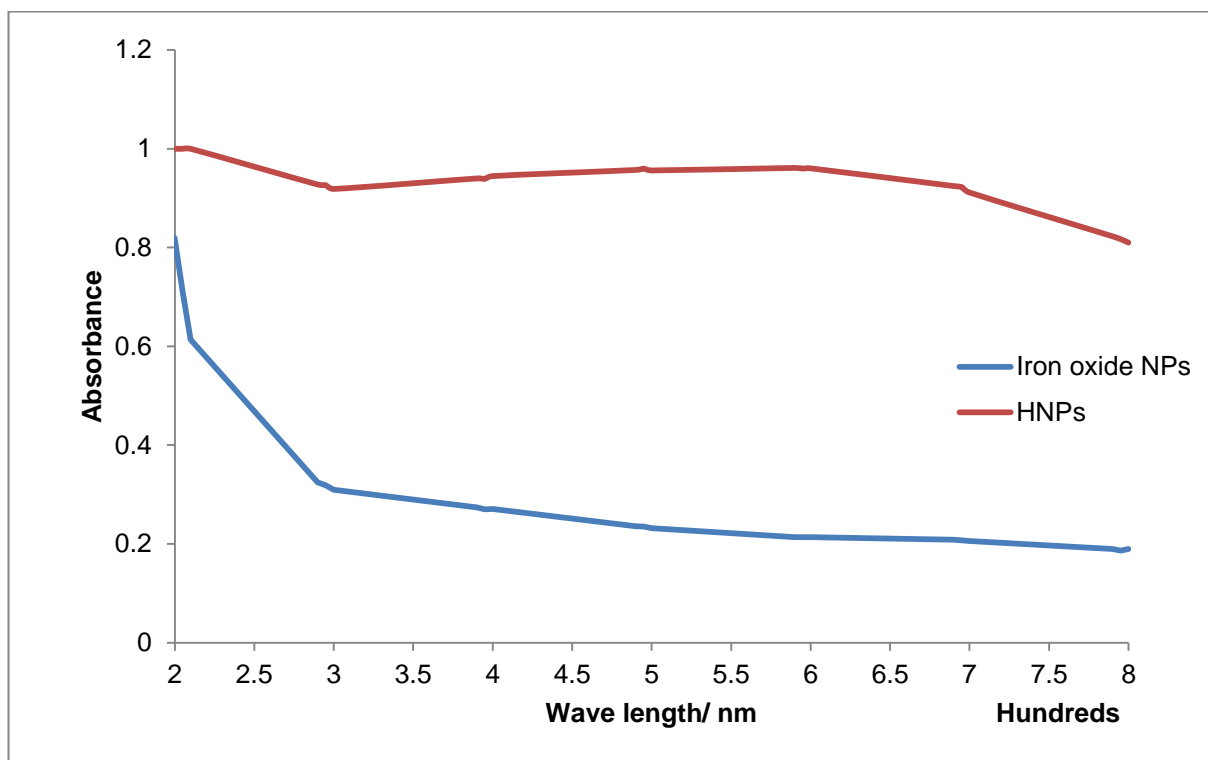
Figure 68: UV/visible spectra comparison between HNPs and iron oxide core

4.4.2 Characterisation using photon correlation spectroscopy and zeta potential measurement

Surface charge, hydrodynamic radius and Polydispersity Index (PDI) data is shown in Table 4. The zeta potential measurements of the nanoparticle suspensions to determine the surface charge show the negative surface charge of the iron oxide core in the first step of synthesis which may be due to the residual surface sulfate association from the synthetic procedure (Hoskins *et al.* 2012). The zeta potential then shifted to a greater value after covering the iron oxide core with the high molecular weight PEI which is mainly due to the presence of positively charged amino groups within the PEI polymer. The data then shows a decrease in

the value of the surface charge concomitant with the next two steps of the hybrid nanoparticle synthesis (gold seeding and gold coating) which is due to negatively charged gold atoms.

The hydrodynamic radius obtained for the iron oxide core shows a large diameter which is due to the magnetic properties of the iron oxide. The diameter was dramatically reduced after coating of the iron oxide with PEI polymer which confirms the ability of the PEI coating to reduce the aggregation of iron oxide.

Polydispersity index (PDI) measurements of the nanoparticles showed a homogenous distribution of particles within each suspension.

Table 4: Hydrodynamic radius, PDI and zeta potential of nanoparticle solution at different step of hybrid nanoparticle synthesis

Particles	Hydrodynamic radius/ nm	PDI	Zeta potential/ mV
Iron oxide	1300	-	-20.82
Iron oxide-PEI	568	0.782	6.93
Gold seeded PEI coated iron oxide nanoparticles	635	0.353	-5.8
HNPs	303	0.629	-16.2

4.4.3 Characterisation using TEM

Transmission electron microscopy (TEM) imaging provides a detailed picture of the nanoparticles where the size and shape of the particles are clearly shown.

Figure 69 shows the naked iron oxide core where the particles are gathered within a colony due to the highly magnetic nature of the particles. The size of the nanoparticles seemed to be higher than expected but this is mainly due to a lack of clearly individual nanoparticles. The shape of the particles was cubic to spherical.
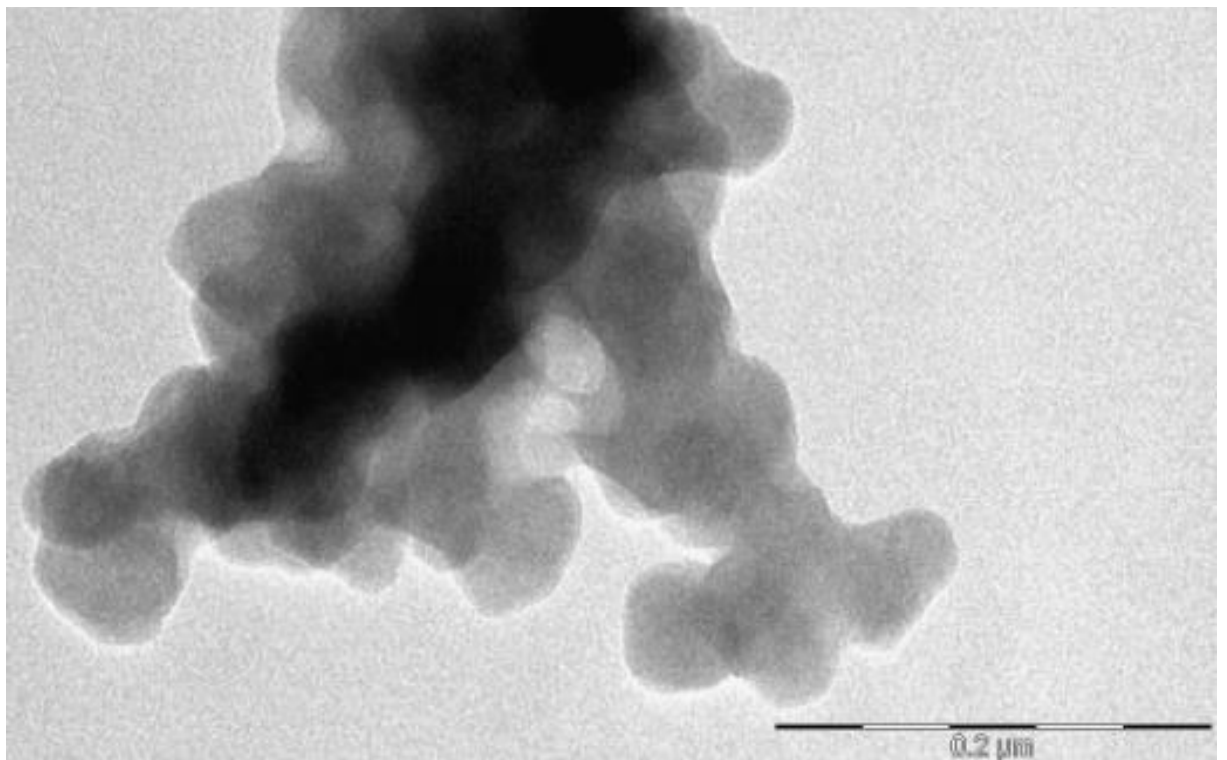
Figure 69: TEM image of iron oxide nanoparticles

Figure 70 shows the effective seeding the gold nano-seeds at the surface of the PEI coated iron oxide core. The small gold nanoparticles (2 nm) appear to be attached to the surface like dots; the picture still shows the particles assembled in groups but to a lesser extent than for the uncoated nanoparticles.
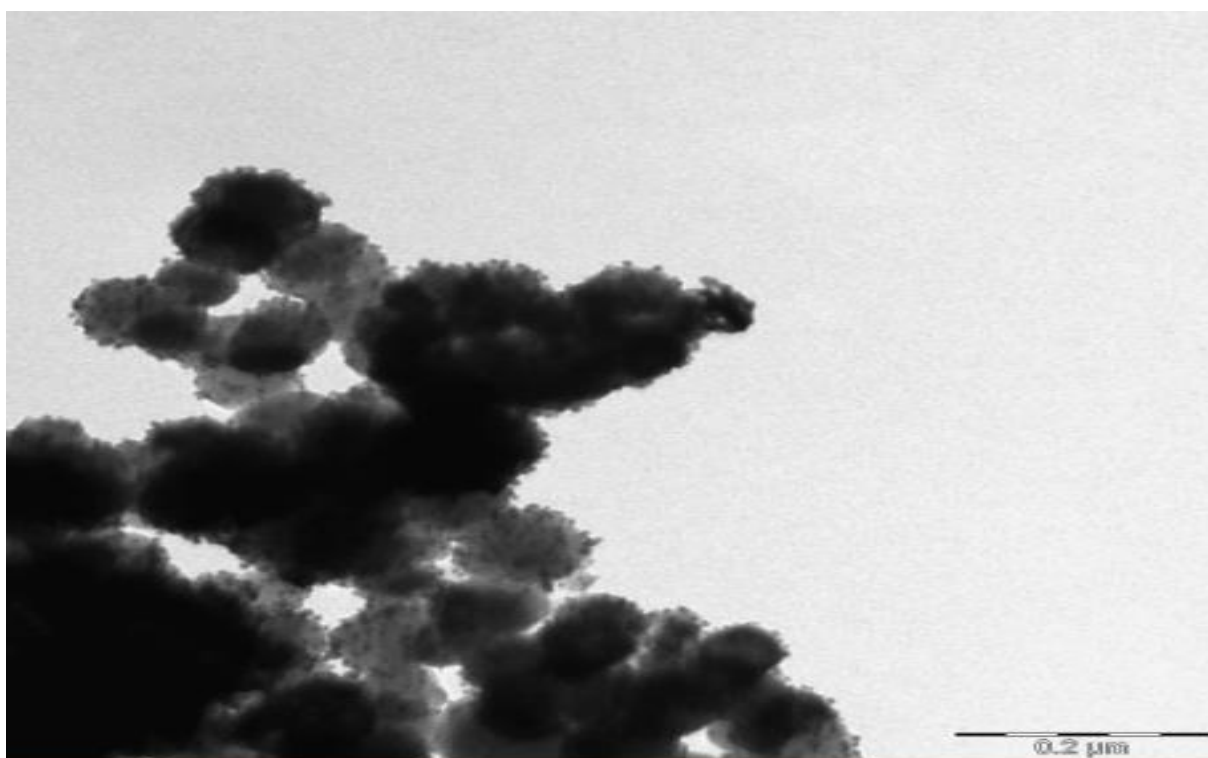
Figure 70: TEM image of gold seeded on the surface of iron oxide nanoparticles

Figure 71 shows the final size and shape of the hybrid nanoparticles (HNPs). At this stage, single nanoparticles with a defined shape could be seen, which could be described as a spherical to star shaped particles. The final size of the particles could be identified as being approximately 100 nm.

It was claimed that the thickness of the gold surface coat of HNPs measured by TEM examination falls within the range of 10-15 nm approximately (Hoskins *et al.* 2012).
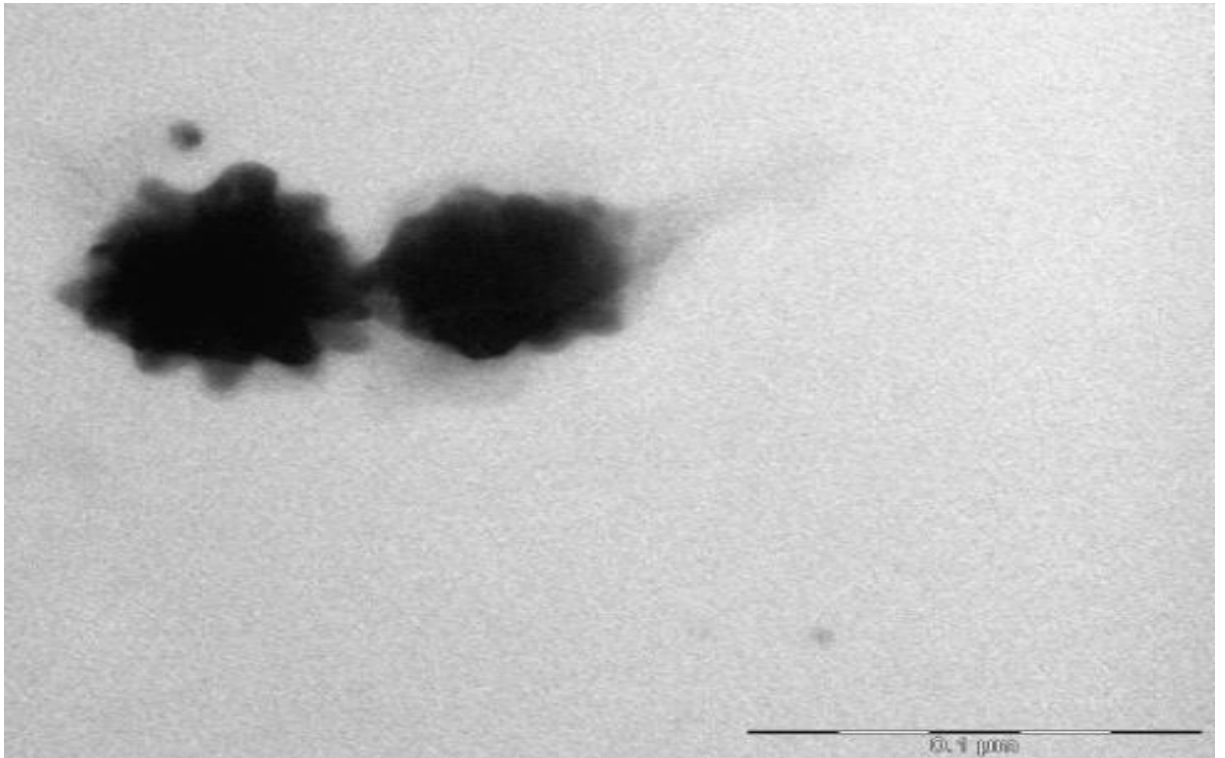
Figure 71: TEM images of HNPs

4.4.4 Gemcitabine-lipoic acid prodrug loading onto the HNPs

Gemcitabine-lipoic acid (GL) prodrug **98** loading studies on the gold surface of HNPs was performed in the presence and absence of thiolated PEG. The data acquired was derived from the equation of the calibration curve ($y = 13350x + 35623$) (Figure 66) previously generated to link the known prodrug concentration and the area under the curve.

In order to find a clear difference between the retention time of GL prodrug and gemcitabine for the subsequent release study, analysis of a solution containing known concentrations of both gemcitabine and GL prodrug was conducted. The results of this HPLC analysis of gemcitabine and GL prodrug are shown in (Figure 72).

The loading capacity of the HNPs was studied by using different ratio of GL prodrug to HNPs, the ratio used started from 1: 1 to 6:1 GL prodrug: HNPs was used to give the highest loading of 5 mg of GL prodrug to 1 mg of HNPs in case of absence of PEG thiol and 2.5: 1 GL: HNPs in case of presence of Peg thiol polymer (

Table 5).

Table 5: The drug loading % for GL prodrug only and GL prodrug + PEG loaded HNPs

	GL prodrug Mass (µg)	%Loading
GL prodrug without PEG-Thiol	25000	96
GL prodrug with PEG-Thiol	25000	50
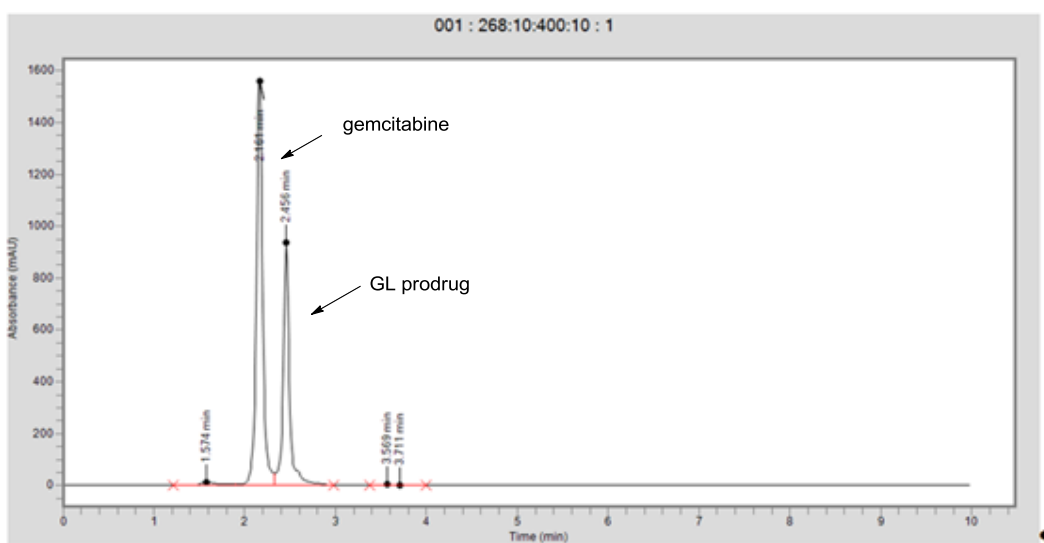
Figure 72: Results of a HPLC analysis to determine the relative retention times of gemcitabine and the GL prodrug **98**

4.4.5 Drug release study

The drug release profile was first determined at 20℃ in aqueous media before starting to study the effect of heat and different pH environments on the release profile of gemcitabine from the PEG GL-HNPs and GL-HNPs formulations. The effect of different pH environments using RPMI media (3.6, 5.6 and 7.4) was chosen to simulate the biological environment faced by the formulation at the time of drug internalisation (Preissler & Williams 1981; Cooper & Hausman 2007). The release profile of gemcitabine from the nanoparticulate formulation in water was undertaken to compare the effect of cell culture media on the release amount and rate. The graph in Figure 73 shows no release of drug at the same pH and temperature between the aqueous environment and the cell media; the small % of burst release in the first hr of the study is thought to be a false reading because of the disappearance of the peak for at the following time point. This is might be because of peak interference between loosely bound GL prodrug and gemcitabine.
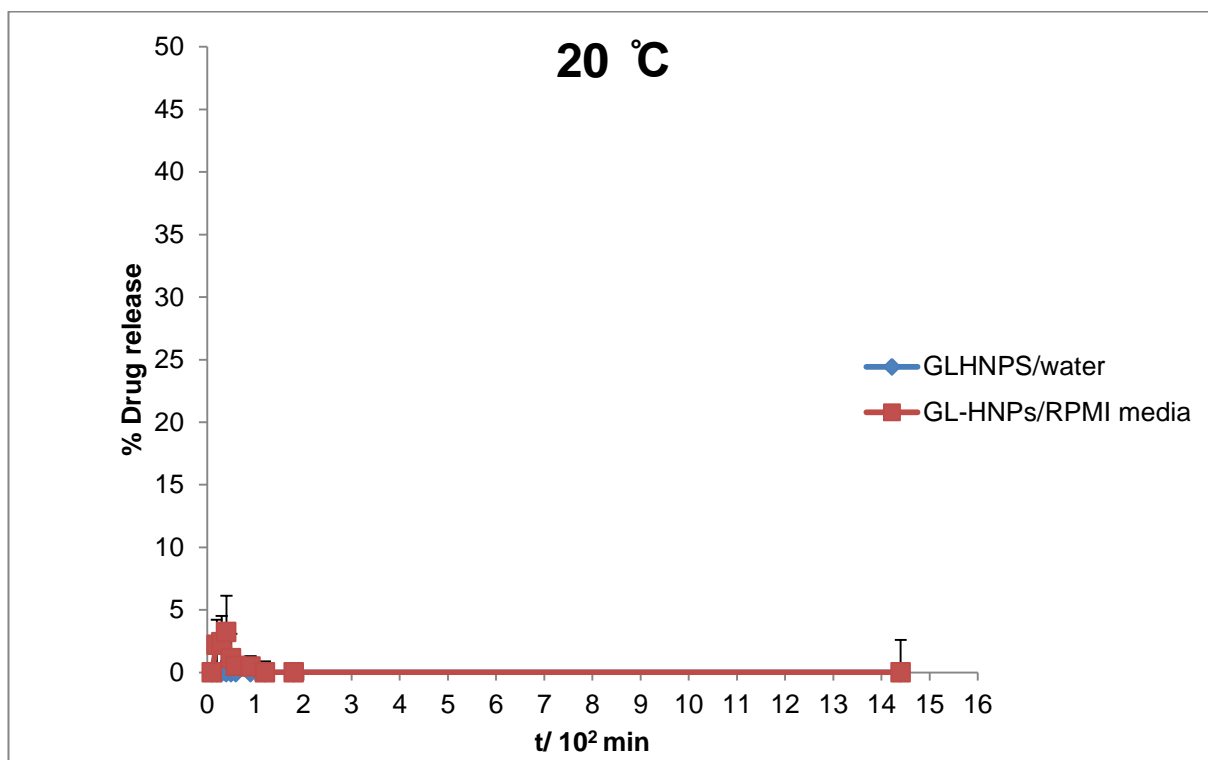
Figure 73: Graph show the comparison between release profile of gemcitabine from GL loaded HNPs over 24 hrs at pH 7.4 (in water and RPMI serum free culture media) at 20 ℃

4.4.5.1 *In vitro* drug release at 20 ℃

The gemcitabine release profile in RPMI media at 20 °C (Figure 74), showed no release at pH 7.4 although up to 2% of loaded gemcitabine was detected in the first 20 minutes which might be due to loosely bound GL prodrug interfering with the result.

The highest release occurred in pH 3.6 which was 11.8% after 24 hrs while at pH 5.6 a 34.7% release was achieved. The PEG GL-HNPs formulation showed no release after 24 hrs at the same pHs mentioned above. These data suggest that

decreasing pH significantly enhanced the release rate of drug from the non-PEG formulation at 20 ℃.
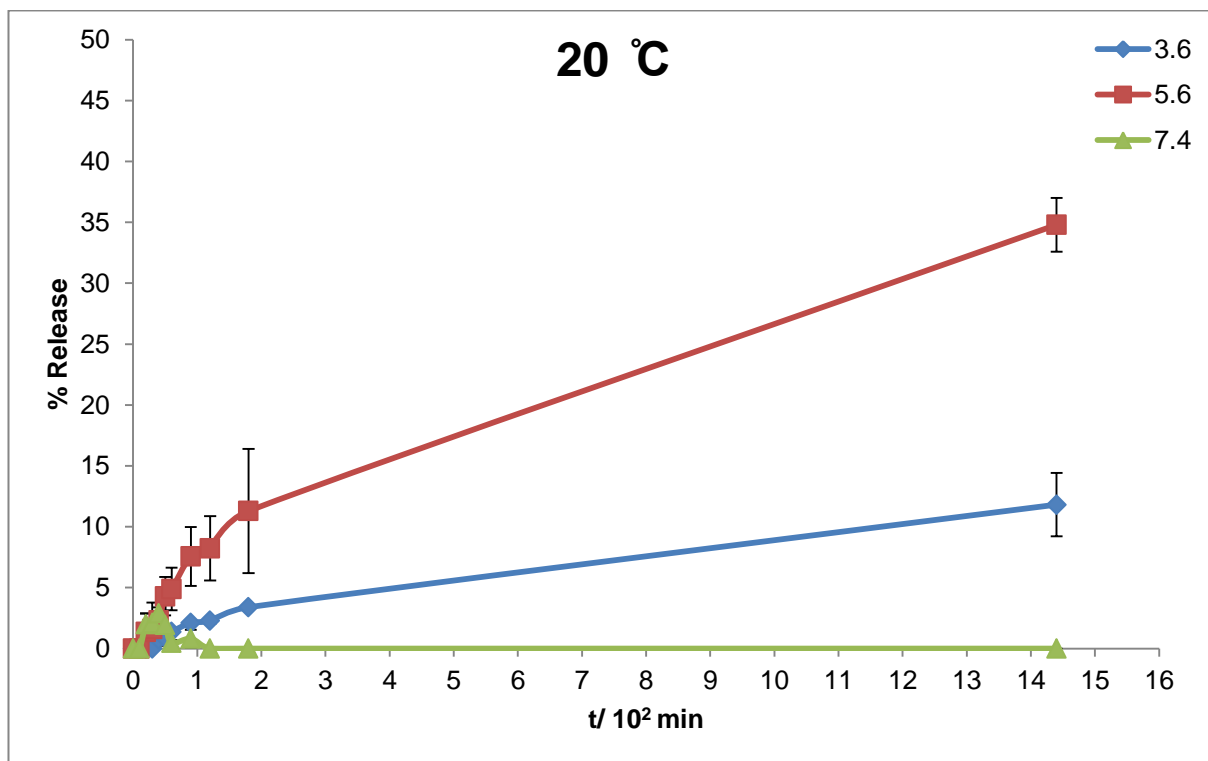
Figure 74: Release profile of gemcitabine from non-PEGylated GL-HNPs formulation over 24 hrs at pH 3.6, 5.6 and 7.4 (RPMI serum free culture media) at 20 ℃

4.4.5.2 *In vitro* drug release at 37 ℃

The gemcitabine release profile in RPMI media at 37 ℃ (Figure 75), showed a significant release at pH 7.4 (24% after 24 hrs) in comparison to the release obtained at pH 3.6 (13.5% after 24 hrs) while at pH 5.6 a maximum of 29.3% of gemcitabine release was recorded. Higher release rates of gemcitabine from the non-PEGylated formulation were recorded at pH 3.6 and 5.6; both showed a burst

release in the first 3 hrs of study (10.8% and 17.3%, respectively). Again, the PEG GL-HNPs formulation showed no release after 24 hrs within the same pH range mentioned above. These data suggest that a temperature of 37 ⁰C triggers the release of gemcitabine from the non-PEGylated formulation at pH 7.4 and it also increases the rate of release at pH 3.6 and 5.6 significantly but at the same time it has negligible effect on the overall release at pH 3.6 and 5.6 after 24 hrs.
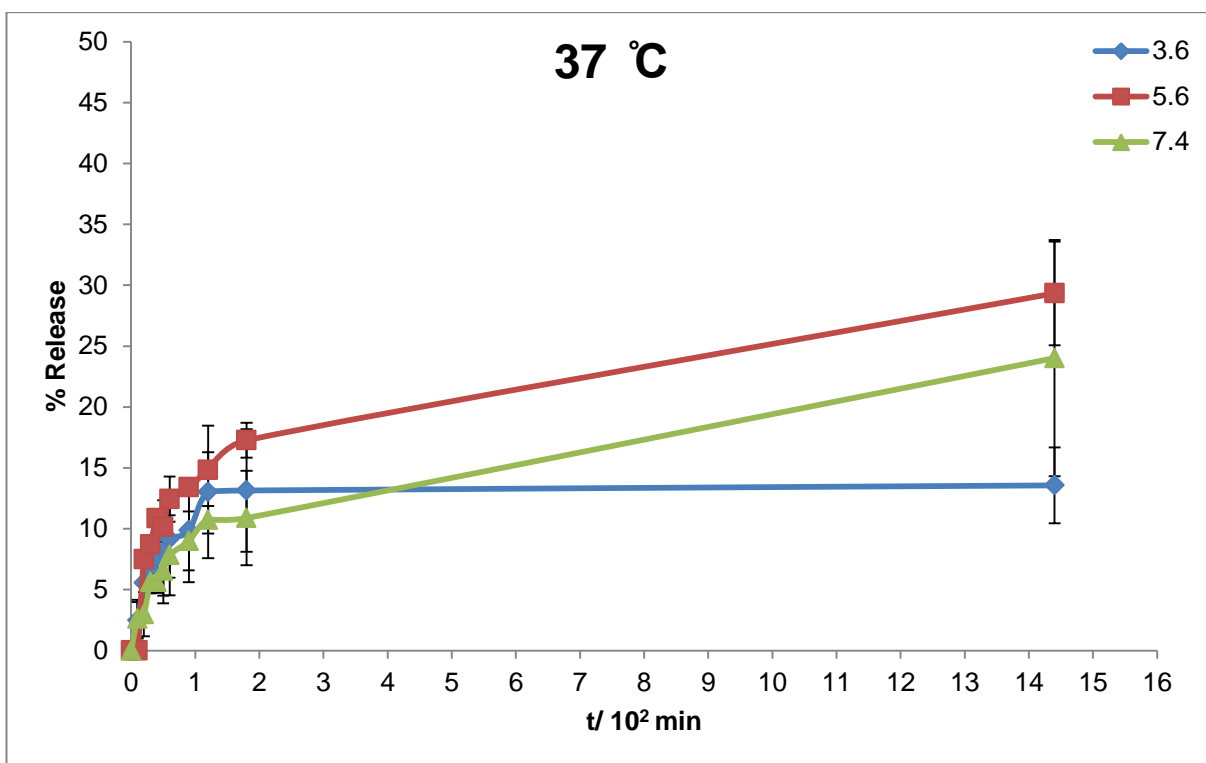
Figure 75: Release profile of gemcitabine from non-PEGylated GL-HNPs formulation over 24 hrs at pH 3.6,5.6 and 7.4 (RPMI serum free culture media) at 37℃

4.4.5.3 *In vitro* drug release at 44 ℃

Gemcitabine release was analysed at 44 °C, this temperature was used to mimic the temperature of the environment surrounding HNPs after laser irradiation with near infrared light. These studies were carried out at pH 3.6, 5.6 and 7.4 as previously discussed. The graph in (Figure 76) demonstrates the rapid release of gemcitabine from the non-PEGylated HNPs formulation when heated to 44 °C.

Gemcitabine release pattern from non-PEGylated formulation (Figure 76), showed a release of 21.9% at pH 7.4, 30.7% at pH 3.6 and a total of 41.1% of gemcitabine release at pH 5.6 after 24 hrs.

A higher release rate of gemcitabine from the non-PEGylated formulation was recorded at pH 3.6, 5.6 and 7.4. A burst release was recorded in the first 3 hrs of study (29.5%, 37.2% and 18.6%, respectively).

PEGylated HNPs formulation showed no release after 24 hrs at all the pHs mentioned above.

These data suggest that the temperature increment has the highest effect on the release rate of gemcitabine from non-PEGylated formulation at pH 7.4 without affecting the overall % released after 24 hrs; both release rate and amount were significantly increased by increasing the temperature to 44 °C.
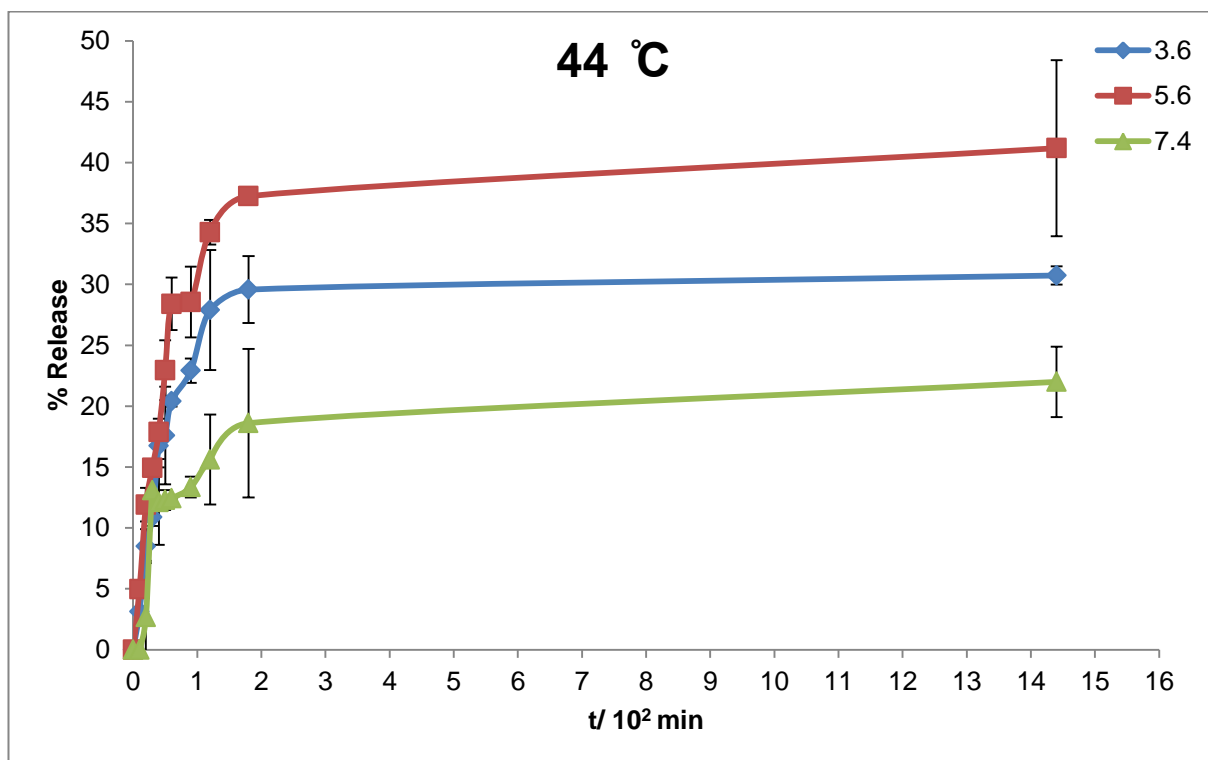
Figure 76: Release profile of gemcitabine from non-PEGylated GL-HNPs formulation over 24 hrs at pH 3.6, 5.6 and 7.4 (RPMI serum free culture media) at 44℃

4.5 Discussion

Regarding the synthesis of the hybrid nanoparticles (HNPs), the data acquired supports the successful synthesis of the particles. The data generated from the surface charge measurements match the expected pattern, from being negatively charged particles for the uncoated iron oxide core (especially due to the surface associated sulfate (Hoskins et al. 2012)) to the positively charged PEI-coated iron oxide core, due to the positively charged amino groups within the PEI structure which is wrapping the iron oxide core. Figure 77 shows a suitable extent of particle separation as determined by the reduction in hydrodynamic radius. Additionally, the opposite charges between the iron oxide core and the PEI polymer favoured a good sort of charge-charge interaction. The continued reduction in the recorded surface charge value after addition of the small gold seed nanoparticles and after the final gold surface application suggests the successful application of both the gold seed and the gold outer layer.
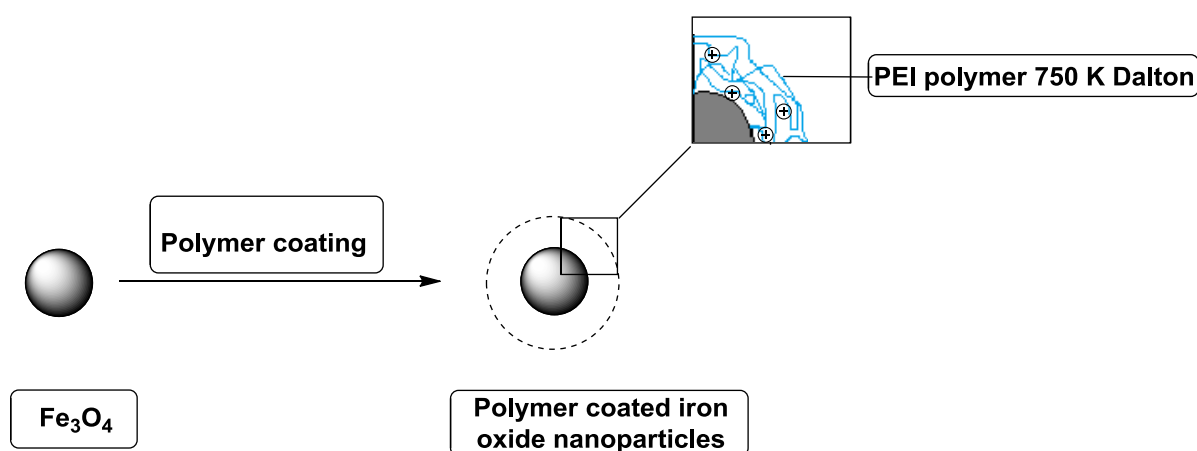
Figure 77: PEI polymer coating step of the naked iron oxide nanoparticles

Another major indication of a successful synthesis of the HNPs is the identification of both gold and iron concentration of the final particles: the ICP-OES instrument measures the amount of gold and iron in each HNPs patch synthesis would provide a strong evidence of presence of both metals in one system, and this is ascertain because of the magnetic way of separation and purification utilised throughout the whole process of HNPs synthesis (i.e. if the gold was washed out (because lacking of magnetic character) it want be available at the time of metal concentration measurement).

UV/Vis spectroscopy data was used to detect the presence of gold on the surface of the HNPs. Gold nanoparticles display an optical feature known as surface plasmon resonance (SPR) and the SPR wavelength for gold nanoparticles is an absorbance in the visible region (500 - 600 nm). The magnitude of the absorbance peak and the absorbance shifting was greatly dependent on the size and shape of gold nanoparticles (the absorbance wavelength rises with large and irregular gold particles) (Huang *et al.* 2007; Hoskins *et al.* 2012).

Finally, the TEM images of the starting, intermediate (gold seeding step) and the final HNPs provide a good sign of the successful synthesis. The TEM images also provide supporting data for the resulting shape and size of the HNPs: the final size of the HNPs appears to be within the range of 100-120 nm and the shape was almost spherical as indicated by the image of the HNPs (Figure 71).

Loading of GL prodrug on the gold surface of the HNPs was confirmed by HPLC by determining the amount of the prodrug left over after the loading procedure. The loading capacity of the synthesised HNPs was assessed by mixing different

ratios of GL prodrug to HNPs and the highest loading capacity was found to be 5 mg of GL prodrug to 1 mg of HNPs. The difference in loading capacity of HNPs in response to the presence of PEG thiol was thought to be due to competition between the GL prodrug and PEG thiol for the binding site of HNPs.

The release profile of gemcitabine from GL prodrug-HNPs formulation was tested in serum free culture media (RPMI) at different pH (3.6, 5.6 and 7.4) to give conditions similar to the environment faced by the formulation inside the cell (endosomal pH 3.6, lysosomal pH 5-6, and blood and intracellular pH 7.4) (Preissler & Williams 1981; Cooper & Hausman 2007).

The effect of heat on the release of gemcitabine from the GL-HNPs formulation was assessed: one of the aims of this research programme is to generate a thermally stimulated release system. The release profile at normal physiological pH and acidic pH environments of endosomal and lysosomal vacuoles was summarised.

The release of gemcitabine from GL-HNPs formulation at pH 3.6 was explained in (Figure 78). Both the overall released amount and the release rate are increased significantly at 44℃ while only the rate of release was affected by increase the temperature from 20℃ to 37℃.

Non-PEGylated formulation also showed a biphasic release profile at 44 ℃ and 37 ℃ due to an initial burst within 3 hrs, which is followed by a constant release.
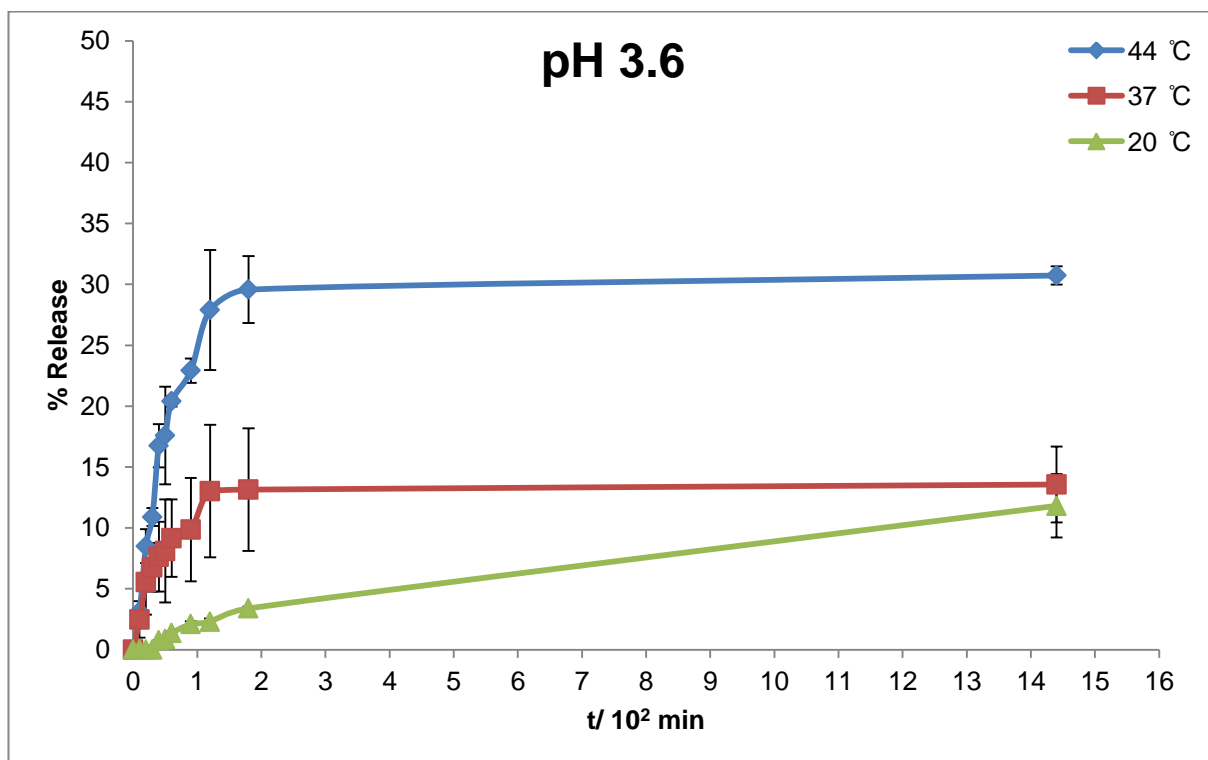
Figure 78: Release profile of gemcitabine from non-PEGylated GL-HNPs formulation over 24 hrs at 20℃, 37℃ and 44℃ (RPMI serum free culture media) at pH 3.6

The effect of temperature on the release profile of gemcitabine from GL-HNPs formulation at pH 5.6 as shown in Figure 79 was that both the overall released amount and the release rate increased significantly at 44℃ while no significant change was recorded by change the temperature change from 20℃ to 37℃.

A continuous phase release profile was noted significantly at 20 ℃ and 37 ℃ while a nearly constant release was achieved after 24 hrs.
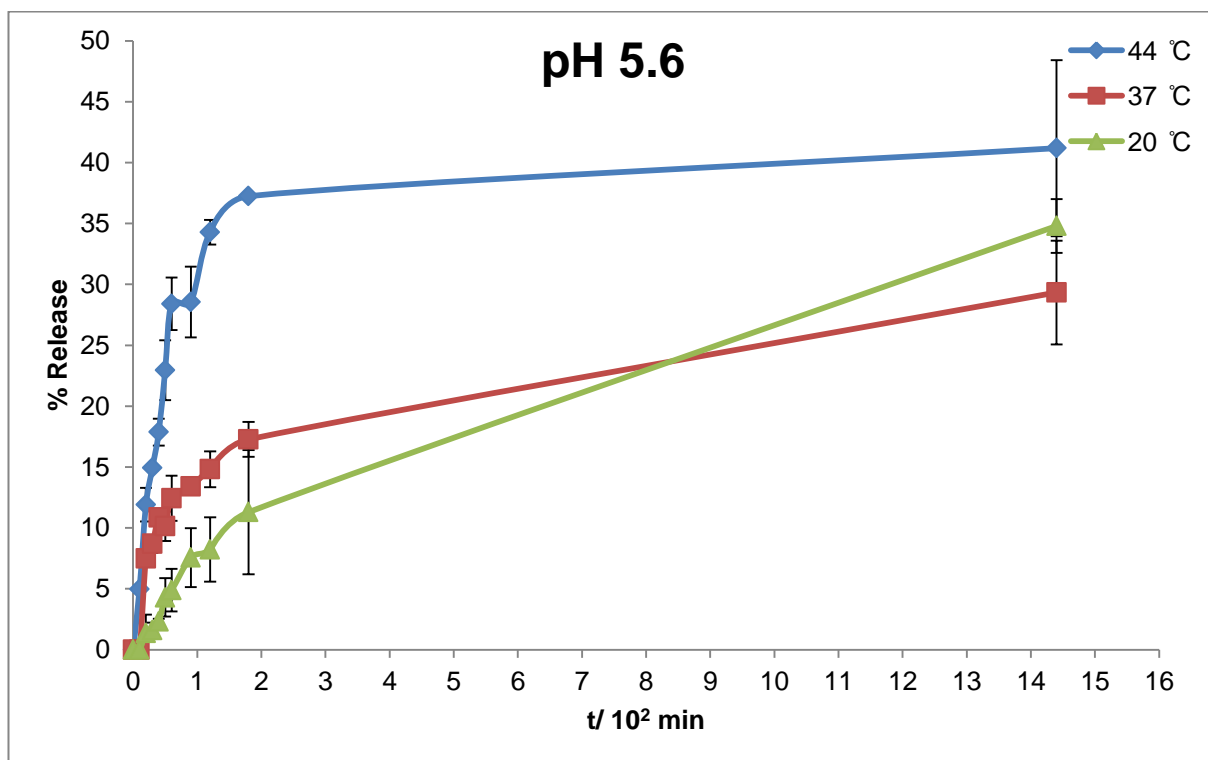
Figure 79: Release profile of gemcitabine from non-PEGylated GL-HNPs formulation over 24 hrs at 20 ℃, 37 ℃ and 44 ℃ (RPMI serum free culture media) at pH 5.6

The effect of temperature on the release profile of gemcitabine from the GL-HNPs formulation at pH 7.4 is shown in Figure 80. The formulation is stable at 20 ºC (no release of gemcitabine was recorded) and similar release profiles were obtained at 44 ºC and 37 ºC.
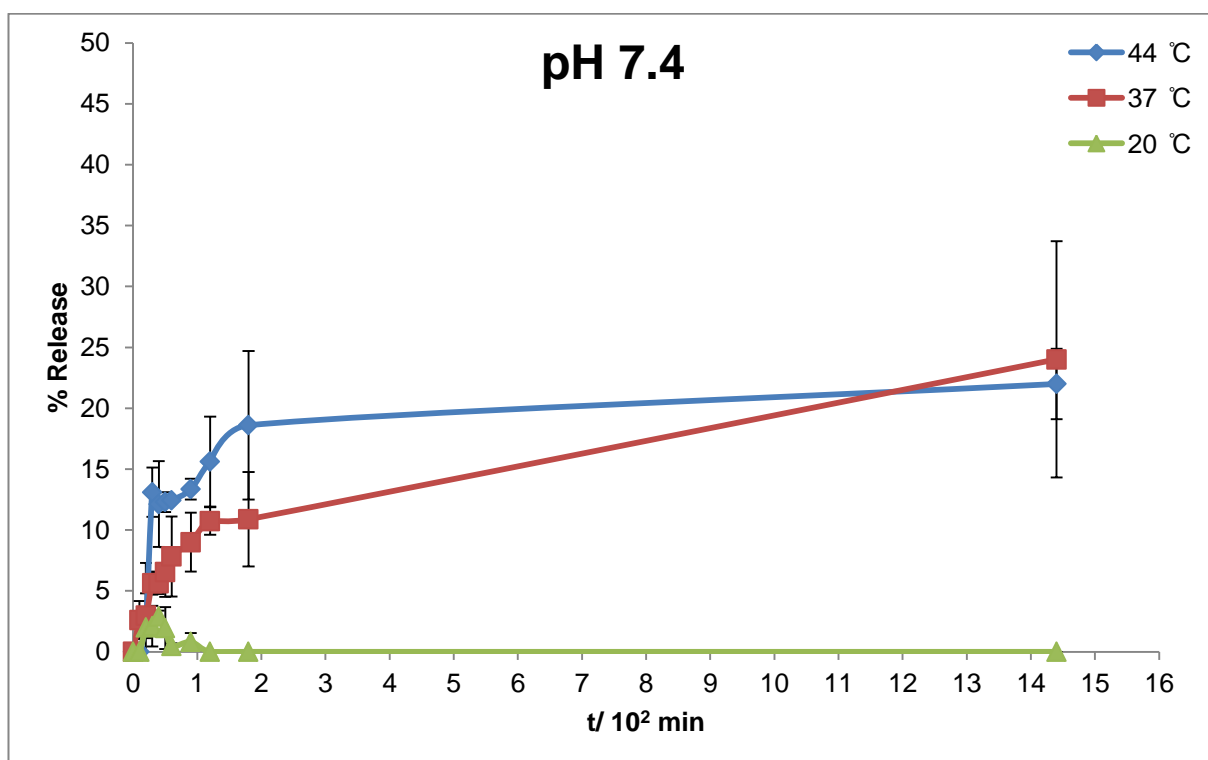
Figure 80: Release profile of gemcitabine from non-PEGylated GL-HNPs formulation over 24 hrs at 20℃, 37℃ and 44℃ (RPMI serum free culture media) at pH 7.4

The release profile of gemcitabine from the nanoparticulate formulation capped with PEG-thiol was expected to be similar to the recorded release from the non-PEGylated formulation. However, it appears that the compound remains trapped within the formulation and no release was detected under any of the conditions

used during the study. The loss of release of the drug from the PEGylated formulation in contrast to the non-PEGylated formulation did not agree with the behaviour of this nanoparticulate system observed in a previous study (Malekigorji *et al.* 2017).

The possible explanation behind the loss of release upon using PEGylated HNPs formulation is that the polymer is shielding the prodrug, preventing the relatively strong amide bond that links gemcitabine to the lipoic acid residue from being directly affected by the low pH and the high temperature conditions.

4.6 Conclusion

The fabrication of the Hybrid iron oxide core gold shell nanoparticles (HNPs) and the following conjugation with GL prodrug **98** onto the surface gold was achieved successfully; conjugation of GL prodrug **98** onto the HNPs in the presence of PEG thiol was achieved but with a significant reduction in loading capacity of the HNPs.

The dative covalent bond between GL prodrug **98** and HNPs is highly stable and cannot be broken with the amount of heat used in this study. Release of gemcitabine from non-PEGylated GL-HNPs formulation was time, pH and temperature dependent.

The release of the drug from the GL-HNPs formulation increases when the pH becomes similar to the environment in endosome/lysosome pH (low pH). Therefore, the release may be accelerated after the intake of the nanosystem by the cells through endocytosis.

A potential clinical benefit has been noticed from the results of the rate of gemcitabine release from the GL-HNPs formulation lacking PEG thiol at various pH and temperatures.

The next stage of this study is the observation of uptake and subsequent effects of the cell proliferation of pancreatic cancer cells.

CHAPTER 5: CELL VIABILITY ASSAYS

OF DRUG- NANOPARTICULATE

CONSTRUCTS

5.1 Background

Pancreatic cancer remains one of the most serious global health issues despite great advances being made in both cancer diagnosis and surgical techniques. The disease is significantly aggressive and challenging, the principal problems arising from the *de novo* chemoresistant behaviour of the disease towards cytotoxic chemotherapeutic agents and the typically advanced stage of the disease at time of diagnosis (Banerjee *et al*. 2005).

In an attempt to address the problems associated with pancreatic adenocarcinoma, several studies utilising combination therapies comprising of different classes of anticancer chemotherapeutic agents have been reported. Such studies show a significant increase in patient response rate but the therapies are highly toxic and there was no significant added benefit in terms of overall patient survival (Hengartner 2000; Arends *et al*. 2005).

Cancer in general is a heterogeneous disease and there is a high diversity in cancer types with dissimilar histopathology, genetic and epigenetic differences, and clinical outcomes, Difficulties in understanding the various forms and stages of such neoplastic processes have hindered the creation of novel therapies (Louzada *et al*. 2012, Ferreira *et al*. 2013).

The early thought of anticancer drug development was based on the anti-proliferative effect of the compounds because of the early recognition of cancer as an uncontrolled cell division. Furthermore the main objective of anticancer drugs was to reduce tumour size, accordingly murine cancer model were developed and utilised for anticancer screening benefiting from the rapidly growing character of

the model. In addition, the success acquired by using a murine cancer cell model was confined to the rapidly growing tumours only (e.g., lymphomas and childhood leukaemia) with little success regarding common solid tumour (e.g., lung and breast cancers) because of the slowly growing character of the tumour (Suggitt & Bibby 2005; Narang & Desai 2009.

In the late 1980s, the United States National Cancer Institute (NCI) set an anticancer drug screening program in the aim of shifting anticancer drug discovery to human solid tumours. This change was based on the relative lack of clinical activity of the compounds for the common human adult solid tumours that had been screened against leukaemia, as modelled in transplantable murine neoplasms (Shoemaker 2006).

Subsequently, new experimental models for many forms of cancer were developed based upon the results of advanced studies of cancer pathobiology which had led to a better understanding of anticancer drug screening (Vargo-Gogola & Rosen 2007).

Experimental models for the study of cancer which use primary tumours, paraffin-embedded samples, cancer cell lines, xenografts, tumour primary cell cultures and/or genetically engineered mice were developed (Vargo-Gogola & Rosen 2007; Louzada *et al*. 2012; Ferreira *et al*. 2013). Studies of cancer chemotherapy usually utilise one of these models because of practical difficulties and ethical limits to undertaking drug testing in animals (Ferreira *et al*. 2013). Culture of cell lines appears as a practical alternative to overcome these ethical and practical difficulties and it is also a relatively simple and easy technique to employ.

182

Cancer cell lines are commonly used for research purposes and have proved to be an excellent model for the study of the biological mechanisms involved in cancer, in addition to providing the facility for high throughput screening for the deduction of large number of experimental parameters (Chiellini *et al.* 2016).

This chapter describes the preliminary evaluation of the *in vitro* effects of gemcitabine-lipoic acid (GL) prodrug alone and also loaded on to the surface of the hybrid iron oxide core gold shell nanoparticles (GL-HNPs formulation), as compared to gemcitabine alone. The reduction in cell viability of pancreatic cancer cells (BxPC-3 cells) was used as an indicator of the effects of the prodrug and formulation.

5.2 Cell viability assays

The measurement of cell viability is routinely used for drug screening and toxicity testing of chemicals. Such assays play a fundamental role in all forms of cell culture and sometimes cell viability tests are the main purpose of the experiment (Stoddart 2011).

Structural integrity of the cell and several cell functions are targets of cytotoxicity assays including: enzyme activity, cell membrane permeability, cell adherence, ATP production, co-enzyme production, and nucleotide uptake activity. Many toxicity assays can be used to correlate cell behaviour to cell number, providing a more accurate picture of, for example, anabolic activity (Louis & Siegel 2011).

There are a wide range of cell viability assays, such as the routine trypan blue dye exclusion assay, colony formation method, crystal violet method, tritium labelled

drug assay, thymidine uptake method, and the MTT assay which is used for counting the number of live cells (Johnson *et al.* 2013).

5.2.1 MTT assay

Active metabolic pathways of viable cells are able to convert the yellow coloured MTT (3-(4,5-dimethylthiazol-2-yl)-2,5-diphenyltetrazolium bromide) dye substrate into a formazan product which is a purple coloured dye (Figure 81), which has an absorbance maximum near 570 nm. Accordingly, dead cells lose the ability to metabolise the MTT into formazan, therefore the purple colour formation acts as a marker for the viable cells only. Reduction of MTT into formazan is expected to be NADH-dependent and because of the involvement of specific mitochondrial enzymes in the reduction of MTT dye it has led to the MTT assay being a tool for measuring mitochondrial activity (Berridge & Tan 1993; Marshall *et al.* 1995; Berridge *et al.* 1996).

Preparation and addition of the MTT solution in a concentration of 0.5 mg/mL is followed by an incubation period of 2-4 hrs before recording changes in absorbance at 570 nm using a plate reading spectrophotometer. The intensity of absorbance, indicating the quantity of formazan produced, is directly proportional to the number of viable cells. The formazan dye is an insoluble compound which accumulates inside cells and around the cell surface in the culture medium, therefore solubilisation of formazan is required prior to recording the absorbance readings; DMSO is routinely used for this.
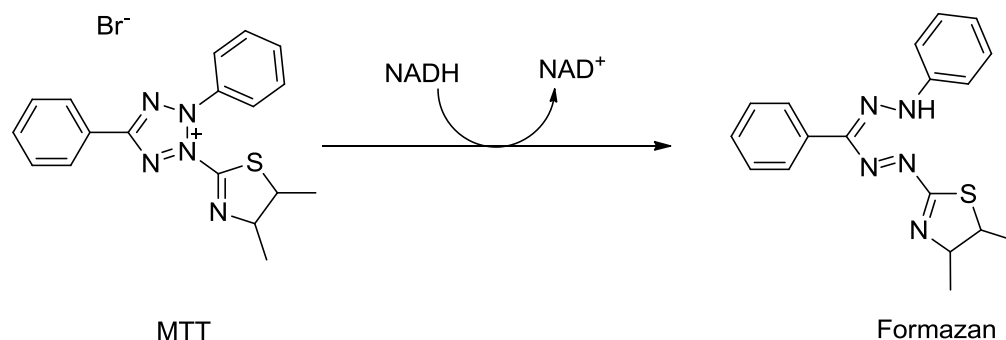
Figure 81: NADH-dependent formation of formazan product from MTT

The amount of formazan product formed by cells is dependent on several parameters including: MTT concentration, the incubation period, and the number and activity of viable cells. The amount of formazan formed is time dependant, in that an extended incubation time results in more dye being accumulated. However, the effect of time of incubation on the accuracy of measurement is limited to a point because of the cytotoxic nature of the MTT which depletes NADH from the cell to generate the product.

In this study, an MTT assay was utilised to investigate the toxicity of GL prodrug and GL-HNPs formulation against pancreatic cancer cell line (BxPC-3) and comparing them to clinically relevant gemcitabine.

5.2.2 Trypan blue exclusion and cell counting

Trypan blue is a diazo stain (Figure 82) commonly used for cell counting microscopy and to assess cell viability.
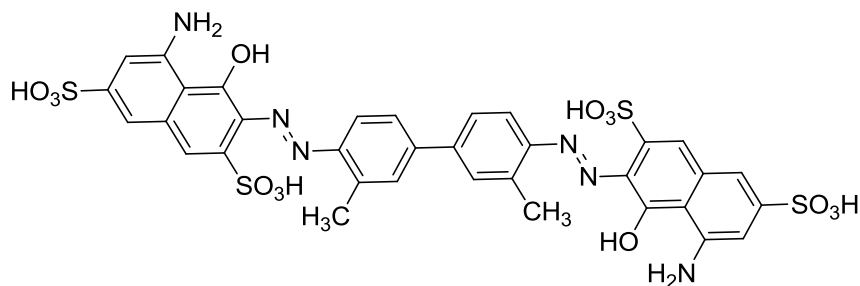
Figure 82: Structure of trypan blue stain

Normal live cells with an intact membrane have a clear cytoplasm and are said to be colourless under the microscope. Because the cell membrane is a selective barrier a stain like trypan blue cannot cross the membrane and stain the cell. However, trypan blue can pass through the membrane if the cells are dead resulting in blue staining of dead cells (Strober 2015).

Based upon selective staining of dead cells by trypan blue an exclusion assay can be established by subtracting the number of live cells from the total number of cells to get the cell viability percentage. Cell counting can be performed either automatically using an automated cell counter or manually by visualising the cells under a microscope. In this study, cells were incubated with formulation for a period of time (24, 48, 72 hrs) and then treated with trypan blue with the ratio of 1:1 and the number of viable cells was counted using an automated cell counter.

An exclusion assay is an easy and fast method, the entire procedure for each sample to be prepared and analysed takes between 5-10 minutes. The main limitations of this technique are the inconvenience of the method for high throughput screening because each sample has to set individually, and cell

viability is determined indirectly from cell membrane integrity. Therefore, it is possible that live cells with an abnormal membrane integrity might be able to repair it again, or the cell viability might be compromised yet the cell membrane integrity is (at least transiently) conserved (Strober 2001).

5.2.3 *In vitro* cellular uptake of GL prodrug and GL-HNPs formulation

Gemcitabine uptake by cells needs the presence of membrane bound proteins responsible for nucleotide transportation, such as the human equilibrate nucleoside transporter-1 (hENT1) (Bildstein *et al*. 2010).

Drug delivery strategies including lipid derivatives (Bersani *et al*. 2014) and nanoparticle drug conjugation (Lee *et al.* 2013) have been examined to demonstrate an increased uptake of gemcitabine by cancer cells as well as to prevent the fast metabolism of the drug molecule. Among several strategies aiming to improve gemcitabine delivery into tumorous tissues the prodrug approach has been investigated, especially conjugation of a gemcitabine molecule onto a lipid, polymeric nanoparticles or cell penetrating peptides (Chitkara *et al*. 2013; Zakeri-Milani *et al.* 2017). In the present work *in vitro* drug accumulation was assayed using HPLC techniques since by knowing the number of the cells in each experiment the concentration of drug taken up in each cell can be calculated (Treuel *et al*. 2013).

5.3 Aim

The aim of the *in vitro* studies was to test the effects of GL prodrug alone and attached to the gold surface of the HNPs nanoparticles (GL-HNPs) in comparison to the effect of gemcitabine on the BxPC-3 pancreatic cell line. The IC_{50} generated

from the percentage cell viability of BxPC-3 cells obtained from both MTT and trypan blue exclusion assays were utilised as preliminary data to confirm the effect of GL prodrug over gemcitabine as well as the effect of GL-HNPs formulation and the potential advantage of the GL-HNPs formulation as a theranostic tool in pancreatic cancer therapy.

The drug uptake rates were determined in order to assess the value of the HNPs as a vehicle to facilitate the uptake of both GL prodrug and gemcitabine.

5.4 Materials and methods

5.4.1 Materials used

Material	Supplier
BxPC-3 Cells	LGC Standards, ATCC (USA)
RPMI Media	Fisher Scientific (UK)
Gemcitabine	Sigma-Aldrich co., (UK)
Cell Culture Flask	Fisher Scientific (UK)
96-Well Plates	Fisher Scientific (UK)
12-Well Plates	Fisher Scientific (UK)
6- Well Plates	Fisher Scientific (UK)
Dulbecco's Phosphate Buffered Saline	Sigma Aldrich co., (UK)
3-(4,5-dimethylthiazol-2-yl)-2,5-diphenyltetrazolium bromide	Sigma Aldrich co., (UK)
Dimethyl sulfoxide	Fisher Scientific (UK)
Trypan Blue Stain 0.4 %	Life Technologies (UK)
Trypsin-EDTA	Life Technologies (UK)
Eppendorf Tubes	Fisher Scientific (UK)
Cell Counting Slides	Life Technologies (UK)
Streptomycin Penicillin	Life Technologies (UK)
Foetal Bovine Serum	Life Technologies (UK)
Acetonitrile	Sigma Aldrich (UK)

5.4.2 Methods

5.4.2.1 MTT cytotoxicity assay

The MTT assay procedure was performed within a 96 well plate seeded by the BxPC-3 human pancreatic cancer cell line. Prior to seeding of the plate, the cells were cultured in RPMI medium supplemented with 10 % foetal bovine serum (FBS) and 1 % penicillin streptomycin (P/S). The BxPC-3 cells were then stored in the incubator at 37 °C in humidified 5 % CO_2 atmosphere. Regular checking of the cell growth was performed and when the cell confluence reached about 80% of the flask, the cells were suspended and re-cultured into two flasks; this step was repeated as necessary.

Preparation of 96 well plates was carried out by seeding each plate with 100 µL of the BxPC-3 cell suspension and then the plates were incubated under the same conditions mentioned above for 24 hrs. When the time lapsed the media was removed and the cells were treated with various concentrations of gemcitabine, GL prodrug and GL-HNPs formulation (Figure 83). The plates were then incubated further for 24, 48 and 72 hrs at 37 °C in humidified 5 % CO_2 atmosphere.

The gemcitabine, GL prodrug and GL-HNPs formulation solutions for cell treatment were prepared using a stock solution of 20 mg/mL of each of gemcitabine, GL prodrug and GL-HNPs formulation. The serial dilutions (Table 6) were prepared by diluting the stock solutions with fresh RPMI media supplemented with FBS and P/S.

Table 6. Preparation of anticancer drug solutions for MTT assay (0.01 - 100 µg/mL)

Drug concentration (µg/mL)	Volume of 20 mg/mL drug stock solution (µL)	Volume of media (mL)
100	22.5	4.5
50	11.5	4.5
25	5.6	4.5
10	2.25	4.5
5	1.125	4.5
*1	90	4.5
*0.1	9	4.5
*0.01	1	4.5

*: Sample was made from 5 µg/mL concentration as a stock solution.

After the incubation of the plates up to the specified time points (24, 48 and 72 hrs), the drug solutions were removed and replaced by a 150 µL solution made up from combining 2/3 (RPMI media with FBS and P/s) and 1/3 MTT solution (5 mg/mL MTT in PBS). The plates were incubated again at the same conditions mentioned above for 4 hrs, then the whole solution was removed from the plate and the formazan crystals formed within the plates were dissolved using DMSO solvent prior to the plate being inserted inside the microplate reader instrument (Tecan, infinite 200 pro, GmbH 5082, Australia) in order to record the absorbance

of the solution at 570 nm. Percentage cell viability and IC_{50} was calculated relative to the controls. All biological studies were run in triplicate and recorded as average values.

	1	2	3	4	5	6	7	8	9	10	11	12	
A	C	C	C	C	0.01	0.1	1	5	10	25	50	100	A
B	C	C	C	C	0.01	0.1	1	5	10	25	50	100	B
C	C	C	C	C	0.01	0.1	1	5	10	25	50	100	C
D	C	C	C	C	0.01	0.1	1	5	10	25	50	100	D
E	C	C	C	C	0.01	0.1	1	5	10	25	50	100	E
F	C	C	C	C	0.01	0.1	1	5	10	25	50	100	F
G	C	C	C	C	0.01	0.1	1	5	10	25	50	100	G
H	C	C	C	C	0.01	0.1	1	5	10	25	50	100	H
	1	2	3	4	5	6	7	8	9	10	11	12	

Figure 83: Plot showing the dosing of 96 well plates for MTT assay by a single compound (C stand for control and each number in the dark blue area refers to the compound concentration in µg/mL)

5.4.2.2 Trypan blue cytotoxicity test

The trypan blue assay was carried out using a 12 well plate: Each plate was seeded by 1 mL of BxPC-3 cell suspension containing approximately 50000 cells and the plate was incubated at 37 °C in a 5 % CO_2 atmosphere for 24 hrs.

When the time lapsed the media were removed and replaced by a 1 mL solution of gemcitabine, GL prodrug and GL-HNPs formulation (prepared by diluting stock solution with RPMI media supplemented with FBS and P/S) in the following order of concentration (0, 0.01, 0.1, 1, 10 and 100 µg/mL). The plates were then placed inside the incubator for 24, 48, and 72 hrs.

Following incubation to the specified time point, the media was removed and the cells were washed 3 times with PBS. The cells were trypsinised and re-suspended in fresh media. A mixture of 50 µL of cells and 50 µL of trypan blue solution was placed in an Eppendorf tube and shake before a 10 µL of the resultant solution was placed into a cell counting slide before cell counting were performed using and automated cell counter (Invitrogen Countess[®], UK).

Viable cells were counted and the percentage cell viability was calculated and compared to the total cell count. IC_{50} were calculated in relation to the number of control cells. All biological studies were run in triplicate and recorded as average values.

5.4.2.3 *In vitro* cellular uptake of formulations

Determination of drug uptake by BxPC-3 cells was achieved by using a 6 well plate seeded by 3 mL of cell suspension (about 150000 cells) and incubated at 37° C with 5 % CO_2 for 24 hrs, then the media was replaced by a drug (gemcitabine, GL prodrug and GL-HNPs formulation) solution at concentrations equal 50 and 100 µg/mL, the plates were then incubated for 24 hrs under the same conditions mentioned above.

When the time laps the medium was removed and each well was washed with 1 mL PBS before the addition of 185 µL trypsin into each well. Cells were re-suspended in 1 mL media and viable cells were counted using an automated cell counter (Invitrogen countess®, UK).

100,000 cells were transferred into the eppendorf tubes and centrifuged (800 rpm, 5 min). The supernatant was removed and cells were re-suspended in acetonitrile: water (1:1).

The drug concentration was quantified using reverse phase high performance liquid chromatography (HPLC) (Perkin Elmer, Flexar Autosampler, column: SPHERISORB ODS2 5 µm, length 250 mm, internal diameter 4.6 mm) and a mobile phase contained H_2O and acetonitrile (50:50).

By determining the drug concentration in the cell population (100,000), a single cell drug accumulation could be determined and compared.

5.5 Results

5.5.1 Cell viability

The cell viability of BxPC-3 cells was examined by treating the cells with known concentrations of gemcitabine, GL and GL-HNPs. The effects of these substances were analysed over a period of 24, 48 and 72 hrs.

The MTT assay was used to determine the IC_{50}, the drug concentration at which only 50 % of the cell population were viable. Drugs with lower IC_{50} values have a greater cytotoxic effect.

5.5.2 MTT assay for cell viability

Percentage cell viability for gemcitabine, GL and GL-HNPs at 24 hrs were compared (Figure 84): the graph shows no IC_{50} for gemcitabine (G) at this time point even at the highest concentration used in this experiment (100 µg/mL), though for GL there is a significant reduction in the cell viability at 50 µg/mL, the IC_{50} obtained for GL prodrug after 24 hrs was 56 µg/mL.

In the case of GL-HNPs formulation there was a significant reduction in the cell viability ($p < 0.05$) starting at a concentration of 5 µg/mL and continued until an IC_{50} was obtained at comparable concentration to the free prodrug 53 µg/mL).
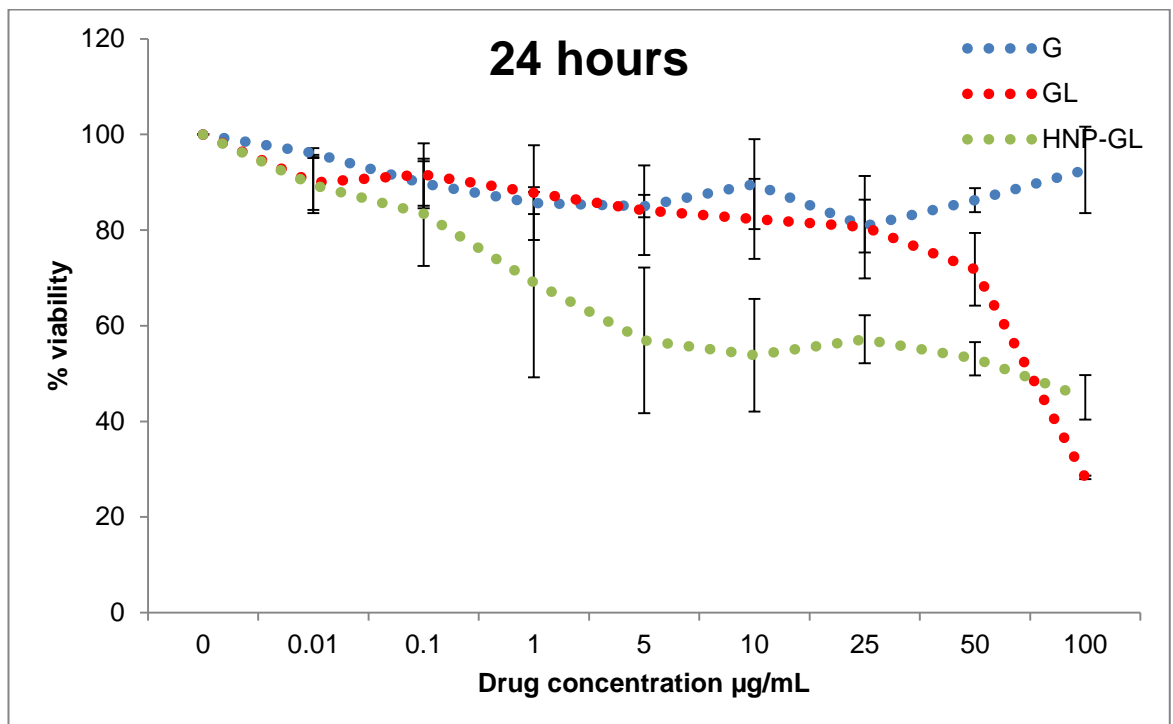
Figure 84: MTT assay graph show the effect of various concentrations of gemcitabine, GL and GL-HNPs on BxPC-3 cells at 24 hrs time points (n=3) (± 19%) ($p< 0.05$)

At 48 hrs (Figure 85), the comparison between the effect of gemcitabine (G), GL prodrug and GL-HNPs formulation show comparable effects on nearly all the time points with no significant differences ($p < 0.05$) except between gemcitabine and GL prodrug at 0.01 µg/mL point where the gemcitabine effect was greater than GL. Even though there is a great difference in the effect of gemcitabine at 0.1 µg/mL and 1 µg/mL the differences are still in significant ($p> 0.05$). The IC_{50} for GL prodrug and GL-HNPs formulation were both obtained at 0.1 µg/mL concentration (exactly calculated IC_{50} for GL and GL-HNPs formulation was 0.098 µg/mL and 0.94 µg/mL respectively). The IC_{50} calculated for gemcitabine was 0.008 µg/mL.
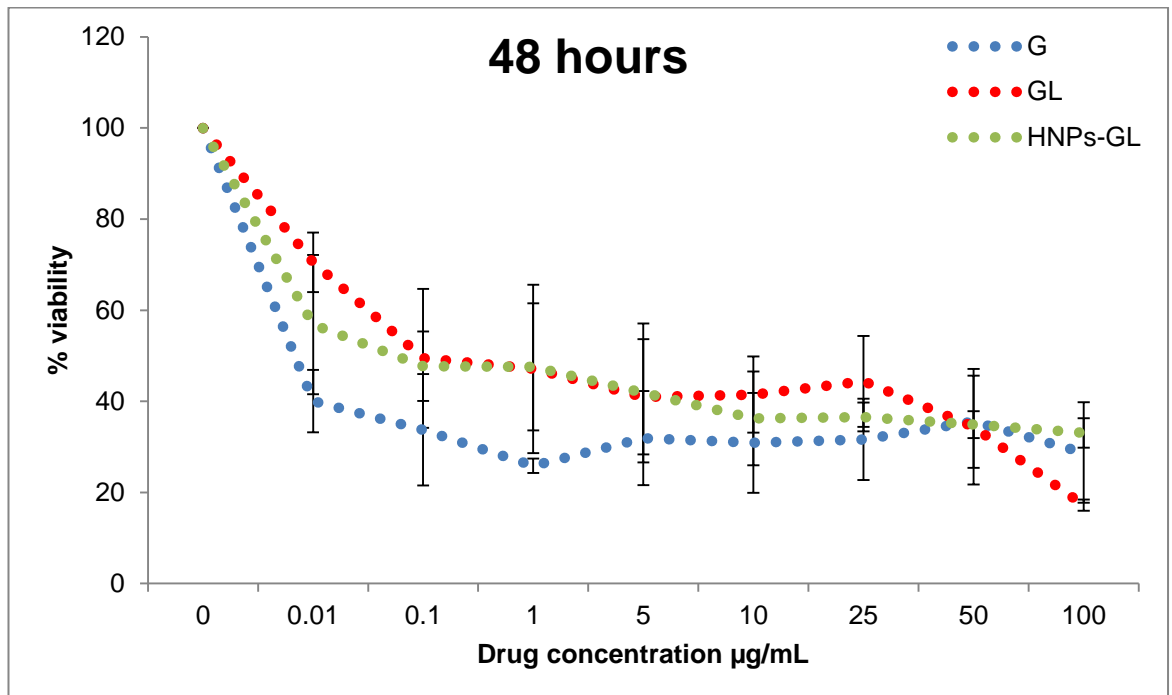
Figure 85: MTT assay graph show the effect of various concentrations of gemcitabine, GL and GL-HNPs on BxPC-3 cells at 48 hrs time points (n=3) (± 18%) ($p < 0.05$)

Figure 86 shows a comparison between the effect of gemcitabine (G), GL and GL-HNPs on BxPC-3 cell viability at 72 hrs: The graph shows significant differences ($p < 0.05$) between the effects on nearly all the concentrations used between GL prodrug and gemcitabine especially at 1, 5, 10, 25, 50 and 100 µg/mL point at which the effect of GL prodrug was observed to be greater than gemcitabine alone while at the point of 0.01 and 0.1 µg/mL the effect of gemcitabine was greater. This kind of effect profile might be due to the cumulative effect of gemcitabine and the lipoic acid on the viability of the cancer cells.
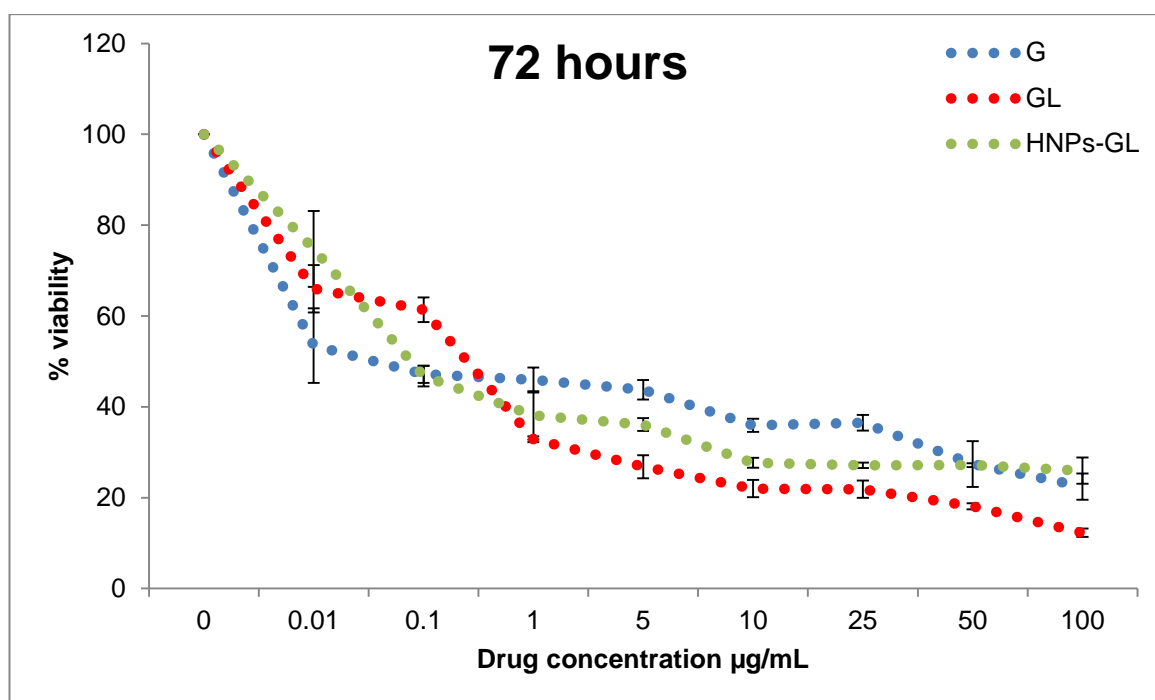
Figure 86: MTT assay graph show the effect of various concentrations of gemcitabine, GL and GL-HNPs on BxPC-3 cells at 72 hrs time points (n=3) (± 12%) ($p < 0.05$)

Another surprising effect of the GL prodrug was observed at 72 hrs where the overall effect of the prodrug was greater than the effect of the prodrug-HNPs formulation at 5, 10, 25, 50 and 100 µg/mL point while both the GL-HNPs formulation and gemcitabine has nearly equal effect. It can be postulated that both the prodrug and the prodrug-HNPs formulation have similar rates of cell internalisation.

5.5.3 Trypan blue assay for cell viability

From the MTT assay the GL prodrug and GL-HNPs formulation were both shown to have a strong effect on cell viability in both a time and concentration dependent manner. Trypan blue assay of BxPC-3 cell viability for the GL prodrug and the prodrug-nanoparticulate formulation GL-HNPs (Figure 87 and Figure 88) displayed a proliferation inhibition profile similar to the profile obtained by the MTT assay at the same concentrations used in the MTT assay. The overall outcome from the trypan blue assay experiment confirmed a comparable effect of the GL prodrug to the GL-HNPs formulation at a given time point for the same concentration.
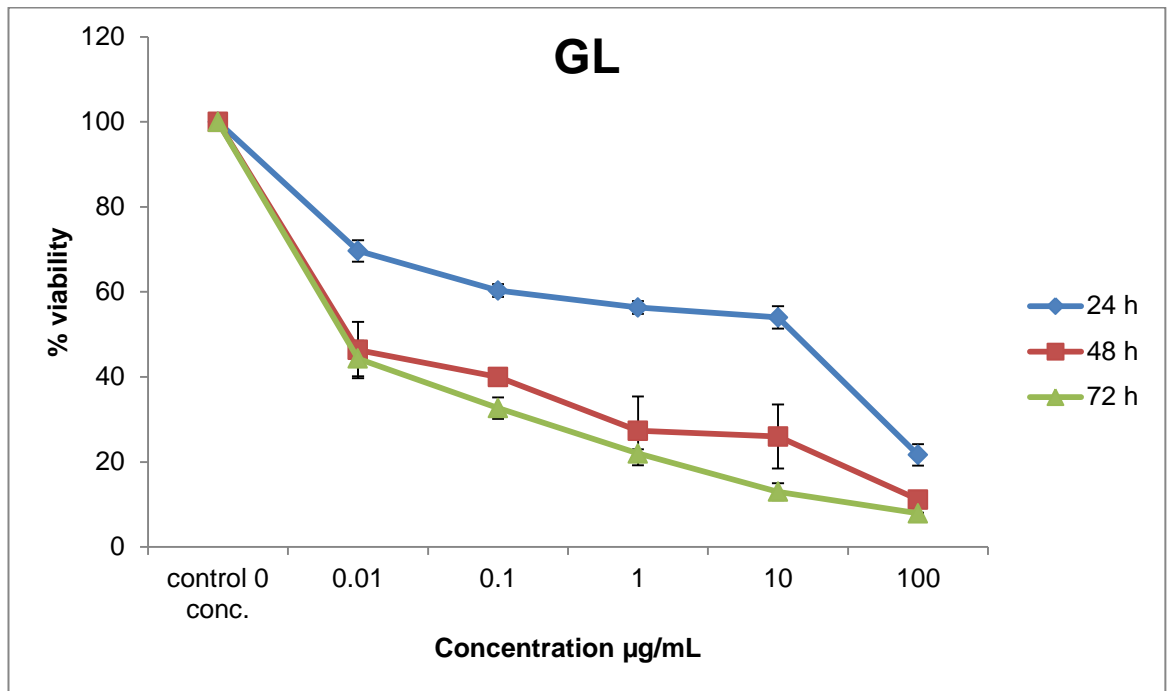
Figure 87: Trypan blue assay graph show the effect of various concentrations of, GL prodrug on BxPC-3 cells at 24, 48 and 72 hrs time points (n=3) (± 12.5%) ($p <$ 0.05)
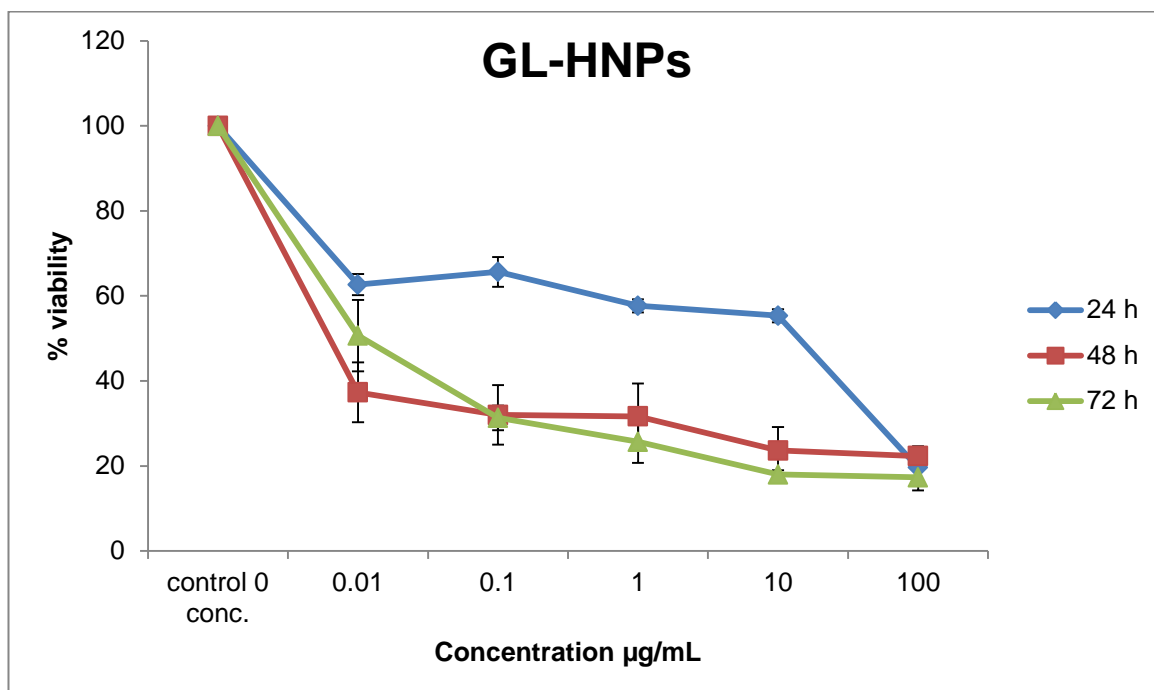
Figure 88: Trypan blue assay graph show the effect of various concentrations of, GL-HNPs formulation on BxPC-3 cells at 24, 48 and 72 hrs time points (n=3) (± 7%) ($p < 0.05$)

5.5.4 *In vitro* cellular uptake of formulations

The bar chart in Figure 89 shows the intracellular amount of both gemcitabine released from the GL-HNPs formulation and from the free GL prodrug used, after a 24 hrs exposure time. In order to best compare the activity of gemcitabine and the GL prodrug, the intracellular concentrations were determined after 24 hrs exposure time; this is to compare between different mechanisms for the internalisation and consequent therapeutic effect.
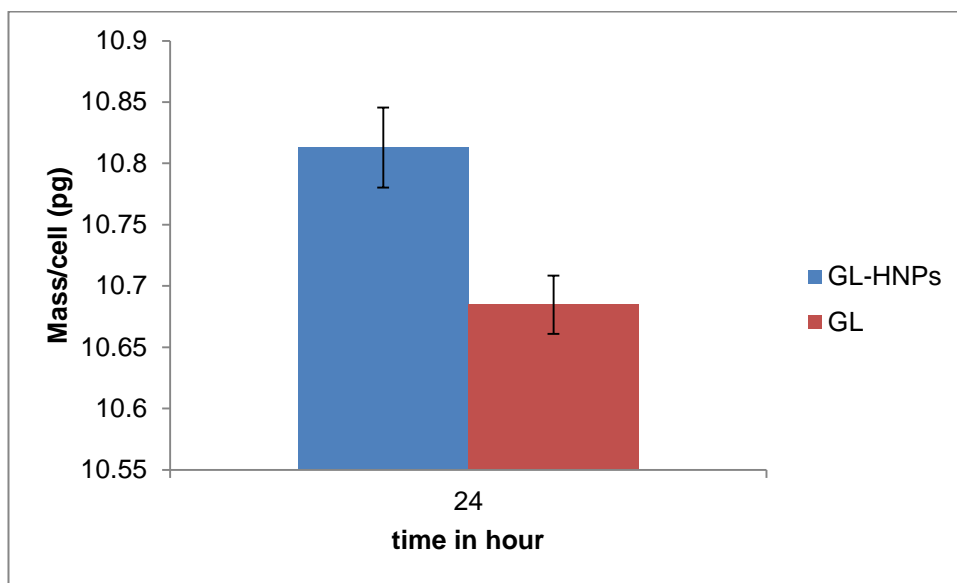
Figure 89: Chart displaying the average amount of gemcitabine inside the BxPC-3 cells after exposure to GL-HNPs (n=3) (± 4.27%) compared to GL (n=3) for 24 hrs exposure time

Free gemcitabine and GL prodrug seems to have different intracellular levels after 24 hrs. No gemcitabine was detected after 24 hrs exposure of BxPC-3 cells to free gemcitabine (data not shown) which suggests that GL prodrug enters the cell via different mechanisms to gemcitabine; gemcitabine enters *via* the tight junction in the cell membrane, as well as being actively transported across the cell membrane with nucleoside transporters (E. Mini *et al*. 2006; Rudin *et al*. 2011b).

Studies have indicated that nanoparticulate vehicles enter cells *via* endocytosis. This is often relatively rapid and results in much higher intracellular concentrations. The amount of gemcitabine detected after exposure to the GL-HNPs formulation is

significantly higher compared to the detected amount of free GL prodrug (bearing

in mind the difference in the mass between gemcitabine and the prodrug).

5.6 Conclusions

The therapeutic activity of gemcitabine against solid tumours is well documented, yet these effects are limited by several factors including the hydrophilic nature of the drug, the short plasma half-life and associated multi-drug resistance (Zakeri-Milani *et al.* 2017). The mechanism of gemcitabine transport into the cells plays a significant role in determining the drug effect. By coupling gemcitabine to lipoic acid to provide a means to bind the prodrug to the gold surface of the HNPs nanoparticles may provide several advantages. It may potentiate the action of gemcitabine due to site-specific activity or raising the amount of drug entering the circulation since the overall physicochemical properties of the prodrug (log P value, plasma half-life and bio-distribution) are different. Additionally, the effect exerted by the lipoic acid residue of the prodrug may affect the activity of the prodrug and the amount of gemcitabine released. For example, lipoic acid has been shown to have antioxidant properties (Geromichalou *et al.* 2015). Nanoparticulate drug delivery systems offer great potential for improving intracellular delivery of therapeutic agents. One of the possible reasons for this effect might be the mechanism of nanoparticulate cellular uptake.

The cytotoxic effect of the GL prodrug and the GL-HNPs formulation is evident. The addition of a lipoic acid residue and coupling of the prodrug to the nanoparticles could improve the efficacy of gemcitabine therapy. The data showed that the coupling of gemcitabine to lipoic acid resulted in an increase in the rate of drug internalisation also.

CHAPTER 6: GENERAL DISCUSSION

AND CONCLUSIONS

The first aim of this study was to provide a library of bisnaphthalimide compounds characterised by having the same total atoms in their linker chain while bearing different numbers of positively charged atoms. The synthetic strategies applied were shown to be successful except for the synthesis of the proposed derivative having six positively charged residues in its linker chain (compound **33**).

The study conducted utilising these compounds as a model for testing the ability of the hybrid iron oxide core-gold shell nanoparticles (HNPs) to act as thermo-responsive carrier revealed the potential benefits of using the HNPs as a drug delivery vehicle in pancreatic cancer therapy, in addition to the potential advantages of the HNPs-drug system to act as a theranostic agent (M. Malekigorji *et al.* 2017).

Malekigorji *et al.* (2017) also provided valuable data regarding the factors most responsible for the effective loading of the drug to the HNPs surface, i.e. number of cationic charged residues and the presence of sulfur atoms in the drug molecule. In addition, it was demonstrated that the effect of heat (44 °C) could reverse the drug HNPs binding if the association was an electrostatic charge-charge interaction (Malekigorji *et al.* 2017).

Following these findings, the second aim was to simulate the structural advantages of bisnaphthalimide based drugs (cationic charges and sulfur) by attempting the synthesis of two gemcitabine derivatives. Unfortunately, the synthesis of a gemcitabine derivative bearing a cationic polyamine chain was unsuccessful although the proposed strategy has been used by other researchers to deliver similar compounds (Geall & Blagbrough 2000).

The successful synthesis of the gemcitabine analogue bearing a sulfur-containing residue was accomplished by utilising amide bond coupling of gemcitabine to lipoic acid. The successful synthesis and reaction scale up was achieved by applying a simple one step reaction and the optimum conditions for the reaction were deduced. The regioselectivity of the coupling of gemcitabine to lipoic acid by amide bond formation was one of the advantages of using DCC as a coupling agent which provided only one product with reasonable yield (40%).

Amide bonds in general are known to be cleaved in acidic pH environments and also by specific enzymes. A gemcitabine prodrug synthesised by introducing a substituent attached to the primary amino group of gemcitabine through an amide bond was described to be enzymatically cleaved by proteases and peptidases. In addition increased temperature had an additive effect on the rate of amide bond hydrolysis (Wickremsinhe *et al.* 2013).

The objective of the synthesis of the GL prodrug was to provide gemcitabine with an arm to actively bind to the gold surface of the HNPs, while conferring the ability of the system prodrug-HNPs to act as a stimuli responsive carrier.

The synthesis of the Hybrid iron oxide core-gold shell nanoparticles (HNPs) was confirmed to be successful by determining the physicochemical properties of the fabricated particles, including confirming the size, shape and effective coating of the iron oxide core of the hybrid system by utilising several techniques (UV/Vis spectroscopy, photon correlation spectroscopy, zeta potential measurement, inductively coupled plasma-optical emission spectroscopy (ICP-OES) and transmission electron microscopy (TEM)). The potential advantages of the HNPs

to act as a theranostic agent is derived from the ability of the system to be imaged using MRI due to the magnetic character of the iron oxide core. The gold surface of the HNPs can be functionalised and loaded with drugs and targeting agents and finally the potential ability of the gold surface to act as a nanoheater when irradiated by near infrared laser light.

Loading of the GL prodrug onto the surface gold of the HNPs was studied at different concentration ratios and a maximum loading concentration of 5 mg of GL prodrug per 1 mg HNPs (based on iron mass) was achieved successfully in the absence of PEG thiol.

The release profile of gemcitabine from the GL-HNPs formulation under sink conditions was studied at fixed time points in different pH and temperature environments: Up to 24 hrs of the release study the highest percentage of drug release from the nanoparticulate formulation was 41% which occurred at pH 5.6 under the effect of elevated temperature (44 °C). In general, the data showed the combined effect of both low pH and heat on the rate and extent of gemcitabine release from the formulation. The drug release profile was performed at different pHs to mimic the cytoplasmic pH and also the pH range of endosomal and lysosomal environments. The drug release pattern followed the order of decreasing the pH of media. Increasing the temperature from 37 °C to 44 °C enhanced the drug release rate however the release rate and extent was higher at pH 5.6 than at pH 3.6 at the same temperature and time point which indicates that the optimum release pH was 5.6.

In vitro biological investigations of the GL prodrug and the GL-HNPs formulation on the human primary pancreatic adenocarcinoma cells (BxPC-3) was performed utilising two techniques, MTT assay and Trypan blue exclusion assay. The MTT assay depends on the metabolic activity of cells and their ability to convert coloured reagent from yellow to violet for absorbance measurements. The Trypan blue exclusion assay depends on the integrity of the cellular structure, in particular cell membranes. Both techniques required careful monitoring of the cell dilutions at the time of cell culture and drug dilution at the time of cell treatment, otherwise a variation in result would happen. Furthermore the MTT assay technique was able to detect the viability more accurately as compared to other techniques, in addition to the advantages of simplicity, high throughput measurement and relatively fast procedure (da Costa *et al.* 1999).

The cell viability in the presence of the GL prodrug and the GL-HNPs formulation measured by MTT assay showed a better effect for the GL-HNPs formulation over both gemcitabine and GL prodrug alone after 24 hrs. The GL prodrug alone showed similar effects to gemcitabine in nearly all the concentrations used except for the highest concentration (100 μg/mL) where the prodrug was shown to be more effective. This finding tie with the result obtained from the cellular uptake study which shows a better uptake of the GL-HNPs formulation over GL prodrug and gemcitabine.

Gemcitabine cytotoxicity on the cancer cell line after 48 and 72 hrs was shown to be more effective than the GL prodrug and the GL-HNPs formulation which might

indicate the importance of the time required for gemcitabine to be internalised and activated before excreting its full action.

In general, according to the uptake study which indicated an enhanced internalisation of the GL prodrug and the GL-HNPs formulation over gemcitabine, the viability effect should show better response for the prodrug and the formulation over gemcitabine. However, gemcitabine requires to be released first from the formulation, or cleaved from the lipoic acid in case of the GL prodrug, and because of the relative stability of the amide bond the variable amount of the drug released from the prodrug and the formulation might be the cause of this behaviour.

By comparing the MTT viability assay results obtained for the GL prodrug and the GL-HNPs formulation with the result obtained for the same compounds using the trypan blue exclusion assay, the IC$_{50}$ appears to be different between the two assays. However, the standard deviation difference in the two experiments appears to be relatively high which might explain the difference between the results.

Moreover, the biological assay required to be performed at the optimum conditions required for drug release from the nanoparticulate formulation (44℃ at pH 5.6) in order to simulate both the physiological conditions faced by the GL-HNPs formulation at the time of uptake and the heat generated by the possible laser irradiation of the gold surface of the HNPs. This was not achieved during this study but could form the basis of future work in this area.

Questions remain concerning the nature of the attachment of prodrug of gemcitabine (GL prodrug **98**) to the gold surface of the HNPs to form GL-HNPs and subsequent release of gemcitabine **7** under various conditions. The amide bond between gemcitabine **7** and the lipoic acid **88** residue is very stable at pH 7.4 and room temperature in deionised water yet it is potentially unstable when the prodrug is attached to the gold surface at elevated temperatures and reduced pH. Laser irradiation of the GL-HNPs formulation using a near infrared laser may show release of gemcitabine **7**. This study could be undertaken *in vitro* but assumes that the formulation will be taken up by bodies within the cell that present an acidic environment. This latter assumption is key and can be resolved by studying cell uptake more closely.

Attachment of gemcitabine **7** to the surface of the HNPs is worth exploring further. Sulfur forms dative bonds to the gold surface but it has been shown that electrostatic interactions can also be used to attach drug substances to gold. Irradiation of a formulation of a polyamine drug derivative coated onto HNPs with near infrared laser light triggers drug release. It therefore follows that a polyamine derivative of gemcitabine would be worth pursuing. As has been mentioned in this thesis, research towards the synthesis of such a prodrug was started but proved to be difficult to achieve in the timeframe allowed due to capricious reactions to synthesise the required polyamine precursors. This could easily form the basis of a further research project.

The nature of the prodrug itself warrants further investigation in the absence of HNPs. It appears that it is potentially more cytotoxic than gemcitabine alone but

not at a level which is yet significant clinically. Again, the nature of the amide bond between gemcitabine **7** and the lipoic acid residue **88** may be important. Many studies into derivatives of gemcitabine have used attachment to the primary amine as a synthetic strategy. As mentioned previously, capecitabine **99** is a structurally related drug which also contains a residue bonded to what was a primary amine functional group on a nitrogen heterocycle. However, the alkyl substituent is not bonded through an amide but through a carbamate linkage. Carbamates are use in drug design as an isosteric replacement for the amide bond (Ghosh & Brindisi 2015). Development of the gemcitabine analogue using a rational drug design approach would be worthy but also being mindful of the research that has already been published on gemcitabine analogues.
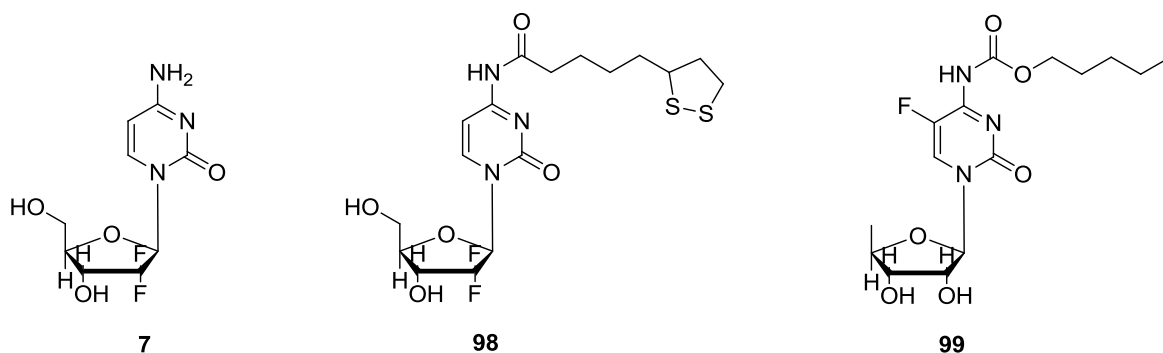
The use of a gemcitabine **7** and capecitabine **99** together as a combination chemotherapy for pancreatic cancer has been reported to be clinically useful (Neoptolemos *et al.* 2017). Taking all of the comments above and being mindful of the potential of HNPs for drug delivery, it would be very interesting to develop a formulation in which capecitabine and gemcitabine prodrugs are attached to HNPs via a suitable responsive linker. Again, this could form the basis of a significant piece of research.

In conclusion, whilst it proved difficult to overcome synthesis of the pharmacologically active compounds and formulations described in this thesis, possible solutions have now been described. There is great potential to develop these findings, both in the presence or absence of HNPs. Future research may yield clinically significant results.

CHAPTER 7: EXPERMENTAL

7.1 Synthesis and characterisation of compounds

All chemicals and solvents were purchased from either Sigma Aldrich or Alfa Aesar company and unless otherwise stated were used without further purification. Anhydrous dimethylformamide were purchased from Sigma Aldrich and used without further treatment.

TLC plates used were silica gel 60 F254 (Merck) and detection was conducted using UV light, potassium permanganate solution or vanillin stain Flash column chromatography was carried out on silica gel 60 (40-63 μm mesh).

Melting point determination was completed using a Bibby Stuart Scientific Melting point apparatus (uncorrected). Infrared spectra were recorded on a Thermo Nicolet Nexus FT-IR spectrometer.

1H NMR and 13C NMR spectra were obtained using Bruker Avance 300 and/or Bruker Avance 400; 19F NMR spectra were obtained using a Bruker Avance 400. Multiplicities were recorded as broad peaks (br), singlets (s), doublets (d), triplets (t), quartets (q), quintets (qu),) double doublets (dd), multiplets (m). All NMR samples were made up in deuterated solvents with all values quoted in ppm relative to tetramethylsilane (TMS) as an internal reference. Coupling constants (J values) are reported in Hertz (Hz).

7.2 *N*-(3-hydroxypropyl) naphthalimide 52
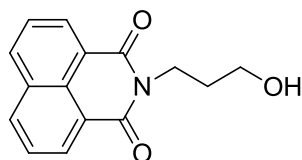
52

The synthetic procedure was adopted from (Lin & Pavlov 2000)

1, 8-Naphthalic anhydride (39.60 g, 0.2 mol) was suspended in absolute ethanol (350 mL) with stirring, followed by drop-wise addition of 3-aminopropan-1-ol (15.00 g 0.2 mol). The mixture was heated to reflux for 15 hrs. The resulting precipitate was collected by vacuum filtration, recrystallised from absolute ethanol and dried in a desiccator to give off-white needle shaped crystals.

Yield: 79%

Mp: 125.5°C

v_{max} (cm^{-1}) 1693 (NC=O), 3425 (OH).

^{1}H NMR (300 MHz CDCl$_3$): δ 8.63, (2H, d, *J* 8.29 ArH) 8.25, (2H, d, *J* 8.48 ArH) 7.78 (2H, t, *J* 8.29 ArH), 4.37 (2H, t, CH$_2$-O); 3.60 (2H, t, N–CH$_2$); 3.01 (br, s, OH); 1.99 (2H, qu, -CH$_2$-).

^{13}C NMR (300 MHz CDCl$_3$): δ164.8 (C=O); 134.2, 131.6, 131.5, 128.1, 127.0, 122.2 (aromatic carbons); 58.7, 36.7, 31.9 (aliphatic carbons).

7.3 *N*-(3-hydroxyethyl) naphthalimide 62
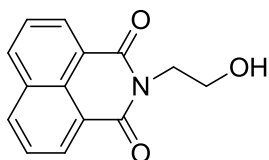
62

The synthetic procedure was adopted from (Lin & Pavlov 2000).

1, 8-Naphthalic anhydride (9.9 g, 50 mmol) was suspended in absolute ethanol (100 mL) with stirring, followed by drop-wise addition of ethanolamine (3.05 g 50 mmol). The mixture was heated to reflux for 15 h. The resulting precipitate was collected by vacuum filtration, recrystallised from absolute ethanol and dried in a desiccator to give off-white needle shaped crystals.

Yield: 84%

MP: 179 °C

^{1}H NMR (300 MHZ CDCl$_3$): δ 8.53, (2H, d, *J* 7.35 ArH), 8.15, (2H, d, *J* 8.48 ArH), 7.69 (2H, t, *J* 8.48 ArH), 4.39 (2H t, CH$_2$-O), 3.92 (2H t, N–CH$_2$), 1.95 (br, s, OH).

^{13}C NMR (300 MHZ CDCl$_3$): δ165.1 (C=O); 134.2, 131.6, 131.5, 128.1, 127.0, 122.3 (aromatic carbons); 61.8, 42.7 (aliphatic carbons).

7.4 *N*-[2-(2-hydroxylethylamino)-ethyl]-1, 8-naphthalimide (HEAEN) 67
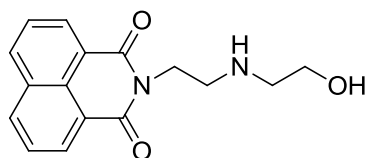
67

The synthetic procedure was adopted from (Chen *et al.* 2009)

1, 8-Naphthalic anhydride **5** (2.0 g, 10.1 mmol) was suspended in absolute ethanol (60 mL) with stirring, followed by drop-wise addition of 2-(2-aminoethylamino) ethanol (1.06 g, 10.2 mmol). The mixture was heated to reflux for 15 hrs. The resulting solution was concentrated by rotary evaporation of most of the solvent and then left to crystallise at room temperature; the resulted pink coloured powder was recrystallised from absolute ethanol and dried in a desiccator to give pale yellow crystals.

Yield: 90%

M.P: 115 $^\circ$C

^{1}H NMR (300 MHZ CDCl$_3$): δ 8.52, (2H, dd, *J* 8.29 ArH), 8.15, (2H, dd, *J* 8.90 ArH), 7.69 (2H, t, *J* 8.10 ArH), 2.82 (t, 2H, *J* 4.90 Hz, –NCH$_2$), 3.02 (t, 2H, *J* 6.40 Hz, CH$_2$-N), 3.62 (t, 2H, *J* 5.20 Hz, CH$_2$CH$_2$-N), 4.32 (t, 2H, *J* 6.40 Hz, CH$_2$-OH),

^{13}C NMR (300 MHZ CDCl$_3$): δ164.53 (C=O); 134.00, 131.48, 131.28, 128.07, 126.98, 122.43 (aromatic carbons); 60.88, 50.98, 47.48, 39.91 (aliphatic carbons).

7.5 *O*-(tosyloxypropyl)naphthalimide 53

53
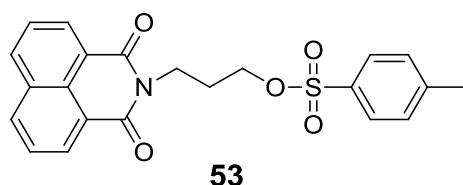
N-(3-Hydroxypropyl)naphthalimide **52** (5.10 g, 20 mmol) was dissolved in anhydrous pyridine (80 mL). The solution was cooled to 0 °C and kept stirring at that temperature for 10 minutes. *para*-Toluenesulfonyl chloride (5.72 g, 30 mmol) was added in small portions over a period of 30 minutes, the pale-yellow solution was kept stirring at 0 °C for extra 10 minutes then the solution was stored in the fridge overnight at 4°C The reaction mixture was poured into icy water (400 mL) with rapid, vigorous stirring, to deliver a viscous liquid that solidified very quickly upon stirring. The precipitate was filtered off and washed thoroughly with water. The crude product was recrystallised from ethanol.

Yield: 58%

Mp: 120.1°C

v_{max} (cm^{-1}) 1698 NC=O, 1093 (C-O)

^{1}H NMR (300 MHZ CDCl$_3$): δ 8.60, (2H, dd, J 7.35 ArH), 8.23, (2H, dd, J 7.35 ArH), 7.78 (2H, t, J 8.29 ArH), 7.79 (2H, d, OTos ArH), 7.31 (2H, d, OTos ArH), 4.22 (4H, p, N-CH$_2$, CH$_2$-O), 2.13 (2H, qu, -CH$_2$-) 2.43 (3H, s, CH$_3$).

^{13}C NMR (300 MHZ CDCl$_3$): δ164.15 (C=O); 144.74, 143.54, 134.13, 132.96, 131.37, 129.78 (naphthalimide aromatic carbons); 128.13, 127.93, 126.98, 122.41 (tosyl aromatic carbons); 68.59, 37.10, 27.63 (CH$_2$) 21.66 (CH$_3$).

7.6 *O*-(tosyloxyethyl) naphthalimide 63

63
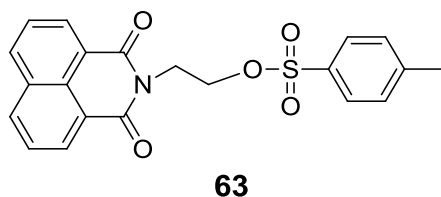
N-(3-Hydroxyethyll)naphthalimide **62** (1.5 g, 6.5 mmol) was dissolved in anhydrous pyridine (20 mL). The solution was cooled to 0 °C and kept stirring at that temperature for 10 minutes. *para*-Toluenesulfonyl chloride (1.25 g, 6.5 mmol) was added in small portions over a period of 30 minutes, the pale-yellow solution was kept stirring at 0 °C for extra 10 minutes then the solution was stored in the fridge overnight at 4°C The reaction mixture was poured into icy water (400 mL) with rapid, vigorous stirring, to deliver a viscous liquid that solidified very quickly upon stirring. The precipitate was filtered off and washed thoroughly with water. The product was purified by column chromatography but it is unstable on the column and so the yield is reduced as a result.

Yield: 53%

Mp: 106℃

v_{max} (cm^{-1}) 1698 (NC=O).

^{1}H NMR (300 MHZ CDCl$_3$): δ 8.63, (2H, dd, *J* 7.16 ArH), 8.25, (2H, dd, *J* 8.29 ArH), 7.78 (2H, t, *J* 8.29 ArH), 7.79 (2H, d, OTos ArH) 7.30 (2H, d, *J* 8.10 OTos ArH); 4.23 (2H m, CH$_2$-O), 2.44 (3H, s, CH$_3$), 2.14 (2H, qu, CH$_2$).

^{13}C NMR (300 MHZ CDCl$_3$): δ164.15 (C=O); 144.74, 143.54, 134.13, 132.96, 131.37, 129.78 (naphthalimide aromatic carbons); 128.13, 127.93, 126.98, 122.41 (tosyl aromatic carbons); 68.59, 37.10 (CH$_2$) 21.64 (CH$_3$).

7.7 Di tosylated *N*-[2-(2-hydroxylethylamino)-ethyl]-1, 8-naphthalimide (HEAEN) 68

68
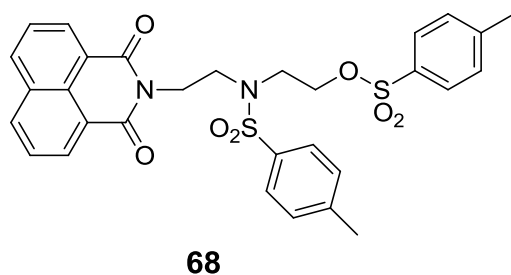
(HEAEN) **67** (2 g, 7.03 mmol) was dissolved in anhydrous pyridine (50 mL). The solution was cooled to 0 °C and kept stirring at that temperature for 10 minutes. *para*-Toluenesulfonyl chloride (4.02 g, 21.12 mmol) was added in small portions over a period of 30 minutes, the yellow solution was left to reach the ambient

temperature spontaneously then kept stirring at room temperature for additional 12 hrs, the aqueous workup of the reaction carried out by pouring the reaction mixture into icy water (400 mL) with rapid, vigorous stirring, to deliver a viscous liquid that solidified very quickly upon stirring. The precipitate was filtered off and washed thoroughly with water. The product was recrystallised from ethanol.

Yield: 40%

^{1}H NMR (300 MHZ CDCl$_3$): δ 8.52, (2H, d, J 6.97 ArH), 8.21, (2H, d, J 7.82 ArH), 7.74 (2H, d, J 7.52 ArH), 7.80 (2H, d, OTos ArH), 7.53 (2H, d, OTos ArH), 7.35 (2H, d, OTos ArH), 6.96 (2H, d, OTos ArH), 4.28 (4H, t, CH$_2$-O), 3.71 (2H, t, CH$_2$), 3.54 (2H, t, CH$_2$), 2.44 (3H, s, CH$_3$), 2.15 (3H, s, CH$_3$).

^{13}C NMR (300 MHz CDCl$_3$): δ164.5 (C=O); 145.11, 143.32, 136.32, 132.48, 131.53 (naphthalimide aromatic carbon), 134.15, 131.24, 129.98, 129.53, 128.058, 127.00, 126.95 (tosyl aromatic carbons); 68.47, 46.48, 46.03, 37.72 (CH$_2$), 21.69, 21.03 (CH$_3$)

7.8 Tetra-mesitylated spermine 56

56

222
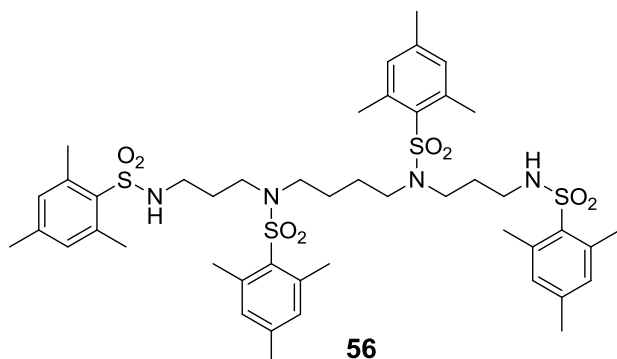
Spermine (4.04 g, 20 mmol) was dissolved in dry pyridine (50mL) the solution was cooled to 0°C. mesitylenesulfonyl chloride (18.57 g 85 mmol) was added in small portion and the mixture was kept stirring in ice for 1 hr and then for 20 hrs at room temperature. The reaction mixture was poured on to icy water (200 mL) with vigorous stirring to obtain a viscous brown precipitate which was collected using Buchner filtration. The precipitate was washed with water and diluted HCl, then dried over the filter paper and the crude product was recrystallised from hot ethanol.

Yield: 30%.

Mp: 162.5°C

v_{max} (cm^{-1}) 1603 Ar, (cm^{-1}) 3266 NH.

^{1}H NMR (300 MHZ CDCl$_3$): 6.95, 6.94 (8H, s, ArH), 3.20 (4H, t, CH$_2$-NH), 3.05 (4H, t, CH$_2$-N), 2.81 (4H, t, CH$_2$-N), 1.60-1.69 (4H, m, CH$_2$–N) 1.29-1.35 (8H, m, CH$_2$–N), 2.6 (12H, s, CH$_3$.Mts), 2.54 (12H, s, CH$_3$.Mts), 2.31 (12H, s, CH$_3$.Mts).

^{13}C NMR (300 MHZ CDCl$_3$): 142.71, 142.11, 139.98, 138.90, 133.70, 133.01, 132.11, 131.96 (aromatic carbons Mts), 45.13, 42.82, 39.33, 27.60, 24.44 (Aliphatic carbon spermine), 22.90, 20.98, 20.93 (CH$_3$.Mts).

7.9 Di-mesitylated diaminododecane 58

58
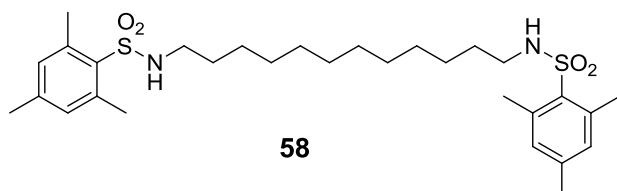
1,12-diaminododecane (2.0 g, 10 mmol) was dissolved in dry pyridine (40 mL) the solution was cooled to 0°C. mesitylenesulfonyl chloride (4.37 g 20 mmol) was added in small portion and the mixture was kept stirring in ice for 1 hr and then for 20 hrs at room temperature. The reaction mixture was poured on to icy water (200 mL) with vigorous stirring to obtain a viscous brown precipitate which was collected using Buchner filtration. The precipitate was washed with water and diluted HCl, then dried over the filter paper and the crude product was recrystallised from hot ethanol.

Yield: 49%

Mp: 102°C.

^{1}H NM (300 MHZ CDCl$_3$): 6.97 (4H, s, ArH), 2.89 (4H, t, CH$_2$-NH), 1.45 (4H, t, CH$_2$–), 2.65 (12H, s, CH$_3$.Mts), 2.31 (6H, s, CH$_3$.Mts), 1.19 (16H, s, –CH$_2$–).

^{13}C NMR (300 MHZ CDCl$_3$): 142–131 (aromatic carbons), 42 (CH$_2$–NH), 29-30 (4×CH$_2$), 26.9 (CH$_2$), 23 (CH$_3$.Mts), 21 (CH$_3$.Mts).

7.10 *N1,N4,N7,N10-tetra*(mesitylenesulfonyl)triethylenetetramine 64

64
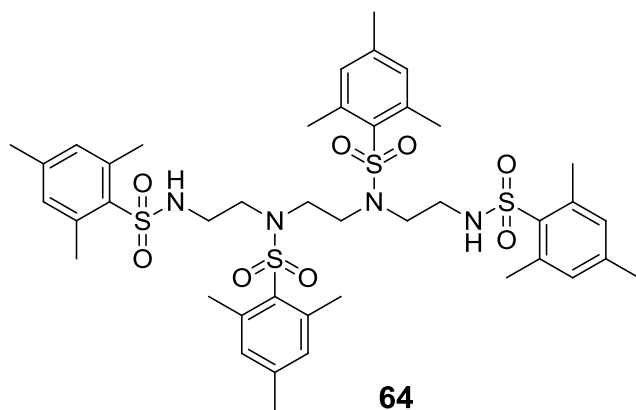
Triethylenetetramine (1.0 g, 6.8 mmol) was dissolved in dry pyridine (25 mL) the solution was cooled to 0°C. mesitylenesulfonyl chloride (6.0 g 28 mmol) was added in small portion and the mixture was kept stirring in ice for 1 hr and then for 20 h at room temperature. The reaction mixture was poured on to icy water (200 mL) with vigorous stirring to obtain a viscous deep brown nearly solid compound which was collected using Buchner filtration. The crude compound was washed with water and diluted HCl, then the pure product was delivered using column separation.

Yield: 33%

^{1}H NM (300 MHZ CDCl$_3$): 6.95 (4H, s, ArH Mts), 6.94 (4H, s, ArH Mts), 3.37 (4H, s, N-CH$_2$-CH$_2$-N), 3.30 (4H, t, *J* 6.03 CH$_2$–N), 2.94 (4H, q, *J* 6.22 CH$_2$–NH), 2.56 (12H, s, CH$_3$.Mts), 2.49 (12H, s, CH$_3$.Mts), 2.32 (6H, s, CH$_3$.Mts), 2.31 (6H, s, CH$_3$.Mts).

^{13}C NMR: (CDCl$_3$) 143.08, 142.36, 140.19, 139.02, 133.10, 132.25, 132.08, 132.05 (aromatic carbons Mts), 46.89, 45.39, 41.19 (aliphatic carbon), 22.92, 22.87, 21.03, 20.96 (CH$_3$.Mts)

7.11 Reaction of 1,4-butane dithiol with acrylonitrile 77
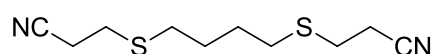
77

1,4-butane dithiol (1.22 g, 10 mmol,) was dissolved in THF (25 mL). at -78℃ in an inert atmosphere, Triton B (1.672g 10 mmol) and after 10 minutes acrylonitrile (1.06 g, 20 mmol) were added and the mixture was allowed to reach the room temperature spontaneously, the reaction was quenched by water (20 mL) after four hrs the crude product was extracted twice with ether (10 mL) the combined organic layer washed with brine and dried over magnesium sulfate, after removal of inorganic salt the solvent was evaporated under reduced pressure.

Yield: 50%

^{1}H NMR (300 MHZ CDCl$_3$): 2.81 (t, CH$_2$-CN); 2.65 (t, CH$_2$-S); 1.69 (m, CH$_2$-)

^{13}C NMR (300 MHZ CDCl$_3$): 118.4 (CN); 31.6 (CH$_2$–S); 28.1(CH$_2$-CH$_2$); 27.5(CH$_2$–S); 18.9 (CH$_2$-CN).

7.12 Reduction of 3,3'-(butane-1,4-diylbis(sulfanediyl))Dipropanenitrile 78
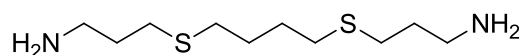
78

3,3'-(butane-1,4-diylbis(sulfanediyl))dipropanenitrile **77** (1.2 g, 5.8 mmol) was dissolved in anhydrous THF (50 mL) under an inert atmosphere BH3.DMS (2.5 mL, 33 mmol) was added and the mixture was heated to reflux for 24 hrs. After cooling, the excess borane was destroyed by very careful drop wise addition of excess methanol. And then the solvents and by products (trimethyl borate and dimethylsulfide) were removed in vacuum to give a colourless, viscous oil.

Yield: 90%

^{1}H NMR: (300 MHZ CDCl$_3$) 3.49 (NH$_2$) 2.81 (t, CH$_2$-N), 2.85 (m, CH$_2$-S), 1.69 (m, CH$_2$-).

^{13}C NMR: (300 MHZ CDCl$_3$) 41.2 (CH$_2$-N); 33.2 (CH$_2$–S); 31.7(CH$_2$-CH$_2$); 29.4(CH$_2$–S); 28.6 (CH$_2$-CH$_2$).

7.13 1,20-Diaminoeicosane 41
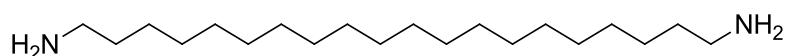
41

The synthetic procedure was adopted from (Norrehed *et al.* 2013)

1,20-Eicosanedicarboxylic acid (2 g, 5.85 mmol) was dissolved in $SOCl_2$ (40 mL) and heated to reflux for 2.5 hrs until gas evolution had ceased completely. The solvent was evaporated and the solid residue was dissolved in dioxane (20 mL). An NH_3-solution (concentrated, in H_2O, 25 mL) was added. A white precipitate was formed then the mixture was stirred for 1 hr, filtered off and left to dry in air over night. The obtained white solid was dissolved in hot dry THF and a suspension of $LiAlH_4$ (0.5 g, 15 mmol) in dry THF (30 mL) was added at room temperature. The mixture was heated to reflux overnight and then quenched with H_2O and filtered over a Buchner funnel. The product was obtained as a waxy white solid the resulted compound was used in the coupling step without further purification.

Yield: 90%

1H NMR: (400 MHZ $CDCl_3$): 1.81-1.58 (30H, m), 1.41-1.25 (10H, m).

7.14 *Tetra-* mesitylated bis(naphthalimidopropyl) spermine 54
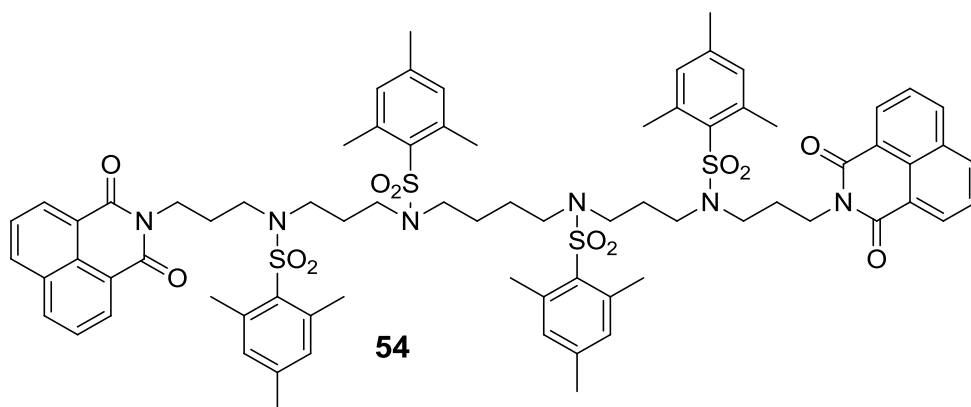
Tetra-mesitylated spermine **56** (3.72 g, 4 mmol) was dissolved in anhydrous dimethylformamide. (50 mL) *O*-(tosyloxypropyl)naphthalimide **53** (3.3065 g, 8.5 mmol) was added followed immediately by caesium carbonate (7 g) the mixture was stirred at 85°C for 8 hrs. the reaction mixture was poured into icy water (500 mL) with vigorous stirring to give a pink solid precipitate. 2M HCl (50 mL) was added with stirring to remove any remaining caesium carbonate. The precipitate was collected by vacuum filtration and washed with water and then air-dried on the filter paper. The crude product was recrystallised from ethanol.

Yield: 54%.

Mp: 189.2°C

^{1}H NMR (300 MHZ CDCl$_3$): δ 8.57, (4H, dd, *J* 7.35 ArH naphthalimide), 8.24, (4H, dd, *J* 8.48 ArH naphthalimide), 7.78 (4H, t, *J* 8.10 ArH naphthalimide), 6.91 (4H, s, ArH Mts), 6.70 (4H, s, ArH Mts); 3.91 (4H, t, *J* 6.97CH$_2$-NH), 3.07 (14H, m, CH$_2$-

N), 1.70 (10H, m, CH$_2$-N), 1.36 (4H, m), 2.55, 2.46 (20H, s, CH$_3$.Mts), 2.27, 2.19, 2.12 (16H, s, CH$_3$.Mts).

^{13}C NMR (300 MHZ CDCl$_3$): 163.98 (CH$_2$ =O), 142.41, 142.33, 140.04, 139.95, 134.08, 133.14, 132.69, 132.00, 131.82, 131.54, 131.27, 128.04, 126.97122.45 (aromatic carbons), 44.93, 43.23, 42.95, 42.82 (CH$_2$–N); 37.51, (CH$_2$–N); 25.73, 25.17, 24.33 (CH$_2$); 22.87, 22.74 (CH$_3$.Mts); 20.99, 20.89 (CH$_3$.Mts).

7.15 Di-mesitylated bis(naphthalimidopropyl)-1,12 diaminododecane 55

33
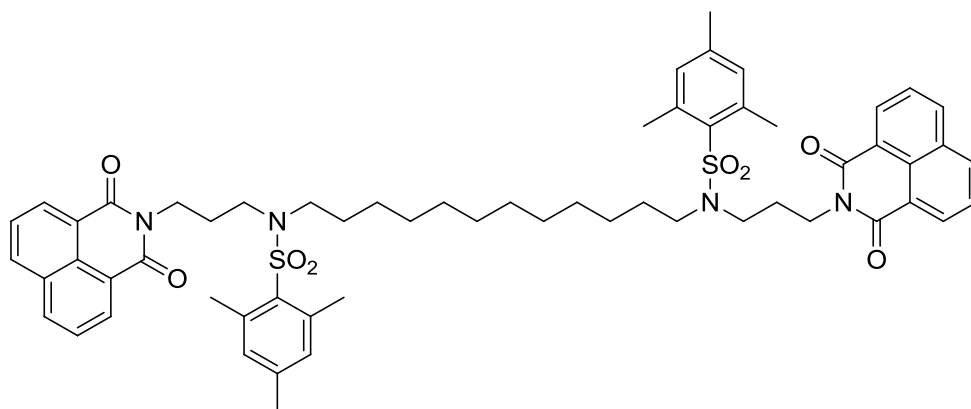
Di-mesitylated diaminododecane **58** (1.13 g, 2 mmol) was dissolved in anhydrous dimethylformamide. (25 mL) O-(tosyloxypropyl)naphthalimide **53** (1.75 g, 4.5 mmol) was added followed immediately by caesium carbonate (3.5 g) the mixture was stirred at 85°C for 8 hrs. the reaction mixture was poured into icy water (500 mL) with vigorous stirring to give a solid precipitate. 2M HCl (25 mL) was added with stirring to remove any remaining caesium carbonate. The precipitate was

collected by vacuum filtration and washed with water and then air-dried on the filter paper. The crude product was recrystallised from ethanol.

Yield: 65%.

Mp: 102°C

^{1}H NMR (300 MHZ CDCl$_3$): δ 8.58, (4H, d, J 7.35 ArH), 8.24, (4H, d, J 8.48 ArH), 7.78 (4H, d, J 8.48 ArH), 6.73 (4H, s, ArH); 4.02 (4H, t, CH$_2$-NH), 3.27 (, m, CH$_2$-N), 2.52 (12H, s, CH$_3$.Mts), 2.15 (6H, s, CH$_3$.Mts), 1.85 (m CH$_2$).

^{13}C NMR (300 MHZ CDCl$_3$): 164.0 (CH$_2$ =O), 142.0–122.5 (aromatic carbons), 45.3, 43.1 (CH$_2$–N), 37.7, 29.5(CH$_2$–N), 29.1, 27.4, 26.8, 25.9, 22.9 (CH$_2$), 22.7 (CH$_3$.Mts), 20.8 (CH$_3$.Mts).

7.16 Bisnaphthalimidopropyldiaminopropyldithiobutane (BNIPds) 34

34
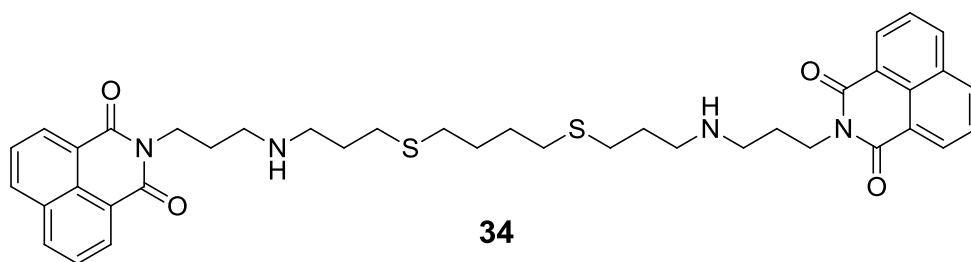
To a solution of **78** (1.0 g, 4.2 mmol) in anhydrous dimethylformamide. (20 mL) O-(tosyloxypropyl)naphthalimide **53** (3.45 g, 8.4 mmol) was added followed immediately by caesium carbonate (7 g) the mixture was stirred at room temperature for 8 hrs under inert atmosphere, the reaction was stopped and the

solvent evaporated under reduced pressure, dissolved in ethyl acetate washed with 2M HCl (20 mL), water (10 mL), brine (10 mL) and dried over magnesium sulfate. The combined extracts were reduced to give a brownie-yellow solid.

Yield: 75%.

^{1}H NMR (300 MHZ CDCl$_3$): δ 8.57, (4H, dd, J 7.16 ArH), 8.22, (4H, dd, J 7.54 ArH), 7.75 (4H, t, J 7.54 ArH), 4.30 (4H, t, J 7.35), 4.19 (4H, t, J 6.22); 3.20 (4H, m, CH$_2$-NH), 2.64 (4H, m, CH$_2$-N), 2.51 (4H, m, CH$_2$-N), 2.10 (4H, m, CH$_2$), 1.99 (4H, t, J 7.35 6.03 CH$_2$), 1.72 (4H, m, CH$_2$).

^{13}C NMR (300 MHZ CDCl$_3$): 164.14 (CH$_2$ =O); 134.13, 134.06, 131.52, 131.26, 127.00. 126.95 (aromatic carbons), 62.84, 58.87, 53.53, 39.24, 37.52, 36.79, 30.89, 27.24 (aliphatic carbons)

7.17 Bis(naphthalimido)diaminoicosan (BNIPDi) 32
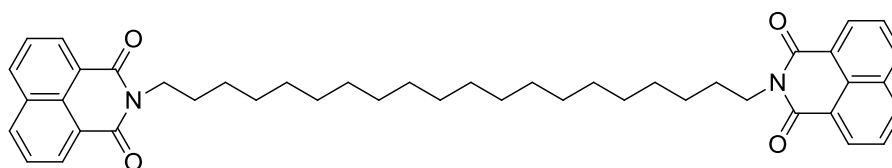
32

1,8-Naphthalic anhydride **35** (8 g ,40mmol) was suspended in absolute ethanol (200 mL) with stirring. Followed by wise addition of 1,20-Diaminoeicosane **41** (.6.2 g 19.8 mmol). The mixture was heated to reflux for 15 hrs. The crude precipitate

was collected by vacuum filtration, recrystallised from absolute ethanol and dried in desiccator, the product was obtained by column separation.

Yield: 15%.

Mp: 120.2℃

^{1}H NMR (400 MHZ CDCl$_3$): δ 8.62, (4H, d, *J* 7.09 ArH), 8.33, (4H, d, *J* 8.19 ArH), 8.09 (4H, d, *J* 7.34 ArH), 3.76-3.68 (8H, m), 1.67-1.51 (8H, m), 1.27-1.22 (24H, m).

^{13}C NMR (400 MHZ CDCl$_3$):164.19 (C=O); 133.81, 131.80, 131.14, 130.35, 126.94, 118.96 (aromatic carbons); 40.50 (N–CH$_2$); 29.70, 29.68, 29.66, 29.61, 29.57, 29.40, 28.20, 27.17(-CH$_2$-).

7.18 BNIPSpm 21

21
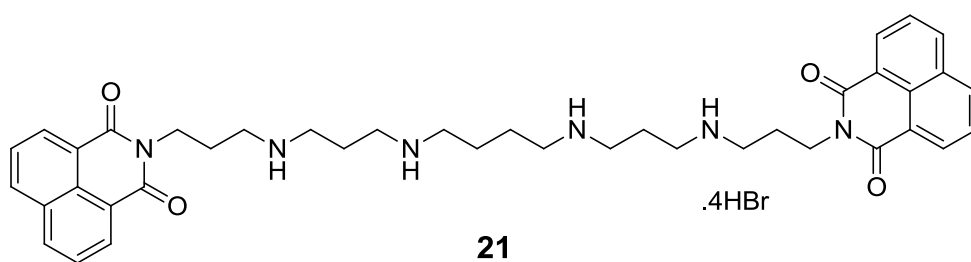
Tetra- mesitylated bis(naphthalimidopropyl) spermine **54** (2.19 g 1.5 mmol) was dissolved in dry dichloromethane (50 mL) HBr as a 33% solution in acetic acid (10 mL) was added and the mixture stirred overnight at room temperature under

nitrogen. On the following day, the formed precipitate was filtered and washed with dry dichloromethane to give a yellow-orange solid. The precipitate was dried on the filter and then in vacuum at 60 °C to remove residual acetic acid.

Yield: 60%

Mp: 272 ℃

^{1}H NMR (300 MHZ DMSO-d6): δ 8.51, (8H, dd, ArH), 7.90 (4H, t, ArH), 4.15 (t, CH_2-N), 3.42 (m, CH_2-NH, CH_2-CH_2).

^{13}C NMR (300 MHZ DMSO-d6):163.7 (C=O), 134.4, 130.7, 127.1, 122.0 (aromatic carbons), 43.9(N–CH_2), 24.5, 22.4 (–CH_2–).

7.19 BNIPDodec 26

26
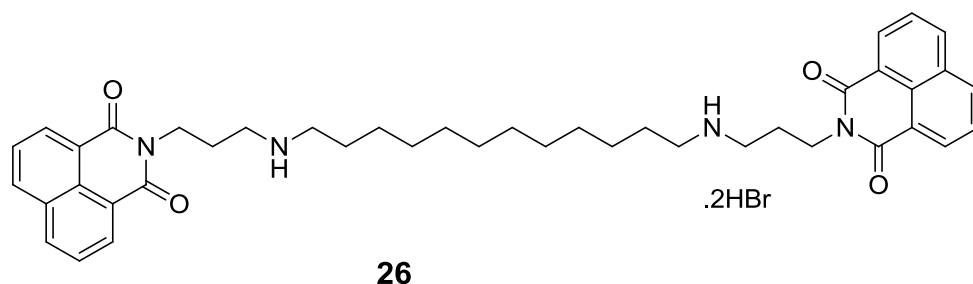
Di-mesitylated bis(naphthalimidopropyl)-1,12 diaminododecane **55** (1.05 g 1 mmol) was dissolved in dry dichloromethane (20 mL) HBr as a 33% solution in acetic acid (3.85 mL) was added and the mixture stirred overnight at room temperature under nitrogen. On the following day, the formed precipitate was

filtered and washed with dry dichloromethane to give a yellow-orange solid. The precipitate was dried on the filter and then in vacuum at 60 °C to remove residual acetic acid.

Yield: 66%

Mp: 216℃

^{1}H NMR (300 MHZ DMSO-d6): δ 8.50, (8H, dd, ArH), 7.89 (4H, t, ArH), 4.12 (t, CH$_2$-N), 3.52 (m, CH$_2$-NH, CH$_2$-CH$_2$).

^{13}C NMR (300 MHZ DMSO-d6):163.6 (C=O); 134.4, 130.7, 127.2, 122.1 (aromaticcarbons); 46.7(N–CH$_2$); 44.8 (NH–CH$_2$); 36.9, 28.8, 28.4, 25.9, 25.5, 24.5. (–CH$_2$–).

7.20 Gemcitabine-lipoic acid prodrug 98

98
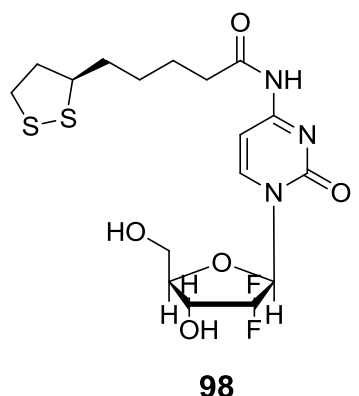
To a solution of Lipoic acid (202 mg, 1 mmol), DCC (202 mg, 1 mmol) in DMF (10 mL) stirred for 10 minutes at room temperature, gemcitabine (263 mg, 1 mmol) was added together with a catalytic amount of DMAP and the reaction mixture was

kept stirring at room temperature for 24 hrs, The reaction was then stopped and filtered, the filtrate was taken, the solvent was evaporated to its half volume under reduced pressure, the residue was mixed with ethyl acetate (20 mL) and the precipitated unreacted gemcitabine was removed by filtration, the solvent was then evaporated and the residue dissolved in ethyl acetate washed with water (10 mL), brine (10 mL) and dried over magnesium sulfate. The combined extracts were reduced to give a yellow solid, this was then purified by column chromatography (ethyl acetate: petroleum ether 10:1 to 1:1, followed by 100% ethyl acetate) to yield the title compound as a pale yellow solid.

Yield 40.0%

Mp: 115℃

^{1}H NMR spectrums (400 MHz DMSO-d6): δ 11.03 (s, 1H,), 8.27 (d, 1H,), 7.30 (d, 1H,), 6.36 (d, 1H), 6.20 (t, 1H,), 5.35 (t, 1H), 4.20 (m, 1H,), 3.91 (m, 1H,), 3.82 (m, 1H,), 3.65 (m, 2H), 3.18 (m, 2H), 2.44 (m, 3H,), 1.93 (m, 1H), 1.68 (m, 1H), 1.25 (m, 1H), 1.58 (m, 2H), 1.39 (m, 2H).

^{13}C NMR spectrums (400 MHz DMSO-d6): δ 174.36, 154.64 (C=O), 163.32, 145.17, 96.44 (Ar carbon), 84.61, 81.45, 68.83, 60.15 59.56, (deoxy ribose carbon), 56.49, 39.39, 38.61, 36.71, 34.53, 28.54, 24.60 (lipoic acid carbo).

CHAPTER 8: REFERENCES

Albericio, F., 2004. Developments in peptide and amide synthesis. *Current Opinion in Chemical Biology*, 8(3), pp.211–221.

Alexakis, N. et al., 2004. Current standards of surgery for pancreatic cancer. *British Journal of Surgery*, 91(11), pp.1410–1427.

Alexander, R.L. et al., 2005. A novel phospholipid gemcitabine conjugate is able to bypass three drug-resistance mechanisms. *Cancer Chemotherapy and Pharmacology*, 56(1), pp.15–21.

Allen, S.L. & Lundberg, A.S., 2011. Amonafide: A potential role in treating acute myeloid leukemia. *Expert Opinion on Investigational Drugs*, 20(7).

Arends, J.J. et al., 2005. A phase II study of raltitrexed and gemcitabine in patients with advanced pancreatic carcinoma. *British journal of cancer*, 92(3), pp.445–448.

Au, M. et al., 2016. Emerging Therapeutic Potential of Nanoparticles in Pancreatic Cancer: A Systematic Review of Clinical Trials. *Biomedicines*, 4(3), p.20. Available at: http://www.mdpi.com/2227-9059/4/3/20/htm.

Aue, W.P., 1976. Two-dimensional spectroscopy. Application to nuclear magnetic resonance. *The Journal of Chemical Physics*, 64(5), pp.2229–2246. Available at:
http://link.aip.org/link/?JCP/64/2229/1&Agg=doi%5Cnpapers3://publication/doi/10.1063/1.432450.

Avendano, C. & Menendez, J.C., 2008. *Medicinal Chemistry of Anticancer Drugs*,

Bachrach, U., 2010. The early history of polyamine research. *Plant Physiology and Biochemistry*, 48(7), pp.490–495.

Bailly, C., Braña, M. & Waring, M.J., 1996. Sequence-selective intercalation of antitumour bis-naphthalimides into DNA. Evidence for an approach via the major groove. *Eur. J. Biochem.*, 240, p.195.

Banerjee, S. et al., 2005. Molecular evidence for increased antitumor activity of gemcitabine by genistein in vitro and in vivo using an orthotopic model of pancreatic cancer. *Cancer Research*, 65(19), pp.9064–9072.

Bardeesy, N. & DePinho, R.A., 2002. Pancreatic cancer biology and genetics. *Nat Rev Cancer*, 2(12), pp.897–909. Available at: http://www.ncbi.nlm.nih.gov/pubmed/12459728.

Bardeesy, N. & DePinho, R. a, 2002. Pancreatic cancer biology and genetics. *Nature reviews. Cancer*, 2(12), pp.897–909.

Barnett, C.M. et al., 2013. Physical stability, biocompatibility and potential use of hybrid iron oxide-gold nanoparticles as drug carriers. *Journal of Nanoparticle Research*, 15(6).

Barron, G.A. et al., 2010. Synthesis, cytotoxicity and DNA-binding of novel bisnaphthalimidopropyl derivatives in breast cancer MDA-MB-231 cells. *European Journal of Medicinal Chemistry*, 45(4), pp.1430–1437.

BARRON, G.A., 2010. *Novel bisnaphthalimidopropyl polyamine derivatives: their mode of action in a breast cancer cell system*. Available at:

http://openair.rgu.ac.uk.

Batmani, Y. & Khaloozadeh, H., 2013. Optimal drug regimens in cancer chemotherapy: A multi-objective approach. *Computers in Biology and Medicine*, 43(12), pp.2089–2095.

Bazak, R., Houri, M., El Achy, S., et al., 2014. Cancer active targeting by nanoparticles: a comprehensive review of literature. *Journal of Cancer Research and Clinical Oncology*, 141, pp.769–784.

Bazak, R., Houri, M., Achy, S. El, et al., 2014. Passive targeting of nanoparticles to cancer: A comprehensive review of the literature. *Molecular and clinical oncology*, 2(6), pp.904–908. Available at: http://www.ncbi.nlm.nih.gov/pubmed/25279172%5Cnhttp://www.pubmedcentral.nih.gov/articlerender.fcgi?artid=PMC4179822.

Bellin, M.-F., 2006. MR contrast agents, the old and the new. *European journal of radiology*, 60(3), pp.314–323.

Bergeron, R.J. et al., 1988. Synthetic polyamine analogues as antineoplastics. *Journal of medicinal chemistry*, 31(6), pp.1183–90. Available at: http://www.ncbi.nlm.nih.gov/pubmed/3373487.

Bergman, A.M. et al., 1999. Decreased resistance to gemcitabine (2',2'-difluorodeoxycitidine) of cytosine arabinoside-resistant myeloblastic murine and rat leukemia cell lines: Role of altered activity and substrate specificity of deoxycytidine kinase. *Biochemical Pharmacology*, 57(4), pp.397–406.

Bergman, A.M., Pinedo, H.M. & Peters, G.J., 2002a. Determinants of resistance to 2',2'-difluorodeoxycytidine (gemcitabine). *Drug Resistance Updates*, 5(1), pp.19–33.

Bergman, A.M., Pinedo, H.M. & Peters, G.J., 2002b. Determinants of resistance to 2',2' -difluorodeoxycytidine (gemcitabine). *Drug Resistance Updates*, 5(1), pp.19–33.

Berridge, M. et al., 1996. The biochemical and cellular basis of cell proliferation assays that use tetrazolium salts. *Biochemica*, (4), pp.4–9.

Berridge, M.V. & Tan, A.S., 1993. Characterization of the Cellular Reduction of 3-(4,5-dimethylthiazol-2-yl)-2,5-diphenyltetrazolium bromide (MTT): Subcellular Localization, Substrate Dependence, and Involvement of Mitochondrial Electron Transport in MTT Reduction. *Archives of Biochemistry and Biophysics*, 303(2), pp.474–482.

Bersani, S. et al., 2014. PH-sensitive stearoyl-PEG-poly(methacryloyl sulfadimethoxine) decorated liposomes for the delivery of gemcitabine to cancer cells. *European Journal of Pharmaceutics and Biopharmaceutics*, 88(3), pp.670–682.

Bhadra, D. et al., 2002. Pegnology: A review of PEG-ylated systems. *Pharmazie*, 57(1), pp.5–29.

Biewenga, G.P., Haenen, G.R.M.M. & Bast, A., 1997. The pharmacology of the antioxidant: Lipoic acid. *General Pharmacology*, 29(3), pp.315–331.

Bildstein, L. et al., 2010. Transmembrane diffusion of gemcitabine by a nanoparticulate squalenoyl prodrug: An original drug delivery pathway. *Journal of Controlled Release*, 147(2), pp.163–170.

Bildstein, L., Dubernet, C. & Couvreur, P., 2011. Prodrug-based intracellular delivery of anticancer agents. *Advanced Drug Delivery Reviews*, 63(1–2), pp.3–23.

Bousquet, P.F. et al., 1995. Preclinical Evaluation of Lu-79553 - A Novel Bis-Naphthalimide with Potent Antitumor-Activity. *Cancer Research*, 55(5), pp.1176–1180. Available at: isi:A1995QJ60000034.

Brana et al., 1980. Synthesis and mode(s) of action of a new series of imide derivatives of 3-nitro-1,8-naphthoic acid. *Cancer Chemother Pharmacol.*, 4(1), pp.61–66.

Brana, M.F. et al., 2001. Intercalators as Anticancer Drugs | BenthamScience. *Current Pharmaceutical Design*, 7(17), pp.1745–1780. Available at: http://www.eurekaselect.com/65102/article.

Braña, M.F. et al., 1993. Bis-naphthalimides: a new class of antitumor agents. *Anti-cancer drug design*, 8(4), pp.257–68. Available at: http://www.ncbi.nlm.nih.gov/pubmed/8240655.

Braña, M.F. et al., 1996. Bis-naphthalimides 3: synthesis and antitumor activity of N,N'-bis[2-(1,8-naphthalimido)-ethyl] alkanediamines. *Anti-cancer drug design*, 11(4), pp.297–309. Available at: http://www.ncbi.nlm.nih.gov/pubmed/8679053.

Brana, M.F. & Ramos, A., 2001. Naphthalimides as Anticancer Agents: Synthesis and Biological Activity. *Current Medicinal Chemistry -Anti-Cancer Agents*, 1(3), pp.237–255. Available at: http://www.ingentaconnect.com/content/ben/cmcaca/2001/00000001/0000000 3/art00002.

Braña, M.F. & Ramos, A., 2001. Naphthalimides as anti-cancer agents: synthesis and biological activity. *Current medicinal chemistry. Anti-cancer agents*, 1(3), pp.237–55. Available at: http://www.ncbi.nlm.nih.gov/pubmed/12678756.

Burris, H.A. et al., 1997. Improvements in survival and clinical benefit with gemcitabine as first-line therapy for patients with advanced pancreas cancer: a randomized trial. *Journal of clinical oncology : official journal of the American Society of Clinical Oncology*, 15(6), pp.2403–13. Available at: http://www.ncbi.nlm.nih.gov/pubmed/9196156.

Cabral, H. et al., 2011. Accumulation of sub-100 nm polymeric micelles in poorly permeable tumours depends on size. *Nature Nanotechnology*, 6(12), pp.815–823. Available at: http://dx.doi.org/10.1038/nnano.2011.166.

Cai, W. et al., 2008. Applications of gold nanoparticles in cancer nanotechnology. *Nanotechnology, science and applications*, 1, pp.17–32. Available at: http://www.pubmedcentral.nih.gov/articlerender.fcgi?artid=3781768&tool=pmc entrez&rendertype=abstract.

Campbell, R., 2006. Tumor Physiology and Delivery of Nanopharmaceuticals. *Anti-Cancer Agents in Medicinal Chemistry*, 6(6), pp.503–512. Available at:

http://www.scopus.com/inward/record.url?eid=2-s2.0-
33750806589&partnerID=tZOtx3y1.

CancerResearch, 2016. Cancer statistics for the UK. *Cancer Research UK*, pp.1–
4. Available at: http://www.cancerresearchuk.org/health-professional/cancer-
statistics.

Cao-Milán, R. & Liz-Marzán, L.M., 2014. Gold nanoparticle conjugates: recent
advances toward clinical applications. *Expert opinion on drug delivery*, 11(5),
pp.741–52. Available at: http://www.ncbi.nlm.nih.gov/pubmed/24559075.

Casero, J.A. & Woster, P.M., 2001. Terminally alkylated polyamine analogues as
chemotherapeutic agents. *Journal of Medicinal Chemistry*, 44(1), pp.1–26.

Casero, R.A. & Pegg, A.E., 2009. Polyamine catabolism and disease. *The
Biochemical journal*, 421(3), pp.323–338. Available at:
http://www.pubmedcentral.nih.gov/articlerender.fcgi?artid=2756025&tool=pmc
entrez&rendertype=abstract.

Casero, R. a & Marton, L.J., 2007. Targeting polyamine metabolism and function
in cancer and other hyperproliferative diseases. *Nature reviews. Drug
discovery*, 6(5), pp.373–390.

Cavallaro, G. et al., 2006. Folate-mediated targeting of polymeric conjugates of
gemcitabine. *International Journal of Pharmaceutics*, 307(2), pp.258–269.

Chen, F., Ehlerding, E.B. & Cai, W., 2014. Theranostic nanoparticles. *Journal of
nuclear medicine : official publication, Society of Nuclear Medicine*, 55(12),

pp.1919–22. Available at: http://www.pubmedcentral.nih.gov/articlerender.fcgi?artid=4255955&tool=pmc entrez&rendertype=abstract.

Chen, J. et al., 2009. Solvatofluorochromism of N-[2-(2-hydroxylethylamino)-ethyl]-1,8-naphthalimide in protic solvent. *Journal of Molecular Structure*, 917(2–3), pp.170–175. Available at: http://linkinghub.elsevier.com/retrieve/pii/S0022286008004997.

Cherukuri, P., Glazer, E.S. & Curley, S.A., 2010. Targeted hyperthermia using metal nanoparticles. *Advanced Drug Delivery Reviews*, 62(3), pp.339–345.

Chiellini, F. et al., 2016. Modelling of Pancreatic Ductal Adenocarcinoma in Vitro with Three-Dimensional Microstructured Hydrogels. *RSC Advances*, 6, pp.54226–54235. Available at: http://dx.doi.org/10.1039/C6RA08420F.

Childs, A.C., Mehta, D.J. & Gerner, E.W., 2003. Polyamine-dependent gene expression. *Cellular and Molecular Life Sciences*, 60(7), pp.1394–1406.

Chitkara, D. et al., 2013. Self-assembling, amphiphilic polymer-gemcitabine conjugate shows enhanced antitumor efficacy against human pancreatic adenocarcinoma. *Bioconjugate Chemistry*, 24(7), pp.1161–1173.

Choi, C.H.J. et al., 2011. Targeting kidney mesangium by nanoparticles of defined size. *Proceedings of the National Academy of Sciences of the United States of America*, 108(16), pp.6656–61. Available at: http://www.pubmedcentral.nih.gov/articlerender.fcgi?artid=3080986&tool=pmc entrez&rendertype=abstract.

De Clercq, E. & Field, H.J., 2006. Antiviral prodrugs - the development of successful prodrug strategies for antiviral chemotherapy. *British journal of pharmacology*, 147(1), pp.1–11. Available at: http://www.pubmedcentral.nih.gov/articlerender.fcgi?artid=1615839&tool=pmc entrez&rendertype=abstract.

Cobley, C.M. et al., 2010. Targeting gold nanocages to cancer cells for photothermal destruction and drug delivery. *Expert opinion on drug delivery*, 7(5), pp.577–587.

Cooper, G.M. & Hausman, R.E., 2007. *The Cell: A Molecular Approach 2nd Edition*,

da Costa, A.O. et al., 1999. Comparative analysis of three methods to assess viability of mammalian cells in culture. *Biocell*, 23(1), pp.65–72. Available at: http://www.ncbi.nlm.nih.gov/pubmed/10904534.

Curtis, A. et al., 2015. Heat Dissipation of Hybrid Iron Oxide-Gold Nanoparticles in an Agar Phantom. *J Nanomed Nanotechnol*, 6. Available at: http://dx.doi.org/10.4172/2157-7439.1000335.

Damaraju, V.L. et al., 2003. Nucleoside anticancer drugs: the role of nucleoside transporters in resistance to cancer chemotherapy. *Oncogene*, 22, pp.7524–7536.

Dance, A.M. et al., 2005. Synthesis and biological activities of bisnaphthalimido polyamines derivatives: Cytotoxicity, DNA binding, DNA damage and drug localization in breast cancer MCF 7 cells. *Biochemical Pharmacology*, 69(1),

pp.19–27.

Davis, M.E., Chen, Z.G. & Shin, D.M., 2008. Nanoparticle therapeutics: an emerging treatment modality for cancer. *Nature reviews. Drug discovery*, 7(9), pp.771–782.

Day, E.S. et al., 2010. Antibody-conjugated gold-gold sulfide nanoparticles as multifunctional agents for imaging and therapy of breast cancer. *International Journal of Nanomedicine*, 5(1), pp.445–454.

Dintzis, S.M. & Liggitt, D., 2012. Pancreas. In *Comparative Anatomy and Histology*. pp. 203–209.

Dreaden, E.C. et al., 2012. Size matters: gold nanoparticles in targeted cancer drug delivery. *Therapeutic Delivery*, 3(4), pp.457–478.

Dreher, M.R. et al., 2006. Tumor vascular permeability, accumulation, and penetration of macromolecular drug carriers. *Journal of the National Cancer Institute*, 98(5), pp.335–344.

Duncan, R., 2003. The dawning era of polymer therapeutics. *Nature reviews. Drug discovery*, 2(5), pp.347–60. Available at: http://www.ncbi.nlm.nih.gov/pubmed/12750738.

Emanuela, B. et al., 2012. Synthetic polyamines as potential amine oxidase inhibitors: A preliminary study. *Amino Acids*, 42(2–3), pp.913–928.

Ernst, R.R., Bodenhausen, G. & Wokaun, A., 1987. Principles of nuclear magnetic resonance in one and two dimensions. In *Principles of Nuclear Magnetic*

Resonance in One and Two Dimensions. pp. 50–60.

Ferreira, D., Adega, F. & Chaves, R., 2013. The Imortance of Cancer Cell Lines as in vitro Models in Cancer Methylome Analysis and Anticancer Drugs Testing. In *Oncogenomics and Cancer Proteomics - Novel Approaches in Biomarkers Discovery and Therapeutic Targets in Cancer*.

Ferrone, C.R. et al., 2012. Pancreatic ductal adenocarcinoma: long-term survival does not equal cure. *Surgery*, 152(3 Suppl 1), pp.S43-9. Available at: http://www.ncbi.nlm.nih.gov/pubmed/22763261%5Cnhttp://www.pubmedcentr al.nih.gov/articlerender.fcgi?artid=PMC3806092.

Filosa, R. et al., 2009. Molecular modelling studies, synthesis and biological activity of a series of novel bisnaphthalimides and their development as new DNA topoisomerase II inhibitors. *Bioorganic and Medicinal Chemistry*, 17(1), pp.13–24.

Fortune, J.M. & Osheroff, N., 2000. Topoisomerase II as a target for anticancer drugs: when enzymes stop being nice. *Progress in nucleic acid research and molecular biology*, 64, pp.221–53. Available at: http://www.ncbi.nlm.nih.gov/pubmed/10697411.

Frese, K.K. et al., 2012. Nab-paclitaxel potentiates gemcitabine activity by reducing cytidine deaminase levels in a mouse model of pancreatic cancer. *Cancer Discovery*, 2(3), pp.260–269.

Fukuda, Y. & Schuetz, J.D., 2012. ABC transporters and their role in nucleoside and nucleotide drug resistance. *Biochemical Pharmacology*, 83(8), pp.1073–

1083.

Galmarini, C.M. et al., 2010. Efficient overcoming of drug resistance to anticancer nucleoside analogs by nanodelivery of active phosphorylated drugs. *International Journal of Pharmaceutics*, 395(1–2), pp.281–289.

Galmarini, C.M., Mackey, J.R. & Dumontet, C., 2001. Nucleoside analogues: mechanisms of drug resistance and reversal strategies. *Leukemia*, 15(6), pp.875–890.

Geall, A.J. & Blagbrough, I.S., 2000. Homologation of polyamines in the rapid synthesis of liospermine conjugates and related lipoplexes. *Tetrahedron*, 56(16), pp.2449–2460.

Geromichalou, E. et al., 2015. Regioselective chemical and rapid enzymatic synthesis of a novel redox-Antiproliferative molecular hybrid. *European Journal of Medicinal Chemistry*, 96, pp.47–57.

Ghosh, A.K. & Brindisi, M., 2015. Organic Carbamates in Drug Design and Medicinal Chemistry. *Journal of Medicinal Chemistry*, 58(7), pp.2895–2940.

Goon, I.Y. et al., 2009. Fabrication and dispersion of gold-shell-protected magnetite nanoparticles: Systematic control using polyethyleneimine. *Chemistry of Materials*, 21(4), pp.673–681.

Gorąca, A. et al., 2011. Lipoic acid - biological activity and therapeutic potential. *Pharmacological reports : PR*, 63(4), pp.849–58. Available at: http://www.ncbi.nlm.nih.gov/pubmed/22001972.

Gottesman, M.M., 2002. Mechanisms of Cancer Drug Resistance. *Annual Review of Medicine*, 53(1), pp.615–627. Available at: http://www.annualreviews.org/doi/10.1146/annurev.med.53.082901.103929.

Gradishar, W.J. et al., 2005. Phase III trial of nanoparticle albumin-bound paclitaxel compared with polyethylated castor oil-based paclitaxel in women with breast cancer. *Journal of Clinical Oncology*, 23(31), pp.7794–7803.

Guo, Y. et al., 2013. Photothermal ablation of pancreatic cancer cells with hybrid iron-oxide core gold-shell nanoparticles. *International Journal of Nanomedicine*, 8, pp.3437–3446.

Guo, Z. & Gallo, J.M., 1999. Selective Protection of 2',2'-Difluorodeoxycytidine (Gemcitabine). *The Journal of Organic Chemistry*, 64(22), pp.8319–8322.

Han, H.K. & Amidon, G.L., 2000. Targeted prodrug design to optimize drug delivery. *AAPS pharmSci*, 2(1), p.E6.

Harris, J.M. & Chess, R.B., 2003. Effect of pegylation on pharmaceuticals. *Nature reviews. Drug discovery*, 2(3), pp.214–21. Available at: http://www.nature.com/doifinder/10.1038/nrd1033%5Cnhttp://www.ncbi.nlm.nih.gov/pubmed/12612647.

Heinemann, V., 2001. Gemcitabine: progress in the treatment of pancreatic cancer. *Oncology*, 60(1), pp.8–18. Available at: http://www.ncbi.nlm.nih.gov/entrez/query.fcgi?cmd=Retrieve&db=PubMed&dopt=Citation&list_uids=11150902.

Hengartner, M.O., 2000. The biochemistry of apoptosis. *Nature*, 407(6805), pp.770–6.

Hezel, A.F. et al., 2006. Genetics and biology of pancreatic ductal adenocarcinoma Genetics and biology of pancreatic ductal adenocarcinoma. *Genes & Development*, 1(30), pp.1218–1249. Available at: http://genesdev.cshlp.org/content/20/10/1218.full.pdf+html.

Hidalgo, M., 2010. Pancreatic Cancer. *New England Journal of Medicine*, 362(17), pp.1605–1617. Available at: http://www.nejm.org/doi/abs/10.1056/NEJMra0901557.

Von Hoff, D.D. et al., 2011. Gemcitabine plus nab-paclitaxel is an active regimen in patients with advanced pancreatic cancer: A phase I/II trial. *Journal of Clinical Oncology*, 29(34), pp.4548–4554.

Von Hoff, D.D. et al., 2013. Increased survival in pancreatic cancer with nab-paclitaxel plus gemcitabine. *The New England journal of medicine*, 369(18), pp.1691–703. Available at: http://www.ncbi.nlm.nih.gov/pubmed/24131140%5Cnhttp://www.pubmedcentral.nih.gov/articlerender.fcgi?artid=PMC4631139.

Hoffmann, E. De & Stroobant, V., 2007. *Mass Spectrometry Principles and Applications*, Available at: http://books.google.com/books?hl=en&lr=&id=pqhr5XQZDtUC&oi=fnd&pg=PR11&dq=mass+spectrometry+principles+and+applications&ots=6l9XvbS0r-&sig=FB4zmdUIyUrmKqG_Y7Hyl-jZ6Kk.

Hoskins, C. et al., 2012. Hybrid gold-iron oxide nanoparticles as a multifunctional platform for biomedical application. *Journal of Nanobiotechnology*, 10(27), pp.1–12.

Huang, X. et al., 2006. Determination of the minimum temperature required for selective photothermal destruction of cancer cells with the use of immunotargeted gold nanoparticles. *Photochemistry and Photobiology*, 82(2), pp.412–7. Available at: http://www.ncbi.nlm.nih.gov/pubmed/16613493.

Huang, X. et al., 2007. Gold nanoparticles: interesting optical properties and recent applications in cancer diagnostics and therapy. *Nanomedicine (London, England)*, 2(5), pp.681–693.

Huang, X. & El-Sayed, M.A., 2010. Gold nanoparticles: Optical properties and implementations in cancer diagnosis and photothermal therapy. *Journal of Advanced Research*, 1(1), pp.13–28.

Hwu, J.R. et al., 2009. Targeted paclitaxel by conjugation to iron oxide and gold nanoparticles. *Journal of the American Chemical Society*, 131(1), pp.66–68.

Jagu, E. et al., 2015. Design, synthesis and in vitro antikinetoplastid evaluation of N-acylated putrescine, spermidine and spermine derivatives. *Bioorganic and Medicinal Chemistry Letters*, 25(2), pp.207–209.

Jain, P.K. et al., 2006. Calculated Absorption and Scattering Properties of Gold Nanoparticles of Different Size, Shape, and Composition: Applications in Biological Imaging and Biomedicine. *The Journal of Physical Chemistry B*, 110(14), pp.7238–7248. Available at:

http://dx.doi.org/10.1021/jp057170o%5Cnhttp://pubs.acs.org/doi/full/10.1021/j
p057170o%5Cnhttp://pubs.acs.org/doi/pdfplus/10.1021/jp057170o.

Jain, R.K., 2012. Delivery of molecular and cellular medicine to solid tumors. *Advanced Drug Delivery Reviews*, 64(SUPPL.), pp.353–365.

Janib, S.M., Moses, A.S. & MacKay, J.A., 2010. Imaging and drug delivery using theranostic nanoparticles. *Advanced Drug Delivery Reviews*, 62(11), pp.1052–1063.

Jazayeri, M.H. et al., 2016. Various methods of gold nanoparticles (GNPs) conjugation to antibodies. *Sensing and Bio-Sensing Research*, 9, pp.17–22.

Jemal, A. et al., 2010. Cancer statistics, 2010. *CA Cancer J Clin*, 60(5), pp.277–300. Available at: http://www.ncbi.nlm.nih.gov/pubmed/20610543.

Jin, Y. et al., 2010. Multifunctional nanoparticles as coupled contrast agents. *Nature communications*, 1(May), p.41. Available at: http://www.ncbi.nlm.nih.gov/pmc/articles/PMC3205955/%5Cnhttp://www.ncbi.nlm.nih.gov/pmc/articles/PMC3205955/pdf/nihms332702.pdf.

Johnson, S., Nguyen, V. & Coder, D., 2013. Assessment of cell viability. *Current Protocols in Cytometry*, (SUPPL.64).

Jokerst, J. V et al., 2011. Nanoparticle PEGylation for imaging and therapy. *Nanomedicine (London, England)*, 6(4), pp.715–728. Available at: http://www.pubmedcentral.nih.gov/articlerender.fcgi?artid=3217316&tool=pmcentrez&rendertype=abstract.

Jokerst, J. V. & Gambhir, S.S., 2011. Molecular imaging with theranostic nanoparticles. *Accounts of Chemical Research*, 44(10), pp.1050–1060.

Jørgensen, M.R. et al., 2005. The effects of conformational constraints and steric bulk in the amino acid moiety of philanthotoxins on AMPAR antagonism. *Journal of Medicinal Chemistry*, 48(1), pp.56–70.

Jun, Y.W., Lee, J.H. & Cheon, J., 2008. Chemical design of nanoparticle probes for high-performance magnetic resonance imaging. *Angewandte Chemie - International Edition*, 47(28), pp.5122–5135.

Kamal, A. et al., 2007. Synthesis, DNA binding, and cytotoxicity studies of pyrrolo[2,1-c][1,4]benzodiazepine-anthraquinone conjugates. *Bioorganic and Medicinal Chemistry*, 15(22), pp.6868–6875.

Kamisawa, T. et al., 2016. Pancreatic cancer. *The Lancet*, 388(10039), pp.73–85.

Kayal, S. & Ramanujan, R. V., 2010. Doxorubicin loaded PVA coated iron oxide nanoparticles for targeted drug delivery. *Materials Science and Engineering C*, 30(3), pp.484–490.

Khan, a U., Mei, Y.H. & Wilson, T., 1992. A proposed function for spermine and spermidine: protection of replicating DNA against damage by singlet oxygen. *Proceedings of the National Academy of Sciences of the United States of America*, 89(23), pp.11426–7. Available at: http://www.pubmedcentral.nih.gov/articlerender.fcgi?artid=50563&tool=pmcen trez&rendertype=abstract.

Kim, J. et al., 2006. Designed fabrication of multifunctional magnetic gold nanoshells and their application to magnetic resonance imaging and photothermal therapy. *Angewandte Chemie - International Edition*, 45(46), pp.7754–7758.

Kim, J. et al., 2008. Multifunctional uniform nanoparticles composed of a magnetite nanocrystal core and a mesoporous silica shell for magnetic resonance and fluorescence imaging and for drug delivery. *Angewandte Chemie - International Edition*, 47(44), pp.8438–8441.

Kleger, A., Perkhofer, L. & Seufferlein, T., 2014. Smarter drugs emerging in pancreatic cancer therapy. *Annals of Oncology*, 25(7), pp.1260–1270.

Knop, K. et al., 2010. Poly(ethylene glycol) in drug delivery: Pros and cons as well as potential alternatives. *Angewandte Chemie - International Edition*, 49(36), pp.6288–6308.

Kölmel, D.K. et al., 2014. Cell-penetrating peptoids: Introduction of novel cationic side chains. *European Journal of Medicinal Chemistry*, 79, pp.231–243.

Kong Thoo Lin, P. et al., 2003. The biological activities of new polyamine derivatives as potential therapeutic agents. *Biochemical Society transactions*, 31(2), pp.407–10. Available at: http://www.ncbi.nlm.nih.gov/pubmed/12653648.

Kusano, T. et al., 2007. Advances in polyamine research in 2007. *Journal of Plant Research*, 120(3), pp.345–350.

Kwon, G.S., 2003. Polymeric Micelles for Delivery of Poorly Water-Soluble Compounds. *Critical Reviews in Therapeutic Drug Carrier Systems*, 20(5), pp.357–403.

Lammers, T. et al., 2011. Theranostic nanomedicine. *Accounts of Chemical Research*, 44(10), pp.1029–1038.

Lee, G.Y. et al., 2013. Theranostic nanoparticles with controlled release of gemcitabine for targeted therapy and MRI of pancreatic cancer. *ACS Nano*, 7(3), pp.2078–2089.

Leung, K.C.-F. et al., 2012. Gold and iron oxide hybrid nanocomposite materials. *Chemical Society reviews*, 41(5), p.1911. Available at: http://www.ncbi.nlm.nih.gov/pubmed/22037623.

Li, C. et al., 2010. Gemcitabine plus paclitaxel versus carboplatin plus either gemcitabine or paclitaxel in advanced non-small-cell lung cancer: A literature-based meta-analysis. *Lung*, 188(5), pp.359–364.

Li, C. et al., 2007. Identification of pancreatic cancer stem cells. *Cancer Research*, 67(3), pp.1030–1037.

Lin, P.K.T. & Pavlov, V.A., 2000. *The synthesis and in vitro cytotoxic studies of novel bis-naphthalimidopropyl polyamine derivatives*,

Ling, K.-S. et al., 2005. Mechanisms Involved in Chemoresistance in Ovarian Cancer. *Taiwanese Journal of Obstetrics and Gynecology*, 44(3), pp.209–217.

Liu, H. et al., 2008. Photothermal therapy of Lewis lung carcinoma in mice using

gold nanoshells on carboxylated polystyrene spheres. *Nanotechnology*, 19(45), p.455101. Available at: http://stacks.iop.org/0957-4484/19/i=45/a=455101%5Cnhttp://www.ncbi.nlm.nih.gov/pubmed/21832760.

Lodish, H. et al., 2000. *Molecular Cell Biology. 4th edition*,

Louis, K.S.K.S. & Siegel, A.C.A.C., 2011. Mammalian Cell Viability. *Methods in Molecular Biology*, 740(1), p.p.7-12. Available at: http://link.springer.com/10.1007/978-1-61779-108-6.

Louzada, S., Adega, F. & Chaves, R., 2012. Defining the sister rat mammary tumor cell lines HH-16 cl.2/1 and HH-16.cl.4 as an In Vitro cell model for Erbb2. *PLoS ONE*, 7(1).

Luo, C. et al., 2014. Prodrug-based nanoparticulate drug delivery strategies for cancer therapy. *Trends in Pharmacological Sciences*, 35(11), pp.556–566.

Mackey, J.R. et al., 1998. Functional nucleoside transporters are required for gemcitabine influx and manifestation of toxicity in cancer cell lines. *Cancer Research*, 58(19), pp.4349–4357.

Madela, K. & McGuigan, C., 2012. Progress in the development of anti-hepatitis C virus nucleoside and nucleotide prodrugs. *Future medicinal chemistry*, 4(5), pp.625–50. Available at: http://www.ncbi.nlm.nih.gov/pubmed/22458682.

Mahato, R., Tai, W. & Cheng, K., 2011. Prodrugs for improving tumor targetability and efficiency. *Advanced Drug Delivery Reviews*, 63(8), pp.659–670.

Mahmoudi, M. et al., 2009. Cell toxicity of superparamagnetic iron oxide

nanoparticles. *Journal of Colloid and Interface Science*, 336(2), pp.510–518.

Malekigorji, M. et al., 2017. Thermally triggered theranostics for pancreatic cancer therapy. *Nanoscale*. Available at: http://xlink.rsc.org/?DOI=C7NR02751F.

Malekigorji, M. et al., 2017. Thermally Triggered Theranostics for Pancreatic Cancer Therapy. *Nanoscale,*.

Mandal, S. et al., 2013. Depletion of cellular polyamines, spermidine and spermine, causes a total arrest in translation and growth in mammalian cells. *Proc Natl Acad Sci U S A*, 110(6), pp.2169–2174. Available at: http://www.ncbi.nlm.nih.gov/pubmed/23345430.

Markman, J.L. et al., 2013. Nanomedicine therapeutic approaches to overcome cancer drug resistance. *Advanced Drug Delivery Reviews*, 65(13), pp.1866–1879.

Marshall, N.J., Goodwin, C.J. & Holt, S.J., 1995. A critical assessment of the use of microculture tetrazolium assays to measure cell growth and function. *Growth regulation*, 5(2), pp.69–84.

Martínez, R. & Chacón-García, L., 2005. The search of DNA-intercalators as antitumoral drugs: what it worked and what did not work. *Current medicinal chemistry*, 12(2), pp.127–151.

Matsumura, Y. & Maeda, H., 1986. A New Concept for Macromolecular Therapeutics in Cancer Chemotherapy: Mechanism of Tumoritropic Accumulation of Proteins and the Antitumor Agent Smancs. *Cancer*

Research, 46(8), pp.6387–6392.

Minelli, C., Lowe, S.B. & Stevens, M.M., 2010. Engineering nanocomposite materials for cancer therapy. *Small*, 6(21), pp.2336–2357.

Mini, E. et al., 2006. Cellular pharmacology of gemcitabine. *Annals of Oncology*, 17(SUPPL. 5).

Mini, E. et al., 2006. Cellular pharmacology of gemcitabine. *Annals of Oncology*, 17(Supplement 5), pp.v7–v12.

Minko, T., Rodriguez-Rodriguez, L. & Pozharov, V., 2013. Nanotechnology approaches for personalized treatment of multidrug resistant cancers. *Advanced Drug Delivery Reviews*, 65(13–14), pp.1880–1895.

Mocan, L. et al., 2016. Advances in cancer research using gold nanoparticles mediated photothermal ablation. *Clujul medical (1957)*, 89(2), pp.199–202. Available at: http://www.pubmedcentral.nih.gov/articlerender.fcgi?artid=4849375&tool=pmc entrez&rendertype=abstract.

Mody, V. et al., 2010. Introduction to metallic nanoparticles. *Journal of Pharmacy and Bioallied Sciences*, 2(4), p.282. Available at: http://www.jpbsonline.org/text.asp?2010/2/4/282/72127.

Mody, V. V et al., 2010. Introduction to metallic nanoparticles. *Journal of pharmacy and bioallied sciences*, 2(4), pp.282–289.

Moghimi, S.M., Hunter, A.C. & Murray, J.C., 2005. Nanomedicine: current status

and future prospects. *The FASEB Journal*, 19(3), pp.311–330. Available at: http://www.ncbi.nlm.nih.gov/pubmed/15746175.

Moiseeva, E.P. & Manson, M.M., 2009. Dietary chemopreventive phytochemicals: Too little or too much? *Cancer Prevention Research*, 2(7), pp.611–616.

Montalbetti, C.A.G.N. & Falque, V., 2005. Amide bond formation and peptide coupling. *Tetrahedron*, 61(46), pp.10827–10852.

Moorthi, C., Manavalan, R. & Kathiresan, K., 2011. Nanotherapeutics to overcome conventional cancer chemotherapy limitations. *Journal of Pharmacy and Pharmaceutical Sciences*, 14(1), pp.67–77.

Morikawa, S. et al., 2002. Abnormalities in pericytes on blood vessels and endothelial sprouts in tumors. *The American journal of pathology*, 160(3), pp.985–1000. Available at: http://www.pubmedcentral.nih.gov/articlerender.fcgi?artid=1867175&tool=pmc entrez&rendertype=abstract.

Moysan, E., Bastiat, G. & Benoit, J.P., 2013. Gemcitabine versus modified gemcitabine: A review of several promising chemical modifications. *Molecular Pharmaceutics*, 10(2), pp.430–444.

Müller, C.E., 2009. Prodrug approaches for enhancing the bioavailability of drugs with low solubility. In *Chemistry and Biodiversity*. pp. 2071–2083.

Muth, A. et al., 2014. Polyamine transport inhibitors: Design, synthesis, and combination therapies with difluoromethylornithine. *Journal of Medicinal*

Chemistry, 57(2), pp.348–363.

Narang, A.S. & Desai, D.S., 2009. Anticancer Drug Development Unique Aspects of Pharmaceutical Development. *Pharmaceutical Perspectives of Cancer Therapeutics*, pp.49–92.

National cancer institute, 2016. About cancer. Available at: https://www.cancer.gov [Accessed January 1, 2017].

Nayvelt, I. et al., 2010. DNA condensation by chiral α-methylated polyamine analogues and protection of cellular DNA from oxidative damage. *Biomacromolecules*, 11(1), pp.97–105.

Neesse, A. et al., 2011. Stromal biology and therapy in pancreatic cancer. *Gut*, 60(6), pp.861–8. Available at: http://gut.bmj.com/content/60/6/861.long.

Neidle, S., 2008. *Principles of Nucleic Acid Structure*,

Neoptolemos, J.P. et al., 2010. Adjuvant chemotherapy with fluorouracil plus folinic acid vs gemcitabine following pancreatic cancer resection: a randomized controlled trial. *JAMA*, 304(10), pp.1073–81. Available at: http://www.ncbi.nlm.nih.gov/pubmed/20823433.

Neoptolemos, J.P. et al., 2017. Comparison of adjuvant gemcitabine and capecitabine with gemcitabine monotherapy in patients with resected pancreatic cancer (ESPAC-4): a multicentre, open-label, randomised, phase 3 trial. *The Lancet*, 389(10073), pp.1011–1024.

Neoptolemos JP et al., 2012. Effect of adjuvant chemotherapy with fluorouracil

plus folinic acid or gemcitabine vs observation on survival in patients with resected periampullary adenocarcinoma: The espac-3 periampullary cancer randomized trial. *JAMA*, 308(2), pp.147–156. Available at: http://dx.doi.org/10.1001/jama.2012.7352%5Cnhttp://jama.jamanetwork.com/data/Journals/JAMA/24421/joc120047_147_156.pdf.

Norrehed, S. et al., 2013. Conformational restriction of flexible molecules in solution by a semirigid bis-porphyrin molecular tweezer. *Tetrahedron*, 69(34), pp.7131–7138.

Nune, S.K. et al., 2009. Nanoparticles for biomedical imaging. *Expert Opinion in Drug Delivery*, 6(11), pp.1175–1194.

O'Reilly, E.M., 2011. Adjuvant therapy for pancreas adenocarcinoma: where are we going? *Expert review of anticancer therapy*, 11(2), pp.173–7. Available at: http://www.ncbi.nlm.nih.gov/pubmed/21342036.

Oliveira, J. et al., 2007. The synthesis and the in vitro cytotoxicity studies of bisnaphthalimidopropyl polyamine derivatives against colon cancer cells and parasite Leishmania infantum. *Bioorganic and Medicinal Chemistry*, 15(1), pp.541–545.

Packer, L., Witt, E.H. & Tritschler, H.J., 1995. Alpha-lipoic acid as a biological antioxidant. *Free Radical Biology and Medicine*, 19(2), pp.227–250.

Pankhurst, Q. a et al., 2003. Applications of magnetic nanoparticles in biomedicine. *Journal of Physics D: Applied Physics*, 36(13), pp.R167–R181. Available at: http://stacks.iop.org/0022-

3727/36/i=13/a=201%5Cnhttp://stacks.iop.org/0022-

3727/36/i=13/a=201?key=crossref.3e466fa3dbc8e71868fa521781326623.

Park, J.H. et al., 2008. Polymeric nanomedicine for cancer therapy. *Progress in Polymer Science*, 33(1), pp.113–137.

Patra, C.R. et al., 2008. Targeted Delivery of Gemcitabine to Pancreatic Adenocarcinoma Using Cetuximab as a Targeting Agent Targeted Delivery of Gemcitabine to Pancreatic Adenocarcinoma Using Cetuximab as a Targeting Agent. *Cancer Research*, (6), pp.1970–1978.

Pavlov, V., Kong Thoo Lin, P. & Rodilla, V., 2001. Cytotoxicity, DNA binding and localisation of novel bis-naphthalimidopropyl polyamine derivatives. *Chemico-Biological Interactions*, 137(1), pp.15–24.

Pedreño, E. et al., 2005. Protecting or promoting effects of spermine on DNA strand breakage induced by iron or copper ions as a function of metal concentration. *Journal of Inorganic Biochemistry*, 99(10), pp.2074–2080.

Peer, D. et al., 2007. Nanocarriers as an emerging platform for cancer therapy. *Nature Nanotechnology*, 2(12), pp.751–760.

Pegg, A.E., 2009. Mammalian polyamine metabolism and function. *IUBMB Life*, 61(9), pp.880–894.

Pegg, A.E., 2014. The function of spermine. *IUBMB Life*, 66(1), pp.8–18.

Peng, X.H. et al., 2008. Targeted magnetic iron oxide nanoparticles for tumor imaging and therapy. *International Journal of Nanomedicine*, 3(3), pp.311–

321. Available at: http://www.scopus.com/inward/record.url?eid=2-s2.0-67650648089&partnerID=40&md5=8fc26e88f71db975a1385e6a3fef0b2c.

Plunkett, W. et al., 1995. Gemcitabine: metabolism, mechanisms of action, and self-potentiation. *Seminars in oncology*, 22(4), pp.3–10. Available at: http://www.ncbi.nlm.nih.gov/pubmed/7481842.

Preissler, M. & Williams, J.A., 1981. Pancreatic acinar cell function: measurement of intracellular ions and pH and their relation to secretion. *J Physiol*, 321, pp.437–448.

Rang, H. et al., 2011. *Rang and Dale's Pharmacology (Seventh ed.)*,

Rautio, J. et al., 2008. Prodrugs: design and clinical applications. *Nature reviews. Drug discovery*, 7(3), pp.255–70. Available at: http://www.ncbi.nlm.nih.gov/pubmed/18219308.

Robinson, I. et al., 2010. Synthesis of core-shell gold coated magnetic nanoparticles and their interaction with thiolated DNA. *Nanoscale*, 2, pp.2624–2630.

Rudin, D. et al., 2011a. Gemcitabine Cytotoxicity: Interaction of Efflux and Deamination. *Journal of drug metabolism & toxicology*, 2(107), pp.1–10. Available at: http://www.pubmedcentral.nih.gov/articlerender.fcgi?artid=3144579&tool=pmcentrez&rendertype=abstract.

Rudin, D. et al., 2011b. Gemcitabine Cytotoxicity: Interaction of Efflux and

Deamination. *Journal of drug metabolism & toxicology*, 2(107), pp.1–10.

Ruiz van Haperen, V.W.T. et al., 1993. 2???,2????-Difluoro-deoxycytidine (gemcitabine) incorporation into RNA and DNA of tumour cell lines. *Biochemical Pharmacology*, 46(4), pp.762–766.

Ruoslahti, E., 2002. Specialization of tumour vasculature. *Nature reviews. Cancer*, 2(2), pp.83–90. Available at: http://www.nature.com/doifinder/10.1038/nrc724%5Cnhttp://www.ncbi.nlm.nih. gov/pubmed/12635171.

Ryan, D.P., Hong, T.S. & Bardeesy, N., 2014. Pancreatic Adenocarcinoma. *The New England journal of medicine*, 35(2 Pt 2), pp.353–354.

Sa Cunha, A. et al., 2005. Surgical resection after radiochemotherapy in patients with unresectable adenocarcinoma of the pancreas. *Journal of the American College of Surgeons*, 201(3), pp.359–365.

Sailor, M.J. & Park, J.-H., 2012. Hybrid nanoparticles for detection and treatment of cancer. *Advanced materials (Deerfield Beach, Fla.)*, 24(28), pp.3779–802. Available at: http://www.pubmedcentral.nih.gov/articlerender.fcgi?artid=3517011&tool=pmc entrez&rendertype=abstract.

Shay, K.P. et al., 2009. Alpha-lipoic acid as a dietary supplement: molecular mechanisms and therapeutic potential. *Biochimica et biophysica acta*, 1790(10), pp.1149–60. Available at: http://www.ncbi.nlm.nih.gov/pubmed/19664690%5Cnhttp://www.pubmedcentr

al.nih.gov/articlerender.fcgi?artid=PMC2756298.

Shilo, M. et al., 2012. Nanoparticles as computed tomography contrast agents: current status and future perspectives. *Nanomedicine (London, England)*, 7(2), pp.257–69. Available at: http://www.ncbi.nlm.nih.gov/pubmed/22339135.

Shoemaker, R.H., 2006. The NCI60 human tumour cell line anticancer drug screen. *Nature Reviews Cancer*, 6(10), pp.813–823.

Shrikhande, S. V et al., 2007. Pancreatic resection for M1 pancreatic ductal adenocarcinoma. *Annals of surgical oncology*, 14(1), pp.118–127.

Siegel, R., Naishadham, D. & Jemal, A., 2013. Cancer statistics, 2013. *CA: a cancer journal for clinicians*, 63(1), pp.11–30. Available at: http://www.ncbi.nlm.nih.gov/pubmed/23335087.

Simons, C., Wu, Q. & Htar, T.T., 2005. Recent advances in antiviral nucleoside and nucleotide therapeutics. *Current topics in medicinal chemistry*, 5(13), pp.1191–203. Available at: http://www.ncbi.nlm.nih.gov/pubmed/16305526.

Singh, D. et al., 2015. Recent advances in pancreatic cancer: biology, treatment, and prevention. *Biochimica et biophysica acta*, 1856(1), pp.13–27. Available at: http://www.sciencedirect.com/science/article/pii/S0304419X15000359.

Singh, Y., Palombo, M. & Sinko, P.J., 2008. Recent trends in targeted anticancer prodrug and conjugate design. *Curr Med Chem*, 15(18), pp.1802–1826. Available at: http://www.ncbi.nlm.nih.gov/pubmed/18691040.

De Sousa Cavalcante, L. & Monteiro, G., 2014. Gemcitabine: Metabolism and

molecular mechanisms of action, sensitivity and chemoresistance in pancreatic cancer. *European Journal of Pharmacology*, 741, pp.8–16.

Stavrovskaya, A.A., 2000. Cellular mechanisms of multidrug resistance of tumor cells. *Biochemistry. Biokhimiia*, 65(1), pp.95–106.

Stoddart, M.J., 2011. Cell viability assays: introduction. *Methods in molecular biology (Clifton, N.J.)*, 740, pp.1–6.

Strober, W., 2001. Trypan blue exclusion test of cell viability. *Current protocols in immunology / edited by John E. Coligan ... [et al.]*, Appendix 3, p.Appendix 3B.

Strober, W., 2015. Trypan Blue Exclusion Test of Cell Viability. *Current protocols in immunology*, 111(November), p.A3.B. 1-A3.B.3.

Suggitt, M. & Bibby, M.C., 2005. 50 Years of preclinical anticancer drug screening: Empirical to target-driven approaches. *Clinical Cancer Research*, 11(3), pp.971–981.

Sugimoto, T. & Matijević, E., 1980. Formation of uniform spherical magnetite particles by crystallization from ferrous hydroxide gels. *Journal of Colloid And Interface Science*, 74(1), pp.227–243.

Sun, C., Lee, J.S.H. & Zhang, M., 2008. Magnetic nanoparticles in MR imaging and drug delivery. *Advanced Drug Delivery Reviews*, 60(11), pp.1252–1265.

Sun, J. et al., 2013. The holistic 3M modality of drug delivery nanosystems for cancer therapy. *Nanoscale*, 5(3), pp.845–59. Available at:

http://www.ncbi.nlm.nih.gov/pubmed/23292001.

Sun, Q. et al., 2013. Polymer-Based Prodrugs for Cancer Chemotherapy. *Functional Polymers for Nanomedicine*, (3), pp.245–260.

Surh, Y.-J., 2003. Cancer chemoprevention with dietary phytochemicals. *Nature reviews. Cancer*, 3(10), pp.768–780.

Szakács, G. et al., 2006. Targeting multidrug resistance in cancer. *Nature Reviews Drug Discovery*, 5(3), pp.219–234. Available at: http://www.nature.com/nrd/journal/v5/n3/full/nrd1984.html%5Cnhttp://www.nature.com/nrd/journal/v5/n3/pdf/nrd1984.pdf.

Tang, L. et al., 2014. Investigating the optimal size of anticancer nanomedicine. *Proceedings of the National Academy of Sciences*, 111(43), pp.15344–15349. Available at: http://www.pnas.org/cgi/doi/10.1073/pnas.1411499111.

Thakor, A.S. et al., 2011. Gold nanoparticles: A revival in precious metal administration to patients. *Nano Letters*, 11(10), pp.4029–4036.

Thorek, D.L.J. et al., 2006. Superparamagnetic iron oxide nanoparticle probes for molecular imaging. *Annals of Biomedical Engineering*, 34(1), pp.23–38.

Treuel, L., Jiang, X. & Nienhaus, G.U., 2013. New views on cellular uptake and trafficking of manufactured nanoparticles. *Journal of the Royal Society, Interface*, 10(82), p.20120939. Available at: http://www.ncbi.nlm.nih.gov/pubmed/23427093%5Cnhttp://www.pubmedcentral.nih.gov/articlerender.fcgi?artid=PMC3627074.

Tsume, Y. et al., 2014. The development of orally administrable gemcitabine prodrugs with d-enantiomer amino acids: Enhanced membrane permeability and enzymatic stability. *European Journal of Pharmaceutics and Biopharmaceutics*, 86(3), pp.514–523.

Tuveson, D.A. & Neoptolemos, J.P., 2012. Understanding metastasis in pancreatic cancer: A call for new clinical approaches. *Cell*, 148(1–2), pp.21–23.

Uster, P.S., Working, P.K. & Vaage, J., 1998. Pegylated liposomal doxorubicin (DOXIL®, CAELYX®) distribution in tumour models observed with confocal laser scanning microscopy. *International Journal of Pharmaceutics*, 162(1–2), pp.77–86.

Valeur, E. & Bradley, M., 2009. Amide bond formation: beyond the myth of coupling reagents. *Chem Soc Rev*, 38(2), pp.606–631. Available at: http://www.ncbi.nlm.nih.gov/pubmed/19169468.

Vallianou, N., Evangelopoulos, A. & Koutalas, P., 2009. Alpha-lipoic Acid and diabetic neuropathy. *The review of diabetic studies : RDS*, 6(4), pp.230–6. Available at: http://www.ncbi.nlm.nih.gov/pubmed/20043035%5Cnhttp://www.pubmedcentral.nih.gov/articlerender.fcgi?artid=PMC2836194.

Vargo-Gogola, T. & Rosen, J.M., 2007. Modelling breast cancer: one size does not fit all. *Nature Reviews Cancer*, 7(9), pp.659–672.

Veltkamp, S. a et al., 2008. New insights into the pharmacology and cytotoxicity of gemcitabine and 2',2'-difluorodeoxyuridine. *Molecular cancer therapeutics*,

7(8), pp.2415–2425.

Vigderman, L. & Zubarev, E.R., 2013. Therapeutic platforms based on gold nanoparticles and their covalent conjugates with drug molecules. *Advanced Drug Delivery Reviews*, 65(5), pp.663–676.

Vincent, A. et al., 2011. Pancreatic cancer. *Lancet*, 378(9791), pp.607–20. Available at: http://www.ncbi.nlm.nih.gov/pubmed/21620466.

Walker, E.J. & Ko, A.H., 2014. Beyond first-line chemotherapy for advanced pancreatic cancer: An expanding array of therapeutic options? *World Journal of Gastroenterology*, 20(9), pp.2224–2236.

Wang, J., Lohman, G.J.S. & Stubbe, J., 2009. Mechanism of inactivation of human ribonucleotide reductase with p53R2 by gemcitabine 5???-diphosphate. *Biochemistry*, 48(49), pp.11612–11621.

Weigt, J. & Malfertheiner, P., 2010. Cisplatin plus gemcitabine versus gemcitabine for biliary tract cancer. *Expert review of gastroenterology & hepatology*, 4(4), pp.395–397.

Wellendorph, P. et al., 2003. A sequential high-yielding large-scale solution-method for synthesis of philanthotoxin analogues. *European Journal of Medicinal Chemistry*, 38(1), pp.117–122.

Wickremsinhe, E. et al., 2013. Preclinical absorption, distribution, metabolism, and excretion of an oral amide prodrug of gemcitabine designed to deliver prolonged systemic exposure. *Pharmaceutics*, 5(2), pp.261–76.

Wu, W., He, Q. & Jiang, C., 2008. Magnetic iron oxide nanoparticles: Synthesis and surface functionalization strategies. *Nanoscale Research Letters*, 3(11), pp.397–415.

Xie, J. & Jon, S., 2012. Magnetic nanoparticle-based theranostics. *Theranostics*, 2(1), pp.122–124.

Xie, J., Lee, S. & Chen, X., 2010. Nanoparticle-based theranostic agents. *Advanced Drug Delivery Reviews*, 62(11), pp.1064–1079.

Xu, C., Wang, B. & Sun, S., 2009. Dumbbell-like au-fe 3O 4 nanoparticles for target-specific platin delivery. *Journal of the American Chemical Society*, 131(12), pp.4216–4217.

Yancik, R., 2005. Population aging and cancer: a cross-national concern. *Cancer journal (Sudbury, Mass.)*, 11(6), pp.437–441.

Yu, B. et al., 2010. Receptor-targeted nanocarriers for therapeutic delivery to cancer. *Molecular membrane biology*, 27(7), pp.286–98. Available at: http://www.pubmedcentral.nih.gov/articlerender.fcgi?artid=3789246&tool=pmc entrez&rendertype=abstract.

Yu, M.K. et al., 2008. Drug-Loaded Superparamagnetic Iron Oxide Nanoparticles for Combined Cancer Imaging and Therapy In Vivo. *Angewandte Chemie International Edition*, 47(29), pp.5362–5365.

Yuan, F. et al., 1995. Vascular Permeability in a Human Tumor Xenograft: Molecular Size Dependence and Cutoff Size. *Cancer Research*, 55(17),

pp.3752–3756.

Zakeri-Milani, P. et al., 2017. Cellular uptake and anti-tumor activity of gemcitabine conjugated with new amphiphilic cell penetrating peptides. *EXCLI Journal*, 16, pp.650–662.

Zhang, L. et al., 2008. Phase II clinical study of gemcitabine in the treatment of patients with advanced nasopharyngeal carcinoma after the failure of platinum-based chemotherapy. *Cancer chemotherapy and pharmacology*, 61(1), pp.33–8. Available at: http://www.ncbi.nlm.nih.gov/pubmed/17909810.

Zhang, L. et al., 2009. Synthesis and applications of polyamine amino acid residues: Improving the bioactivity of an analgesic neuropeptide, neurotensin. *Journal of Medicinal Chemistry*, 52(6), pp.1514–1517.